POLYMER DYNAMICS STUDIED BY NMR AND LIGHT SCATTERING METHODS

A thesis presented in partial fulfilment of the requirements

for the degree of Doctor of Philosophy in Physics

at Massey University

PETER JOHN DAIVIS

1989

Massey University Library. Thesis Copyright Form

Title of thesis: Polymer dynamics studied by NMR and light scattering methods.

(1) (a) I give permission for my thesis to be made available to readers in the Massey University Library under conditions determined by the Librarian.

~~(b)~~ I do not wish my thesis to be made available to readers without my written consent for _____ months.

(2) (a) I agree that my thesis, or a copy, may be sent to another institution under conditions determined by the Librarian.

~~(b)~~ I do not wish my thesis, or a copy, to be sent to another institution without my written consent for _____ months.

(3) (a) I agree that my thesis may be copied for Library use.

~~(b)~~ I do not wish my thesis to be copied for Library use for _____ months.

Signed Peter Dain

Date 26/9/89

The copyright of this thesis belongs to the author. Readers must sign their name in the space below to show that they recognise this. They are asked to add their permanent address.

NAME AND ADDRESS	DATE

DEDICATION

To my grandparents; Bob and Florence Turner, who lived in Narrandera, Jonas Burbulevicius, who lived in Vilnius and Stefanija Fugaru who lives in Adelaide.

ABSTRACT

Theoretical treatments of static and dynamic properties of polymer solutions are reviewed. Particular emphasis is placed on the discussion of diffusion in polymer solutions. The relationship between the mutual diffusion coefficient defined in non-equilibrium thermodynamics and the diffusion coefficient measured in a dynamic light scattering experiment is discussed. The blob model is applied to the calculation of the concentration and solvent quality dependence of the polymer self diffusion coefficient.

An introduction to the theory of Pulsed Gradient Spin Echo (PGSE) NMR and Dynamic Light Scattering (DLS) is given. The possibility of directly measuring a nonlinear mean square displacement for a diffusing polymer molecule by Pulsed Gradient Spin Echo NMR is considered.

Experimental techniques involved in PGSE NMR and DLS measurements are discussed. The variance of the normalized echo attenuation is derived and related to the weighting of least squares fits to PGSE NMR data. A run rejection scheme is proposed for DLS experiments. This scheme can be used to discriminate against data which may be distorted by the scattering from a small number of strongly scattering particulate contaminants in the sample.

The concentration dependences of the polymer and solvent self diffusion coefficients in polystyrene-cyclohexane solutions have been measured. Cyclohexane is a theta solvent for polystyrene and the measurements were made at a temperature near the theta temperature. The polystyrene molar mass was 350,000 g mol^{-1}. The exponent found for the concentration dependence was in good agreement with the theoretical prediction of the reptation model combined with scaling theory. The contribution of local friction effects, which often become apparent near the glass transition, is estimated from the solvent diffusion measurements.

The preparation and characterization of poly(vinyl methyl ether) fractions is described. The fractionation was achieved by batch fractional precipitation from toluene solution with petroleum spirit. Gel permeation chromatography, dynamic light scattering and ultracentrifugation were used to characterize the fractions.

The results of dynamic light scattering measurements on ternary polymer solutions are reported. Three sets of experiments are described. The first set of experiments was performed on the PS-PVME-toluene system. The PS and PVME molar masses were 929,000 g mol^{-1} and 102,000 g mol^{-1}. PVME and toluene are very nearly isorefractive and the polystyrene was present only at trace concentrations. It has often been assumed in the

literature that the self diffusion coefficient of the "visible" polymer is obtained in such measurements, but the range of the validity of this assumption has not been fully defined. Agreement with results in the literature is found, and the diffusion coefficient measured in these experiments is identified as the self diffusion coefficient of the polystyrene. However, in the second set of experiments, it is shown that the self diffusion coefficient of the polystyrene is not obtained from similar measurements when the solvent, toluene, is replaced by carbon tetrachloride. The difference is attributed to thermodynamic factors.

The third set of experiments on ternary polymer solutions also investigated PS-PVME-toluene solutions. The polystyrene and PVME molar masses were 110,000 g mol^{-1}. The effect of an increasing the polystyrene concentration was investigated. Both PGSE NMR and DLS experiments were performed on these samples. A direct comparison of the diffusion coefficients given by these two techniques showed that the self diffusion coefficient of the polystyrene was obtained from the DLS experiments, even when the polystyrene comprised 25% of the total polymer concentration in the samples. Although a cooperative mode of decay was expected to appear in the correlation functions measured in DLS experiments, it was not observed. These experiments are discussed using theoretical results from the literature.

ACKNOWLEDGEMENTS

It is a pleasure to acknowledge the assistance provided by my supervisors. My chief supervisor, Dr D. N. Pinder, provided encouragement, insight and constructive criticism in the right proportions at the appropriate times. He was always available whenever I needed to discuss any aspect of the project. Prof. P. T. Callaghan gave me the opportunity to expand my toolkit of experimental techniques by offering a project involving PGSE NMR - an opportunity from which I feel that I have profited greatly. His sound advice and his willingness to provide assistance with various different aspects of the project is genuinely appreciated. Dr R. C. O'Driscoll also deserves thanks. Without his active involvement, the improvement of the dynamic light scattering apparatus to its present state would not have been possible.

The staff of the Departments of Physics and Biophysics and Chemistry and Biochemistry have been very helpful throughout the duration of my Ph D project. The close proximity and cooperation of the two departments has been a real advantage.

To all those who made or repaired equipment for me, those who freely loaned equipment, and those who instructed me in the use of various items of specialized apparatus, I offer my thanks. Dr Ken Jolley, Mr Dick Poll and Dr James Lewis deserve special mentions for their help with NMR, GPC and ultracentrifugation experiments.

It has been a pleasure to associate with the postdoctoral fellows and Ph D students I have met here at Massey during the past few years. Their good humour, friendship and cooperation have made my stay an enjoyable one. Some of them have become fearsome adversaries - they must be kept in check!

I am particularly thankful for the encouragement and support given to me by my housemates, present and past; John, Phil, Margaret, Beth and James and also my parents and sister, who, despite distance, have been with me all the way.

For her help with the typing of Chapter Two and her phone calls, letters and postcards which kept my spirits high during the completion of this work, my special thanks go to Jessica.

TABLE OF CONTENTS

LIST OF FIGURES

LIST OF TABLES

1 INTRODUCTION

1.1 Background

Polymer solutions have strikingly different dynamic behaviour from that of simple liquids. They flow slowly and may display viscoelastic behaviour combining features seen in rubbery solids and viscous liquids. These unusual attributes have prompted many theoretical and experimental investigations of polymer dynamics, and rapid advances in the understanding of the subject have been made in recent years. Many questions, however, remain unanswered, so more incisive experimental investigations and more powerful theoretical methods are constantly being applied to the remaining problems.

The properties of polymer solutions often exhibit a high degree of universality. For example, the relationship between the chain length and the radius of a randomly coiled polymer takes the form of a power law, with an exponent that is largely independent of the microscopic details of the monomers making up the chain. Scaling concepts, which rely on the validity of the assumption of universality for their derivation, have been very successful in describing the static properties of polymer solutions [7]. Most of the recent theoretical and experimental work in the dynamics of polymer solutions has also been directed at the definition and refinement of universal relationships.

The present understanding of the theory of polymer dynamics is mainly due to the work of de Gennes [7], Doi and Edwards [15] and Graessley [59]. The "tube" or "reptation" model, developed by Edwards and de Gennes, which envisages entangled chains moving in a snake-like fashion through the solution, has been very influential. The reptation model has not been entirely successful, but the generally accepted view now is that any new theories will need to retain the essential features of the reptation model.

This thesis deals mainly with experimental studies of self diffusion in polymer solutions. The self diffusion coefficient is probably the most conceptually simple of all of the dynamic properties. It is a measure of how rapidly a single molecule diffuses by random motion through a solution of uniform concentration. The polymer chain length, the concentration of the solution and the thermodynamic quality of the solvent all influence the self diffusion coefficient. Measurements of the self diffusion coefficient as a function of these parameters provide data which can be used to test and improve the theories of polymer dynamics.

The range of experimental techniques available for the study of self diffusion in polymer solutions has expanded rapidly. The older studies used radioactive tracer methods to monitor the flux of labelled molecules through the solution. In more recent times, various other labelling techniques have been used. The problem with many of these methods is that

chemical modification of the labelled molecules may also occur, leading to a change in the behaviour of the system. What is required is that the labelling technique be minimally perturbative. This ideal is very well achieved by Pulsed Gradient Spin Echo NMR, one of the techniques used in this work. PGSE NMR uses the Larmor precession frequencies of nuclei within the sample to label molecules [78]. The spin states of the nuclei have a negligible effect on the interactions between molecules.

Another experimental technique which has been used extensively to study polymer dynamics in recent years is Dynamic Light Scattering. Whereas time-averaged light scattering is capable of measuring the static properties of polymers such as the molar mass, mean radius and thermodynamic interactions, DLS can measure dynamic properties such as the diffusion coefficient. In a DLS experiment, the mean lifetime of fluctuations in the intensity of the scattered light is measured. Intensity fluctuations are related to concentration fluctuations, which decay by diffusion, so DLS provides a method of measuring diffusion in polymer solutions. The mean rate of decay of concentration fluctuations in a binary polymer solution depends on the mutual diffusion coefficient, which is fundamentally different from the self diffusion coefficient, so PGSE NMR and DLS experiments on binary solutions generally measure different quantities. In the limit of infinite dilution, however, the self and mutual diffusion coefficients are equal. Similarly, the diffusion coefficient measured in a DLS experiment on a ternary solution comprising two solutes and a solvent may be equal to the self diffusion coefficient under certain conditions. These conditions are investigated in Chapter Six of this thesis.

1.2 Research Goals

The overall aim of the research presented in this thesis was to add to the understanding of the dynamics of polymer solutions in two ways; firstly, by performing new measurements of dynamic properties and secondly, by contributing to the development of the techniques which are used for these measurements.

The object of the work presented in Chapter Four was to investigate the effect of solvent quality on self diffusion in polymer solutions. Earlier experiments on self diffusion in polymer solutions tended to concentrate on polymers in solvents which were thermodynamically "good". A good solvent is one in which a single flexible polymer molecule exists as an expanded random coil. The solution is far from phase separation and the monomers of dilute polymer coils in a good solvent tend to repel each other because of the excluded volume effect.

As the solvent quality is reduced, the swelling effect decreases and the net interaction between polymer segments goes to zero. The condition of zero net segment-segment

interaction (or zero excluded volume) is known as the theta condition. Under theta conditions, the polymer conformation is described by a gaussian random walk and the second virial coefficient of the osmotic pressure is equal to zero. An increase in the concentration of a solution of a polymer in a good solvent leads to an analogous effect, because in the limit of pure polymer, the excluded volume interaction is completely screened.

The scaling laws were originally derived for polymers in good solvents, and scaling laws for theta solvent systems followed later. The introduction of the reptation model, combined with scaling laws, provided a comprehensive set of predictions of the molar mass (i.e. chain length) and concentration dependence of dynamic properties including the self diffusion coefficient. However, the change in effective solvent quality in going from a polymer in a good solvent at low concentration to an effective theta solvent at high concentration, resulted in some ambiguity in the interpretation of the experimental results. The effect on the self diffusion coefficient of the "crossover" from good solvent to theta conditions with increasing concentration has been approximately treated theoretically [62], but the ambiguity can be totally removed by making the measurements on a system under theta conditions. This was the aim of Chapter Four. At the time when this work was started, there were virtually no results in the literature on self diffusion in a theta solvent. In fact, Tirrell called for more measurements in a review published in 1984 [54].

Another source of ambiguity in the interpretation of self diffusion data is the increase in local friction which occurs as the glass transition temperature of a polymer is approached. The same effect can often seen if the concentration of a polymer solution is increased sufficiently. This effect is not included in the original form of the reptation model and it is still not thoroughly understood. Solvent diffusion measurements were conducted on the theta solvent system discussed in Chapter Four so that the local friction effects could be investigated simultaneously with the self diffusion of the polymer.

Chapters Five and Six are directed towards an investigation of the use of a new light scattering technique for the measurement of self diffusion in polymer solutions. It has been known for some time [97] that dynamic light scattering experiments on solutions containing two macromolecular solutes would give an autocorrelation function composed of two modes of decay. For dilute ternary solutions, this result is trivial - the two modes of decay correspond to the free particle diffusion coefficients of the two solutes. However, the results become more difficult to interpret when the solutes interact with each other. Phillies [97] showed that the two modes of decay were related to combinations of the ternary diffusion coefficients of the solutes. The mode amplitudes for interacting spherical solutes were calculated by Pusey, Fijnaut and Vrij [98] and experiments on spherical solutes

verifying the essential features of the theory were conducted by Kops-Werkhoven et al. (these are reviewed in section 4.8 of Pusey's paper in [26]).

The application of the technique to polymer solutions proceeded along slightly different lines. From the outset, the emphasis was on solutions in which one solute is isorefractive with the solvent. Hadgraft, Hyde and Richards [191] produced early experimental work in the field, followed by Lodge [192], Cotts [193] and Hanley, Balloge and Tirrell [99]. The only experiments so far which have concentrated on non-isorefractive polymer solutions appear to have been those of Daivis et al. [194].

It has usually been assumed, with some theoretical justification, that the self diffusion coefficient of the visible polymer is obtained from such measurements provided that the concentration of the visible polymer is low enough; hence the name "optical tracer" dynamic light scattering. An opportunity to directly test this assumption existed at Massey University because of the availability of both DLS and PGSE NMR apparatus, so the work in Chapters Four and Five was directed at this task. A theory of dynamic light scattering from ternary polymer solutions has recently appeared in the literature [100]. This theory has been used extensively in the discussion of the results in Chapter Six. Sample preparation and characterization constituted a major portion of the work in these experiments, and it is discussed fully in Chapters Five and Six.

1.3 Thesis Organization

Chapter Two contains a review of the relevant polymer theory and a discussion of the theoretical basis of the two main experimental techniques used in this work, Pulsed Gradient Spin Echo NMR and Dynamic Light Scattering.

Chapter Three covers general experimental considerations which are common to most of the experiments discussed in later chapters.

The main body of the thesis is constituted by Chapters Four to Six. The PGSE NMR studies of polymer (polystyrene) and solvent (cyclohexane) self diffusion under theta conditions are reported in Chapter Four.

The fractionation and characterization of poly(vinyl methyl ether) (PVME) in preparation for the optical tracer dynamic light scattering experiments is described in Chapter Five.

Chapter Six contains the PGSE NMR and DLS experiments on self diffusion in polystyrene-PVME-solvent samples. Three different sets of experiments are discussed.

During the course of the project, several points which had not been adequately covered in the literature were pursued in some detail. This work has been placed in the Appendices so as not to interrupt the flow of the text. However, some new results are contained in these sections, and their importance is stressed in the text.

2 THEORY

This chapter consists of a survey of polymer theory relevant to the experiments reported in this thesis followed by a brief discussion of the theoretical basis of pulsed gradient spin echo NMR and dynamic light scattering.

2.1 Static Properties of Polymers

2.1.1 Phase Diagram for a Binary Solution

The static properties of polymers can be determined by measuring time averaged equilibrium properties such as the osmotic pressure or the absolute intensity of scattered light [1]. One of the most useful static properties is the root mean square radius of gyration, R_G, which is a measure of the average size of a polymer molecule. The static properties of polymer solutions depend strongly upon molar mass, M, polymer volume fraction, ϕ and temperature, T for a given solute-solvent combination.

A qualitative phase diagram for a binary (polymer - solvent) solution is shown in Fig. 2.1. Phase separation occurs in the shaded regions. As the molar mass is increased, the upper critical point (UCP) moves up and to the left. In the limit of infinite molar mass, the UCP approaches the T axis. The limiting value of T is called the theta temperature, θ [2]. A polymer solution may possess both an upper critical solution temperature (UCST) and a lower critical solution temperature (LCST). At each of these extremes, precipitation will occur. Between these temperatures, a continuum of solvent quality exists.

For solutions which have no lower critical solution temperature (or a LCST which is far from the UCST) Daoud and Jannink [2] deduced the temperature - concentration diagram shown in Fig. 2.2. The T - ϕ plane is divided into five regions:

I	Dilute region
I'	Dilute theta region
II	Semidilute region
III	Semidilute theta region
IV	Collapsed chain region
V	Two phase region

The parameter $1-2\chi$ is a measure of solvent quality. The Flory interaction parameter χ is equal to zero for an athermal solvent and 1/2 for a theta solvent. The solvent quality is proportional to the segment - segment excluded volume υ;

$$1-2\chi=\frac{\upsilon}{a^3} \tag{2.1}$$

where a^3 is the volume of a polymer segment or solvent molecule (assumed to be equal in lattice models). The excluded volume can often be written in terms of the reduced temperature $\tau = (T-\theta)/T$ as [3, 6]

$$\left(\frac{\upsilon}{a^3}\right)^2=\tau^2/k_1 \tag{2.2}$$

where k_1 is a constant which is expected to depend insensitively on the solvent and monomer type [6]. Note that τ is sometimes [2] defined as $\tau = (T-\theta)/\theta$ which agrees with the above definition at small deviations from the theta temperature.

The ideas of Daoud and Jannink have been extended by Schaefer to include a newly defined semidilute marginal region [3] lying between the semidilute good and semidilute theta regions, but for the purposes of this thesis, the simpler diagram of Daoud and Jannink will be used.

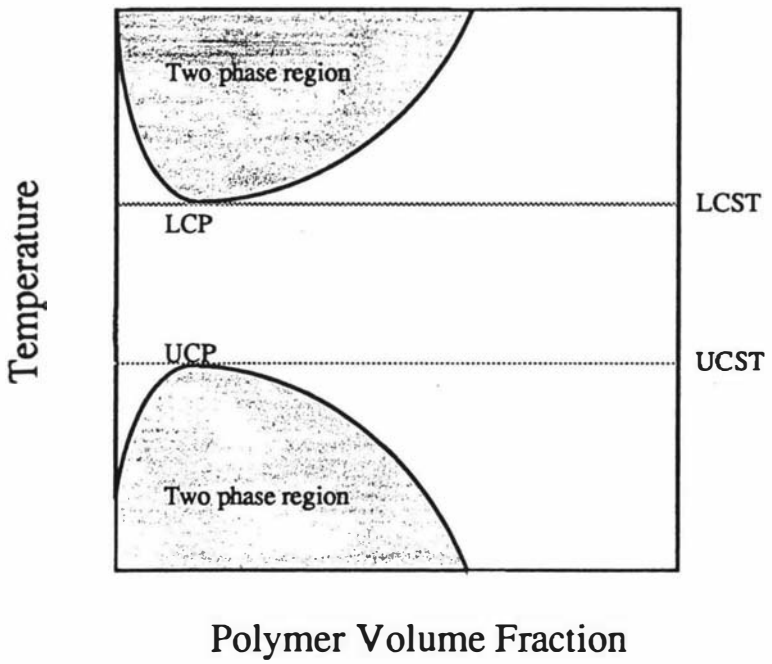

Figure 2.1 Qualitative phase diagram for a polymer solution. The upper and lower critical points (UCP and LCP) may be much more widely separated than is shown here.

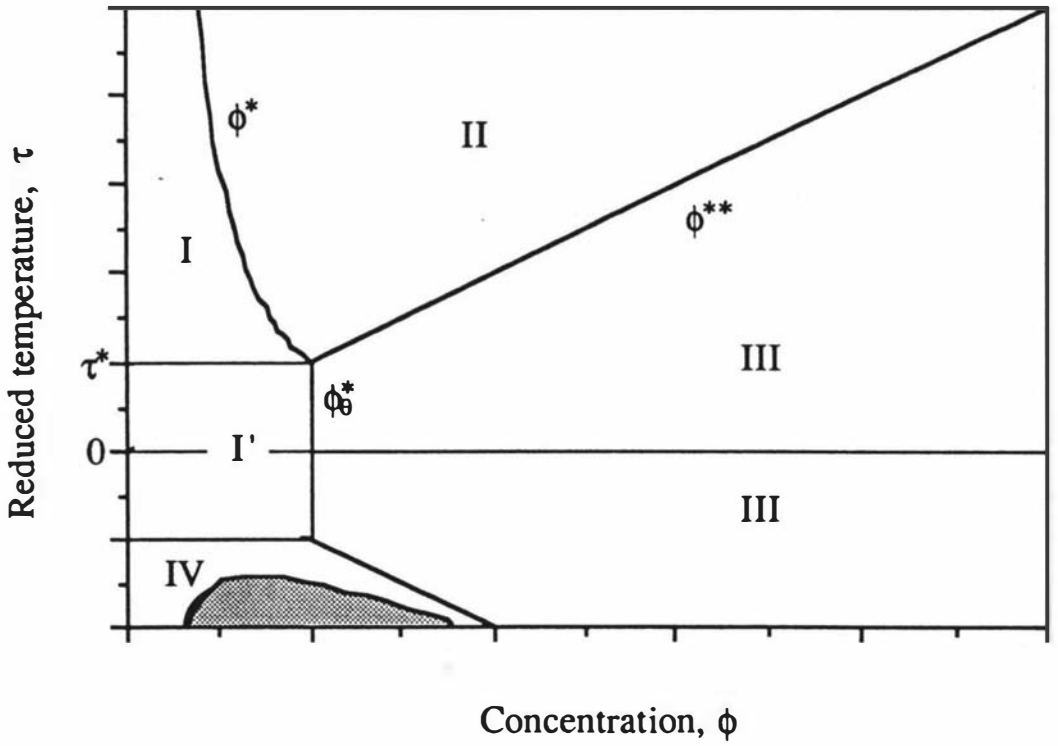

Figure 2.2 Temperature-concentration diagram for a polymer solution far from the LCP according to Daoud and Jannink [2]. The different regions are; I Dilute good solvent region, I' Dilute theta region, II Semidilute good solvent region, III Semidilute theta solvent region, IV Collapsed chain region. The shaded region represents the lower two phase region shown in Fig. 2.1. For a polymer of infinite molar mass, the dilute theta region I' is vanishingly small and the UCST corresponds to the theta temperature ($\tau = 0$).

2.1.2 Infinite Dilution

Fig. 2.2 shows that a dilute polymer solution could be in any one of three different regions, depending on the temperature.

Under poor solvent conditions below the theta temperature (region IV), the polymer chains are collapsed and verging on phase separation. The shaded region of Fig. 2.2 corresponds to the two phase region of Fig. 2.1. Between the theta temperature and the precipitation temperature, polymer molecules in a dilute solution undergo a coil to globule transition [7].

In the dilute theta region, attractive and repulsive interactions between different parts of a chain cancel each other and the polymer conformation can be treated as a random walk of N steps with effective step length a. The effective step length is generally greater than the

length of a monomer, due to the effects of fixed bond angles and hindered rotation [4]. The root mean square radius of gyration of a polymer molecule in the dilute theta region can be calculated using the properties of a random walk to be [4]

$$R_G = \frac{a}{\sqrt{6}} N^{1/2} \tag{2.3}$$

where a is the unperturbed effective bond length and N is proportional to the molar mass or degree of polymerization.

The radius of gyration of a polymer molecule in a dilute solution under good solvent conditions (region I) is increased by the repulsive excluded volume interactions between segments. The polymer chain must then be described in terms of a self-avoiding walk [7].

One way of describing the effect of solvent quality on the swelling of a chain is to use the blob model of chain statistics [5, 6]. The mean squared distance between two segments separated by n segments along the chain is assumed to follow the form

$$R^2(n) = a^2 n \qquad n \le N_\tau \tag{2.4}$$

$$R^2(n) = a^2 n^{2\nu} N_\tau^{1-2\nu} \qquad n \ge N_\tau \tag{2.5}$$

so that at small n the chain is ideal but at large n the chain is swollen. The parameter N_τ is a temperature dependent cutoff determined by experiment ($N_\tau = k_1 / \tau^2$) [6]. If $N_\tau \ge N$, the entire chain is gaussian. In terms of the molar mass, N is M / nA with n being the number of monomers per statistical segment and A the molar mass of a monomer. Therefore, the condition for the onset of swelling is that

$$\tau \ge \tau^*$$

where $\tau^* = (k_1 nA / M)^{1/2}$ (see Fig. 2.2).

The radius of gyration for a polymer molecule in a very good solvent (the athermal limit; $\chi = 0$) has been calculated according to the blob model as [6]

$$R_G = a\, N^{\nu} / [\, 2\,(\nu+1)\,(2\nu+1)\,]^{1/2}\,. \tag{2.6}$$

The value of ν calculated by Flory is 3/5, which is close to the accurate numerical result, 0.588. A general expression which describes the dependence of R_G on N / N_τ can be calculated using the blob model [6].

Since interactions between different polymer molecules are absent at infinite dilution regardless of the solvent quality, the osmotic pressure Π of such a solution obeys van't Hoff's law [8]

$$\Pi = \frac{RT}{M} C \qquad (2.7)$$

where R is the gas constant, T is the temperature in Kelvin, M is the polymer molar mass and C is the polymer concentration in units of mass per unit volume. (The concentration C can be written in terms of the volume fraction ϕ as $C = \phi / \bar{v}$, where $\bar{v}$ is the partial specific volume of the polymer.)

2.1.3 The Virial Regime

The properties of solutions in the dilute theta and dilute good solvent regions are often approximated by the behaviour at infinite dilution. In reality, intermolecular interactions gradually become more important as the polymer concentration is increased, even in the dilute region. Below ϕ^* (in the dilute regions I and I'), a virial expansion adequately describes the concentration dependence of the osmotic pressure [4]

$$\Pi = RT \left(\frac{C}{M} + A_2 C^2 + A_3 C^3 + \ldots \right). \qquad (2.8)$$

Here, A_2, A_3, are the second, third etc. virial coefficients. At the theta temperature $A_2 = 0$ and since the concentration is low, the higher order coefficients need not be considered. Therefore, eqn (2.7) can once again be used for the osmotic pressure.

However, as the temperature is increased, A_2 increases and the higher order virial coefficients may also become important.

Provided that $\tau > (k_1 / N)^{1/2}$, a polymer in a solvent at infinite dilution will be swollen, as mentioned in section 2.1.2. As ϕ is increased, keeping τ constant, this swelling decreases until, in a polymer melt, R_G once again has the same molar mass exponent as it does for a polymer in a theta solvent. The decrease of R_G with increasing concentration is often assumed to be negligible below ϕ^*, with most of the contraction occurring in the semidilute region [7, 9].

2.1.4 Semidilute Solutions

The crossover from the virial regime to the semidilute regime occurs when the domains of polymer molecules in a solution begin to overlap. The concentration at which the effects of interpenetration are observed in static properties is designated ϕ^* as shown in Fig 2.2. A simple interpretation of ϕ^* is that it is the value of the overall concentration which is equal to

the concentration in an isolated coil under the same solvent conditions. If the volume of a coil is taken as R_G^3, the overlap concentration is

$$C^* \approx \frac{M}{N_A R_G^3} \tag{2.9}$$

$$\phi^* \approx \frac{a^3 N}{R_G^3} . \tag{2.10}$$

Equation (2.9) is an example of a scaling law [7] which is correct to within a dimensionless proportionality constant. The use of scaling arguments is insufficient to determine numerical prefactors, but more recently developed renormalization group methods [10, 11] can be used to determine these useful quantities.

An expression for C^* has been found by expanding the equation for Π from renormalization group theory and comparing the result to eqn (2.8) (see e.g. [11]). The result is

$$A_2 M C^* = \frac{9}{16} . \tag{2.11}$$

Equation (2.11) is clearly invalid at the theta temperature, but it has the same scaling behaviour as eqn (2.9) in the athermal limit.

Given that the crossover from one region of the T - ϕ diagram to another often involves a slow change in the measured quantity over a finite range of ϕ or T, eqn (2.10) provides an adequate [1] estimate of ϕ^*. It is possible to express ϕ^* in terms of the radius of gyration using eqns (2.3) and (2.6). In the case of a theta solvent,

$$\phi^* \approx N^{-1/2} . \tag{2.12}$$

Since R_G varies with solvent quality when $\tau \geq \tau^*$, ϕ^* will also vary. In the asymptotic region before the athermal solvent limit for R_G (eqn (2.6)) is reached, the radius of gyration at zero concentration varies as

$$R_G \approx a \tau^{0.2} N^{0.6} \tag{2.13}$$

and ϕ^* therefore varies as [7]

$$\phi^* \approx \tau^{-0.6} N^{-0.8} . \tag{2.14}$$

Once ϕ^* has been reached, R_G will begin to decrease, varying as

$$R_G \approx a N^{1/2} \phi^{-1/8} . \tag{2.15}$$

Equation (2.15) has been verified by both neutron scattering [12] and viscosity [13] measurements.

The decrease in R_G is the result of the screening of the excluded volume effect which takes place gradually as the concentration is increased. This is easily visualized in terms of the self correlation function $g_s(r)$ which gives the excess probability of finding a segment at a distance r from one on the same chain whose location is taken as the origin. At small values of r, $g_s(r)$ behaves as it would for an isolated chain in a good solvent. However, at a distance ξ, $g_s(r)$ changes to the form for an ideal chain because of interactions with segments from other chains. As the concentration is increased, the value of ξ becomes smaller until, in a polymer melt, the swelling effect is entirely absent. The interpretation of ξ is slightly different in the case of a solution at the theta temperature. In this case, the chain dimensions are ideal already, and the correlation function for the total segment density obeys the Ornstein-Zernicke law with a correlation length ξ [7].

Scaling theories also provide predictions of the behaviour of the osmotic pressure at semidilute concentrations. In terms of the correlation length ξ, the osmotic pressure can be expressed as

$$\Pi \approx \frac{RT}{\xi^3} \tag{2.16}$$

In the semidilute θ region of Fig. 2.2 the correlation length varies as

$$\xi \approx a\,\phi^{-1} \tag{2.17}$$

whereas in the semidilute good solvent region it is found that

$$\xi \approx a\,\tau^{-1/4}\,\phi^{-3/4}\ . \tag{2.18}$$

These two expressions for ξ provide us with an estimate of the crossover between regions II and III. When the two values of ξ are equal, it is found that

$$\phi^{**} \approx \tau\ . \tag{2.19}$$

The expressions for ξ given above allow us to write scaling laws for the osmotic pressure in firstly, the semidilute theta region;

$$\Pi \approx \frac{RT}{N_A}\,a^{-3}\,\phi^3 \tag{2.20}$$

and secondly, the semidilute good solvent region;

$$\Pi \approx \frac{RT}{N_A} a^{-3} \tau^{3/4} \phi^{9/4} . \qquad (2.21)$$

For athermal solvents τ is constant and the temperature dependence disappears.

The scaling laws for the asymptotic behaviour of the osmotic pressure in semidilute solutions are well verified [1, 12, 14]. The variation of the radius of gyration with solvent quality as calculated with the aid of the blob model of chain statistics agrees reasonably well with experiment [6], although modifications are required in the non-asymptotic (small N/N_τ) region [10]. The concentration dependence of the radius of gyration in the semidilute region has been measured by neutron scattering [12] and x-ray scattering (see references in [9]). The results agree with scaling predictions [7, 12] but an alternative theory has been presented which also describes the data well [9].

Overall, scaling theories provide simple expressions which describe the static properties of dilute and semidilute polymer solutions reasonably well. The development of renormalization group methods promises improvements over the scaling laws, plus predictions of numerical prefactors which will aid experimental tests.

2.1.5 Polymer Melts

Although it is not marked on Fig. 2.2, there must be a crossover from the semidilute region to the concentrated region which has the pure polymer as its limit. As was mentioned earlier, in the limit of pure polymer, the dimensions of a polymer coil must return to an $N^{-1/2}$ scaling law, since there is no solvent present to cause swelling. In addition, for very concentrated solutions, the polymer segment density will be almost totally uniform. Under these conditions the Flory-Huggins theory [7, 19] adequately describes the thermodynamics of polymer solutions.

Edwards [15] gives a more sophisticated theory, which is valid for concentrated solutions and defines a concentration ϕ_c for the onset of the concentrated regime as

$$\phi_c = \left(\frac{\bar{v} A n}{N_A} \right) \frac{v}{a^6} \qquad (2.22)$$

where $\bar{v}$ is the partial specific volume of the polymer, A is the polymer molar mass per monomer and n is the number of monomers per segment.

Alternatively, Schaefer [3] also gives expressions for the semidilute - concentrated crossover based on his model for semiflexible polymers.

Little experimental work has been done on concentrated polymer solutions, one of the likely reasons being that the best characterized model polymer, polystyrene, becomes glassy at high concentrations near room temperature.

2.1.6 The Glass Transition

If a liquid is cooled quickly enough, crystallization cannot take place and instead a glass is formed. In the case of some polymer liquids, crystallization over any timescale may prove impossible and a glass is always formed upon cooling [16].

A qualitative plot of volume against temperature for three different polymer samples is shown in Fig. 2.3. Curve (a) is the volume-temperature relationship for a polymer which does not crystallize. Instead, it undergoes a glass transition which is marked by a change in the coefficient of thermal expansion, α, at the glass transition temperature T_g. Curve (b) shows the V-T relationship for a polymer which undergoes crystallization at the crystalline melting point T_m. The crystallization is a first order phase transition involving a discontinuous change in the volume, whereas the glass transition has features more reminiscent of (but not totally consistent with) a second order phase transition [16, 17]. Curve (c) shows the V-T curve for the common case of a partially crystalline and partially amorphous polymer, exhibiting both crystallization and vitrification.

The fundamental nature of the glass transition in polymers is still a subject of controversy [16, 17]. Transport properties such as diffusion and viscosity undergo dramatic changes near the glass transition owing to extremely reduced chain mobility, which can be correlated with a steep reduction in free volume near T_g [18]. This will be discussed further in section 2.2.5.

2.1.7 Ternary Solutions

Many of the ideas presented in previous sections can be generalized to the ternary solution case.

Beginning with the simplest example, it is a straightforward extension of van't Hoff's equation (eqn (2.7)) to write the osmotic pressure of a multicomponent solution with several solutes and one solvent in the dilute limit as [19]

$$\frac{\Pi}{RT} = \sum_{i=1}^{r} \frac{C_i}{M_i} \tag{2.23}$$

where the index i enumerates solutes. Likewise, in the virial regime, a multicomponent virial expansion can be written [19].

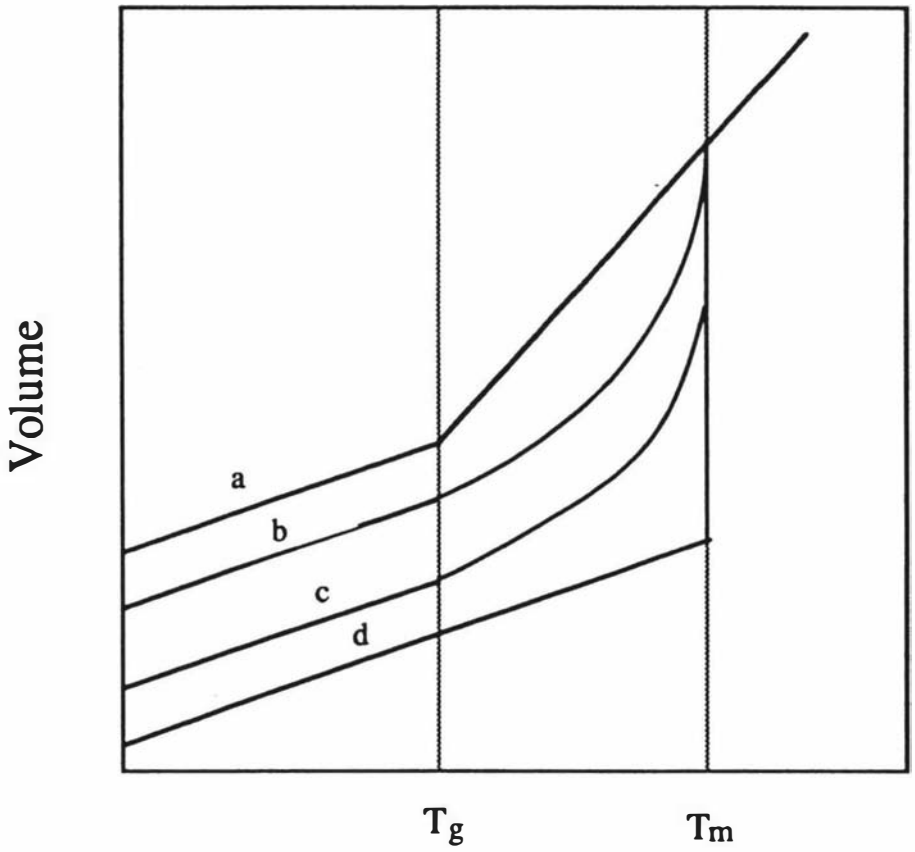

Figure 2.3 Qualitative volume-temperature plot for various liquids. Case (a) represents an amorphous material which shows no crystalline melting behaviour at all. The volume changes continuously, but the slope of the plot changes at the glass transition temperature. Cases (b) and (c) apply to partially crystalline materials and case (d) is for a material which undergoes complete crystallization at the crystalline melting temperature, T_m.

Once the total polymer concentration in a ternary solution reaches the overlap concentration, phase separation is a possibility [7]. In fact, compatibility is the exception rather than the rule in ternary polymer solutions [20]. Polymer-polymer compatibility is usually discussed in the context of the Flory-Huggins theory. The Flory-Huggins theory works better for polymer-polymer mixtures than it does for polymer-solvent mixtures due to the closer match of molecular parameters between components in the polymer-polymer case [20]. The compatibility of ternary polymer solutions is discussed by Kurata [19], de Gennes [7] and Krause [20]. If both polymers are individually soluble in the solvent under

consideration a dilute ternary solution can be made, no matter how mutually incompatible the polymers are. On the other hand, two polymers of infinite molar mass will never form a compatible blend if their Flory interaction parameter χ_{12} is positive [20]. In many cases, a negative value of χ_{12} is found for compatible polymer pairs, suggesting a tendency towards the formation of complexes between the polymer species [19].

Some simpler cases will be considered before semidilute ternary solutions are discussed in more detail.

For a melt of two chemically identical polymers with different molar masses, Joanny et al. [21], following Flory, showed that a single long chain with degree of polymerization N in a melt of shorter chains with degree of polymerization P will be swollen, provided that $P < N^{1/2}$. This is analogous to the case of a polymer in a good solvent (section 2.1.2.).

As the concentration of the N chains is increased, an overlap concentration analogous to ϕ^* (eqn (2.10)) is reached, beyond which the radius of the N chains decreases until the ideal dimensions (c.f. eqn (2.3)) are reached. The results of [21] for the case of long N polymers in a melt of P polymers are summarized in Table 2.1.

Table 2.1 Conformation of long N polymers in a bimodal melt ($P < N^{1/2}$)

Concentration regime	Radius of long chains
$\phi_N < N^{-4/5} P^{3/5}$	$R_G \approx a N^{3/5} P^{-1/5}$
$N^{-4/5} P^{3/5} < \phi_N < P^{-1}$	$R_G \approx a N^{1/2} P^{-1/8} \phi_N^{-1/8}$
$\phi_N > P^{-1}$	$R_G \approx a N^{1/2}$

The more complicated case of N and P chains in an athermal solvent is also discussed in [21]. It is found that the ϕ_N - ϕ_P plane contains seven regions exhibiting different scaling laws for the N, P, ϕ_N and ϕ_P dependence of the radius of gyration of the N chains. In view of the complicated nature of this problem, the reader is referred to the original work [21] for more information.

The cases treated in [21] still involve simplifications because the N and P chains are assumed to be chemically identical and the solvent is assumed to be athermal for them.

Nose [22] has treated the case in which the N and P chains may be chemically different for a restricted set of circumstances. The solvent is assumed to be athermal for both polymers, so that $\chi_{01} = \chi_{02} = 0$ (where the subscript 0 denotes solvent). However, the interaction parameter between the two polymers χ_{12} is non-zero. Nose has additionally assumed that the N polymer is present only as a trace, whereas the solution is semidilute with respect to the P polymer. The degrees of polymerization N and P are both allowed to vary. Using the thermal and concentration blob models and an expression for χ_{12} which accounts for the excluded volume effect of the P chains on the N chains, Nose finds expressions for R_G and A_2 as functions of N, P, ϕ_P and χ_{12}. He also finds scaled forms of these equations and defines several regions in terms of them. The results agree with those of Joanny [21] in the case where $\chi_{12} = 0$.

2.2 Dynamic Properties of Polymers

2.2.1 Diffusion Coefficients

The dynamic properties studied in this work are the mutual and self diffusion coefficients. The macroscopic and microscopic definitions of these quantities are discussed in this section.

The mutual diffusion coefficient will be considered first. De Groot and Mazur [23] define the diffusion coefficients D_{ij}^{ax} in a relationship between macroscopic gradients in the composition variables x_j for components j and the resultant macroscopic flux (relative to a reference velocity v^a) of component i;

$$J_i^a = C_i (v_i - v^a)$$

$$= - \sum_{j=1}^{n-1} D_{ij}^{ax} \, \mathrm{grad}(x_j) \quad . \tag{2.24}$$

This equation refers to an n component solution in which component 0 has arbitrarily been designated as solvent. Note that the fluxes of only n–1 of the n components need be specified because the fluxes are not independent. Equation (2.24) points out clearly that both the composition variables and the reference velocity need to be specified before the definition of a diffusion coefficient is complete. In most experimental situations, the simplest form of the diffusion equations is obtained by selecting the mass/volume concentrations C_j as the concentration variables (giving D units of m^2s^{-1}) and the mean volume weighted velocity of the system as the reference velocity [23]. When this is done, the relationship between flux and gradient becomes

$$J_i^a = -\sum_{j=1}^{n-1} D_{ij}\, \mathrm{grad}(C_j) \quad . \tag{2.25}$$

For a binary solution, there is only one independent diffusion coefficient, called the mutual diffusion coefficient, which will be designated as D from here on. The form of eqn (2.25) which applies to a binary solution is called Fick's first law and the diffusion coefficients appearing in eqn (2.25) are generally referred to as Fick's Law diffusion coefficients. The mutual diffusion coefficient can be written in terms of a product of a thermodynamic term and a friction term (eqn (203) in [23]).

$$D = \frac{M}{f} C_1 \left(\frac{\partial \mu_1}{\partial C_1}\right)_{T,P} \tag{2.26}$$

where f is the molar friction factor (or inverse mobility) defined with respect to the mean volume weighted velocity (units : N $(ms^{-1})^{-1}$ mol^{-1}) and μ_1 is the chemical potential of the solute expressed in J kg^{-1}. Equation (2.26) can be written in a number of different ways depending on the definition of f and the expression used for the thermodynamic term. Some of those expressions are considered in Appendix 1.

Since the friction factors for mutual diffusion and the sedimentation coefficient are the same, they are related by the following equation:

$$\frac{D}{s} = \frac{C_1}{1-\rho\,\bar{v}} \left(\frac{\partial \mu_1}{\partial C_1}\right)_{T,P} \tag{2.27}$$

where ρ is the solution density. In the dilute limit, this becomes

$$\frac{D}{s} = \frac{RT}{M(1-\rho\bar{v})} \tag{2.28}$$

which is known as the Svedberg equation.

Microscopic expressions for transport coefficients including D can be written in terms of the correlation functions of microscopic fluxes due to fluctuations in the equilibrium state [24, 25]. These equations are called Green-Kubo relations.

A Green-Kubo equation for the mutual diffusion coefficient can be derived using linear response theory [25, 29]. The result (see Appendix 2) is

$$D = (S(0)\ 3\ N)^{-1} \int_0^{\infty} \sum_{i=1}^{N} \sum_{j=1}^{N} \langle\ v_i(0).v_j(t)\ \rangle\ dt \qquad (2.29)$$

where S(0) is proportional to the osmotic compressibility, κ_π ;

$$S(0) = \frac{RT}{M}\left(\frac{\partial \Pi}{\partial C}\right)_T^{-1} \qquad (2.30)$$

$$= RTC\kappa_\pi / M$$

and the summations are performed over a small but macroscopic volume containing N solute molecules.

The self diffusion coefficient, in contrast to the mutual diffusion coefficient, is the transport coefficient describing the migration of a labeled particle in a system without chemical potential gradients. Strictly speaking, this process should be called intradiffusion, with the term self diffusion being restricted to (pseudo-) one component systems in which a minimally perturbative label is applied to some of the otherwise identical particles. Diffusion in the presence of gradients in chemical potential has been called interdiffusion to distinguish it from intradiffusion [30]. The terms intradiffusion and self diffusion will be used interchangeably here, with the understanding that in systems containing more than one component, intradiffusion is implied.

A macroscopic definition of the self diffusion coefficient can be given in terms of eqn (2.25) with the concentration gradients of all species except the labeled one being equal to zero. The concentration gradients of the labeled and unlabeled members of the species being studied must be equal and opposite [30];

$$\text{grad } C_1 = -\text{ grad } C_{1^*} .$$

The most direct microscopic interpretation of the self diffusion coefficient is in terms of the mean square displacement [24, 31]

$$D_s = \lim_{t\to\infty} \frac{\langle \Delta r^2 \rangle}{6t} . \qquad (2.31)$$

Here, $\langle \Delta r^2 \rangle$ is a shorthand notation for $\langle |\mathbf{r}(t)-\mathbf{r}(0)|^2 \rangle$.

This equation leads to a Green-Kubo relation for D_s [24, 31];

$$D_s = 1/3 \int_0^\infty \langle v_1(0) \cdot v_1(t) \rangle \, dt \qquad (2.32)$$

$$= \frac{RT}{f_s}.$$

The subscript 1 indicates that D_s is an ensemble averaged single particle property. Clearly, there is a fundamental difference between f_s and f if equations (2.29) and (2.32) are compared. The difference between f_s and f has also been demonstrated experimentally by Callaghan and Pinder [140] and Brown, Stilbs and Johnsen [141].

At infinite dilution, D_s and D are equal [24], and equation (2.26) becomes

$$D = \frac{RT}{f} = \frac{RT}{f_s}$$

so that in this limit $f = f_s$.

2.2.2 Infinite Dilution

The polymer self diffusion coefficient in an infinitely dilute solution is equal to the mutual diffusion coefficient. Furthermore, the friction factor of a hydrodynamically equivalent sphere can be used for f_s (= f). Therefore

$$D_s = D_m = \frac{RT}{f}$$

$$= \frac{k_B T}{6\pi\eta_0 R_H} \qquad (2.33)$$

where η_0 is the solvent viscosity and R_H is the equivalent hydrodynamic radius of the polymer coil.

Like the radius of gyration, the hydrodynamic radius depends not only on molar mass but also on solvent quality. The hydrodynamic radius can be calculated in the dilute limit by combining the blob model with the Kirkwood equation for R_H [6]. The result for a theta solvent is

$$R_H = \frac{(6\pi)^{1/2}}{16} a N^{1/2} \qquad (2.34)$$

whereas in a good solvent it is found that [6]

$$R_H = \frac{(6\pi)^{1/2}}{12} (1-\nu)(2-\nu) a N^{\nu}. \qquad (2.35)$$

It is now well known that dynamic quantities approach the long chain, good solvent limit [6, 11, 32] more slowly than static properties. The asymptotic behaviour of equation (2.35) is not usually observed and it has been necessary to use the blob model to interpolate between the two limits [6, 32]. A plot of the effective dynamic exponent ν_H versus the effective static exponent ν_G calculated using renormalization group methods (which do not contain the arbitrariness inherent in the blob model) also shows the slow crossover behaviour of R_H [11].

Renormalization group methods have been applied to the dynamic properties of dilute polymer solutions [11]. The most useful predictions are in the form of universal ratios of readily measured quantities containing no adjustable parameters. Values of universal ratios containing various static and dynamic quantities have been calculated in the swollen and gaussian chain limits using renormalization group methods. For example, in the nondraining limit [11],

$$U_{f/s} = \frac{f}{\eta_0 R_G} \tag{2.36}$$

has been calculated as 12.067 for a swollen chain and 15.189 for a gaussian chain. The swollen chain result has been verified experimentally [33].

2.2.3 The Virial Regime

The concentration dependence of dynamic properties in the virial regime is most easily described by power series expansions similar to the osmotic pressure virial expansion (eqn (2.8)).

If the friction factor f is written as [4]

$$f = f_0 \ (1 + k_f C + \ldots) \tag{2.37}$$

and the virial expansion for the osmotic pressure (eqn (2.8)) is used in equation (A1.2), a power series expansion for D is obtained;

$$D/D_0 = 1 + k_D C + \ldots \tag{2.38}$$

where

$$k_D = 2A_2M - \bar{v} - k_f \ . \tag{2.39}$$

The sedimentation coefficient s is inversely proportional to f (eqn (2.27)) so an expression similar to eqn (2.37) holds for 1/s.

Since f and f_s are not equal except at infinite dilution (section 2.2.1) k_{fs} must be distinguished from k_f;

$$f_s = f_0 (1 + k_{fs} C + \ldots)$$

$$\frac{D_s}{D_0} = \frac{f_s}{f_0}$$

$$= (1 + k_{fs} C + \ldots)^{-1}$$

$$= (1 - k_{fs} C + \ldots) \ . \qquad (2.40)$$

Note that whereas k_D may be positive or negative, k_{fs} is always positive because its only contribution comes from an increase in friction with concentration [34].

2.2.4 Semidilute and Entangled Solutions

The static properties of polymer solutions in the semidilute region are now well understood [1, 7, 11]. The theoretical discussion of dynamic properties, however, is still in progress. The most difficult aspects of dynamic properties are the hydrodynamic interaction and the effect of entanglements.

De Gennes was able to simplify the analysis and apply scaling methods when he assumed that the hydrodynamic screening length was equal to the static correlation length for polymers in good solvents [35]. This assumption has been criticised [36] but a recent reconsideration of hydrodynamic screening [37] has given results which agree with the scaling analysis in the asymptotic good solvent case. Assuming that the hydrodynamic screening length was proportional to the static correlation length, de Gennes [7] calculated the sedimentation coefficient and combined the result with the scaling law for the osmotic (see equations (2.27), (A1-1) and (2.21)) to find the scaling law for the cooperative diffusion coefficient;

$$D_c \approx \frac{k_B T}{6\pi\eta_0 \xi} \ . \qquad (2.41)$$

The cooperative diffusion coefficient must be distinguished from the mutual diffusion coefficient because D_c describes the short time "respirational" response to a concentration fluctuation rather than the long time decay of a macroscopic concentration gradient which may involve slow structural relaxation processes [38]. Therefore, entanglements are relatively unimportant in a calculation of D_c [39]. When equation (2.18) is applied to equation (2.41), the exponent for the concentration dependence of D_c in good solvents is found to be 3/4, which is higher than exponents found experimentally [40, 41, 42, 43]. Similar discrepancies exist for the sedimentation coefficient [40, 44]. In theta solvents,

however, the agreement between theory and experiment for both s and D_c is much better [40, 45]. The slow approach of dynamic properties to their asymptotic long chain, good solvent behaviour is probably responsible for the discrepancies in the good solvent cases. The blob model has been applied to the calculation of D_c showing the variation of the effective exponent with solvent quality and concentration (see Appendix 3 and [46]).

Shiwa [39] has presented results for D_c obtained by renormalization group methods. The calculations of Shiwa represent an improvement over scaling methods and calculations based on the blob model because the sudden change in chain statistics in the blob model can be avoided and the assumption used in scaling theories that the hydrodynamic screening length is equal to the correlation length is unnecessary. On the other hand, the application of renormalization group methods is still limited to the good solvent case. This is clearly so in Shiwa's calculations which predict no concentration dependence of ξ_H when $A_2 = 0$.

A discussion of the self diffusion coefficient D_s, in contrast to D_c, must explicitly consider the effect of entanglements. The clearest evidence of the effect of entanglements on the dynamic properties of polymers is found in the molar mass dependence of the viscosity of a polymer melt (p 244 of [50]). It is found experimentally that for low molar masses, the melt viscosity varies as

$$\eta \sim M \tag{2.42}$$

whereas at higher molar masses, η varies as

$$\eta \sim M^{3.4} \ . \tag{2.43}$$

The higher exponent is attributed to the effect of entanglements and the molar mass at which the change from M to $M^{3.4}$ behaviour is observed is called the critical molar mass for the onset of entanglement coupling M_c and is characteristic of a given polymer. Equation (2.42) may not be strictly obeyed because the monomer friction coefficient varies with molar mass at low values of M due to chain end effects. When this effect is normalized out, the predicted M dependence is observed (Ferry [50] p 227).

The effect of entanglements on the viscosity of a polymer solution is observed when [50, 51]

$$\alpha_s^2 \, \phi M > M_C \tag{2.44}$$

where α_s^2, the expansion factor for the radius of gyration is a function of solvent quality, molar mass and concentration. The expansion factor has the value 1 in a theta solvent and in concentrated solutions.

Berry and Fox [51, 13] have presented extensive experimental data supporting the following empirical equation for the viscosity of a polymer solution, based on a similar relation for the melt viscosity;

$$\eta = \frac{N_A}{6} X_C \left(\frac{X}{X_C}\right)^a \zeta_b \ . \tag{2.45}$$

In equation (2.45),

N_A = Avogodro's number

$$X = \frac{R_G^2 \ \phi \ M \ \rho_1}{nl^2 \ M_L^2}$$

$$X_C = \frac{R_G^2(\theta) \ M_C \ \rho_1}{nl^2 \ M_L^2}$$

$a = 3.4$ for $X > X_C$

$= 1.0$ for $X \leq X_C$

and ζ_b is the friction factor per chain bond. Also, $R_G(\theta)$ is R_G under theta conditions, ρ_1 is the density of undiluted polymer, nl is the contour length of a polymer of n bonds, each of length l, and M_L is M / nl. Equation (2.45) shows that if the change in ζ_b with concentration, temperature and molar mass is accounted for, the viscosity obeys a simple power law.

Berry and Fox [51] have discussed the variation of ζ with molar mass and temperature for a polymer melt. The temperature variation cannot generally be described by a simple relation holding over a wide temperature range. However, at temperatures much higher than the glass transition temperature ($T-T_g > 200$) nearly linear plots of ln η against 1/RT are obtained, the slope E^* being interpreted as an activation energy for flow. At the other extreme, when the temperature is not far above the glass transition temperature, the Vogel relation

$$\zeta = \zeta_0 \exp[1 / (\alpha(T-T_0))] \tag{2.46}$$

is found to account for the temperature dependence of the melt viscosity adequately. However, the parameters T_0 and α remain constant only within a restricted temperature range [51]. Equation (2.46) can be cast in a slightly different form which is suggested by free volume theory;

$$\zeta = \zeta_0 \exp\left(\frac{B}{f_g+\alpha_f(T-T_g)}\right) \tag{2.47}$$

where B is the critical fractional free volume required to allow the motion of a chain segment (usually B≈1), f_g is the fractional free volume at the glass transition temperature and α_f is the coefficient of thermal expansion for the free volume of the polymer liquid. The coefficient of expansion of free volume α_f is the difference between the total expansion coefficient for the liquid state α_l and the expansion coefficient of the occupied volume α_0. The value of α_0 is often taken as zero [51].

For low molar mass polymers, T_g varies with molar mass and can be approximated by

$$T_g = T_g^{\infty} - \frac{k}{M} \tag{2.48}$$

where T_g^{∞} is the glass transition temperature for a polymer of infinite molar mass and k is a constant. The variation of ζ with the concentration of a diluent can still be described by equations (2.46) and (2.47), but the parameters B, f_g and T_g will vary with the solvent volume fraction. In practice, B and f_g for solutions seem to be independent of solvent volume fraction ϕ_0 until $\phi_0 > 0.8$. At very high solvent volume fractions the free volume interpretation of ζ is generally not valid.

Berry [52] has stressed that values of the parameters in (2.47) are best determined by measuring the temperature dependence of η (or D_s). Values determined in this way may then be used to correct viscosity or diffusion data for the influence of ζ. However, the range of temperatures available for a temperature dependence study is often limited by the low boiling point of the solvent.

The experimental data on self diffusion in polymer melts and solutions published before 1984 have been reviewed by von Meerwall [53] and Tirrell [54]. In the melt, polymer self diffusion data seem to indicate that the self diffusion coefficient varies as

$$D_s - \zeta_m^{-1} M^{-2} \tag{2.49}$$

both above and below M_c [54, 56, 57]. The absence of a change in the molar mass scaling of D_s at M_c contrasts with the drastic change observed in the melt viscosity (equation (2.45)). The monomer friction factor ζ_m becomes molar mass dependent at low molar masses [54] as was mentioned previously in relation to the melt viscosity. An empirical relation similar to eqn (2.45) for the concentration dependence of D_s has been proposed by Nemoto et al. [56] but self diffusion behaviour in solutions is more complicated than in the melt and a purely empirical description of self diffusion seems likely to become more

complicated and less satisfactory than equation (2.45) has been for viscosity. Therefore, it is appropriate to consider the theoretical descriptions of self diffusion.

The most prominent theory of polymer dynamics which includes the effect of entanglements is the reptation model which was proposed by de Gennes and Edwards (see [7], [15] and [50] for references to the original papers). The basic premise of the reptation model is that in a system of entangled chains, the lateral motion of a test chain is restricted by the presence of other entangled chains. Therefore, motion can only proceed along the length of the chain and only the ends are allowed unconstrained motion. In the original reptation model, it was assumed that the entanglement constraints on the test chain are static. Experimentally, this would be equivalent to a short chain moving in a matrix of very long chains [7].

The reptation model takes a particularly simple form for the case of a polymer melt. A derivation beginning with the equation for the mean square displacement (eqn (2.31)) can be used to calculate the self diffusion coefficient. The time taken for a polymer molecule to move totally out of the tube defined by its initial topological constraints is called the reptation time τ_R. By the end of this time interval, a chain will have moved along a curvilinear distance approximately equal to the length of the tube, $(N/N_e)\, aN_e^{1/2}$ where N_e is the number of segments between entanglements. The motion along this path can be treated as one dimensional Brownian motion so the mean square displacement divided by the reptation time defines a diffusion coefficient for curvilinear motion within the tube;

$$D_{tube} \approx \frac{a^2N^2}{2\tau_R N_e} \quad . \tag{2.50}$$

When the Rouse expression for the friction factor is used, the Einstein relation for D_{tube} is

$$D_{tube} \approx \frac{k_B T}{N\zeta_a} \tag{2.51}$$

where ζ_a is the friction factor per statistical unit. The reptation time emerges from (2.50) and (2.51) as

$$\tau_R \approx \frac{a^2\zeta_a}{2k_B T}\frac{N^3}{N_e} \sim N^3 \quad . \tag{2.52}$$

Graessley [59] defines τ_R as the longest relaxation time of an equivalent Rouse chain representing the tube. Combined with the Rouse expression for the self diffusion coefficient, this definition gives a result differing from eqn (2.52) only by a dimensionless constant.

If the overall three dimensional motion of the chain is now considered, the mean square displacement of the chain during a time τ_R is approximately equal to the mean square end to end distance of the chain R^2 [58, 59], or, in terms of the radius of gyration ($R_G^2 = R^2 / 6$),

$$D_s \approx \frac{R_G^2}{\tau_R} \tag{2.53}$$

In the melt, R_G is given by equation (2.3) so that

$$D_s \approx \frac{a^2 N}{6\tau_R} \tag{2.54}$$

$$= \frac{k_B T N_e}{3\zeta_a} N^{-2}$$

The N^{-2} dependence of D_s in the melt has been verified experimentally [54]. Other predictions of the reptation model have not been as successful. The viscosity goes as $N^{3.4}$ rather than N^3 as the reptation model predicts. This is a serious discrepancy which has prompted modifications to the reptation model. Doi and Edwards [15] discuss possible explanations for the discrepancy and note that Graessley has found that the reptation prediction for η is actually higher than the observed values (despite the lower exponent). Furthermore, the discrepancy decreases with increasing M and becomes negligible at molar masses of $M \approx 800\ M_c$. Therefore a large crossover region between Rouse behaviour and reptation behaviour can be expected. This discussion points to the conclusion that additional mechanisms for relaxation are required to reduce the theoretical estimates of η. Two of the additional mechanisms for the relaxation of entanglement constraints which have been considered in the literature are constraint release and tube contour length fluctuation. Constraint release is the relaxation of entanglement constraints due to the motion of surrounding chains which form the constraints. Contour length fluctuation ("tube leakage") occurs when a portion of the test chain bulges out between entanglements, shortening the length of chain within the tube and allowing the chain end to choose a new path when the fluctuation subsides [15, 59]. For very high molar masses, these effects are expected to disappear. Recent melt viscosity measurements on samples with M/M_c up to approximately 300 show a tendency towards $\eta \sim N^3$ at the highest molar masses [60].

The extension of the reptation model from melts to solutions was first made by de Gennes [35] for the good solvent case using scaling arguments. It is also possible to use an extension of the method leading to equation (2.54). Assuming that the static and hydrodynamic lengths are equal, i.e. $\xi_S = \xi_H = \xi$, and that one "concentration blob" of radius ξ contains g segments, the reptation time is

$$\tau_R \approx \frac{(N/g)^2 \xi^2}{2}$$

but

$$D_{tube} \approx \frac{k_B T}{6\pi\eta\ (N/g)\ \xi}$$

so

$$\tau_R \approx \frac{6\pi\eta}{2k_B T}\ (N/g)^3\ \xi^3 \qquad (2.55)$$

therefore

$$D_S \approx \frac{R_G^2}{\tau_R} = \frac{k_B T}{18\pi\eta_0} (N/g)^{-2}\ \xi^{-1}. \qquad (2.56)$$

The polymer volume fraction is $\phi = a^3 g / \xi^3$, and equation (2.18) gives ξ, so

$$D_S \approx \frac{k_B T}{18\pi\eta_0}\ a^{-1}\ \tau^{-5/2}\ N^{-2}\ \phi^{-7/4}\ . \qquad (2.57)$$

Deschamps and Leger [61] have discussed the derivation of equation (2.56) for the θ - solvent case. Although the correlation length ξ is not equal to the distance between binary contacts (i.e. entanglement points) in a theta solvent, they found that ξ could still be identified as the distance between entanglement *constraints* because a polymer chain in a theta solvent is self - entangled. Therefore the form of equation (2.56) is unchanged in the theta solvent case and the result is

$$D_S \approx \frac{k_B T}{18\pi\eta_0}\ a^{-1}\ N^{-2}\ \phi^{-3}\ . \qquad (2.58)$$

Tirrell [54] has discussed the agreement of equations (2.57) and (2.58) with experiment. By plotting $D_S M^2 \eta_0$ against concentration, Tirrell was able to remove the main effects of solvent and molar mass variation and data for several different polystyrene-good solvent systems were superimposed. Rather than a definite $\phi^{-7/4}$ scaling region, the data showed a continuous curvature in the log-log plot. Two effects are probably responsible for the absence of an extended concentration scaling region. First, due to the crossover from good solvent to theta solvent conditions as the concentration increases (the crossover concentration is ϕ^{**} in Fig. 2.2), a transition from $\phi^{-7/4}$ to ϕ^{-3} scaling is expected. The blob model has been used by Callaghan and Pinder [62] to investigate the effective exponents resulting from the crossover effect. A detailed analysis of the blob model is given in Appendix 3. Fleischer and Straube [55] have applied a slightly different model of

the concentration crossover effect to the calculation of the self diffusion coefficient. Their Fig. 4 displays unexpected behaviour for $\xi_{H\theta} / \xi_H$ (their α_H^{-1}). These quantities are expected to have the same concentration scaling behaviour as $D_c / D_{c\theta}$, which goes as $C^{3/4} / C^1 = C^{-1/4}$ in the semidilute good solvent region. Their plot decreases at low C rather than increasing as would be expected (see Fig. A3.2 for example).

At high polymer concentrations, the effective exponent of ϕ may become less than -3 [54] due to an increase in the effective local friction. For theta solvent systems, the agreement with the concentration scaling shown in equation (2.58) is good ([61] and Chapter 4) until local friction effects become important.

The exponent for the molar mass dependence of D_s predicted by the reptation plus scaling theory is -2 throughout the semidilute region. This prediction has not been unequivocally verified, but seems to be correct for concentrations well above C* [54].

Hess [63, 64] has recently presented a model of the diffusion of entangled polymers which includes reptation as a limiting case. Hess' model predicts the onset of reptation at a critical value of an entanglement parameter ψ which is defined in terms of the mean interaction energy of the polymer and is proportional to its number of entanglements. Hess gives

$$\psi = \frac{G^V M \bar{v}_1}{2 RT \phi_1} \tag{2.59}$$

where G^V is the free energy of mixing per unit volume. In Appendix 4 it is shown that G^V is related to the osmotic pressure so that ψ can be found by integrating the osmotic pressure.

In Hess' model, the reptation transition occurs at $\psi = 1$ and for higher values of ψ motion of a polymer perpendicular to its contour is quenched. For a given molar mass, ψ will equal one at a critical value of ϕ. On the other hand, when the concentration is constant ψ will reach one at a critical value of M. Nemoto et al. [65] found that a direct estimate of the critical molar mass using equation (2.59) gave values which were smaller than experimental values by a factor of ten.

Hess' model predicts that the self diffusion coefficient is given by

$$D_s = D_R \left(1 - \frac{2\psi}{3} \right) \qquad \text{for } 0 \le \psi \le 1 \tag{2.60}$$

$$= \frac{D_R}{1+2\psi} \qquad \text{for } \psi \ge 1$$

where

$$D_R = \frac{k_B T}{N\zeta(C)} \tag{2.61}$$

is the effective Rouse diffusion coefficient and $\zeta(C)$ is the effective friction per segment. Note that $\zeta(C)$ should be interpreted as the total chain friction (including the effect of hydrodynamic interactions) divided by N, rather than the simple monomer friction factor appearing in equation (2.45).

Hess [63] was able to show that his expression for D_s when $\psi > 1$ is equivalent to the scaling result for good solvents when the appropriate scaling laws for G^V and $\zeta(C)$ are used. Since Hess' theory neglects 3 body contributions to ψ, it cannot be applied to solutions at the theta temperature.

Shiwa has presented theoretical calculations of D_s for both unentangled [37] and entangled [39] solutions which use recent calculations of the concentration dependent effective segment friction factor $\zeta(C)$. For entangled solutions, Shiwa uses Hess' model to obtain D_s. The concentration exponent agrees with the scaling theory exponent in the asymptotic good solvent case. Furthermore, the molar mass exponent changes from -1 to the scaling plus reptation exponent of -2 as the concentration is increased. However, the theory of Shiwa is still deficient because the crossover to theta solvent behaviour at high concentrations cannot be calculated. In addition, Shiwa uses an expression for $\zeta(C)$ which involves a complicated integral equation which can only be solved numerically.

2.2.5 Matrix Effects

The reptation model can be incisively tested by studying the self diffusion of a tracer polymer in a solution or melt of another polymer. As was mentioned earlier, the unmodified reptation model relies on the assumption that the entanglement constraints on the test polymer are static. In practice, this situation will only be well approximated by a test polymer moving through a matrix formed by very long polymers.

Theoretical studies of matrix effects have mainly been concerned with the self diffusion of a tracer polymer in a melt of another polymer.

Daoud and de Gennes [66] considered the case of a polymer of N statistical segments diffusing in a melt of chemically identical polymers of P statistical segments. When $N<<P$ (but $P>P_C$ so that the matrix is entangled), the P chains form a network which is static during the reptation time of the N chain. The reptation model applies in this case. On the other hand, when $N>>P$ the P chain matrix can be treated as a viscous medium through

which the N chains move like spheres with a diffusion coefficient given by the Stokes-Einstein equation, i.e.

$$D_{SE} = \frac{k_B T}{6\pi\eta_P R_H(N)} \quad . \tag{2.62}$$

The viscosity η_P can be calculated using the reptation model if the P chains are entangled, and scales according to

$$\eta_P \sim P^3 P_e^{-2} \quad . \tag{2.63}$$

The hydrodynamic radius $R_H(N)$ of the N chain can be expected to depend on the matrix molar mass and chemical type in a similar way to the radius of gyration which was discussed in section 2.1.7.

When the ratio of D_{SE} to the reptation D is large, Stokes-Einstein diffusion will be the dominant transport process. This occurs when [66]

$$N > P^2 P_e^{-2/3} \quad . \tag{2.64}$$

A discussion of the intermediate case, $N \approx P$, must consider the effects of constraint release and contour length fluctuations, as was mentioned in section 2.2.4. Recent experiments on self diffusion in polystyrene melts have confirmed the existence of these effects and demonstrated that they diminish as the matrix molar mass increases [67].

When the N and P polymers are not chemically identical similar ideas to those mentioned above will apply, but the thermodynamic effects of the matrix polymer on the probe polymer must also be taken into account (see section 2.1.7).

The case of two polymers dissolved in a solvent which is good for both of them has been discussed theoretically by Martin [68] and Numasawa, Kuwamoto and Nose [69]. Martin applied the analysis of Daoud and de Gennes to a dilute solution of long N chains in a matrix solution of shorter P chains in a solvent which is good for both polymers. Using an analysis similar to that leading to eqn (2.64) Martin was able to define a crossover concentration ϕ_{SR} between the Stokes-Einstein and reptation regimes. Martin assumed that unless the N and P polymers are chemically identical, the interactions within the N chain are not screened by the P chains. Therefore, the N chains are swollen and a concentration dependent excluded volume parameter is used to describe the interactions between the blobs of the N polymer and the P polymers. Martin found that the reptation diffusion coefficient is

$$D_S \sim N^{-9/5} \phi^{-3/2} \upsilon^{2/5} \tag{2.65}$$

where υ is the excluded volume parameter and ϕ is the volume fraction of the P chains. In the case of chemically identical N and P chains in a good solvent the standard reptation-scaling result (eqn (2.57) with $\tau = 1$) was obtained.

Numasawa et al. [69] extended Martin's analysis to the case of an incompatible N, P combination, using Daoud and de Gennes' discussion as a guide and taking specific results for R_G from Nose's paper [22].

2.2.6 Solvent Diffusion

Theoretical treatments of solvent diffusion in polymer solutions can be divided into two classes; those which apply near the glass transition temperature of the solution and those which apply far above T_g.

It is most often the case that a dilute solution is far above its glass transition temperature. Several theoretical expressions have been derived which consider the obstruction effect of macromolecular or colloidal solutes [70, 72, 73].

In a study of the self diffusion of water in protein solutions, Wang [70] derived a result which includes the obstruction effect and the effect of hydration of the protein;

$$\frac{D}{D_0} = (1-\bar{\alpha}\phi)\,(1-f) \qquad (2.66)$$

where D_0 is D_S for pure solvent, $\bar{\alpha}$ is a geometrical factor which accounts for the shape and orientation of solute molecules ($\bar{\alpha} = 1.5$ for spheres) and f is the ratio of the concentrations of bound and unbound solvent.

Clark et al. [71] have noted that Wang's equation should contain an extra factor of $(1-\phi)$;

$$\frac{D}{D_0} = \frac{1-\bar{\alpha}\phi}{1-\phi}\,(1-f)\ . \qquad (2.67)$$

Using a different approach, Mackie and Meares [72] derived an expression for the mobility of a small molecule in a swollen ion exchange resin membrane which led to the following expression for self diffusion of solvent in a network;

$$\frac{D}{D_0} = \left(\frac{1-\phi}{1+\phi}\right)^2\ . \qquad (2.68)$$

More recently, Jönsson et al. derived an expression for the obstruction effect of colloidal particles which represents an improvement over Wang's equation [73];

$$\frac{D}{D_0} = \frac{1}{1+\phi/2} \cdot \tag{2.69}$$

The hydration effect is also considered in reference [73].

The solvent friction factor for polymer-solvent systems which are near the glass transition temperature can be expected to be dominated by free volume effects. In this case, D is written as

$$D = \frac{k_B T}{\zeta_s} \tag{2.70}$$

with ζ_s being the solvent friction factor. The concentration and temperature dependence of ζ_s can then be described by eqn (2.47).

2.3 Pulsed Gradient Spin Echo NMR

2.3.1 Nuclear Magnetic Resonance

The purpose of this section is to introduce some basic concepts of Nuclear Magnetic Resonance (NMR) and provide a theoretical basis for the interpretation of the experiments discussed in later sections. More detailed information can be found in the classic texts by Abragam [74] and Slichter [75].

When a material is placed in a magnetic field, the resultant magnetization of the material is dominated by electronic contributions because nucleon magnetic moments are negligible in comparison to the magnetic moment of an electron. Therefore, nuclear magnetism is an extremely weak effect and methods which make use of resonance are almost essential if nuclear magnetic phenomena are to be observed.

The main contribution to the nuclear magnetic susceptibility of a nucleus possessing a non-zero value of the nuclear spin, I comes from spin paramagnetism. The hamiltonian operator used in a quantum mechanical description of a single nuclear spin in a magnetic field is therefore

$$\boldsymbol{H_0} = -\gamma\hbar \mathbf{B}_0 \boldsymbol{I} \tag{2.71}$$

where $\boldsymbol{I}$ is the nuclear spin operator and $\mathbf{B}$ is the magnetic field. Assuming that the field is oriented along the z axis ($\mathbf{B} = B_0\,\mathbf{k}$) the hamiltonian becomes

$$\boldsymbol{H_0} = -\gamma\hbar B_0 \boldsymbol{I_z} \tag{2.72}$$

The eigenvalues of $\boldsymbol{H_0}$ are therefore simply the eigenvalues of $\boldsymbol{I_z}$ multiplied by $\gamma\hbar B_0$, i.e. $m\gamma\hbar B_0$, where

$$m = I,\ I-1, \ldots, -I$$

For a spin 1/2 nucleus, I=1/2 and only two energy eigenvalues, $\pm\gamma\hbar B_0/2$ exist, corresponding to the spin up (m = 1/2) and spin down (m = -1/2) states.

A general spin state of a nucleus is represented by a superposition of spin eigenstates

$$|\psi\rangle = \sum_m a_m |m\rangle \tag{2.73}$$

where the a_m are complex amplitudes. The time evolution of $|\psi\rangle$ is found by solving Schrödinger's equation

$$-\frac{\hbar}{i}\frac{\partial}{\partial t}|\psi\rangle = H|\psi\rangle\ . \tag{2.74}$$

When the hamiltonian in (2.74) is the time independent one given by eqn (2.72) the time evolution of $|\psi\rangle$ is given by

$$|\psi(t)\rangle = \exp\left[-\frac{i}{\hbar}H_0\, t\right]\ |\psi(t_0)\rangle\ . \tag{2.75}$$

Equation (2.75) corresponds to a rotation of $|\psi(t_0)\rangle$ about the z axis at an angular frequency of $\omega_0 = \gamma B_0$ which is called the Larmor frequency. Nuclear spin transitions can be selectively induced by irradiating the sample at the resonant frequency $f = \gamma B_0 / 2\pi$, hence the name nuclear magnetic resonance. For values of B_0 and γ commonly encountered, f is in the radiofrequency region of the electromagnetic spectrum.

The state of a macroscopic sample containing many nuclei is conveniently described using the density matrix formalism [76]. Elements of the density matrix may be defined by the following expression using any convenient complete set of basis states;

$$\rho_{mn} = \langle m|\rho|n\rangle$$

$$= \sum_i W_i \langle m|i\rangle\langle i|n\rangle\ . \tag{2.76}$$

Here, ρ is the density operator and W_i is the probability of finding a member of the spin ensemble in the state $|i\rangle$. The ensemble averaged expectation value of an observable $\boldsymbol{A}$ is conveniently represented using the density matrix formalism as

$$\overline{\langle A \rangle} = \mathrm{Tr}\,(\rho A) \tag{2.77}$$

assuming that ρ and the basis states are properly normalized. Note that the trace operation in (2.77) can only be performed after the matrix elements of the product of operators ρA have been evaluated. The population of state i is given by the diagonal element ρ_{ii} of the density matrix. Various other properties of the density matrix are summarized in references [74-77]. The state of an ensemble of spin I nuclei in a magnetic field is completely specified by the density matrix. When the spins are in equilibrium with the field **B**, the density operator is

$$\rho_0 = \exp(-\beta H_0) / Z \tag{2.78}$$

where $\beta = k_B T$, H_0 is given by eqn (2.72) and Z is the partition function defined as

$$Z = \mathrm{Tr}\,[\exp(-\beta H_0)] \ . \tag{2.79}$$

The nuclear magnetization of a spin 1/2 system can be calculated using (2.78) and (2.79) in (2.77) where the observable in (2.77) is the z component of magnetization M_z. Using the high temperature approximation (which is always valid at commonly encountered temperatures) and taking I = 1/2 it is found that at equilibrium, the expectation value of M_z is

$$\begin{aligned} \langle M_z \rangle &= N\gamma\hbar \langle I_z \rangle \\ &= N\gamma\hbar\, \mathrm{Tr}\,(\rho I_z) \\ &= \frac{N(\gamma\hbar)^2 B_0}{4k_B T} \ . \end{aligned} \tag{2.80}$$

The difference between the relative populations of the m = +1/2 and m = -1/2 states for a spin 1/2 system is $2\gamma\hbar B_0/k_B T$, which at room temperature (say 25°C) with B_0 = 1.4 T equals roughly 2×10^{-5} for hydrogen nuclei. This value results from the small value of $\gamma\hbar B_0$ compared to $k_B T$, and justifies the use of the high temperature approximation. For a spin 1/2 system, the magnetization can be thought of as a consequence of the population difference between the m = +1/2 and m = -1/2 states.

In general, an NMR experiment consists of three phases. First, the sample is allowed to achieve equilibrium in the presence of the polarizing field $B_0\mathbf{k}$. Next, a perturbation is applied to the sample, placing the spin system in a non-equilibrium state. This step may include various rf pulses and periods of evolution. Then the response of the spin system is measured. The theoretical description of the time evolution of a spin system will now be considered.

The time evolution of the macroscopic magnetization is often well described by the Bloch equations, which are written in vector form as

$$\frac{\partial \mathbf{M}}{\partial t} = \gamma(\mathbf{M} \times \mathbf{B}) - \frac{M_x \mathbf{i} + M_y \mathbf{j}}{T_2} + \frac{M_0 - M_z}{T_1}\mathbf{k} \,. \tag{2.81}$$

The first term represents the precessional motion of **M** due to the field **B**. The spin-lattice or longitudinal (along the z axis) relaxation time T_1 describes the rate at which the spin system approaches thermal equilibrium with its surroundings. The spin-spin or transverse relaxation time T_2 is related to the rate at which transverse magnetization (i.e. the component of magnetization in the x-y plane) decays. The Bloch equations are not always valid, but they do provide a good description of NMR in liquids. By themselves, they provide only a macroscopic description of the behaviour of **M** in terms of the phenomenological parameters T_1 and T_2. On the other hand, the density matrix description provides a microscopic theory from which the Bloch equations may be derived [75].

The density operator at time t is related to the density operator at time 0 by the Liouville-von Neumann equation [77]

$$\frac{\partial}{\partial t}\rho = -\frac{i}{\hbar}[H,\rho] \tag{2.82}$$

which has the formal solution

$$\rho(t) = U(t)\,\rho(0)\,U^{-1}(t) \,. \tag{2.83}$$

The evolution operator $U(t)$ is given by

$$U(t) = T \exp\left(-\frac{i}{\hbar}\int_0^t H(t)\,dt\right) \tag{2.84}$$

where T is the time ordering operator [77]. Provided that the hamiltonian H is known during the evolution of the density operator, the expectation value of any observable at time t can then be calculated.

The effect of rf pulses on the state of the spin system is described mathematically by rotation operators acting on the density matrix. An rf field oscillating along the y axis applied for time t_w corresponds to the rotation operator

$$R_y = \exp(-i\gamma B_1 t_w) \tag{2.85}$$

where B_1 is the amplitude of the rf field. If the quantity $\gamma B_1 t_w$ is interpreted as an angle, it is clear that rotations of $\pi/2$ and π may be achieved by adjusting the value of t_w.

2.3.2 Spin Echoes

Consider an experiment using the pulse sequence shown in Fig. 2.4. At time t = 0 a $\pi/2$ pulse is applied, creating a detectable magnetization in the x-y plane. Due to spin-spin relaxation and field inhomogeneity, the signal decays. This signal is called a free induction decay (FID).

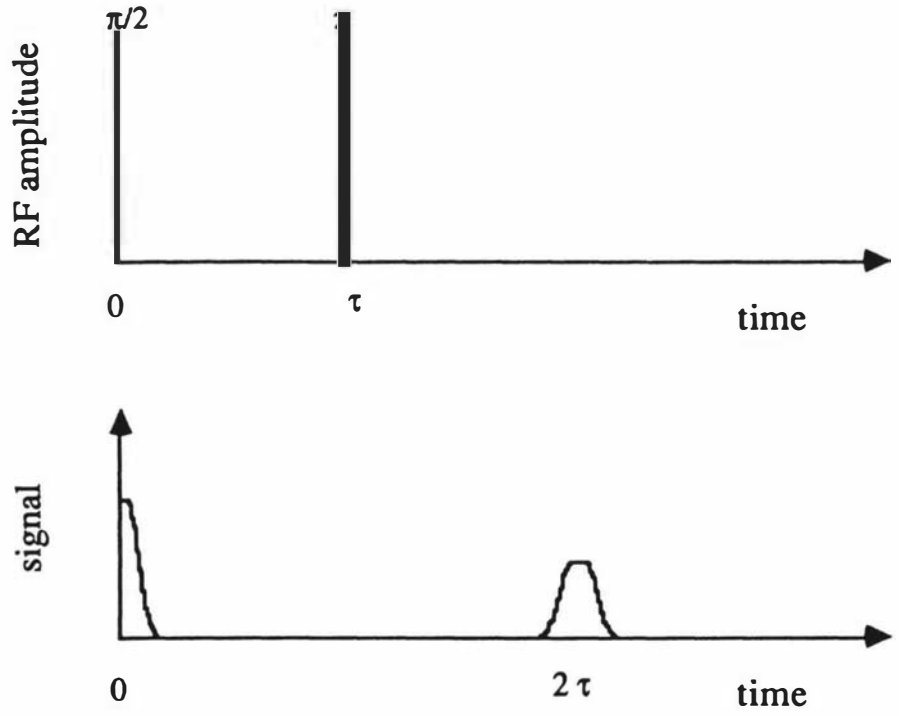

Figure 2.4 Production of a spin echo by a $\pi/2$–τ–π rf pulse sequence. The signal is detected in the x-y plane, perpendicular to the direction of the main field B_0.

The effect of a $\pi/2$ pulse on the populations of the m = +1/2 and m = -1/2 states for a spin 1/2 system can be calculated by using eqn (2.85) with $\gamma B_1 t_w = \pi/2$ in eqn (2.83). The result [77] is that for both m = +1/2 and m = -1/2 the populations are 1/2 immediately after the $\pi/2$ pulse. There is no macroscopic magnetization in the z direction immediately after the pulse, but due to T_1 relaxation the z magnetization subsequently returns to its equilibrium value.

The equations of motion for the x and y components of the macroscopic magnetization can be derived using eqn (2.83) and eqn (2.77) with M_x and M_y as the observables. The result shows that **M** precesses in the x-y plane (neglecting the slow T_1 relaxation) at the Larmor

frequency. However, if the field $B_0\mathbf{k}$ is not perfectly uniform the Larmor frequency will vary in space. The sample can be divided into regions in which the variation of B_0 is negligible. Each of these has a Larmor frequency ω_n and a group of spins which all have the same value of ω_n is called an isochromatic group. In a frame of reference rotating at the mean Larmor frequency, the magnetization vectors of some isochromatic groups will lag behind and others will move ahead of the mean. At time $t = \tau$, a π pulse is applied which reverses the dephasing effect of the field inhomogeneity (provided that the spins do not move from one isochromatic group to another) and a spin echo appears. The signal is attenuated because the effects of spin-spin interactions are not reversed by the π pulse. The echo attenuation can be written as

$$A(2\tau) / A(0) = \exp(-2\tau / T_2) \tag{2.86}$$

where T_2 is the spin-spin relaxation time.

The sequence $\pi/2$ (FID) - τ - π - 2τ (echo) is useful for measuring the spin-spin relaxation time because the effects of field inhomogeneity are nullified.

Lenk [77] gives a derivation in the density matrix formalism of the effect of the pulse sequence shown in Fig. 2.4. The signal, V(t) is proportional to $\mathrm{Tr}(\rho I_+)$ where $I_+ = I_x + iI_y$. The complete expression for V(t) is

$$V(t) = \mathrm{Tr}(\rho I_+) = \mathrm{Tr}(U_{tot}\, \rho(-\infty)\, U_{tot}^{\dagger}\, I_+) \tag{2.87}$$

where

$$Utot = T_2\, R_2\, T_1\, R_1$$

is the ordered product of operators for the $\pi/2$ rotation (R_1), the first period of time evolution (T_1), the π rotation (R_2) and the second period of time evolution (T_2). When the explicit forms of the operators are inserted into eqn (2.87) it is found that V(t) has a maximum value at $t = 2\tau$, when the echo appears.

2.3.3 The Effect of Gradient Pulses

It was mentioned in the previous section that the dephasing effect of field inhomogeneity can be nullified by the spin echo technique provided that the spins do not move from one isochromatic group to another during the experiment. In reality this effect is always present in liquid samples, although it may be neglected if the field inhomogeneity is small enough. On the other hand, it suggests a method of measuring diffusion.

In this section, the Pulsed Gradient Spin Echo (PGSE) method of measuring diffusion will be discussed.

Whereas early measurements of diffusion by NMR used steady field gradients to provide the field inhomogeneity, pulsed field gradients have been used increasingly in modern work. Another important point is that Fourier transform spectroscopy is now standard. Fourier transform spectroscopy offers the advantage that the area of a peak in the frequency domain is equal to the contribution made by the species corresponding to that peak to the time domain echo amplitude. This means that the diffusion coefficients of species having different chemical shifts can be measured separately. When echo amplitude is mentioned, remember that it is the peak area in the frequency domain that is actually measured.

Stejskal and Tanner proposed the PGSE method of measuring diffusion in 1965 [78, 79]. The PGSE technique has two important advantages over the steady gradient technique. Since the gradient is absent during detection of the signal, there is no loss of resolution in the spectrum and a narrow spectral range is covered resulting in a higher signal to noise ratio. Also, the timescale over which motion is detected is a well defined quantity. Stejskal and Tanner described the PGSE experiment theoretically using the Bloch equations as modified by Torrey to include the effects of diffusion and flow. Here, it is assumed that there is no bulk flow in the sample. In vector form the Bloch Torrey equations are

$$\frac{\partial \mathbf{M}}{\partial t} = \gamma(\mathbf{M} \times \mathrm{B}) - \frac{M_x\mathbf{i} + M_y\mathbf{j}}{T_2} + \frac{M_0 - M_z}{T_1}\mathbf{k} + \nabla \cdot \mathbf{D} \cdot \nabla \mathbf{M} \qquad (2.88)$$

where **D** is the diffusion tensor, allowing for anisotropic diffusion. This approach is based on the use of purely macroscopic quantities.

The PGSE pulse sequence is shown in Figure 2.5. The result of Stejskal and Tanner's analysis of the PGSE experiment is an equation for the echo amplitude;

$$A(2\tau,G) = A_0 \exp(-2\tau/T_2) \exp[-D_s\gamma^2G^2\delta^2(\Delta-\delta/3)] \qquad (2.89)$$

where G is the magnitude of the applied magnetic field gradient. This equation is often used in a normalized form to remove T_2 effects;

$$A(G)/A(0) = \exp[-D_s\gamma^2G^2\delta^2(\Delta-\delta/3)]\,. \qquad (2.90)$$

When the value of δ is small (i.e. in the narrow pulse limit), the diffusion time is Δ and a PGSE experiment is analogous to an incoherent scattering experiment at scattering vector $\mathbf{q} = \gamma\delta\mathbf{G}$. When δ is not small, the effective diffusion time is $\Delta_r = \Delta - \delta/3$.

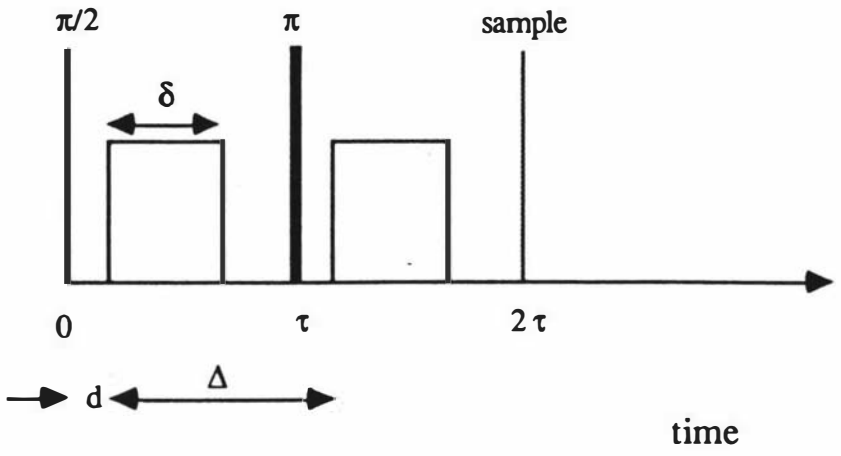

Figure 2.5 The pulsed gradient spin echo NMR pulse sequence. The magnetic field gradient pulses have width δ and separation Δ. Usually, Δ is set equal to τ. Sampling of the spin echo signal begins at time 2τ (compare with Fig. 2.4).

Stepisnik [81] has formulated a theory of the PGSE experiment using density matrix methods which allows a direct microscopic interpretation to be applied to the theory. A brief outline of Stepisnik's approach will now be given. The hamiltonian including all interactions which occur during the experiment is

$$H(t) = H_0 + H_G + H_{rf} + H_L \tag{2.91}$$

where H_0 describes the effect of B_0, H_G describes the effect of the gradient field, H_{rf} describes the effect of the rf pulses and H_L includes all other interactions.

The spin echo amplitude is proportional to

$$\langle I_x(2\tau)\rangle = \mathrm{Tr}\,(\rho(2\tau)I_x) \tag{2.92}$$

with

$$\rho(2\tau) = U(t)\,\rho(0)\,U^{-1}(t)\ . \tag{2.93}$$

In the high temperature approximation the equilibrium density matrix $\rho(0)$ is given by

$$\rho(0) = \mathbf{1} - \beta\omega_0 I_z \tag{2.94}$$

and $U(t)$ is given by eqn (2.84). Stepisnik's approach is to simplify the calculation of $\rho(t)$ by successive transformations of $\rho(0)$ into different interaction representations. The result shows that the effect of diffusion is to produce an echo attenuation given by exp $[-\beta(t)]$with

$$\beta(t) = \frac{\gamma^2}{2\pi} \int_{-\infty}^{\infty} C_{xx}(\omega)\, S(\omega,t)\, d\omega \tag{2.95}$$

where

$$C_{xx}(\omega) = \frac{1}{2} \int_{-\infty}^{\infty} C_{xx}(t)\, e^{i\omega t}\, d\omega \quad . \tag{2.96}$$

Here, x is the direction of the magnetic field gradient, $C_{xx}(t)$ is the velocity autocorrelation function defined as

$$C_{xx}(t) = \langle\, v_{ix}(0)\, v_{ix}(t)\, \rangle$$

and v_{ix} is the x component of the velocity of nucleus i. The spectrum of the magnetic field gradient is defined as

$$S(\omega,t) = \frac{|G(\omega,t)|^2}{\omega^2} \tag{2.97}$$

where

$$G(\omega,t) = \int_0^t G_{eff}(t')\, e^{i\omega t'}\, dt' \quad . \tag{2.98}$$

For mathematical convenience, Stepisnik defines the effective magnetic field gradient G_{eff} as

$$G_{eff} = \begin{cases} G(t) & 0 < t < \tau \\ -G(t) & t > \tau \end{cases} \quad . \tag{2.99}$$

The velocity autocorrelation function is related to D_s by the well known relation eqn (2.32) which is equivalent to eqn (2.96) with $\omega = 0$ and $C_{xx}(0) = D_s$.

The explicit form of $S(\omega,t)$ for the usual PGSE pulse sequence (Fig. 2.5) is

$$S(\omega,t) = \frac{4G}{\omega^2}\left(\sin\frac{\omega\delta}{2}\sin\frac{\omega\Delta}{2}\right)^2 \tag{2.100}$$

where it has been assumed that $\Delta = \tau$.

Equation (2.95) indicates that if $C(\omega)$ remains near its value at zero frequency ($C(0) = D_s$) while $S(\omega,t)$ is large, the following expression for $\beta(t)$ is valid;

$$\beta(t) = \frac{8\gamma^2G^2D_s}{\pi} \int_{-\infty}^{\infty} \omega^{-4} \left(\sin\frac{\omega\delta}{2} \sin\frac{\omega\Delta}{2}\right)^2 d\omega \ . \tag{2.101}$$

Making the substitutions

$$a = \frac{\Delta+\delta}{2} \ , \tag{2.102}$$

$$b = \frac{\Delta-\delta}{2} \tag{2.103}$$

and applying some trigonometric identities, it is found that

$$\beta(t) = \frac{2\gamma^2G^2D_s}{\pi} \int_{-\infty}^{\infty} \omega^{-4} \left(\cos^2a\omega + \cos^2b\omega - 2\cos a\omega \cos b\omega\right) d\omega \tag{2.104}$$

which can be simplified using integration by parts and standard integrals to give

$$\beta(t) = D_s\gamma^2G^2\delta^2(\Delta-\delta/3) \tag{2.105}$$

in agreement with (2.90).

Several other cases can be investigated with the help of eqn (2.95). When $C(\omega)$ is not constant over the range of $S(\omega,t)$, (i.e. D_s effectively varies with time) a simple result for $\beta(t)$ is available in the narrow pulse approximation (δ small). Assuming that $G_{eff}(t)$ consists of a pair of Dirac delta functions (normalized so that each has area $G\delta$) it is straightforward to show that

$$\beta = \frac{\gamma^2G^2\delta^2}{2}(\Delta x)^2 \tag{2.106}$$

where $(\Delta x)^2$ is the x component of the mean square displacement during time Δ. The derivation of eqn (2.106) is given in Appendix 5. The same result can be obtained by other methods [80]. In the long time limit $(\Delta x)^2 = D_s\Delta$ and the narrow pulse approximation to eqn (2.105) agrees with eqn (2.106).

The question arises as to how the measurement of $(\Delta x)^2$ would be affected by the use of finite width pulses. The general form of $\beta(t)$ when $C(\omega)$ is not constant is

$$\beta(t) = \frac{\gamma^2 G^2}{2}\left(\frac{1}{2}I(2\alpha) + \frac{1}{2}I(2\beta) - I(\Delta) - I(\delta)\right) \qquad (2.107)$$

where

$$I(t) = \int_0^t \int_0^t \langle|\Delta x(t_2-t_1)|^2\rangle\, dt_1 dt_2 \ . \qquad (2.108)$$

In the case where D_s is independent of time, it is given by

$$D_s = \frac{\langle|\Delta x(t_2-t_1)|^2\rangle}{2(t_2-t_1)}$$

and eqn (2.107) is reduced to the usual Stejskal-Tanner relation, eqn (2.105). Otherwise, it seems that the usual PGSE pulse sequence will not allow a straightforward measurement of a nonlinearly increasing mean square displacement except in the narrow pulse limit. Stepisnik [81] has discussed the measurement of $(\Delta x)^2$ from a different point of view. If a gradient pulse sequence including an oscillating gradient (square wave or sinusoidal) is used $\beta(t)$ contains a term in $C(\omega_m)$ where ω_m is the gradient modulation frequency, as well as the $C(0) = D_s$ term. Therefore, by varying ω_m, a plot of $C(\omega_m)$ could be obtained, the Fourier transform taken, giving C(t) and the mean square displacement found by integrating C(t).

2.3.4 PGSE and Polymer Solutions

Several details of PGSE experiments specific to polymer solutions will be considered in this section.

Polydispersity must be considered in any experiments involving polymers. For a dilute, monodisperse polymer solution, the echo amplitude corresponding to a given peak in the spectrum is

$$A(G) = A_0 \exp(-2\tau/T_2) \exp[-\gamma^2 G^2 \delta^2 D_s(\Delta - \delta/3)] \ .$$

If the polymer is polydisperse and the solution is dilute, A(G) will consist of a weighted sum over the molecular weight distribution. (Note that polydispersity does not affect the chemical shift). The signal resulting from polymers of molar mass M_i is proportional to $n_i M_i$ where n_i is the number of molecules in the sample having molar mass M_i. In terms of a continuous distribution this is M n(M) dM so

$$A(G) = \frac{1}{F}\int_0^\infty A(G,M)\ M\ n(M)\ dM \qquad (2.109)$$

where

$$F = \int_0^\infty M\, n(M)\, dM \tag{2.110}$$

is required for normalization and

$$A(G,M) = A_0 \exp(-2\tau/T_2(M)) \exp[-\gamma^2 G^2 \delta^2 D_s(M) (\Delta - \delta/3)] \ . \tag{2.111}$$

If T_2 is independent of molar mass as was found by Callaghan and Pinder for polystyrene in carbon tetrachloride [82] this becomes

$$\frac{A(k)}{A(0)} = \frac{1}{F}\int_0^\infty \exp[-kD_s(M)]\, M\, n(M)\, dM \tag{2.112}$$

if

$$A(0) = A_0 \exp(-2\tau/T_2)$$

and

$$k = \gamma^2 G^2 \delta^2 (\Delta - \delta/3) \ .$$

The analysis of PGSE NMR data on polydisperse polymer samples is very similar to the polydispersity problem in dynamic light scattering and similar solutions have been applied. Two approaches to the analysis of PGSE NMR data have been suggested in the literature. One is to assume a form for n(M) and fit eqn (2.112) (or a discrete approximation) to the data [84]. The other is to fit ln[A(k)/A(0)] with a power series to obtain the weight averaged diffusion coefficient, the higher order terms giving the higher order moments of the distribution of diffusion coefficients [83]. The echo attenuation is

$$\frac{A(k)}{A(0)} = \frac{1}{F}\exp(-k\langle D\rangle_w)\int_0^\infty \exp[-k\,(D-\langle D\rangle_w)]\, M\, n(M)\, dM \ . \tag{2.113}$$

The signal from molecules with molar masses in the interval M to M+dM can be written as $M\, n(M)\, dM = G(D)\, dD$. Making this substitution, expanding the exponential factor in the integral and then using the approximation $\ln(1+x) \approx x$ the result to second order in k is [83]

$$\ln[A(k)/A(0)] = -k\langle D\rangle_w + \frac{k^2}{2}(\langle D^2\rangle_w - \langle D\rangle_w^2) \tag{2.114}$$

where $\langle D\rangle_w$ designates the weight averaged D_s, given by

$$\langle D\rangle_w = \frac{1}{F}\int_0^\infty D\ M\ n(M)\ dM \quad .$$

The second order term contains information about polydispersity. It is possible to relate the second order term directly to M_w/M_n by assuming a form for the molar mass distribution. The normalized log normal (Lansing-Kraemer) distribution for the weight fraction is given by [85]

$$W(M) = \frac{\exp(-\beta^2/4)}{\beta M_0 \pi^{1/2}} \exp[-(\ln^2 M/M_0)/\beta^2] \qquad (2.115)$$

where M_0 and β are related to the weight average molar mass M_w and polydispersity M_w/M_n by

$$M_w = M_0 \exp(-3\beta^2/4) \qquad (2.116)$$

and

$$M_w/M_n = \exp(\beta^2/2)\ . \qquad (2.117)$$

Assuming that $D - M^\alpha$ and using

$$\langle D^n\rangle_w = D^n(M_0) \exp[\beta^2 \alpha n(\alpha n+2)/4] \qquad (2.118)$$

the result is

$$\langle D^2\rangle_w - \langle D\rangle_w^2 = \langle D\rangle_w^2[(M_w/M_n)^{\alpha^2} - 1] \quad . \qquad (2.119)$$

If $\langle D\rangle_w$ obtained from measurements on polydisperse fractions is to be plotted against molar mass, an appropriate measure of the average molar mass M_{Dw} must be defined. The correct expression for the average molar mass corresponding to a value of $\langle D\rangle_w$ can be derived in the same way as has been done for the z-average diffusion coefficient obtained from dynamic light scattering [138]. The weight averaged diffusion coefficient is given by

$$\langle D\rangle_w = \frac{\sum N_i D_i M_i}{\sum N_i M_i} = a(M_{Dw})^{-\alpha} \qquad (2.120)$$

so that

$$M_{Dw} = \left(\frac{\sum N_i M_i}{\sum N_i M_i^{\,1-\alpha}}\right)^{1/\alpha} \quad . \qquad (2.121)$$

Another point of particular interest in discussing PGSE experiments on polymer solutions is the time scale over which diffusion is measured [86]. The effective diffusion time in a PGSE experiment is $\Delta_r = \Delta - \delta/3$. In an entangled polymer solution, the motion of a polymer molecule is constrained to motion within a tube according to the reptation model. For times Δ_r less than the reptation time T_r, the mean square displacement is expected to be nonlinear in time. Under favourable circumstances, this effect might be measurable using PGSE NMR.

2.4 Dynamic Light Scattering

2.4.1 The Dynamic Structure Factor

The theory of Dynamic Light Scattering (DLS) is discussed in detail in the excellent book by Berne and Pecora [87] and in several excellent collections of lectures and conference proceedings [26, 88-91]. A review by Pusey and Vaughan [92] provides a particularly clear introduction to the field. Here, a brief review is given to provide an introduction to the discussion of recent developments which follows.

Consider the scattering geometry shown in Figure 2.6. The light which is incident on the sample has an electric field vector of the form

$$\mathbf{E}_i(r,t) = \mathbf{n}_i E_0 \exp[i(\mathbf{k}_i.\mathbf{r} - \omega_i t)] \qquad (2.122)$$

where $\mathbf{n}_i$ is a unit vector in the direction of the incident field.

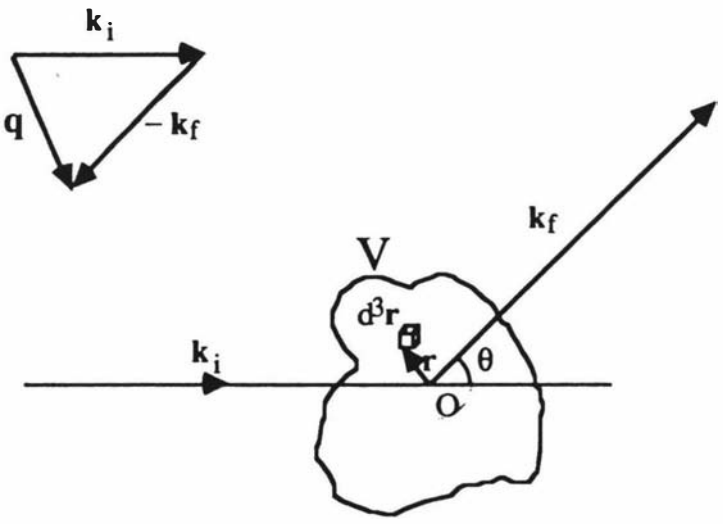

Figure 2.6 Scattering geometry in a dynamic light scattering experiment. The scattering vector $\mathbf{q}$ is obtained by the subtraction of $\mathbf{k}_f$ from $\mathbf{k}_i$.

The instantaneous electric field at a point on the detector can be represented as the sum of the electric fields due to scattering from small volume elements within the scattering volume V. The scattering medium can be characterized by a local dielectric constant which varies in space and time. The local value of ε can be written as the mean value plus a fluctuation;

$$\varepsilon(\mathbf{r},t) = \varepsilon_0 + \delta\varepsilon \ .$$

Berne and Pecora show that the scattered field detected at a distance R from the sample ($|\mathbf{R}| >> |\mathbf{r}| >> \lambda$) is

$$E_s(R,t) = \frac{E_0}{4\pi R\varepsilon_0}\exp(ik_fR) \int d^3r \exp[i(\mathbf{q}.\mathbf{r}-\omega_i t)]\{\mathbf{n}_f.[\mathbf{k}_f\times(\mathbf{k}_f\times(\delta\varepsilon(r,t).\mathbf{n}_i))]\} \quad (2.123)$$

where $\mathbf{q} = \mathbf{k}_i - \mathbf{k}_f$. If it is assumed that $|\mathbf{k}_i| \cong |\mathbf{k}_f|$ the magnitude of the scattering vector $\mathbf{q}$ is given by

$$q = \frac{4\pi n}{\lambda_i} \sin(\theta/2) \quad (2.124)$$

where n is the refractive index of the sample and θ is the scattering angle (see Fig. 2.6).

Equation (2.123) can be written in terms of the spatial Fourier transform of the fluctuation in the dielectric constant

$$\delta\varepsilon(\mathbf{q},t) = \int d^3r \exp(i\mathbf{q}.\mathbf{r})\ \delta\varepsilon(\mathbf{r},t) \quad (2.125)$$

showing that q can be interpreted as a spatial frequency. In terms of $\delta\varepsilon(\mathbf{q},t)$ the scattered field is

$$E_s(R,t) = \frac{E_0}{4\pi R\varepsilon_0}\exp[i(k_fR-\omega_t t)]\ \{\mathbf{n}_f.[\mathbf{k}_f\times(\mathbf{k}_f\times(\delta\varepsilon(\mathbf{q},t).\mathbf{n}_i))]\} \quad (2.126)$$

The cross products can be simplified to

$$\delta\varepsilon_{if} = \mathbf{n}_f.\delta\varepsilon(\mathbf{q},t).\mathbf{n}_i \quad (2.127)$$

giving the result

$$E_s(R,t) = \frac{-E_0k_f^2}{4\pi R\varepsilon_0}\exp[i(k_fR-\omega_t t)]\ \delta\varepsilon_{if}(\mathbf{q},t) \ . \quad (2.128)$$

The time dependence of the dielectric constant fluctuations can be studied by measuring the electric field autocorrelation function, written in normalized form as

$$g^{(1)}(\tau) = \frac{\langle E_s^*(R,0)\, E_s(r,\tau)\rangle}{\langle |E_s|^2\rangle} \tag{2.129}$$

$$= \langle \delta\varepsilon_{if}^*(q,0)\, \delta\varepsilon_{if}(q,\tau)\rangle \exp(-i\omega_i\tau)\,. \tag{2.130}$$

To make a connection between molecular properties and light scattering measurements it is convenient to introduce the assumption that the light is scattered from particles and that the dielectric constant fluctuations are due solely to fluctuations in the number density of particles. The fluctuation in the polarizability density can be written as

$$\delta\alpha_{if}(r,t) = \sum_{j=1}^{N} \alpha_{if}^{j}(t)\, \delta(\mathbf{r}-\mathbf{r}_j(t)) \tag{2.131}$$

where $\alpha_{if} = \mathbf{n}_i.\alpha.\mathbf{n}_f$ is the component of the polarizability tensor defined by the incident and detected polarizations. The spatial Fourier transform of the polarizability fluctuation is

$$\delta\alpha_{if}(\mathbf{q},t) = \sum_{j=1}^{N} \alpha_{if}^{j} \exp[i\mathbf{q}\cdot\mathbf{r}_j(t)] \tag{2.132}$$

so the field autocorrelation function can be written as

$$g^{(1)}(\tau) = \frac{\langle \delta\alpha_{if}^*(\mathbf{q},0)\, \delta\alpha_{if}(\mathbf{q},\tau)\rangle}{\langle |\delta\alpha_{if}(\mathbf{q})|^2\rangle}\,. \tag{2.133}$$

If all the particles have the same polarizability α_{if}^{j}, $g^{(1)}(\tau)$ can be written as

$$g^{(1)}(\tau) = \frac{S(\mathbf{q},\tau)}{S(\mathbf{q})} \exp(-i\omega_i\tau) \tag{2.134}$$

where $S(\mathbf{q},\tau)$ is the dynamic structure factor;

$$S(\mathbf{q},\tau) = \frac{1}{N}\sum_{i=1}^{N}\sum_{j=1}^{N} \langle \exp[i\mathbf{q}\cdot(\mathbf{r}_i(\tau)-\mathbf{r}_j(0)] \rangle \tag{2.135}$$

and $S(\mathbf{q}) = S(\mathbf{q},0)$ is the static structure factor. Simplifications of eqn (2.135) can be made when a dilute solution of small, non-interacting polymer molecules is considered. By

small, it is meant that each molecule can be considered to act as a Rayleigh scatterer (i.e. $qR_G \leq 1$) and intramolecular interference effects are negligible. Then a single exponential decay is found;

$$|g^{(1)}(\tau)| = \exp(-D_0 q^2 \tau) \tag{2.136}$$

where D_0 is the infinite dilution diffusion coefficient.

For large, non-interacting polymer molecules, the summation in eqn (2.135) must be performed over all of the segments (in a single molecule, since the cross terms between segments from different molecules vanish for non-interacting systems) and $P(\mathbf{q}) = S(\mathbf{q})$ for a single molecule is called the particle form factor.

Eqn (2.136) can easily be generalized to the case of a dilute polydisperse solution. The field autocorrelation function becomes a weighted sum of exponentials

$$|g^{(1)}(\tau)| = \int_0^\infty G(\Gamma)\, e^{-\Gamma\tau}\, d\Gamma \tag{2.137}$$

where $\Gamma = D_0 q^2$ and

$$G(\Gamma)\, d\Gamma \propto P(\mathbf{q},M)\, \alpha^2\, n(M)\, dM$$

is the fraction of the scattered intensity scattered due to particles having decay rates in the range Γ to $\Gamma+d\Gamma$.

The molecular polarizability can be written in terms of the polarizability per unit mass (which is constant) as

$$\alpha \propto \alpha_m\, M$$

so that

$$G(\Gamma)\, d\Gamma \propto P(\mathbf{q},M)\, M^2\, n(M)\, dM\ . \tag{2.138}$$

Koppel [93] and Pusey [94] have shown that $\ln|g^{(1)}(\tau)|$ can be represented as a power series (called the cumulant expansion)

$$\ln|g^{(1)}(\tau)| = -\langle\Gamma\rangle\tau + \frac{1}{2}\frac{\mu_2}{\langle\Gamma\rangle^2}\langle\Gamma\rangle^2\tau^2 - \frac{1}{3!}\frac{\mu_3}{\langle\Gamma\rangle^3}\langle\Gamma\rangle^3\tau^3 + \frac{1}{4!}\frac{\mu_4 - 3\mu_2^2}{\langle\Gamma\rangle^4}\langle\Gamma\rangle^4\tau^4 + \ldots \tag{2.139}$$

with

$$\langle\Gamma\rangle = \int_0^\infty \Gamma\, G(\Gamma)\, d\Gamma \tag{2.140}$$

and

$$\mu_n = \int_0^\infty (\Gamma - \langle\Gamma\rangle)^n\, G(\Gamma)\, d\Gamma \ . \tag{2.141}$$

Therefore $\langle D\rangle = \langle\Gamma\rangle / q^2$ can be extracted and takes the form

$$\langle D\rangle = \frac{1}{q^2}\int_0^\infty \Gamma\, G(\Gamma)\, d\Gamma$$

$$= \frac{\int_0^\infty D(M)\, M^2\, n(M)\, P(q,M)\, dM}{\int_0^\infty M^2\, n(M)\, dM} \ . \tag{2.142}$$

When $P(q,M) = 1$ for all species (this can always be satisfied by taking measurements at small enough values of q) the z-average diffusion coefficient $\langle D\rangle_z$ is obtained from the initial slope [95].

Many methods of extracting information about polydispersity from DLS data have been proposed. A survey of this subject has recently been given in the review by Bloomfield in [26].

2.4.2 Dynamic Regimes

For dilute solutions of polymers, the neglect of correlations between segments from different molecules leads to the simplification of eqn (2.135). Additionally, when the condition $qR_G < 1$ is satisfied, only the motions of the centres of mass of the molecules need be considered and further simplification is achieved. In semidilute solutions, correlations between segments from different molecules cannot be neglected so that the summations in $S(q,\tau)$ must be performed over all segments. By writing eqn (2.133) in terms of fluctuations in the Fourier components of the number density of segments, de Gennes was able to derive an expression for $S(q,\tau)$ for a polymer in a good solvent; [7, 35]

$$S(q,\tau) = \exp(-D_c q^2 \tau) \tag{2.143}$$

where D_c is the cooperative diffusion coefficient.

De Gennes [35] defined several different dynamic regimes in the qR_G vs ϕ/ϕ^* plane (Fig. 2.7) which are useful in a discussion of DLS applied to a solution of a polymer in a good solvent [41].

In region 1 the polymer molecules are independent and interactions between segments from different molecules are absent. The polymer molecules can be treated as independent spherical particles when $qR_G < 1$ and $\phi/\phi^* < 1$ so that $S(\mathbf{q},\tau)$ is given by eqn (2.33). In the virial regime, it is adequate to replace D_0 by D evaluated using eqn (2.38). When $qR_G > 1$ and $\phi < \phi^*$, internal relaxations within a polymer molecule may be measured. Pecora [87] proposed that $S(\mathbf{q},\tau)$ could be resolved as a sum of exponentials but experimental studies have shown that this procedure is very difficult. An alternative approach of fitting $S(\mathbf{q},\tau)$ with a theoretical shape function has been proposed by Akcasu [96].

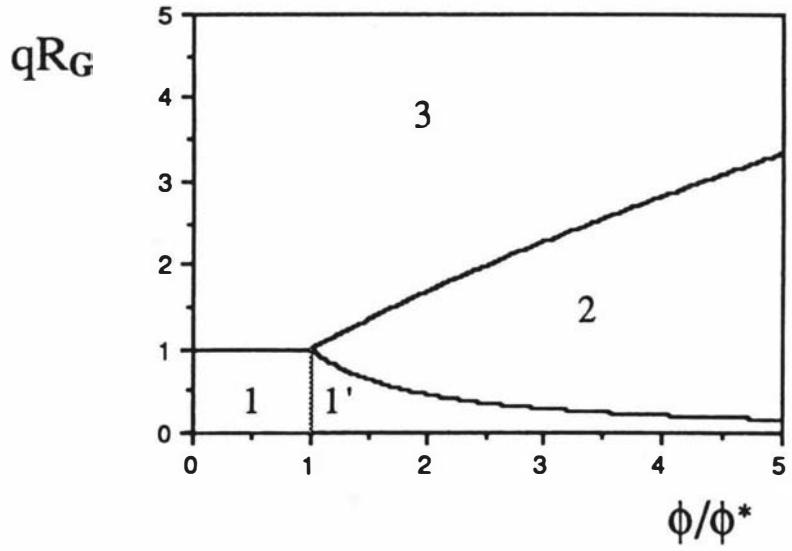

Figure 2.7 Dynamic regimes for the coherent dynamic structure factor. 1: the dilute small q region; 1': the semidilute small q region; 2: the pseudogel region; 3: the internal modes region.

For concentrations $\phi > \phi^*$, a solution of a polymer in a good solvent can be viewed as a transient network and in region 2, $S(\mathbf{q},\tau)$ is given by eqn (2.143) with D_c representing the "pseudo gel" cooperative diffusion coefficient. When the distance between contact points ξ is less than $2\pi/q$, region 3 is entered. The transient network model is only valid for high

frequency fluctuations (i.e. at small values of τ). In terms of the reptation time τ_R, the condition

$$\tau = D_c^{-1} q^{-2} \leq \tau_R$$

must be satisfied, giving the equation for the line $q_{min}R_G$ in Fig. 2.7. Provided that no slow structural relaxations occur, eqn (2.143) can be expected to hold in region 1' with $D_c = D_m$ in regions 1' and 2.

The situation becomes more complicated when theta solvent systems are considered. Although the division of the qR_G - ϕ/ϕ^* plane into regions is expected to be similar to that for good solvent systems, the form of $S(\mathbf{q},\tau)$ is made more complicated by the tendency of polymers in a theta solvent to self-entangle [45].

2.4.3 Scattering from Ternary Solutions

Dynamic light scattering experiments on ternary (polymer-polymer-solvent) systems are featured in this work. Here, the theoretical form of $S(\mathbf{q},\tau)$ for ternary polymer solutions will be discussed.

The dynamic scattering from ternary solutions in the dilute solution case is simply a special case of the polydispersity problem discussed in section 2.4.1. The extension to concentrations in the virial regime (but still below ϕ^*) can be made by analogy with the situation for spheres, because it is valid to approximate polymer molecules by spheres in the virial regime. The dynamic structure factor for scattering from a system consisting of a solvent and two different spherical solutes was considered by Phillies in 1974 [97]. He found that $S(\mathbf{q},\tau)$ consisted of a sum of two exponentials having decay rates not simply related to the diffusion coefficient of either of the solutes. This problem was also considered by Pusey, Fijnaut and Vrij [98], who were able to calculate the mode amplitudes using the hard sphere model. Their treatment will now be summarized.

When the time dependent part of eqn (2.133) is rewritten in terms of fluctuations in the refractive index $\delta n(q,t)$, the result is

$$S(\mathbf{q},\tau) \propto \langle\, \delta n(-\mathbf{q},0)\, \delta n(\mathbf{q},\tau)\, \rangle \qquad (2.144)$$

where the right hand side is the spatial Fourier transform of the space-time correlation function for refractive index fluctuations, $\langle \delta n(0,0)\, \delta n(\mathbf{r},\tau) \rangle$.

The space-time correlation function for refractive index fluctuations can be written in terms of the correlation function for number density fluctuations by the following procedure.

Number density fluctuations can be assumed to decay according to the linear laws analogous to eqn (2.25);

$$\frac{\partial}{\partial t}\delta\rho_1(\mathbf{r},t) = D_{11}\nabla^2\delta\rho_1(\mathbf{r},t) + D_{12}\nabla^2\delta\rho_2(\mathbf{r},t) \tag{2.145}$$

$$\frac{\partial}{\partial t}\delta\rho_2(\mathbf{r},t) = D_{21}\nabla^2\delta\rho_1(\mathbf{r},t) + D_{22}\nabla^2\delta\rho_2(\mathbf{r},t)\ . \tag{2.146}$$

The matrix of diffusion coefficients can be diagonalized, yielding two uncorrelated modes

$$\delta\rho_+ = \alpha_+\delta\rho_1 + \delta\rho_2 \tag{2.147}$$

$$\delta\rho_- = \alpha_-\delta\rho_1 + \delta\rho_2 \tag{2.148}$$

which decay as

$$\frac{\partial}{\partial t}\delta\rho_+(\mathbf{r},t) = D_+\nabla^2\delta\rho_+ \tag{2.149}$$

$$\frac{\partial}{\partial t}\delta\rho_-(\mathbf{r},t) = D_-\nabla^2\delta\rho_-\ . \tag{2.150}$$

The values of $\alpha_\pm$ and $D_\pm$ are determined by

$$\alpha_\pm = \frac{(D_{11}-D_{22})\pm[(D_{11}-D_{22})^2 + 4D_{12}D_{21}]^{1/2}}{2D_{12}} \tag{2.151}$$

and

$$D_\pm = \tfrac{1}{2}(D_{11}-D_{22})^2 \pm \tfrac{1}{2}[(D_{11}-D_{22})^2 + 4D_{12}D_{21}]^{1/2}\ . \tag{2.152}$$

Ignoring constants which are later normalized out, the refractive index fluctuations are related to the density fluctuations by

$$\delta n(\mathbf{r},t) = f_1\,\delta\rho_1(\mathbf{r},t) + f_2\delta\rho_2(\mathbf{r},t) \tag{2.153}$$

where f_1 and f_2 are scattering amplitudes. Substitution of eqns (2.147) and (2.148) into (2.153), followed by formation of the correlation function and then Fourier transformation leads to an expression for $S(\mathbf{q},\tau)$ (see eqn (2.144)). The final form of $S(\mathbf{q},\tau)$ is

$$S(\mathbf{q},\tau) = A_+\exp(-D_+\,q^2\tau) + A_-\exp(-D_-q^2\tau)\ . \tag{2.154}$$

The diffusion coefficients D_+ and D_- represent the rates of decay of two different types of density fluctuation. The + mode can be interpreted as a compression-dilation or collective mode, with the relative concentrations fixed ($\delta\rho_1/\rho_1 = \delta\rho_2/\rho_2$). The – mode can be interpreted as an exchange of species at fixed total number density (i.e. $\delta\rho_1 + \delta\rho_2 = 0$).

The scattering from polymer-polymer-solvent systems was considered by Hanley, Balloge and Tirrell [99] who obtained the same general form as eqn (2.154) but did not make any detailed theoretical predictions.

There have been two recent publications dealing with the theory of DLS experiments on ternary systems. Benmouna et al. [100] found two relaxation modes in $S(\mathbf{q},\tau)$, identifying one as a cooperative mode and the other as an interdiffusion mode. The theory of Foley and Cohen [101] is similar to that of Benmouna et al. [100]. They also identify two modes of relaxation for $S(\mathbf{q},\tau)$, but do not attempt detailed calculations of the decay rates.

The theoretical approach of [100] is to use the random phase approximation to find an approximate expression for the effect of interactions on $S(\mathbf{q},\tau)$. For static properties, use of the RPA results in the Flory-Huggins expression for S(0) [102]. This is a mean field theory which is only valid above C^* [103]. The initial slope of ln $S(\mathbf{q},\tau)$ is found and it is assumed that both modes decay exponentially. Additionally, hydrodynamic interactions are assumed to be totally screened. (Rouse mobilities are used.) Two special cases are considered in detail:

Case A; two interacting polymers with equal molar masses and sizes, one having no contrast with the solvent, in a solvent of the same solvent quality for both polymers

Case B; a solution of two polymers differing only in their molar masses

Case A will be considered in detail. Two decays are found, having decay rates

$$\Gamma_I = q^2 D_I(q) = \Gamma_S(q) \left[1 - 4A_2\, MCx(1-x)\, P(q)\chi/\upsilon \right] \qquad (2.155)$$

and

$$\Gamma_C = q^2 D_c(q) = \Gamma_S(q) \left[1 + 2A_2\, MCP(q)\right] . \qquad (2.156)$$

In the small q limit, the diffusion coefficients D_I and D_c are analogous to D_- and D_+ in eqn (2.154). Here, x is the relative concentration of the visible polymer (e.g. $C_1/(C_1+C_2)$), C is the total polymer concentration, A_2 is a generalized virial coefficient which may depend on C (expressing the dependence of the osmotic pressure on the total polymer concentration), υ is the excluded volume parameter (assumed to be the same for both polymers) and χ ($= \chi_{12}$) is the Flory interaction parameter for polymer-polymer interactions [103, 104]. The parameter $\Gamma_S(q)$ is the "bare" decay rate; i.e. the decay rate of the self dynamic structure factor [104] which in this theory is given by

$$\Gamma_S = q^2 \frac{k_B T}{N\zeta\, P(q)}$$

$$= \frac{q^2 D_s}{P(q)} \,. \qquad (2.157)$$

Unless P(q) is equal to one, a q-dependent effective diffusion coefficient is obtained. In the limit of small q, the self diffusion coefficient is measured. Since the friction factor $N\zeta$ in eqn (2.157) takes the Rouse form it is clear that this theory does not account for the effect of hydrodynamic interactions or entanglements on chain dynamics.

The limiting forms of eqns (2.155) and (2.156) are consistent with the known limits of ternary diffusion coefficients [99, 105];

$$\lim_{C_1 \to 0} D_{12} = 0 \qquad (2.158)$$

$$\lim_{C_2 \to 0} D_{11} = D_{10} \qquad \text{(mutual diffusion)} \qquad (2.159)$$

$$\lim_{C_1 \to 0} D_{11} = D_1(C_2) \qquad (2.160)$$

where $D_1(C_2)$ represents the self diffusion coefficient of a trace of component 1 in the presence of a variable concentration C_2 of component 2. Eqn (2.160) is equivalent to eqn (2.155) with $x \to 0$. This is the condition which must be satisfied in order to perform an "optical tracer" dynamic light scattering experiment. However, a note of caution must be made at this point. Equation (2.155) indicates that the degree to which D_I approximates D_s depends not only upon the value of x, but also upon the thermodynamic quantities A_2 and χ/υ. An interesting limit of eqn (2.155) is found when χ/υ tends to zero. Then Γ_I becomes equal to $\Gamma_S(q)$ regardless of the value of x. Such a situation is realized when the polymers are compatible and the solvent is good for both of them.

Full expressions for the mode amplitudes are given in Borsali et al. [104]. In the limit of low values of x, the amplitude of the cooperative mode approaches zero, so that only the interdiffusion mode is measured. When $x \neq 0$ both modes are expected to contribute to $S(q,\tau)$, even though one of the polymers is "invisible". (These considerations apply to solutions of interacting polymers - not dilute solutions). Another interesting case is the one discussed very recently by Borsali et al. [104]; the "zero average contrast condition". In this case, the refractive index increments satisfy

$$(\partial n / \partial \phi)_1 = -(\partial n / \partial \phi)_2$$

where ϕ is the total polymer volume fraction. The cooperative mode disappears if x = 1/2.

3 EXPERIMENTAL

This chapter contains a general discussion of the experimental aspects of PGSE NMR and DLS. More specific information is given in the experimental sections of the following chapters.

3.1 PGSE Experiments

3.1.1 Apparatus

The excellent texts by Fukushima and Roeder [106] and Martin, Delpuech and Martin [107] give general discussions of the apparatus and techniques of Fourier transform NMR spectroscopy. Here, the discussion will focus on the Pulsed Gradient Spin Echo NMR apparatus at Massey University.

The PGSE NMR experiments were performed on a JEOL FX-60 Fourier transform NMR spectrometer which has been modified for PGSE NMR [108] and NMR imaging experiments [109, 110]. The main components of the modified spectrometer are shown schematically in Fig. 3.1.

The static field B_0 is produced by a 1.4T electromagnet giving a resonant frequency of 60 MHz for ^1H nuclei. The value of B_0 is stabilized by a lock circuit which senses the resonant frequency of a small sample (usually heavy water, D_2O) located near the sample coil in the probe.

The spectrometer is controlled by a Texas Instruments 980A computer. The TI 980A computer is provided with programs which allow the user to prepare and run various pulse sequences, display the digitized data and perform limited data analysis. Parameters such as the rf pulse phase, duration and separation can all be set via the light pen user interface. Fourier transformation, baseline correction and first and second order phase correction are also available. Signal averaging is used (on the Fourier transformed data) to improve the signal to noise ratio. In addition, the phase of the π rf pulse and the sign of the A/D converter are alternated to cancel any spurious dc components in the signal. (In the spectrometer software this mode of operation is called coherent noise cancellation.) The JEOL software has been supplemented by a program written by Callaghan [112] specifically designed to run PGSE experiments. A pulse sequencer designed and built by Eccles [109] allows the TI 980A to control the rf and magnetic field gradient pulses.

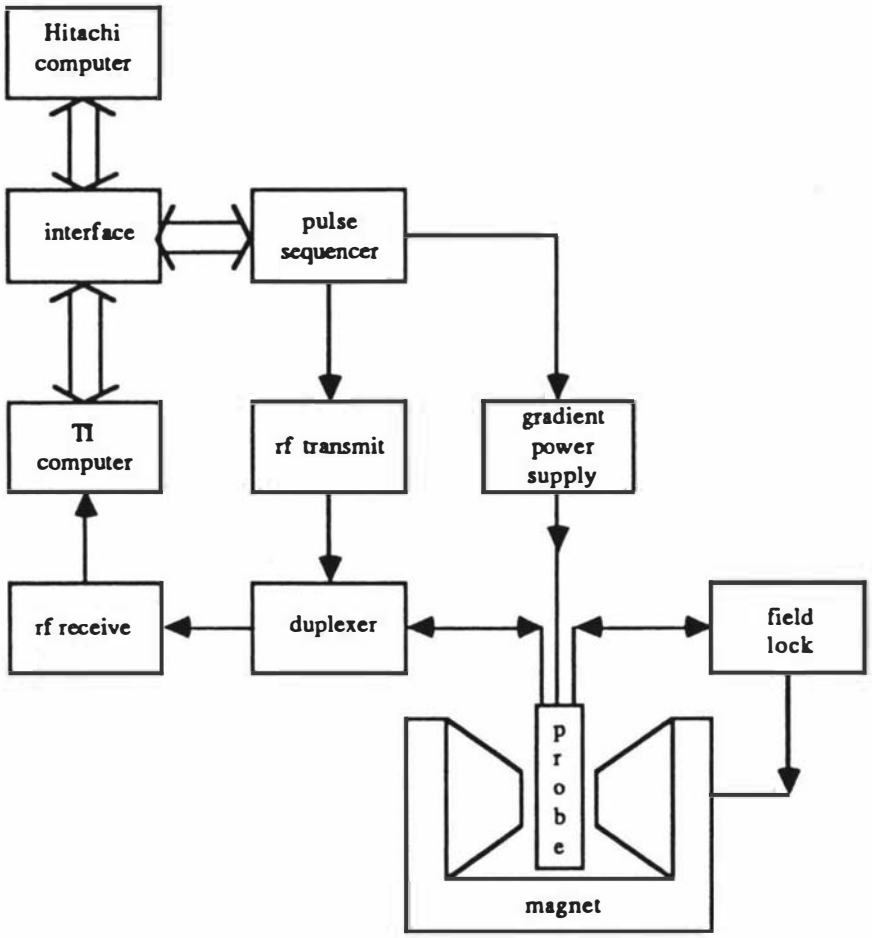

Figure 3.1 Pulsed gradient spin echo NMR apparatus.

The rf pulses which excite the sample and produce a detectable magnetization are transmitted by a solenoidal coil into which the sample is placed. The same coil is also used to detect the signal induced by the oscillating nuclear magnetization. Therefore, a duplexer is required to route a high voltage (typically 60V p-p) to the sample coil in the transmit phase and transfer a small signal (typically in the μV range) to the rf preamplifier with minimal loss in the receive phase. The duplexer used in this work has been described by Eccles [109].

After passing through the duplexer, the signal enters a preamplifier. The original JEOL preamplifier has been replaced by one with greater gain and signal to noise ratio [109]. This is followed by an rf amplification stage and mixing with a local oscillator to produce an intermediate frequency signal. The IF signal is further amplified and then enters another mixer which acts as a phase sensitive detector. The output from the psd is in the audio frequency range and can then be digitized and stored. The local oscillator frequencies are

chosen so that the Larmor frequency corresponds approximately to zero frequency after the mixing stages. Detected frequencies are therefore measured relative to the frequency of the rotating frame. Quadrature detection is achieved by shifting the reference phase of the phase sensitive detector by 90° after every pair of accumulations (in coherent noise cancellation mode). The in-phase and quadrature-phase data comprise the real and imaginary parts of a complex data set.

The gradient pulses are produced by electronically switching the current from a commercial power operational amplifier (Kepco ATE 75-15M) operated in constant current mode as described by Callaghan, Trotter and Jolley [108]. Precise matching of the gradient pulses is necessary for the production of stable and reproducible spin echoes. In this apparatus, the current is maintained at a constant value and is switched to either the gradient coils or to ground through two Darlington transistor networks. The transistors are switched by logic pulses from the pulse sequencer. This method has the advantage that no current can flow through the gradient coils while the transistors are off [108].

The Kepco ATE 75-15M power supply has been modified by Xia [110] to reduce the ripple on the output. The modifications consisted of separating the cooling fans and transformer from the sensing resistor which is used to monitor the output current. The efficiency of cooling has, however, been reduced. When the power supply was operated at high currents, it was necessary to set the current level to zero between signal accumulations to prevent overheating. The level was increased to the desired value under software control about 0.8 s before each accumulation to avoid any problems due to slow stabilization of the level.

The pulsed field gradient system satisfies all of the requirements to produce stable, reproducible spin echoes so that signal averaging can be used to improve the signal to noise ratio.

The Hitachi MB16000 personal computer is used to load software into the TI 980A and also accepts spectra from the TI 980A for display and analysis. A Fortran program (called PGSE) which was written by Callaghan [113] was used for data collection and analysis. After each run of N accumulations, a set of data consisting of the resultant digitized spin echo signals for the two quadrature phases is Fourier transformed in the TI 980A computer which then sends the real and imaginary spectra to the Hitachi computer. The value of the detector phase may not be the one required to make the real spectrum a pure absorption spectrum, so a phase correction which can differ from one experiment to the next is usually required. Program PGSE performs phase correction by searching for the linear combination of the real and imaginary spectra which produces the maximum integral over a selected spectral window. The peak integrals A(k) and the normalized echo amplitudes

A(k)/A(0) are then calculated over each preselected window. The first run of each set must have zero gradient so that A(k)/A(0) can be calculated for the following runs. After the third run, a least squares fit is performed on the data for each window and plotted on the Hitachi's colour monitor. The plots and fits are updated after each following run and the results may be printed at the end of the set.

Three different probes were used in this work. The probe described previously by Callaghan, Trotter and Jolley [108] having a gradient of 0.1577 T $m^{-1}A^{-1}$ was used in the earlier measurements. A new probe [114] with G = 1.215 T $m^{-1}A^{-1}$ was used for the later measurements. The higher gradients available with the new probe make it possible to measure lower diffusion coefficients. The new probe has other advantages over the older one. The resolution is slightly better and the quadrupolar geometry [109] of the gradient coil provides better gradient uniformity along the vertical (y) axis than the Maxwell pair used in the old probe. This means that longer samples can be used than with the old probe. Some deuterium PGSE NMR experiments were also performed (see Chapter 4). The probe used for these experiments was the imaging probe [109, 110]. Prof. Callaghan kindly retuned this probe to operate at the deuterium resonant frequency, reconfigured the spectrometer to receive at deuterium frequency and swapped the lock from deuterium to proton operation. The y gradient available from the imaging probe is 0.0936 T $m^{-1}A^{-1}$ [110]. All of the probes have homogeneity coils which are used to improve the spectral resolution by making fine adjustments to the main field.

The temperature of the sample was controlled with the standard JEOL hot air temperature controller (see e.g. [108]). The temperature in the sample space was measured with a dummy sample containing a calibrated thermistor. The temperature of the sample could be controlled to within ±0.5°C.

3.1.2 Preparation of Samples for PGSE NMR

Samples were contained in 4 or 5 mm NMR tubes (Wilmad Glass Co., N.J., U.S.A.). The tubes were washed with detergent, thoroughly rinsed with water, rinsed with analytical grade acetone and allowed to dry before the sample was added. For some experiments, the polymer and solvent were dispensed directly into the tubes. For others, the solutions were made before being added to the tubes. Concentrations were determined by weight on a Mettler balance reading to 0.01 mg. Spectroscopic or similar quality solvents were used to make the solutions. The tubes were flame sealed and usually stored at 30-40°C in the dark.

3.1.3 Experimental Technique

The JEOL temperature controller was allowed at least a half hour to stabilize after being switched on and the temperature in the sample space was checked periodically between measurements.

Signal averaging and coherent noise cancellation were always employed.

An exponential filter was applied to the digitized data in the time domain, giving spectral broadening of 20 - 30 Hz.

The calibration of the probes was frequently checked by measuring D_s for water and checking the results against the precise measurements of Mills [111].

3.1.4 Data Analysis

For routine analysis, linear least squares fits were used to find the slope and intercept of the plots of $\ln[A(k)/A(0)]$ against k ($k = \gamma^2G^2\delta^2(\Delta-\delta/3)$), the slope being interpreted as D_s (see eqn (2.90)).

It is of interest to estimate the error in a determination of the echo attenuation. In practice, a value of the normalized echo amplitude is calculated from A(k)/A(0) where

$$A(k) = I/N,$$

I is the integral over a given window in the frequency domain (actually the sum since the data is digitized) and N is the number of accumulations.

The variance in A(k)/A(0) is given by

$$\sigma_a^2 / a^2 = \sigma_G^2 / (I/N)^2 + \sigma_0^2 / (I_0/N_0)^2 \qquad (3.1)$$

where $a = A(k) / A(0)$.

Assuming that the noise is uncorrelated from one point to another, the variance in I after N accumulations is $wN\sigma_y^2$ where w is the number of points in the window. Therefore,

$$\sigma_G^2 = w\sigma_y^2 / N$$

and with an analogous expression for σ_0^2, it is found that

$$\sigma_a^2 / a^2 = w\sigma_y^2[N/I^2 + N_0/I_0^2] \; . \qquad (3.2)$$

The standard deviation in the natural log of A(k)/A(0) is then [133]

$$\sigma = \frac{\sigma_a}{a}$$

$$= w^{1/2}\,\sigma_y\,[N/I^2 + N_0/I_0^2]^{1/2}\,. \qquad (3.3)$$

For the common case in which A(k)/A(0) decays exponentially, it is found that

$$\sigma = \frac{\sigma_y w^{1/2}}{A(0)}\,\{[\exp(2kD)]/N + 1/N_0\}^{1/2} \qquad (3.4)$$

i.e. if N remains constant, the standard deviation increases exponentially as kD increases.

In a least squares fit each point is given a weighting inversely proportional to its variance [133]. An alternative to including the variance explicitly in the fit is to increase N as k increases so as to keep the variance constant. In this case, the number of accumulations must be increased as

$$N/N_0 = \exp(2kD) \qquad (3.5)$$

(assuming that $N=N_0$ when $k=0$) which approximately equals 7^{kD}. When the number of accumulations was set for an experiment this rule was approximately observed so that uniform weighting could be used in the linear least squares fits.

In addition to the linear least squares fitting program which was used for routine data analysis, polynomial fits on a commercial software package (Cricket Graph, Cricket Software, USA) and a non-linear curve fitting program (see section 3.2.4) were also available.

3.2 DLS Experiments

3.2.1 Apparatus

A schematic diagram of the apparatus used in dynamic light scattering experiments is shown in Fig. 3.2.

The laser and spectrometer are securely located on a heavy table designed by Dr R. C. O'Driscoll [115] to give good vibration isolation. The table top consists of a steel frame filled with concrete and surfaced with steel plate. The steel surface allows optical components to be screwed directly to the table or secured with magnetic mounts. The table top rests on a thick layer of foam rubber supported by steel legs.

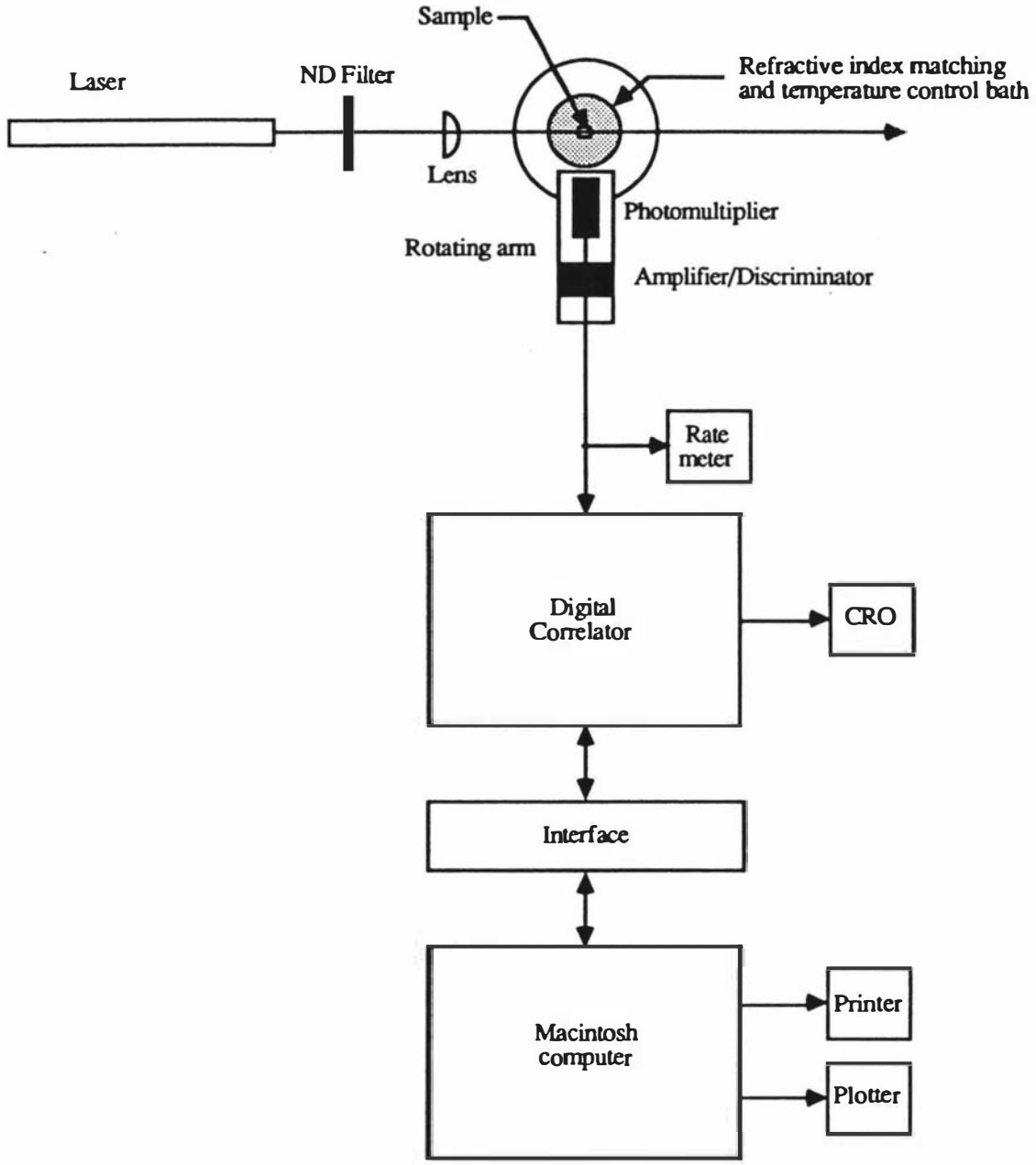

Figure 3.2 Dynamic light scattering apparatus.

The light source is a Spectra Physics 165-08 Argon Ion laser operated at 488.0 nm or 514.5 nm. The incident beam is weakly focused with a 10 cm focal length lens to give a high intensity in the scattering volume. A closed circuit cooling system [116] containing distilled water in thermal contact with a heat exchanger was used to cool the laser. For some measurements a PMS Electro-Optics tunable Helium-Neon laser (model no. LSTP-0020) operated at 632.8 nm was used. The lasers were always operated well above

threshold and if necessary, the beam was attenuated with a variable neutral density filter (Ealing Optics).

The measurements were made with a Malvern Instruments RR102 spectrometer, consisting of a refractive index matching and temperature control bath, a spectrometer rotation unit and a photomultiplier assembly including collection optics, photomultiplier tube and photoelectron pulse amplifier/discriminator. The purpose of the refractive index matching bath is to reduce unwanted reflections and flare from the glass cells used to contain the samples. The refractive index matching fluid was water containing 0.4 g/litre of sodium azide to inhibit the growth of microorganisms. Water has too low a refractive index to perfectly match the refractive index of glass, but it is reasonably effective and has the additional advantages that it has a high boiling point, low viscosity and is harmless. The refractive index matching fluid is recirculated and filtered with a Malvern Instruments RR98 recirculating pump and filtration system to remove particulate contamination before the spectrometer is used. It is important to use surfactant free filters such as Millipore GVWP, HVLP or low water extractable (TF) types for this purpose. The bath also contains a heated copper block for temperature control. A Malvern Instruments RR56 temperature controller was used to control the temperature.

A microscope stage with x and y translation verniers was adapted to fit onto the top of the Malvern Instruments refractive index matching bath so that NMR tubes could be precisely positioned for DLS measurements. The NMR tubes were held in a nylon collar which could be clamped to a movable arm on the x-y translation stage. Every time a tube was placed in this holder, its position was carefully adjusted. The position perpendicular to the direction of the incident beam (in the horizontal plane) was adjusted so that the back reflections from the tube returned along the direction of the incident beam. The position parallel to the incident beam was adjusted by setting the photomultiplier at 90°, noting the tube positions at which the count rate decreased to zero and returning the tube to the precise centre of these two points. (The vernier scales on the microscope stage were particularly useful in this procedure.)

Attempts to perform time averaged light scattering measurements on the Malvern spectrometer were made, but were not successful. After some investigation it was found that the glass vat used in the Malvern spectrometer does not have parallel walls and is slightly eccentric, making it impossible to achieve good optical alignment at all angles. This point has also been noted by Butler [117]. Measurements of the angular dependence of the absolute intensity would require better optical alignment than is currently available on our instrument. However, for photon correlation experiments, the existing spectrometer is perfectly adequate.

The photomultiplier is an ITT FW 130 which was operated at the recommended voltage of -1740 V. This particular photomultiplier is often chosen for photon correlation experiments due to its low dark count and minimal afterpulsing [118]. The photomultiplier was mounted in the standard Malvern Instruments photomultiplier housing which also includes the collection optics and a pulse amplifier and discriminator. The collection optics are designed to provide coherent detection of the scattered light (ideally, a point detector would be used). A good discussion of the collection optics in the Malvern Instruments spectrometer is given by Jolly and Eisenberg [119]. The amplifier and discriminator produce standardized pulses corresponding to photoelectron detections.

The standardized pulses are processed by a digital correlator made by O'Driscoll [120, 121]. This correlator has 48 correlation channels with an available range of sample times from 0.05 μs to 9.95×10^5 μs. Four monitor channels are provided for the normalization of correlation functions. The O'Driscoll correlator is a "one bit" correlator, which means that one of the channels is reduced to binary form before the correlation function is computed. Provided that a one bit correlator is operated correctly, no distortion of the correlation function need occur [122]. The reduction of the signal to one bit form was achieved either by clipping or by scaling. The output of a clipper is zero if the number of counts detected in a given sample time T is less than or equal to the clipping level k and one if the number of counts detected exceeds the clipping level. A scaler outputs one count for every s counts which enter it. In practice, scaling is always followed clipping at zero.

A digital correlator calculates the correlation function of photodetection pulses by accumulating the products

$$NG^{(2)}(iT-rT) = \sum_{i=1}^{N} n(iT)\, n_k(iT-rT) \tag{3.6}$$

where T is the sample time, r is the delay channel number, N is the number of samples and n and n_k are the unclipped and clipped numbers of photodetections counted in a given sampling period. For a stationary, ergodic process, the time average is equal to the ensemble average, so

$$NG^{(2)}(iT-rT) = N\langle n(iT)\, n_k(iT-rT)\rangle \tag{3.7}$$

is independent of the time origin iT. The lag time (iT–rT) is usually given the symbol τ and the correlation function is even so that $G^{(2)}(-\tau) = G^{(2)}(\tau)$.

The normalized intensity autocorrelation function $g^{(2)}(\tau)$ is equal to the normalized photocount correlation function [122] and the estimator for $g^{(2)}(\tau)$ obtained in an experiment is given by

$$\hat{g}^{(2)}(\tau) = \frac{\langle n(iT)n_k(iT-rT)\rangle}{\langle n\rangle\langle n_k\rangle}$$

$$= N \times \frac{NG^{(2)}(\tau)}{B} \quad . \tag{3.8}$$

where B is the product of the measured values of $N\langle n\rangle$ and $N\langle n_k\rangle$. It is appropriate to think of the measured $\hat{g}^{(2)}(\tau)$ as one member of an ensemble which has the population mean $g^{(2)}(\tau)$.

All of the quantities in eqn (3.8) are available from the stores and monitor channels of a digital correlator. This normalization method is sometimes called self-normalization. Oliver [130] has discussed normalization methods and concluded that self-normalization generally gives the best performance.

If the scattered field has gaussian statistics, the electric field autocorrelation function and the intensity autocorrelation function are related by the Siegert relation [122]

$$g^{(2)}(\tau) = 1 + C\left|g^{(1)}(\tau)\right|^2 \tag{3.9}$$

where the constant C is an experimental factor which accounts for the effects of clipping (or scaling) , the finite area of the detector and the finite length of the sample time. In the data analysis, C is treated as a free parameter .

A novel feature of the O'Driscoll correlator is the incorporation of a hardware device (the "blinker") designed to prevent the distortion of correlation functions due to scattering from dust. The blinker can suspend the accumulation of data or reset the correlator store if the number of counts detected is higher than a preset level during three consecutive sample times. The introduction of software control of the correlator has, to a certain extent, made the use of the blinker unnecessary in this work.

A digital-analogue ratemeter constructed by Trotter [123] can be connected to the output from the amplifier/discriminator unit to aid fine adjustments of the optical alignment.

The correlator is connected to an Apple Macintosh computer (512 kbyte memory) which is used for remote control of the correlator and data collection and analysis. Data is transferred to and from the correlator through the RS 232 serial port on the computer using an interface constructed by O'Driscoll [124]. The data transfer rate is 9600 baud. An Apple Imagewriter printer and Hewlett-Packard 7470A plotter are connected to the computer to provide printed output and plots of data. The computer programs which control the flow of data through the serial port were written in Fortran 77 and compiled

with the Absoft MacFortran compiler, version 2.3. Standard Macintosh Toolbox routines are used to control the serial port.

3.2.2 Preparation of Samples for Light Scattering

It is well known that particulate contamination of light scattering samples can severely distort the data [126, 127]. Therefore it is necessary to ensure that both the sample itself and its container are free of such contamination before experiments are performed. Procedures for cleaning light scattering cells and solutions vary [126]. The methods adopted in this work will now be described.

Light scattering samples were contained in 1 cm square fluorimeter cells (Hellma, England) sealed with teflon stoppers or 4 or 5 mm NMR tubes (Wilmad Glass Co., N.J., U.S.A.). In both cases, the cleaning procedure was to:

1. Wash with detergent and water
2. Soak in chromic acid
3. Wash thoroughly in water
4. Rinse with distilled water
5. Rinse with analytical grade acetone
6. Flush with condensing acetone vapour
7. Dry under vacuum
8. Stopper immediately after drying

Step six was carried out using the apparatus shown in Fig. 3.3. This apparatus is based on a design discussed in reference [126]. The cells were rinsed clean in an appropriate solvent after use.

Solutions were always made with analytical or spectroscopic grade solvents. Good results were usually obtained by filtering solutions directly into a cleaned cell using a Millipore filter (usually type FGLP chosen for its solvent resistance) held in a stainless steel filter holder (Millipore Swinny). Glass syringes and stainless steel hypodermic needles were used to filter samples. The procedure for filtering samples was as follows:

1. Clean and dry the filter holder, syringe and needle
2. Hold in retort stand (see Fig. 3.4)
3. Transfer sample to syringe
4. Insert plunger
5. Discard the first few drops
6. Filter the solution into a cell and seal

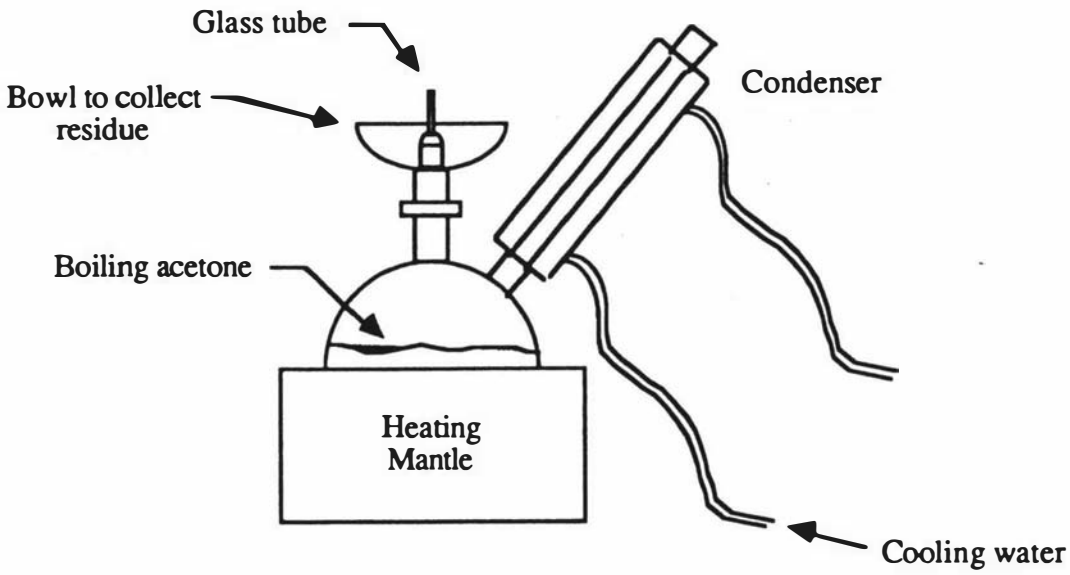

Figure 3.3 Apparatus for cleaning light scattering cells.

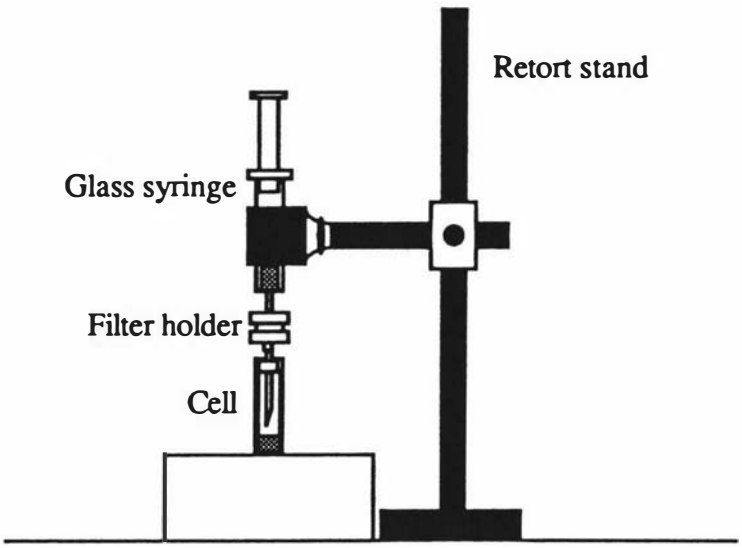

Figure 3.4 Apparatus for filtering light scattering samples.

Concentrated solutions were made by slowly evaporating solvent from filtered, dilute solutions. The cell was placed in a vacuum dessicator which was then evacuated to an appropriate pressure. If the solvent had a low boiling point, care was taken to ensure that the pressure was not so low as to boil the solution.

Filtered solvents were used for dilutions.

Concentrations determined by weighing in a temperature and humidity controlled room on a Mettler balance reading to 0.01 mg.

3.2.3 Experimental Technique

It is necessary to ensure that the optical alignment is correct before measurements are made with the spectrometer. The alignment procedure employed for this purpose is summarized as follows:

1. Remove the input lens and empty, remove and clean the vat containing the refractive index matching fluid
2. Align the incident beam to the optical axis of the spectrometer
3. Replace the vat and adjust its position and the incident beam direction until the back reflections from the entrance and exit windows of the vat are symmetrical and centred
4. Fill the vat with the refractive index matching fluid
5. Replace the input lens and align it so that the back reflections from its front and back surfaces are central
6. Focus the incident beam in the centre of the vat
7. Place a strongly scattering sample in the spectrometer
8. With the angle set at 90°, adjust the vertical alignment of the detection optics for maximum count rate
9. Reduce the laser power to minimum and attenuate the beam
10. Gradually move the photomultiplier to 0°, further attenuating the beam if necessary
11. Adjust the angle for maximum count rate, adjust the horizontal and vertical alignment of the detection optics for maximum count rate and set the angle vernier to zero

It may also be necessary to adjust the focus of the detection optics. This is done most easily by plotting the maximum count rate versus the distance of the photomultiplier assembly from the scattering volume at a scattering angle of 90°.

Because of the poor optical quality of the Malvern vat, it is occasionally necessary to adjust the vertical alignment of the detection optics to maximize the count rate when the angle is changed.

The sample time was usually chosen so that the correlation function decayed to a value of approximately e^{-3} at the largest value of τ.

Both clipping and scaling were used in these measurements. Clipping was often chosen when the count rate was low because it makes more efficient use of the signal. On the other hand, scaling is useful because the intercept is less sensitive to the mean count rate and correlation functions measured at different sample times and count rates therefore superimpose when plotted against $q^2\tau$. Scaling also has the advantage that unlike clipping, it gives the true correlation function even when the scattered field does not have gaussian statistics [122]. Of course, for count rates less than one per sample time, the true correlation function is obtained on a one bit correlator in any case. The clipping level was set to the mean number of counts per sample time $\langle n \rangle$ (rounded to the nearest integer value) and the scaling level was chosen as $10\langle n \rangle$ to ensure that the probability of getting two scaled counts in any sampling period was small [122].

The intensity of the incident beam was usually adjusted to give $\langle n \rangle$ between 1 and 10 if possible. In general, the recommendations of Oliver [129, 130] were followed.

When weakly scattering samples are studied or extreme precision in the measured correlation function is required, it is often advantageous to average many shorter runs rather than accumulating one run over a long period. Store overflows can be avoided and the effective number of counts recorded can be increased far in excess of the store capacity by this method. A single long measurement on an otherwise very clean sample is easily spoiled by the scattering from a large dust particle passing momentarily through the scattering volume. The averaging of individually normalized runs is a very convenient way of overcoming this problem. Runs can be scrutinized before being included in the average and those which are obviously distorted can be excluded. Individual normalization of shorter runs has the additional advantage that errors in normalization due to long term drifts in the laser power or detector gain can be expected to decrease as the run length decreases [128]. One drawback of this technique is that $\hat{g}^{(2)}(\tau)$ is actually a biassed estimator of $g^{(2)}(\tau)$, the bias terms being of order $1/N$ [122, 130]. Provided that N is large enough (say $> 10^3$) this effect is negligible [128].

When the data collection process is placed under software control a run rejection scheme with objective criteria can be applied to the data. O'Driscoll [120] has summarized various schemes which appeared in the literature before 1982. The basic idea of all of these

schemes is the same; the count rate is monitored and data showing evidence of an unusually high scattered intensity are rejected. Haller et al. [131] have given a detailed discussion of a dust discrimination scheme for time averaged intensity measurements based on a statistical test. In their scheme, the standard deviation of ten measurements of the ratio of the scattered to transmitted intensity is calculated. If this value is more than 1.3 times the expected standard deviation, the data set is tested for outlying values which may then be rejected and the standard deviation is tested again. The variance must be calculated theoretically before this criterion can be applied.

In general, the variance depends on ΓT and $\langle n \rangle$. However, when the count rate is low, the fluctuations in n are dominated by photon noise and the variance depends only on $\langle n \rangle$. Therefore, if $\langle n \rangle$ is small enough ($\langle n \rangle < 1$) an estimate of $\langle n \rangle$ is sufficient to allow a calculation of the variance. A detailed discussion of this point is given in Appendix 6.

The run rejection scheme used in this work required only a simple modification to the software once the run averaging facility was included. First, the mean number of counts per run is measured in a given number of preliminary runs. Each run provides an estimate of the mean number of counts per sample time, $\hat{n}$. The values of $\hat{n}$ obtained in the preliminary runs are stored in an array and their average is calculated. Each time a run is completed, the new value of $\hat{n}$ is compared to the mean value. If the new value is within five standard deviations of the mean, the new run is included in a running average of $\hat{g}^{(2)}(\tau)$ and the new value of $\hat{n}$ replaces the oldest value of $\hat{n}$ in the array. The process is repeated until a predetermined number of runs has been accepted. In the current implementation of this scheme, only the Poisson noise term of the variance is included, but there is no reason why a cumulant fit could not be used to obtain Γ (and C; see Appendix 6) from the preliminary runs and eqn (A6.5) used to calculate the variance, with a running average of Γ also being maintained.

This scheme has the advantage that the mean value of $\hat{n}$ is self-correcting, even if a small number of the preliminary runs are affected by dust. The mean will also adapt to small drifts in the average intensity.

Short runs give the best dust discrimination, but this is offset by a loss of data collection efficiency since there is a small time delay between runs for data transfer and the small amount of computation required. If the runs are too short, the bias terms in $g^{(2)}(\tau)$ will become important. A practical rule is that N should be greater than 10^3 but still small enough to provide reasonable dust discrimination. Of course, there is no substitute for good sample preparation. If the proportion of runs which are rejected is too large, the experiment takes a long time and the results may not be meaningful anyway.

3.2.4 Data Analysis

Two computer programs controlling data collection and storage were written. The first, "DLS", is described in Fig. 3.5. Program DLS was used for routine experimental work. Each run is analysed using a cumulant fit after it is stored. Another program called "DLSEXPRESS" was used for the collection of a large number of runs without any operator intervention or data analysis. This program was used when it was necessary to collect data over a very long period. A separate data analysis program, "DLSFIT" was written for the analysis of data which had already been stored on disk. Program DLSFIT provides the option of fitting the data with cumulant fits or single or double exponential fits with or without a floating baseline.

All of the fits include the option of neglecting the initial points of the correlation function in the data analysis. This is necessary when measurements are made at very short sample times or at very low count rates because of the distortion caused by correlated afterpulsing in the photomultiplier tube.

In general, the intensity autocorrelation function can be written as

$$g^{(2)}(\tau) = 1 + (C|g^{(1)}(\tau)| + \Delta_1)^2 + \Delta_2 \qquad (3.10)$$

where $g^{(1)}(\tau)$ is a model provided by theory and Δ_1 and Δ_2 are constants which may be included to allow for small experimental artefacts which cannot be eliminated [132]. For example, Δ_2 could represent the misnormalization of $g^{(2)}(\tau)$ due to drifts in the source intensity or detector gain [128] or a number fluctuation term due to a small number of large particles moving through the scattering volume [127]. The Δ_1 term could represent the practically constant correlation function of any dust particles in the scattering volume [127]. In practice, the most straightforward method of data analysis is to ignore Δ_2 and fit

$$S_i = (\hat{g}^{(2)}(\tau_i) - 1)^{1/2} \qquad (3.11)$$

or $\ln S_i$ directly.

One advantage of this is that when a complicated model for $g^{(1)}(\tau)$ is being fitted, it is easier to fit it directly rather than fitting the square, which would be necessary if $g^{(2)}(\tau)$ were to be fitted. On the other hand, this method makes it more difficult to include Δ_2 in the fit. Provencher et al. [132] have remarked that in their measurements on polystyrene in cyclohexane, Δ_1 appeared to be more important than Δ_2. It is interesting to note that they also used a dust discrimination scheme in their data collection. It may be the case that the need for Δ_2 is eliminated when such a scheme is employed.

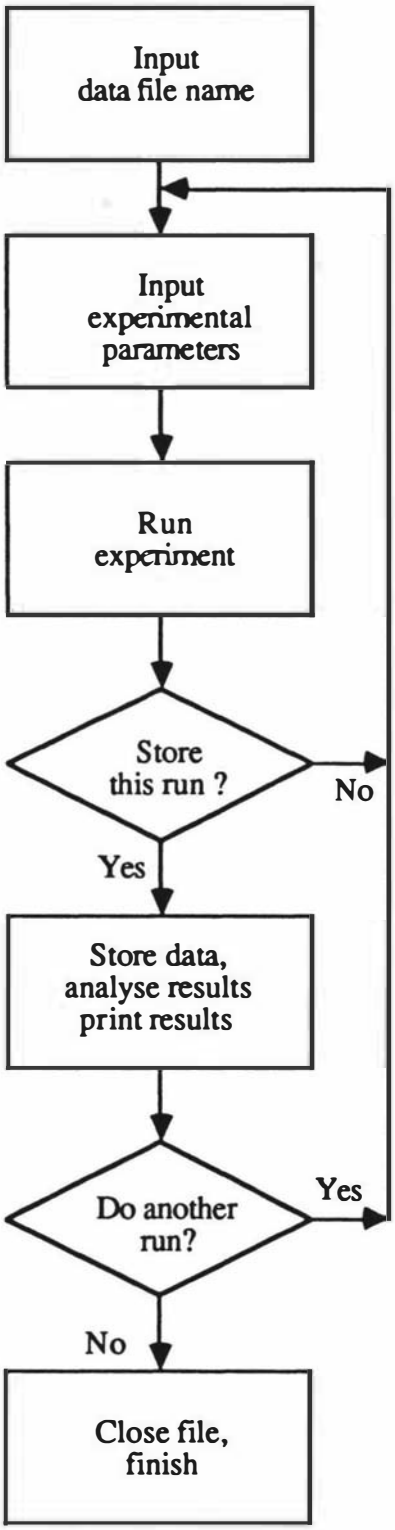

Figure 3.5a Flow diagram for program DLS.

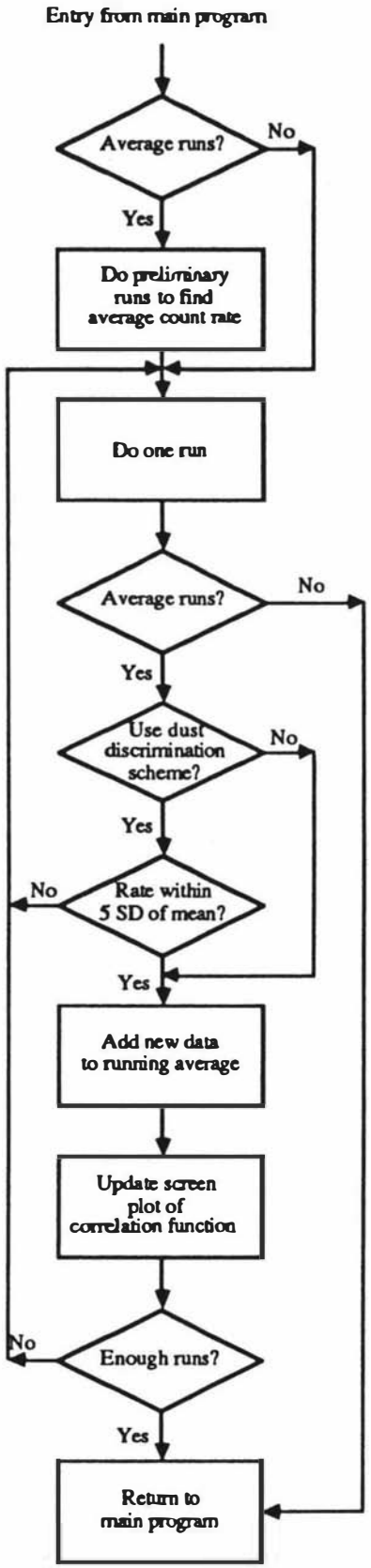

Figure 3.5b A more detailed description of the "Run Experiment" module in Fig. 3.5a.

All of the fits to data used the method of least squares. In the method of least squares, the quantity

$$\chi^2 = \sum_{i=1}^{M} w_i \, [y_i - y(x_i)]^2 \tag{3.12}$$

is minimized [133] with respect to the parameters of the fitting function. Here, the y_i represent the data and $y(x_i)$ are the values of the fitting function at particular values of the independent variable x. If $y(x_i)$ is written as $y(a_i, x_i)$ where the a_i represent the parameters of the fitting function, (for example, the slope and intercept in the case of a straight line) the minimization conditions read as

$$\frac{\partial \chi^2}{\partial a_i} = 0. \tag{3.13}$$

The weighting factors w_i in eqn (3.12) may be set to 1 for uniformly weighted data or $1/\sigma_i^2$ (where σ_i^2 is the variance in y_i) for the correct least squares weighting.

In the case of cumulant fits, the cumulant expansion, eqn (2.139) (including an additional term ln C; see eqn (3.10)) represents the fitting function $y(x_i)$ in eqn (3.12) and the data y_i are the measured values of ln S_i. In this case both Δ_1 and Δ_2 are neglected, but large values of Δ_1 or Δ_2 will increase the quadratic term in the results of the cumulant fit. The cumulant fit is a polynomial fit which is easily accomplished using the method of least squares. The derivatives in eqn (3.13) are calculated analytically and the results are equated to zero. This gives a set of simultaneous linear equations (see [133] for example) which can be solved by direct methods. In the programs discussed here, Gauss-Jordan elimination was used to solve the set of linear simultaneous equations.

For single exponential fits, the data y_i were fitted to

$$C\exp(-\Gamma\tau) + \Delta_1 \tag{3.14}$$

with Δ_1 being optional. The function fitted in double exponential fits is

$$C[A\exp(-\Gamma_1\tau) + (1-A)\exp(-\Gamma_2\tau)] + \Delta_1 \tag{3.15}$$

with Δ_1 once again optional. The convergence of the non-linear least squares algorithm was assisted by constraining the decay rates Γ_1, Γ_2 and Γ, the mode amplitude A and the baseline correction Δ_1 to be positive. This constraint was imposed by setting the theoretical parameter equal to the square of the parameter in the algorithm. For example, $A = a^2$.

The simultaneous equations resulting from the minimization of χ^2 are not linear in the parameters a_i for the fitting functions of equations (3.14) and (3.15) so they cannot be solved by direct methods. Instead, iterative methods must be used. The Levenberg-Marquardt algorithm is used in program DLSFIT. This is a non-linear least squares algorithm incorporating the best features of the steepest descent and Gauss-Newton algorithms. A detailed discussion is given in Bevington's book [133] which also contains Fortran code upon which the non-linear least squares subroutines in DLSFIT are based. The non-linear fits performed well when they were tested on synthetic data sets to which realistic noise had been added.

If the correct least squares weights are used in equation (3.12) the variances in the parameters of the fitting function will be minimized. The variance of $\hat{g}^{(2)}(\tau)$ for scattered light having an exponential correlation function is given by Jakeman [122]. The result is a complicated equation which requires Γ to be known for its evaluation. A simpler result is obtained for the case $\langle n \rangle << 1$;

$$\mathrm{Var}\,\hat{g}^{(2)}(\tau) = \frac{g^{(2)}(\tau)}{B}. \tag{3.16}$$

In the fitting routines discussed here, the weighting factors are calculated approximately by assuming that eqn (3.16) is valid regardless of the count rate and it is also assumed that the estimator $\hat{g}^{(2)}(\tau)$ is an adequate approximation to $g^{(2)}(\tau)$. The usual rules for calculating the errors in derived quantities [133] give the weighting factors for fits to S_i and ln S_i as

$$w_i = \frac{4B[\hat{g}^{(2)}(\tau_i)-1]}{\hat{g}^{(2)}(\tau_i)} \tag{3.17}$$

and

$$w_i = \frac{4B[\hat{g}^{(2)}(\tau_i)-1]^2}{\hat{g}^{(2)}(\tau_i)} \tag{3.18}$$

respectively.

Two methods of evaluating the quality of a fit are provided in program DLS. In the first, the value of the reduced χ^2 is computed using

$$\chi_F^2 = \frac{\chi^2}{F} \tag{3.19}$$

where F is the number of degrees of freedom in the fit, i.e. the number of data points minus the number of parameters in the fit. A value of χ_F^2 close to 1 indicates that the fit is good,

whereas values greater than 1 indicate a poor fit [133]. Stated more precisely, if $\chi_F^2 > 1.5$ there is a 98% probability that the model is incorrect, given that the data are not distorted. (Note that values of less than 1 do not, however, signify any improvement in the fit [133].)

The quality of a fit can also be gauged by plotting the weighted residuals which are the summed terms appearing in equation (3.12). If the fit is poor, a plot of the residuals will show trends, whereas if the fit is good the points should be uniformly distributed above and below zero. Also, the validity of the least squares weights can be determined. If the magnitude of the scatter of the points about zero shows a trend, the weights have not been evaluated correctly.

Another useful function which program DLSFIT can perform is the averaging of runs recorded at different times. The individual runs may have different values of C so it is necessary to calculate C with a cumulant fit first and renormalize each run to an intercept of 1 (for S_i) before the averages are calculated.

4 POLYMER AND SOLVENT SELF DIFFUSION IN POLYSTYRENE-CYCLOHEXANE SOLUTIONS NEAR THE THETA TEMPERATURE

4.1 Polymer Diffusion

4.1.1 Experimental

Pulsed gradient spin echo NMR was used to measure the concentration dependence of the self diffusion coefficient of polystyrene in deuterated cyclohexane (C_6D_{12}). It was essential to use deuterated cyclohexane in these experiments because the spin echo signal from a protonated solvent would have overwhelmed the much smaller polymer proton signal, providing dynamic range problems and making the polystyrene proton signal unresolvable.

The polystyrene used in these experiments was nominally a 390,000 g mol^{-1} fraction with M_w/M_n <1.10 obtained from the Pressure Chemical Co. (batch no. 3b). However, the D_0 and k_{fs} values obtained for this material in previous experiments are more consistent with a molar mass of 350,000 g mol^{-1} [62]. This value will be adopted here.

The C_6D_{12} was >99 atom % deuterated cyclohexane manufactured by Merck (lot no. 1867-E) or similar quality deuterated solvent.

Some properties of polystyrene-cyclohexane solutions are summarized in Table 4.1.

Table 4.1 Properties of polystyrene-cyclohexane solutions

	C_6H_{12}	C_6D_{12}
Solvent M / (g mol^{-1})	84.16	96.23
Solvent ρ / (kg m^{-3})	779 (20°C) [134]	909 (20°C) [136]
	764 (35°C) [135]	
Polymer $\bar{v}$ / m^{3}kg^{-1}	0.934×10^{-3}[135]	
Theta temperature / °C	34.5 [135]	38-40 [136]

Concentrations were determined by weight, giving mass fractions which were then converted to mass/volume concentrations and volume fractions using the data given in Table 4.1.

The partial specific volume of C_6H_{12} at 40.5°C was calculated from the densities of the pure solvent given in Table 4.1 assuming a linear increase with temperature. (A very useful table of the refractive indices and densities of solvents is given by Johnson and Smith in [125].) The partial specific volume of C_6D_{12} at 40.5°C was calculated from the value at 20°C assuming the same rate of increase with temperature as for C_6H_{12}.

The critical concentration C^* for the crossover from the dilute regime to the semidilute regime for polystyrene in cyclohexane at the theta temperature was found by Stepanek et al. [137] (using osmotic pressure measurements) to be approximately given by

$$C^* = \frac{4\times10^4}{\sqrt{M_w}} \tag{4.1}$$

with C expressed in kg m^{-3} and M in g mol^{-1}. This gives C^* a value of 68 kg m^{-3} (ϕ^* = 0.063) for M = 3.5×10^5 g mol^{-1}. Equation (4.1) was actually derived by substituting an experimental relation for R_G into eqn (2.9). The result is within a factor of two of the value obtained by equating R_G and the measured correlation length $\xi\sqrt{3}$ at C^*. (See Adam and Delsanti [45] and Stepanek et al. [137] for a discussion of the measurement of ξ.)

The critical concentration for the onset of entanglement coupling in viscosity measurements C_e can be estimated using eqn (2.37). With M_c = 36,000 g mol^{-1} and α_ξ^2 = 1, it is found that ϕ_e = 0.103 or C_e = 112 kg m^{-3}.

The samples for these experiments were made by adding the solvent directly to a predetermined mass of polymer in 5 mm NMR tubes. The tubes were weighed, flame sealed and allowed to equilibrate at a temperature of 40°C for at least three months before the measurements were started. Cyclohexane is a theta solvent for polystyrene, and phase separation will occur if the temperature of the sample falls below the critical solution temperature (which may be several degrees below θ, depending on the molar mass and concentration). The relatively concentrated solutions studied here would probably require at least a few weeks to achieve equilibrium again even if partial phase separation were to occur. Therefore, the samples were kept warm in a dewar when they were transferred to the NMR spectrometer and the transfer was made as quickly as possible so as to prevent phase separation.

The self diffusion measurements were made at a temperature of 40.5±0.5°C using the lower field gradient probe (G = 0.1577 T $m^{-1}A^{-1}$).

4.1.2 Results

Typical echo attenuation plots for low and high concentration samples are shown in Figs 4.1 and 4.2. In both cases, there is a fast component in the echo attenuation due to residual undeuterated hydrogen nuclei in the deuterated cyclohexane. Consequently, the intercept is less than zero in the log plot. This effect is enhanced by the long T_2 of the solvent compared to that of the polymer. The solvent diffusion is much faster than the polymer diffusion so the solvent signal is attenuated at very low values of k and only contributes to the first point of A(k)/A(0) if at all. The first point was ignored in the data analysis if it was clearly affected by the solvent signal.

When very low diffusion coefficients are being measured, large gradients and large values of Δ and δ are necessary. However, large values of Δ and δ also require large values of τ. Due to spin-spin relaxation, the available signal decreases exponentially as τ is increased so the signal to noise ratio also decreases. In practice, Δ and τ could only be increased to 50-60 ms before the signal became too weak. The result is that for the highest concentration samples, only a small echo attenuation due to diffusion could be observed within the available range of experimental parameters (Fig. 4.2).

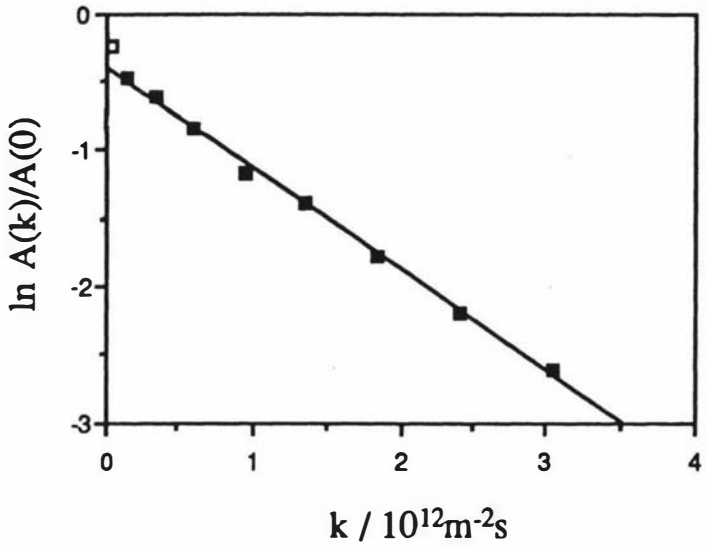

Figure 4.1 Echo attenuation plot for polystyrene diffusion in C_6D_{12}, C = 78.9 kg m^{-3}. On the horizontal axis, $k = \gamma^2G^2\delta^2(\Delta-\delta/3)$. The values of Δ and δ were 40 ms and 26 ms and the current in the gradient coil was varied from 1 A to 9 A. A linear least squares fit to the data represented by filled squares gives a diffusion coefficient of $(7.4 \pm 0.2) \times 10^{-13}$ m^2s^{-1}.

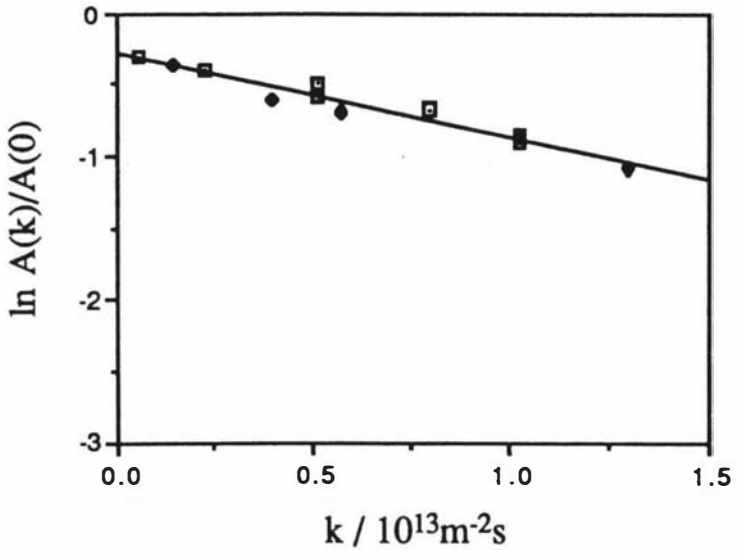

Figure 4.2 Echo attenuation plot for polystyrene diffusion in C_6D_{12}, C = 162.1 kg m^{-3}. The current in the gradient coil was varied and the values of Δ and δ were 53 ms and 46 ms (▫) and 55 ms and 48 ms (•). From the slope of the graph, $D_S = (5.8 \pm 0.5) \times 10^{-14}$ $m^2 s^{-1}$.

The results are given in Fig. 4.3 which shows a plot of log D_S against log c at 40.5°C. The error bars are approximately the same size as the points on the graph except where otherwise indicated. These errors reflect the uncertainty in a given determination of D_S; that is, the error in the slope of an echo attenuation plot. However, the reproducibility of the measurements, which is indicated by the scatter in the plot, was slightly poorer. Occasionally, very high values of D_S were measured in the dilute region. These high values were probably caused by convection in the sample. It is known that the hot air temperature control system used in NMR spectrometers can produce a small temperature gradient from the bottom to the top of the NMR tube containing the sample. Even if the effect of the temperature gradient across the sample itself is negligible, small droplets of solvent vapour can condense near the meniscus, flow down and cause convection in the sample. This produces non-exponential decay of the echo attenuation plots. Any measurements exhibiting this behaviour were rejected and repeated later. This effect became less evident as the concentration was increased due to the increased viscosity and lowered solvent vapour pressure.

A linear least squares fit to the data represented by filled squares in Fig. 4.3 gives a slope of -3.1 ± 0.1 which agrees with the prediction of the reptation model (section 2.2.4) to within experimental error. The low concentration points were excluded because they were not in

the semidilute region and the highest concentration point was excluded because it had a large uncertainty. Note also that the high concentration data are later shown to have been the points most strongly affected by local friction effects which become important near the glass transition (see section 4.1.3 and Fig. 4.15 in section 4.2.3). An approximate correction for this increase in local friction is discussed in section 4.2.3.

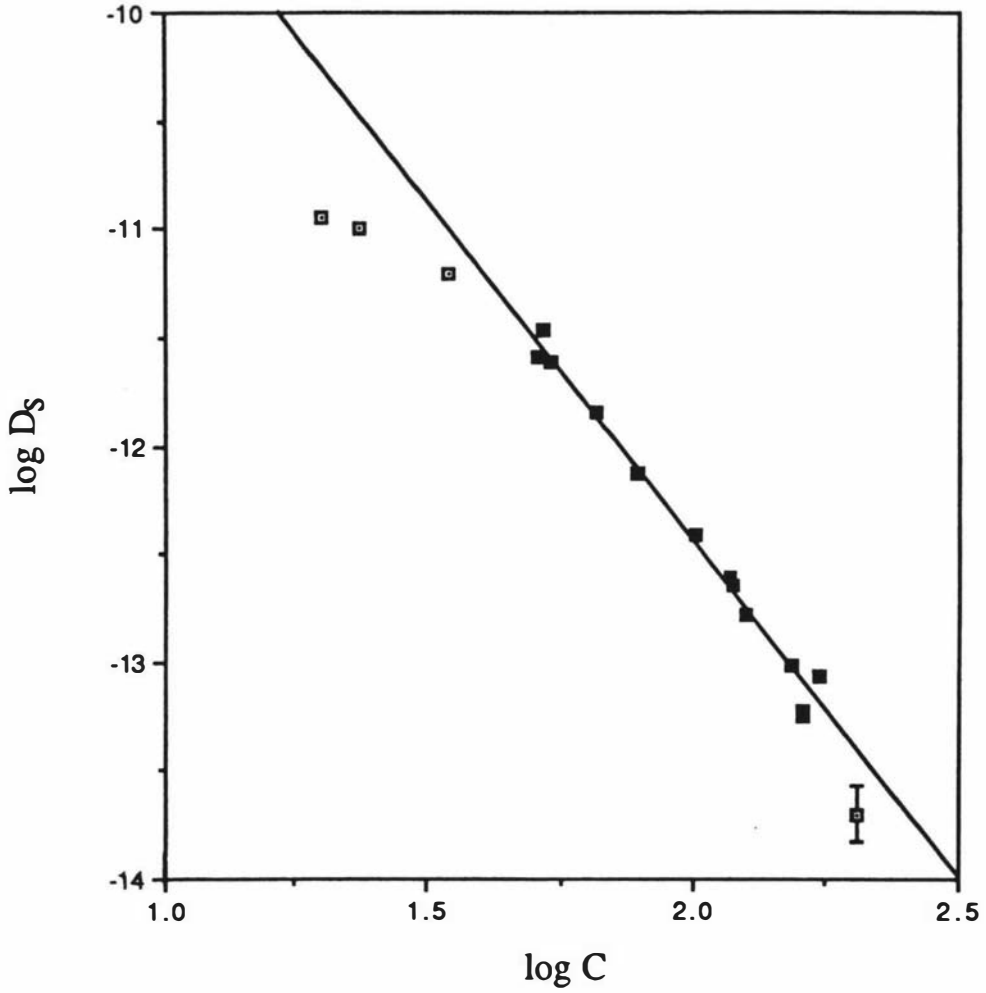

Figure 4.3 The concentration dependence of the self diffusion coefficient of 350 kg mol^{-1} polystyrene in C_6D_{12} measured by PGSE NMR at 40.5°C. A linear least squares fit to the filled points gives a slope of -3.1 ± 0.1.

The low concentration data are plotted separately in Fig. 4.4. The arrow indicates the value of D_0 (2.54×10^{-11} m^2s^{-1}) which was calculated from the molar mass dependence of the sedimentation coefficient given by Vidakovic [135]. Specifically, Vidakovic's molar mass dependence of s_0 was converted into a relation between D_0 and M;

$$D_0 = 1.34 \times 10^{-8} M^{-1/2} \quad \text{(PS in } C_6H_{12} \text{ at 34.5°C)} \qquad (4.2)$$

using the dilute limit of eqn (2.21). This expression is in agreement with previously reported results [138]. Assuming that the hydrodynamic radius is the same in C_6D_{12} at the theta temperature as it is in C_6H_{12} at the theta temperature, a temperature and viscosity correction was then applied to the value of D_0 (see equation (2.33)) to give D_0 for polystyrene in C_6D_{12} at 40.5°C.

According to the arguments presented in section 2.2.3, a plot of $1/D_s$ against concentration should yield a straight line at sufficiently low concentrations. This method was used by Callaghan and Pinder [139] to determine D_0 and k_{fs} for polystyrene-carbon tetrachloride solutions. The data shown in Fig. 4.4a do not extend to low enough concentrations to enable a reliable extrapolation to be made, even with a quadratic fit. On the other hand, the plot of log D_s against C shown in Fig. 4.4b is quite linear. Although there is no theoretical justification for such a plot, it seems to be quite a useful way of estimating D_0 from self diffusion data when the measurements do not go to low enough concentrations for a linear extrapolation to be made. The value of D_0 obtained from this plot is $(2.9\pm0.3) \times 10^{-11}$ m^2s^{-1}. The initial slope of D_s versus C can also be estimated from the linear fit to log D_s because 10^{-ax} has an initial slope of -a/log e. The value of k_{fs} obtained in this way was (0.045 ± 0.002) $kg^{-1}m^3$. (Note that the uncertainty quoted here does not include an estimate of any systematic error involved in the extrapolation.)

4.1.3 Discussion

The low concentration data will be discussed first.

The value of D_0 obtained from a linear fit to the plot of log D_s against C ($2.9\pm0.3 \times 10^{-11}$ m^2s^{-1}) is slightly higher than the value of D_0 (2.54×10^{-11} m^2s^{-1}) calculated from the empirical relationship between D_0 and M [135]. The method of extrapolation was checked by analysing the self diffusion data of Callaghan and Pinder [62] for polystyrene in CCl_4 and comparing the resultant values of D_0 with those evaluated from low concentration data using a $1/D_s$ - C plot [139]. The plots of log D_s against C were not always as linear as Fig. 4.4b and the curvature increased at higher molar masses. The values of D_0 obtained from the log plot extrapolations for good solvent systems were systematically lower than the values obtained from the low concentration data.

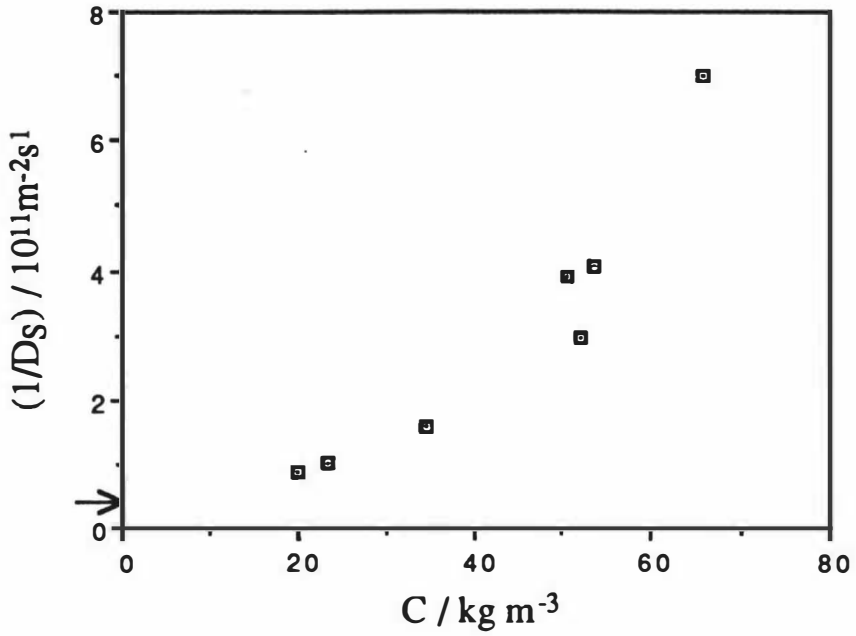

Figure 4.4a The low concentration polymer self diffusion data plotted as $1/D_s$ vs C. The arrow indicates the value of D_0 (2.54×10^{-11} m^2s^{-1}) calculated from the molar mass dependence of the sedimentation coefficient as discussed in the text.

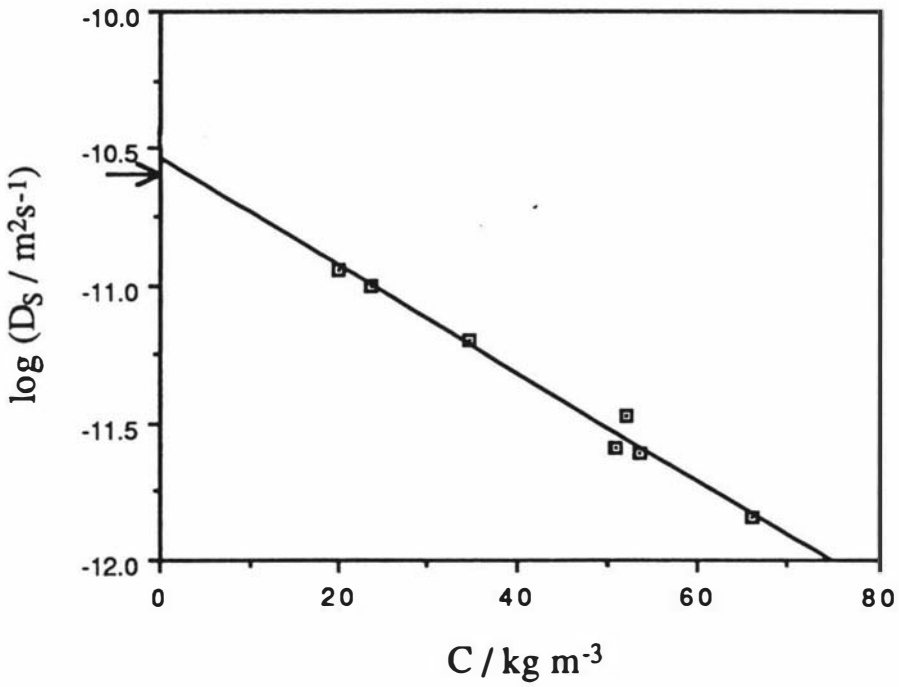

Figure 4.4b The low concentration polymer self diffusion data plotted as log D_s vs C. A linear least squares fit gives $D_0 = (2.9 \pm 0.3) \times 10^{-11}$ m^2s^{-1} and $k_{fs} = (0.045 \pm 0.002)$ $kg^{-1}m^3$. The arrow has the same meaning as in Fig. 4.4a.

Due to the expansion of a polymer in a good solvent, the C^* values in good solvents are much lower than in theta solvents, limiting the concentration range available below the semidilute region. In addition, k_f is greater for a polymer in a good solvent than it is in a theta solvent. Therefore, this extrapolation method must be applied with care, especially when it is applied to good solvent systems. Provided that the maximum concentration is below C^* it is probably possible to estimate D_0 to within 20%.

As a further check on the value of D_0, a few dynamic light scattering experiments were performed on dilute solutions of the 350,000 g mol^{-1} polystyrene in C_6D_{12}. At 18.9 kg m^{-3}, the mutual diffusion coefficient obtained from DLS was 1.5×10^{-11} m^2s^{-1}, and at 2.83 kg m^{-3}, D_m was found to be 2.2×10^{-11} m^2s^{-1}. A crude extrapolation using these two points gives a D_0 value of 2.3×10^{-11} m^2s^{-1} which agrees fairly well with the expected value of D_0, 2.54×10^{-11} m^2s^{-1}. These experiments were performed on unfiltered samples which were originally prepared for PGSE NMR experiments.

The k_{fs} value obtained from the fit to log D_s is 0.045 $kg^{-1}m^3$ which is smaller than the value obtained by Callaghan and Pinder [139] for the same molar mass polystyrene in carbon tetrachloride, 0.14 $kg^{-1}m^3$. This is to be expected, because k_f, the analogous quantity for the friction factor for mutual diffusion, includes a term which is proportional to the hydrodynamic volume of the polymer molecule divided by the molar mass [138]. For a given molar mass, this quantity must decrease as the solvent quality decreases. It must be emphasized here that k_{fs} and k_f are not expected to be equal because, as was mentioned in sections 2.2.1 and 2.2.3, f_s and f are fundamentally different quantities. Indeed, it has been shown experimentally [140, 141] that for a polymer in a good solvent, f_s increases less rapidly than f as the concentration is increased, implying that $k_{fs} < k_f$. The value of k_f for 350,000 g mol^{-1} polystyrene in cyclohexane at the theta temperature calculated from the relationship

$$k_f = 4.5 \times 10^{-5} M^{1/2} \qquad (4.3)$$

given by King et al. [138] is 0.027 m^3kg^{-1} which is less than the value of k_{fs} (0.045 m^3kg^{-1}) measured here. A similar analysis of Callaghan and Pinder's results for 110,000 g mol^{-1} polystyrene in C_6D_{12} gives $k_{fs} = 0.021$ m^3kg^{-1} compared with $k_f = 0.015$ m^3kg^{-1}. A more detailed investigation of k_{fs} in theta solvent systems at lower concentrations than those examined here would be required before any definite conclusions could be drawn.

Equation (2.58) shows that for theta solvent systems, the reptation model predicts that D_s scales with molar mass as M^{-2} in the semidilute region. Therefore, a plot of D_sM^2 against log ϕ should unify data above ϕ^* for different molar masses under the same solvent conditions. Variations due to temperature T and solvent viscosity η_0 will also be removed

if $D_s M^2 \eta_0/T$ is plotted. Diffusion data for different molar mass polystyrenes in deuterated and undeuterated cyclohexane (C_6D_{12} and C_6H_{12}) at the theta temperatures for these two systems are plotted this way in Fig. 4.5. The viscosities of C_6H_{12} and C_6D_{12} were taken to be equal and were calculated using an expression given in [135]. The data for M = 130,000 and 360,000 g mol^{-1} in C_6H_{12} were measured by Wesson et al. [142] using forced Rayleigh scattering. The data for 110,000 g mol^{-1} polystyrene in C_6D_{12} were measured by Callaghan and Pinder [143] using PGSE NMR. The two points for M = 360,000 g mol^{-1} from [142] agree well with the data from this work and the M = 130,000 g mol^{-1} data merge well with the M = 110,000 g mol^{-1} data of Callaghan and Pinder. However, the 350,000 g mol^{-1} data differ slightly from the 110,000 g mol^{-1} data at higher concentrations. Similar behaviour is observed when the self diffusion coefficient of polystyrene in carbon tetrachloride [62] is plotted as $\log(D_s M^2)$ against C, and also, to a lesser extent, for the polystyrene-benzene system.

Data for the 350,000 g mol^{-1} polystyrene in benzene and carbon tetrachloride are also available [62], so it is possible to examine the dependence of D_s on solvent quality by plotting $D_S\eta_0/T$ against concentration for polystyrene in deuterated benzene, (C_6D_6), deuterated cyclohexane, (C_6D_{12}) and carbon tetrachloride, (CCl_4) as is done in Fig. 4.6. At low concentrations, D_s is higher in the theta solvent than it is in good solvents. This is to be expected because the hydrodynamic radius at infinite dilution decreases with decreasing solvent quality. Above C^*, the reptation model predicts that D_s has a concentration scaling exponent of -1.75 in a good solvent and -3 in a theta solvent. The exponent for the good solvent data is expected to approach -3 as the concentration increases and the semidilute theta region is entered. This behaviour is observed in Fig. 4.6 which clearly shows that the theta solvent data and the good solvent data merge at high concentrations.

Relatively few measurements of the self diffusion of a polymer in a theta solvent are available for comparison. The measurements of D_s for polystyrene in cyclohexane reported by Wesson et al. [142] cover only a limited range of concentration. More recently, Deschamps and Léger [144] have published the results of forced Rayleigh scattering measurements of D_s for polystyrene in cyclopentane, C_5H_{10}. Their results are plotted in Fig. 4.7 along with the cyclohexane results which were mentioned previously. The assumption of M^2 scaling reduces the data to a reasonably well defined common line with a slope of approximately -3. However, at high concentrations, the measurements reported here fall below this curve.

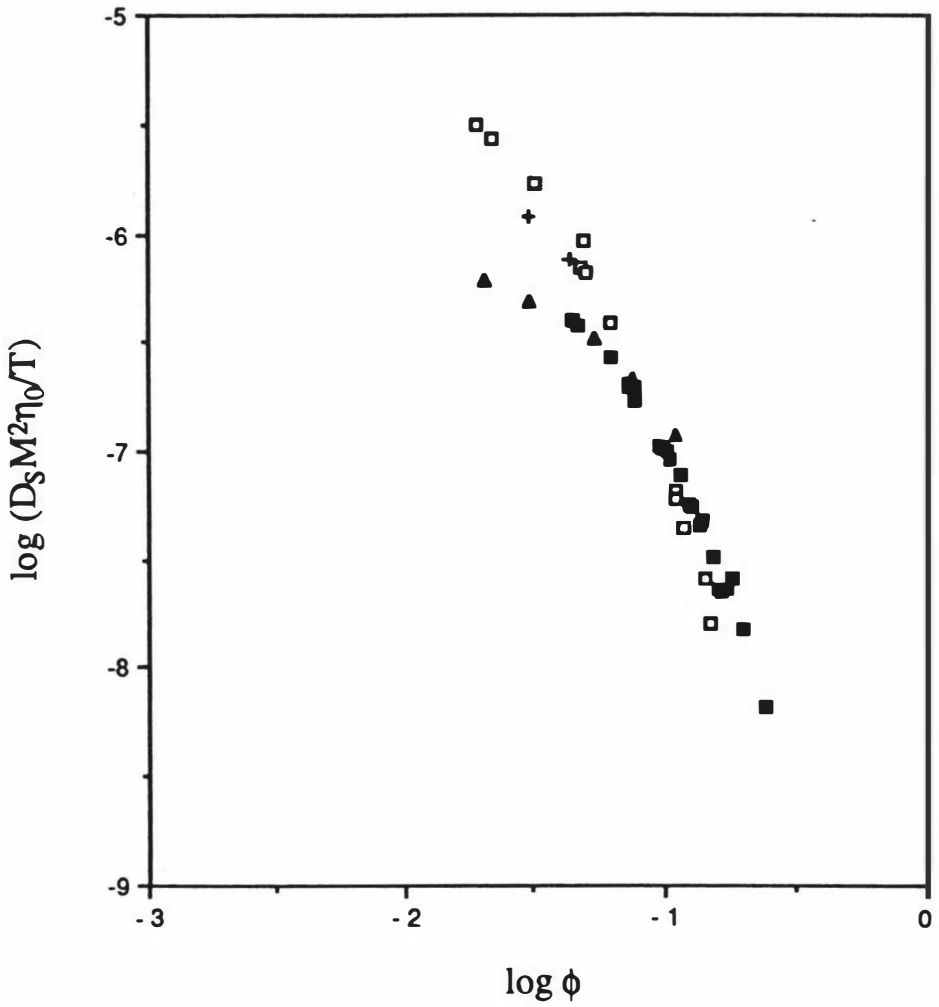

Figure 4.5 Collected data for polystyrene self diffusion in cyclohexane plotted as $\log(D_sM^2\eta_0/T)$ vs $\log \phi$, where ϕ is the polymer volume fraction. The data were obtained from; this work (▫ 350 kg mol^{-1}), Callaghan and Pinder, [143] (■ 110 kg mol^{-1}) and Wesson et al., [142] (▲ 130 kg mol^{-1} and + 360 kg mol^{-1}). The solvent was C_6D_{12} in the first two cases and C_6H_{12} in the second two.

It should be noted at this stage that there are considerable experimental difficulties in the forced Rayleigh scattering (FRS) measurements on polymers in theta solvents. Wesson et al. and Deschamps and Léger have both remarked on anomalous signals detected in their experiments, particularly at higher concentrations. After an exhaustive investigation, Deschamps and Léger concluded that the anomalous signal was due to a local change in the polymer concentration caused by the photoexciting pulse employed in an FRS experiment. The FRS technique requires the labeling of a proportion of the polymer molecules with photochromic groups which are excited during a measurement. The solvent quality is

poorer for the photoexcited molecules than for those which are not excited and localized partial phase separation occurs after the initial exciting pulse. Deschamps and Léger concluded that the long time part of their signal was unaffected because the decay of the concentration modulation by mutual diffusion is expected to be a much more rapid process than self diffusion. However, an element of doubt about these measurements must persist, because the time taken for the decay of a concentration fluctuation depends not only on the magnitude of the mutual diffusion coefficient, but also on the extent of the initial concentration gradient.

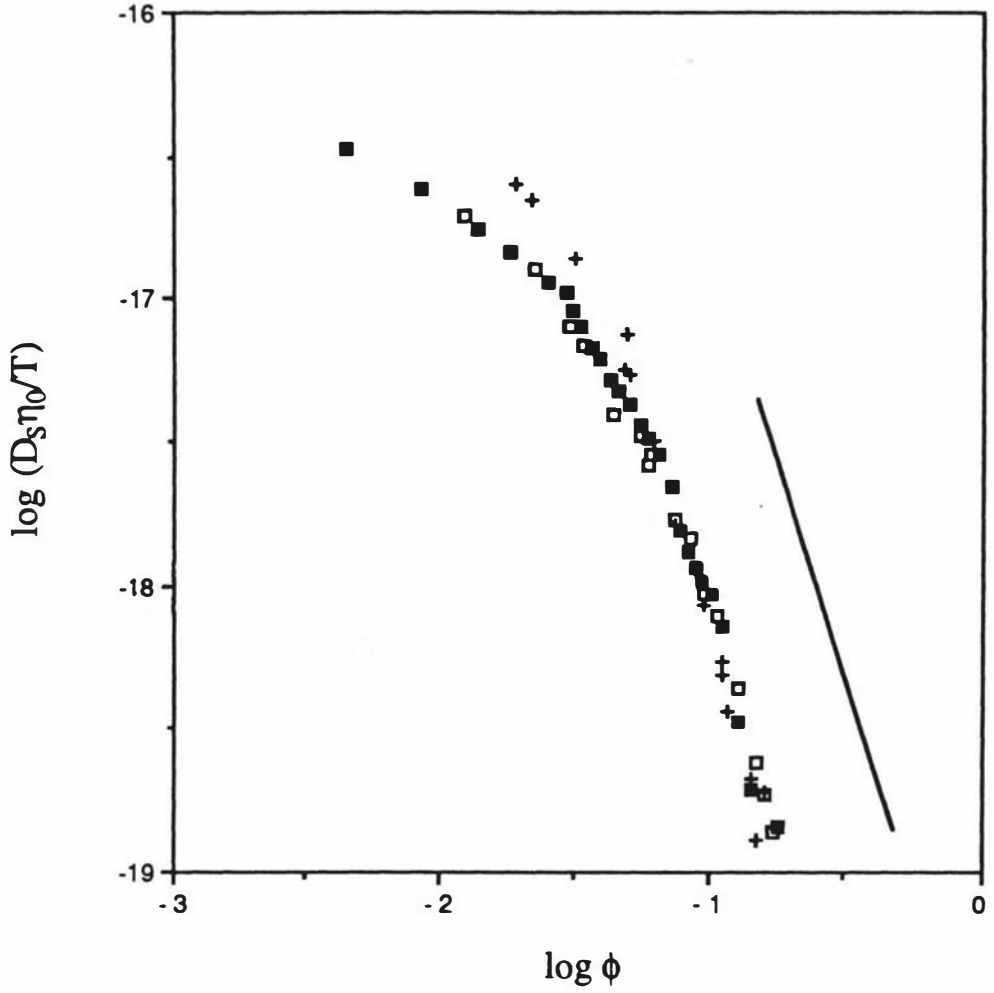

Figure 4.6 The reduced self diffusion coefficient of 350 kg mol^{-1} polystyrene in; C_6D_6 (□), CCl_4 (■) and C_6D_{12} (+). At low concentrations, the self diffusion coefficient of polystyrene in the theta solvent is greater because of the smaller value of R_H in dilute solutions at the theta temperature. A line of slope –3 is shown for comparison.

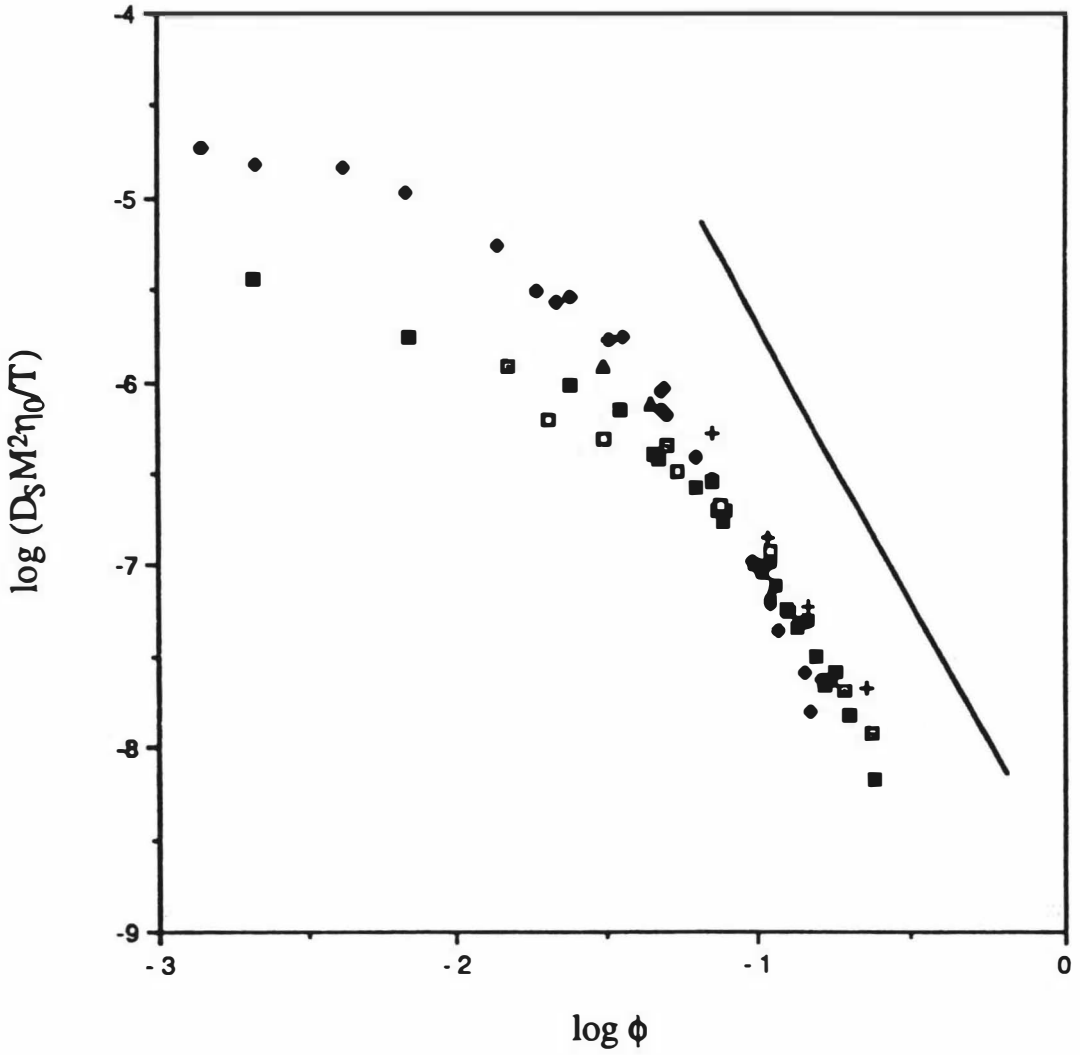

Figure 4.7 Polystyrene self diffusion in theta solvents. The molar masses (in kg mol^{-1}) and solvents are; 262 (■), 657 (+), 861 (●) in C_5H_{10} (Léger, [144]); 130 (□), 360 (▲) in C_6H_{12} (Wesson, [142]); 110 (■) in C_6D_{12} (Callaghan and Pinder, [143]); 350 (●) in C_6D_{12} (this work). A line of slope –3 is shown for comparison.

Marmonier and Léger [145] have remarked that a universal curve is obtained when $\log(D_S/D_0)$ is plotted against C/C^*. In their experiments on matrix effects on self diffusion in a good solvent, they found that for a probe polymer (N) of much lower molar mass than the matrix polymer (P), the exponent for the concentration dependence agreed with that expected from the reptation model (-1.75). This result is consistent with the expectation that the reptation model should be most successful in describing the motion of a shorter labeled chain in a matrix of long polymers which effectively provide fixed constraints. When N = P, they found that the concentration scaling region was narrower and the exponent changed gradually towards -3 as C was increased. This behaviour would be

predicted on the basis of crossover effects as the concentration approaches C^{**}. They corrected their raw data for the increase in the effective local viscosity which occurs as the glass transition is approached. This correction was made by multiplying their D_s values by $D_{spiro}(\phi=0) / D_{spiro}(\phi)$ where $D_{spiro}(\phi)$ is the self diffusion coefficient of a small dye molecule (approximately the size of a monomer) in a solution of small, unentangled polymer chains at volume fraction ϕ.

In their discussion, they attribute the difference between the $N << P$ results and the $N = P$ results to effects (such as constraint release) which are additional to pure reptation. As was noted earlier, the theta solvent data show C^{-3} scaling which is in agreement with the prediction of the reptation model. This is rather surprising in view of the fact that the good solvent data show clear evidence of constraint release and/or contour length fluctuation effects. Deschamps and Léger used the following argument to resolve this apparent inconsistency. In the presence of constraint release effects, D_s is usually written as

$$D_s = D_{rept} + D_{cr} \ . \tag{4.4}$$

When the expression for D_{cr} is adapted from its original form, relevant to polymer melts, to the semidilute solution case, the result is

$$D_{cr} = k_{cr} D_{rept} (g/N)^2 (N/P)^3 \tag{4.5}$$

where D_{rept} is the reptation diffusion coefficient and k_{cr} is a constant which varies according to the model used for the calculation. If $N = P$, the value of D_{cr} depends on $(g/N)^2$. In the good solvent limit, $(g/N)^2$ scales as $(\phi/\phi^*)^{-5/4}$ whereas the theta solvent limit gives $(\phi/\phi^*)^{-2}$. This indicates that the constraint release contribution to D_s decreases more rapidly with increasing concentration in the theta solvent case than it does in the good solvent case.

Kim et al. [146] have also performed experiments to investigate matrix effects on self diffusion in semidilute solutions. They measured D_s as a function of matrix molar mass for different values of the probe molar mass and matrix concentration. The value of D_s decreased and then became independent of P as P was increased to 3-4 times N. The limiting value of D_s was designated as D^{∞}. Kim et al. [146] found that a plot of $\log[D^{\infty}/D^{\infty}(C^*)]$ against C/C^* brought their data for four different molar masses onto a single curve. No corrections for the increase in the effective local viscosity near the glass transition were made.

The combined good and theta solvent data plotted in previous figures are plotted as $\log[D_s/D_0]$ against C/C^* in Fig. 4.8. The values of D_0 for polystyrene in the solvents represented in Fig. 4.8 were obtained from the following sources; [139] for CCl_4, [41] for

C_6H_6 and [135] for C_5H_{10} and C_6H_{12}. The value of C^* for the good solvent data was calculated using Adam and Delsanti's equation for C^* for polystyrene in benzene [41]. (It should be remembered that C^* is not an experimentally well defined quantity.) Where necessary, temperature and solvent viscosity corrections were made to the values of D_0 found in the literature.

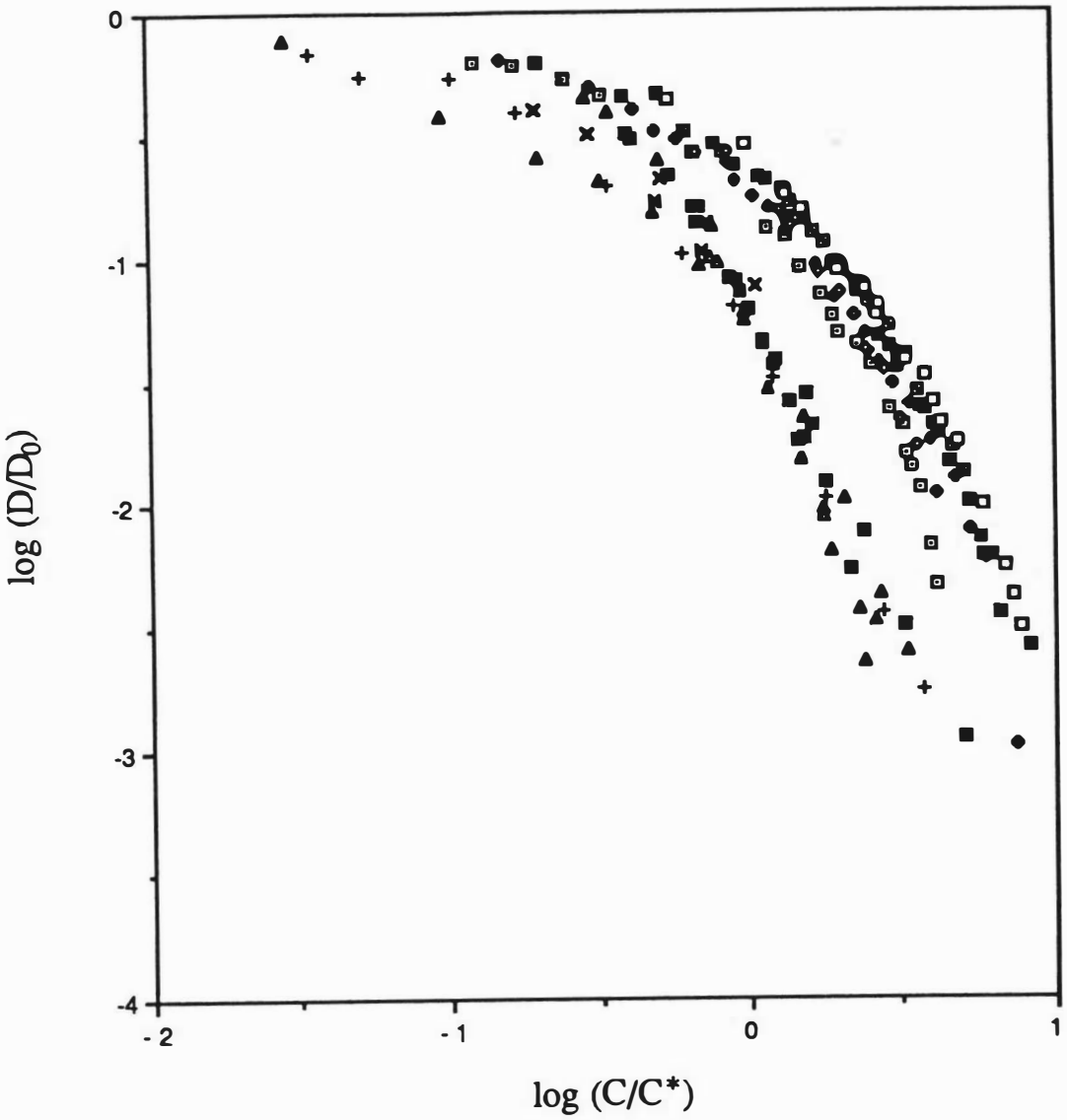

Figure 4.8 Collected data for polystyrene self diffusion in good and theta solvents plotted as $\log(D_s/D_0)$ vs C/C^*. The molar masses (in kg mol^{-1}) and solvents are:

▫ 110, CCl_4	• 110, C_6D_6	▲ 262, C_5H_{10}	■ 110, C_6D_{12}
• 233, CCl_4	■ 233, C_6D_6	■ 657, C_5H_{10}	× 130, C_6H_{12}
■ 350, CCl_4	▫ 350, C_6D_6	+ 861, C_5H_{10}	▲ 350, C_6D_{12}
			✖ 360, C_6H_{12}

Fig. 4.8 is similar to the plot given by Deschamps and Léger [144]. The good solvent data form one curve and the theta solvent data form another. However, in contrast to the plot given in [144], Fig. 4.8 shows a molar mass dependence in the good solvent data. It becomes more pronounced at high values of C/C^* and is most severe for the 110,000 g mol^{-1} points. The theta solvent data do not show any sign of a spread according to molar mass. If the spread in the good solvent data is due to local friction effects, these effects would therefore appear to be solvent dependent. On the other hand, if the spread is due to constraint release or contour length fluctuation corrections to D_s, these results differ from those of Léger, who found a universal curve independent of N after applying corrections for the increase in the effective local viscosity, even for N=P [145]. Note that Léger appears to have corrected the good solvent data, but not the theta solvent (cyclopentane) data for local friction effects [144]. Another possible explanation for the spread of the good solvent data is the crossover from semidilute good to semidilute theta conditions as the concentration is increased. The concentration at which this crossover occurs is expected to be the same for all molar masses (eqn (2.19)) so it will occur at a different value of C/C^* for each molar mass for the good solvent data in Fig. 4.8. The crossover does not occur for solutions which are already at the theta condition.

Crossover effects can be accounted for by using the blob model. The analysis in Appendix 3 suggests that when the mechanism for diffusion is purely reptation, a universal plot should be obtained by plotting $D_s/D_s(\theta)$ against $(C/C^*_\theta)/(\tau/\tau^*)$. The data of Kim et al. [146] probably satisfy the requirement for pure reptation, but $D_s(\theta)$ is unknown for the polystyrene-toluene system. One way of avoiding this problem would be to simply plot D_s/C^{-3} because D_s would be expected to scale as C^{-3} under theta conditions. It is possible to do slightly better than that by using an approximate fit to the theta solvent data collected in Fig. 4.7. The data in the power law region of the plot of log $(D_sM^2\eta_0/T)$ against C can be approximately described by

$$\log (D_sM^2\eta_0/T) = -1 - 3 \log C \ . \qquad (4.6)$$

Taking θ = -41°C [6] for polystyrene in toluene and C^*_θ / τ^* = 7400 kg m^{-3} (see Appendix 3), the plot shown in Fig. 4.9 is obtained. Data measured at concentrations below C^* have been omitted as have data for probe molar masses less than 100,000 g mol^{-1}. Fig. 4.9 shows some interesting features. For each molar mass, the slope just above C^* is consistent with the asymptotic slope of the theoretical curve. This is in agreement with the -1.75 exponent expected for the concentration dependence of D_s in a good solvent. (Note that the asymptotic slope in Fig. 4.9 is determined by log $D_s/D_s(\theta)$ giving -1.75+3 = 1.25.) As the concentration is increased, the curve for each molar mass flattens out, indicating a change in the effective exponent from -1.75 to -3. The concentration at which

the change occurs increases with decreasing molar mass, a feature which was also noted by Callaghan and Pinder [62] in their work on the self diffusion of polystyrene in good solvents with N = P. If the change in slope was due to crossover from the semidilute good to the semidilute theta regions of the τ - C diagram, it would be expected to occur at the same concentration, C^{**}, for all molar masses. An alternative explanation is that the change in slope occurs due to a molar mass dependent increase in the effective local friction. Attempts have often been made to quantify the local friction effect by measuring the self diffusion coefficient of a small molecule in the solution. Such measurements give a friction factor having a concentration dependence which is approximately independent of the polymer molar mass (provided that the molar mass is high enough for T_g to be molar mass independent - see eqn (2.48)). However, the friction factor of a small probe molecule cannot give a completely adequate analogue of the effect of concentration on the effective friction on a polymer chain. Kim et al. [146] have pointed out that a small probe molecule is not equivalent to the hydrodynamically screened unit (blob) which determines dynamic behaviour in the semidilute region. They estimated the concentration at which the effective local friction becomes important by plotting the value of D_s at C^* for each molar mass (obtained by interpolation of their data) against C. This assumes that the effective local friction does not depend on molar mass. The deviation of this quantity from power law behaviour was taken as indicative of a deviation of the local effective viscosity from η_0. An alternative indirect measurement of the effective local friction might be possible by observing the deviation of the cooperative diffusion coefficient D_c from power law behaviour with a plot similar to Fig. 4.9. Such an investigation would be free of the extra complexities introduced by constraint release and contour length fluctuations which affect self diffusion measurements.

In summary, the discussion above indicates that crossover effects, the increase in local friction near the glass transition, constraint release and contour length fluctuations probably all affect the self diffusion coefficient of a monodisperse polymer in a good solvent. The crossover effect is eliminated when a polymer in a theta solvent is studied, and the arguments of Deschamps and Léger discussed above indicate that constraint release effects are also less important under theta conditions. The differences between the theta solvent data of this work and the data of Deschamps and Léger [144] seen in Fig. 4.7 are probably due to local friction effects, which can be expected to be solvent dependent. The local friction effect appears to be less severe in the cyclopentane data of Deschamps and Léger [144] than it is for the cyclohexane or carbon tetrachloride data. It is worth noting that the viscosity of cyclopentane is considerably lower than that of cyclohexane or carbon tetrachloride, even after the difference in temperature is taken into account. If the plot given by Ferry (Fig. 17.1 of [50]) is used as a guide, it seems to indicate that low viscosity solvents tend to be more effective than high viscosity solvents in lowering the glass

transition temperature of polystyrene solutions. The data of Fig. 4.5 and the discussion of the results of Kim et al. given above imply that when the local friction effect appears, it is molar mass dependent.

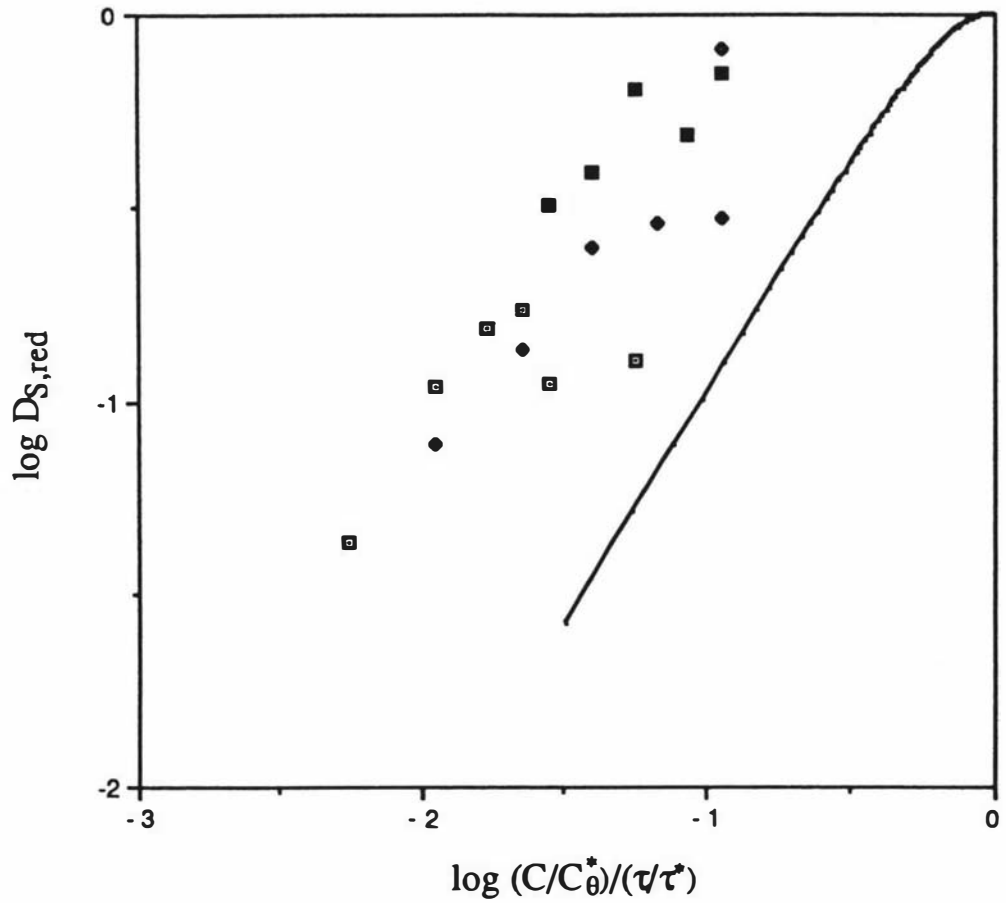

Figure 4.9 The reduced self diffusion coefficient $(D_S M^2 \eta_0/T)/(D_{S\theta} M_\theta^2 \eta_{0\theta}/T_\theta)$ obtained from the data of Kim et al. [146]. The molar masses in kg mol^{-1} are: ▫ 1800; • 900; ▪ 390; • 100. The curve is the theoretical prediction of the blob model (see Appendix 3). The values of τ and C^*_θ/τ^* were taken as 0.208 and 7400 kg m^{-3}. These quantities are very difficult to estimate for a polymer in a good solvent so the horizontal shift between the theoretical curve and the data points is not a serious problem.

4.2 Solvent Diffusion

4.2.1 Experimental

Two sets of experiments on the concentration dependence of solvent diffusion in polystyrene-cyclohexane solutions were performed. In the first set, the solvent was undeuterated cyclohexane (C_6H_{12}) and in the second it was deuterated cyclohexane (C_6D_{12}). The polystyrene was the same as that used in the polymer diffusion measurements (M = 350,000 g mol^{-1}).

The initial experiments were done on the samples containing C_6H_{12} as the solvent. The range of concentrations covered was comparable with that investigated in the polymer diffusion experiments. Due to the convection effects which were discussed in section 4.1.1, it was difficult to obtain consistent measurements of D_s for C_6H_{12} at low polymer concentrations (below approximately 30 kg m^{-3}). The value of D_s measured for pure cyclohexane was occasionally up to 20% higher than the value inferred from published data. Therefore, it was necessary to use an improved temperature control system for the low concentration samples. The temperature control system adopted for these experiments uses water for heat transfer, so that proton NMR was not suitable for these experiments. Instead, samples were made with C_6D_{12} as the solvent and the deuterium NMR signal was used for the PGSE experiments. The gyromagnetic ratio γ of the deuterium (^2H or D) nucleus is smaller by a factor of 6.5 than that of the ^1H nucleus, giving a decrease in the signal to noise ratio by a factor of approximately 100 [74]. The reduced signal to noise ratio was not a problem because the samples were almost 100% deuterated cyclohexane.

All measurements were made at 40.5°C, which was also the temperature at which the polymer diffusion measurements were made. Although the theta temperature for the polystyrene C_6H_{12} system is several degrees lower than it is for the polystyrene C_6D_{12} system, no difference in the solvent diffusion coefficients was detected.

The JEOL air flow temperature controller was used to maintain the temperature for the proton NMR measurements. A much more stable temperature controller kindly loaned by Dr K. Jolley was used for the deuterium NMR measurements. Water is pumped from a very stable thermostat to a double pass water jacket surrounding the entire sample tube. The flow rate is high enough so that a minimal drop in the temperature of the control water occurs in the circuit. The temperature is measured using a thermocouple placed in the water outlet pipe of the sample holder. The temperature stability provided by this system is ±0.0008 °C which is more than adequate for these experiments. Temperature gradients

along the tube are eliminated with this temperature control system. A detailed description of the temperature controller is available in reference [147].

The polystyrene gave a small contribution to the signal in the proton PGSE NMR experiments. The diffusion coefficients of the polymer and solvent differ by a factor of 80 at infinite dilution with the difference increasing rapidly as C is increased. The polymer signal was therefore hardly attenuated at all over the range of k values used in the solvent diffusion measurements. At the lowest polymer concentrations the polymer signal was negligible. For polymer concentrations above 30 kg m^{-3} the echo attenuation plots were analyzed by approximating the data by an exponential decay plus a constant baseline. The exponential decay was due to the attenuation of the solvent signal and the constant baseline is a good approximation to the comparatively very slowly attenuated polymer signal. A first approximation to the baseline was obtained from the large k portion of the echo attenuation plot. The baseline was then subtracted from A(k)/A(0) and ln[A(k)/A(0)] was replotted. The baseline was modified and the data replotted until ln[A(k)/A(0)] gave a straight line, the slope of which was calculated using a linear least squares fit to yield D_s. This procedure gave results in good agreement with a direct fit to A(k)/A(0) using a nonlinear curve fitting program which became available later.

There was no signal from the polymer in the deuterium NMR experiments so the diffusion coefficient was obtained by a straightforward linear least squares fit to the plot of ln[A(k)/A(0)] against k.

4.2.2 Results

Representative echo attenuation plots for PS-C_6H_{12} and PS-C_6D_{12} solutions respectively are shown in Fig. 4.10 and 4.11. The effect of the polystyrene signal is clearly seen in Fig. 4.10. With no baseline subtracted, the echo attenuation plot levels off at approximately ln[A(k)/A(0)] = –3.5 giving an approximate value of B as 0.03. The initial slope of the echo attenuation plot is only weakly influenced by such a small value of B. For concentrations less than 30 kg m^{-3}, B was taken as zero.

The concentration dependence of D_s for C_6H_{12} in PS-C_6H_{12} solutions is shown in Fig. 4.12. Each error bar represents the error in the slope obtained from a linear least squares fit to an echo attenuation plot.

Fig. 4.13 shows the concentration dependence of D_s for C_6D_{12} in dilute PS-C_6D_{12} solutions. Each point is the average value obtained by repeating the experiment three or four times and the error bar represents the spread of values.

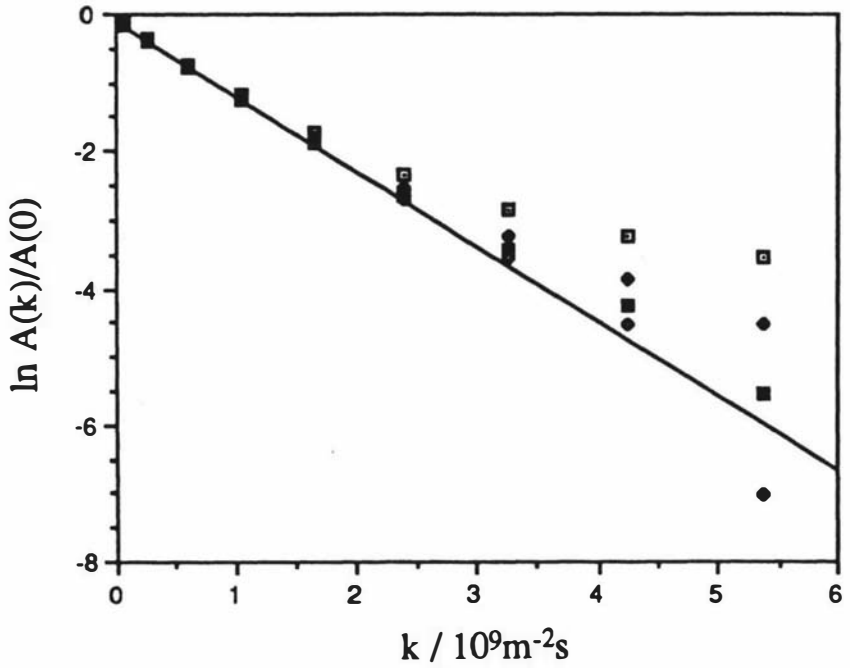

Figure 4.10 The echo attenuation plot for a solvent diffusion measurement using proton PGSE NMR. The sample was a solution of polystyrene (M = 350,000 g mol^{-1}) in cyclohexane (C_6H_{12}) with C = 167 kg m^{-3}. The polymer signal is not attenuated over the range of k values used in this experiment and is well approximated by a flat baseline. The echo attenuation plots after baseline subtraction are shown: ▫ B = 0; • B = 0.018; ▪ B = 0.025; • B = 0.028. The baseline was increased until the resultant echo attenuation plot was a straight line. After the baseline was subtracted from the data, the solvent diffusion coefficient was obtained from a linear least squares fit to the first four points.

4.2.3 Discussion

The self diffusion of pure cyclohexane has been studied by several groups [148, 149, 150]. The most precise measurements are those of Mills [149] which were made using radioactive tracer methods. Mills measured D_s for $C_6H_{11}T$ and $C_6D_{11}T$ at 25°C and concluded that there was no isotope effect to within experimental error (±0.3%). The average of Mills' results taken to three significant figures is 1.46×10^{-9} m^2s^{-1}. The measurements presented here were made at 40.5°C so Mills' result is not directly comparable. However, if it is assumed that the Stokes-Einstein relation is valid for cyclohexane and that the hydrodynamic radius does not change with temperature (see [150] for an interesting discussion of this point), D_s at 40.5°C can be estimated by using a simple temperature and viscosity correction. Taking the viscosity of cyclohexane at 25°C and 40.5°C as 8.89×10^{-4} Pa s and 6.95×10^{-4} Pa s respectively, it is found that $D_s(40.5°C) = 1.96 \times 10^{-9}$

m^2s^{-1}. Both O'Reilly et al.[148] and Jonas et al.[150] have studied the temperature dependence of the self diffusion coefficient of cyclohexane by NMR methods. The expression given by O'Reilly et al. for the temperature dependence of D_S gives $D_S = 1.34 \times 10^{-9}$ m^2s^{-1} at 25°C which clearly disagrees with the results of Mills. On the other hand, Jonas et al., whose measurements were all performed at temperatures greater than or equal to 40°C found $D_S(40°C) = 1.92 \times 10^{-9}$ m^2s^{-1} which agrees with the estimate given above. Since NMR measurements of diffusion require accurate calibration to give accurate values of D_S, it is possible that the calibration factor used by O'Reilly et al. was incorrect. When the normalization of the expression for the temperature dependence of D_S given by O'Reilly et al. is adjusted to give Mills' value at 25°C, the result is $D_S(40.5°C) = 1.93 \times 10^{-9}$ m^2s^{-1} which is consistent with the values given above. This value will be used in all further discussion.

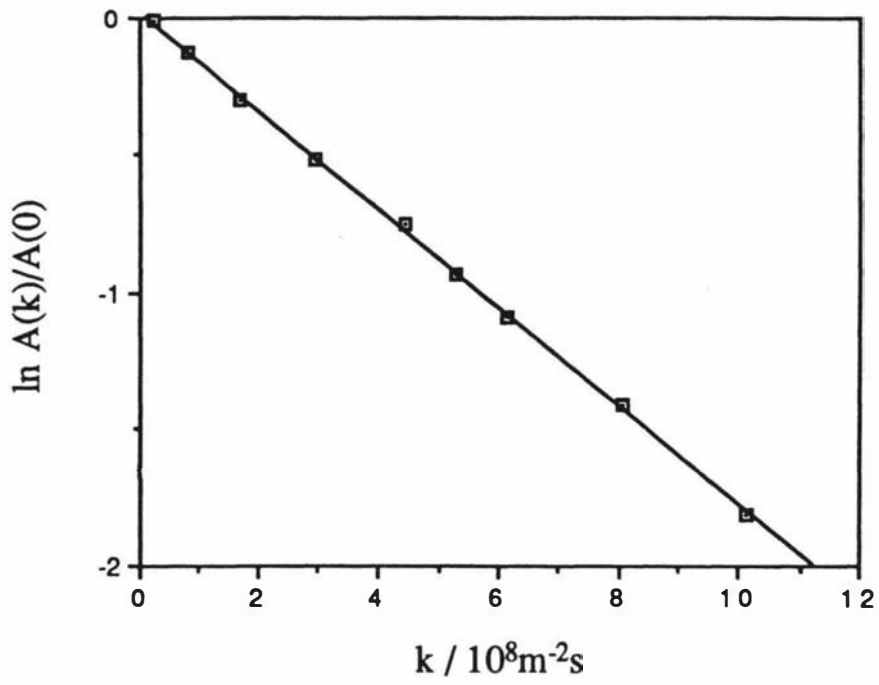

Figure 4.11 The echo attenuation plot for a solvent diffusion measurement using deuterium PGSE NMR. The sample was a solution of polystyrene (M = 350,000 g mol^{-1}) in deuterated cyclohexane (C_6D_{12}) with C = 17.3 kg m^{-3}. A linear least squares fit to the data gives $D_S = (1.79 \pm 0.01) \times 10^{-9}$ m^2s^{-1}.

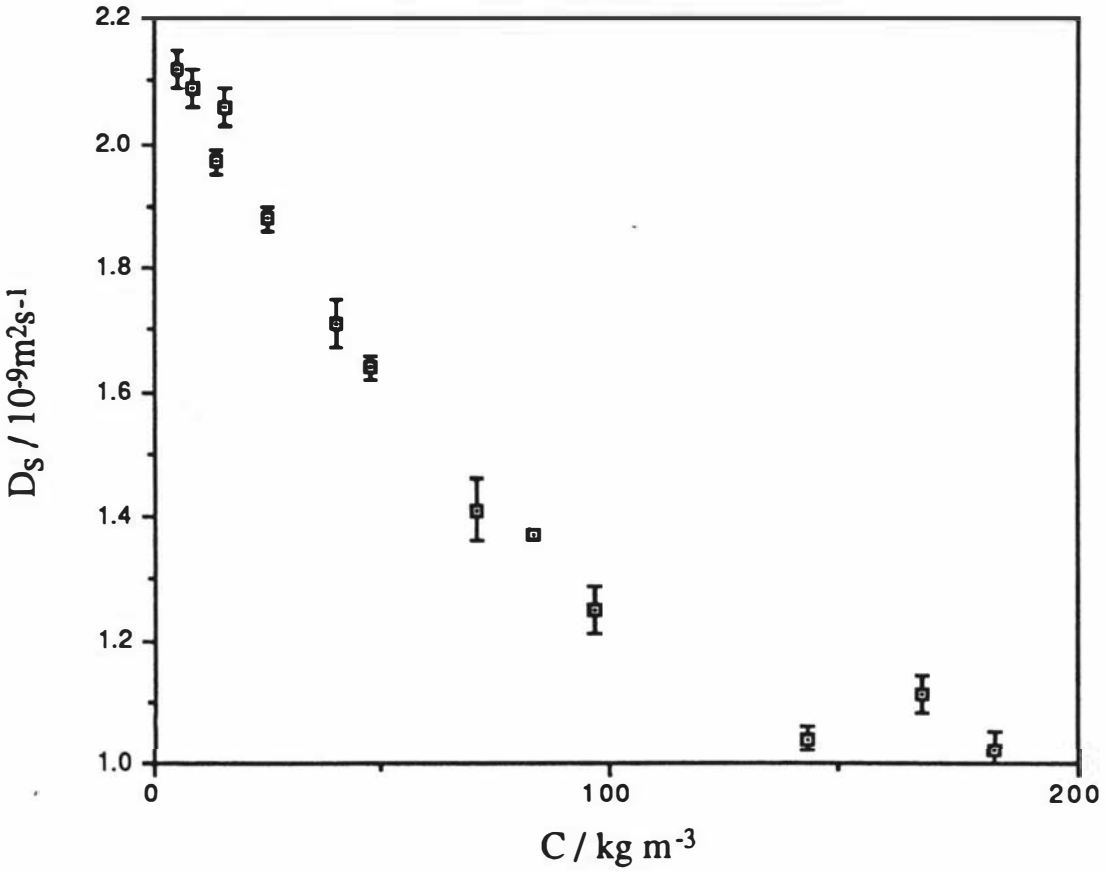

Figure 4.12 The concentration dependence of solvent self diffusion in PS-C_6H_{12} solutions.

The value of the solvent self diffusion coefficient at infinite dilution, D_0, is higher than the expected value in the case of the proton NMR measurements on PS-C_6H_{12} solutions. This can be attributed to the convection effects mentioned earlier. The deuterium NMR measurements on the PS-C_6D_{12} solutions give a value of D_0 which is within experimental error of the expected value. In this case, the convection effects have been eliminated by using a more effective temperature control system.

Measurements of solvent self diffusion in PS-C_6H_{12} solutions have also been made by Kosfeld and Goffloo [151] and Blum, Pickup and Foster [152] by NMR methods. Yu and Torkelson [153] have recently measured diffusion limited phosphorescence quenching interactions between benzil and anthracene in various polymer solutions including PS-C_6H_{12}. They identified the ratio of quenching rate constants k_q/k_{q0} with the ratio of solvent self diffusion coefficients D_s/D_0. The results from this work and some of the data from the papers mentioned above [151, 152, 153] are plotted together in Fig. 4.14.

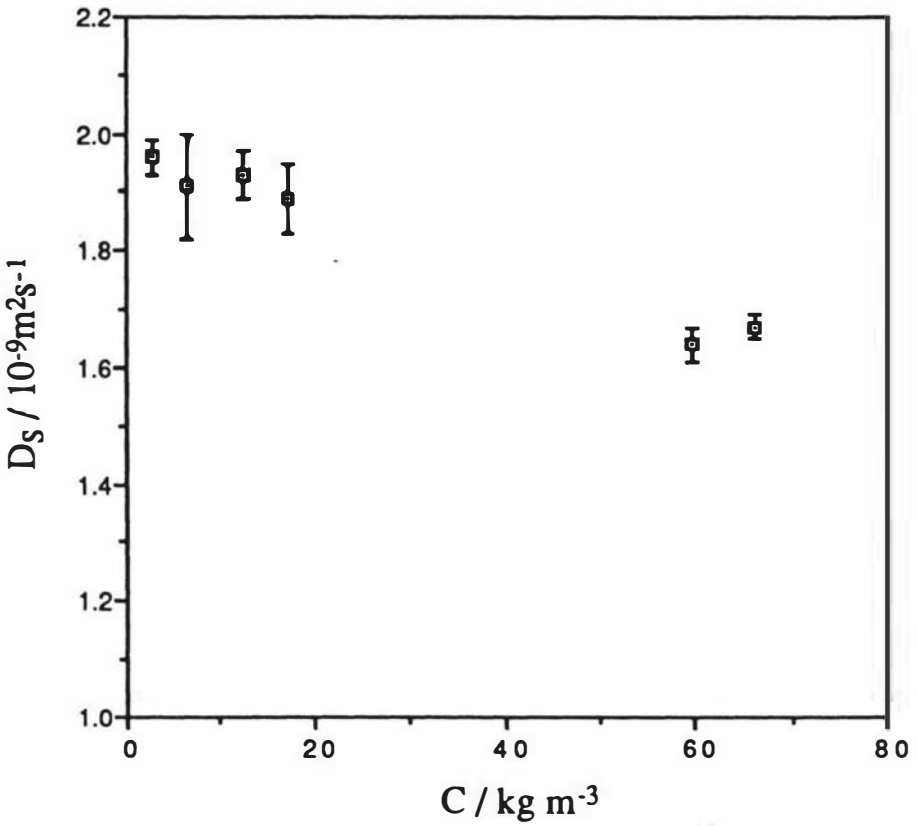

Figure 4.13 The concentration dependence of solvent self diffusion in PS-C_6D_{12} solutions.

Fig. 4.14 shows that the results of this work are generally consistent with the results of Kosfeld and Goffloo [151] and Blum, Pickup and Foster [152]. Kosfeld and Goffloo's value of D_0 (taken as accurately as possible from the 40°C curve on the plot in [151]) seems high and could indicate that convection effects were also present at low concentrations in their experiments. The results of Yu and Torkelson [153] are clearly inconsistent with the rest of the data at concentrations below 300 kg m^{-3}. This may mean that their identification of k_q/k_{q0} with D_s/D_0 is in error.

A striking feature of solvent diffusion measurements noted by several workers [152, 157] is the general insensitivity of a plot of D/D_0 against concentration to solvent quality and polymer molar mass.

In 1967, Boss, Stejskal and Ferry [154] reported measurements of benzene self diffusion in benzene-polyisobutylene solutions at 70.4°C. Their results showed an enhancement of D_s at low polymer concentrations. However, when their reported value of D_0 for pure benzene at 70.4°C (5.40×10^{-9} m^2s^{-1}) is compared with the value obtained from the very accurate expression for the temperature dependence of D_s given by Collings and Woolf

[155], (4.23×10^{-9} m^2s^{-1}) a significant discrepancy is apparent. It is likely that this discrepancy also results from convection effects associated with the air flow temperature control system.

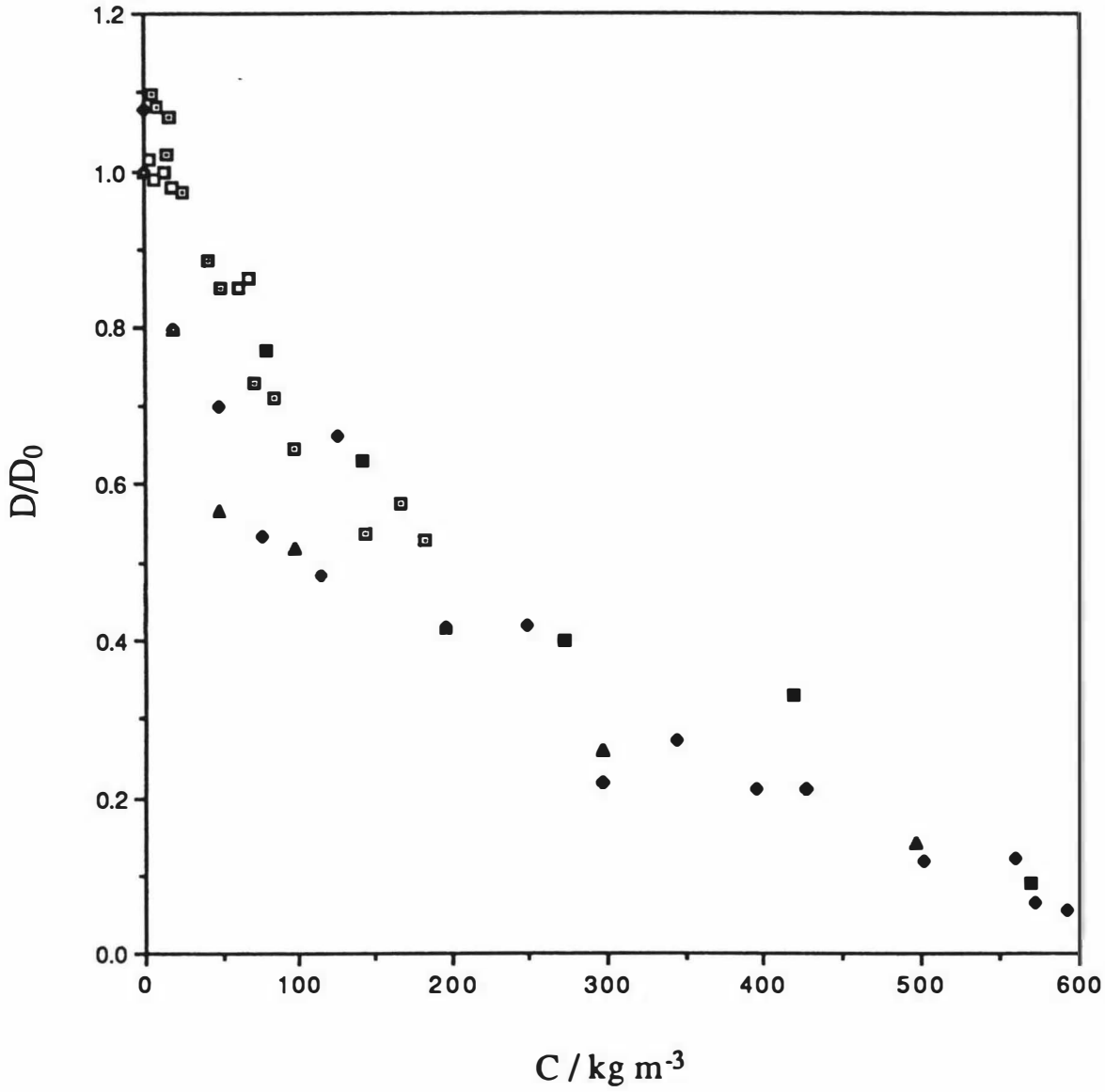

Figure 4.14 Concentration dependence of the reduced self diffusion coefficient D_S/D_0 for cyclohexane in polystyrene-cyclohexane solutions.

Key:

▫ PS-C_6H_{12}, ▫ PS-C_6D_{12}, T = 40.5°C, M = 350,000 g mol^{-1} (this work)

• PS-C_6H_{12}, T = 40°C, M not specified (Kosfeld [151])

■ PS-C_6H_{12}, T = 25°C, M = 25,000 g mol^{-1} (Blum [152])

▲ PS-C_6H_{12}, M = 4,000 g mol^{-1}, ● PS-C_6H_{12}, M = 47,000 g mol^{-1} (Yu [153])

Free volume theory is usually used to interpret solvent self diffusion data at high polymer concentrations. The usual way of describing the concentration dependence at a fixed value of T is to use the following extension of the argument leading to eqn (2.47).

The friction factor for self diffusion is expected to vary as

$$\zeta = \zeta_r \exp B\left(\frac{1}{f} - \frac{1}{f_r}\right) \tag{4.7}$$

where ζ_r and f_r are the friction factor and the fractional free volume at an arbitrary reference concentration. If the free volumes contributed by polymer and solvent are assumed to be linearly additive, the total free volume at a given concentration becomes

$$f = f_r + \beta(\phi_0 - \phi_{0r}) \tag{4.8}$$

where ϕ_0 is the solvent volume fraction. A straightforward rearrangement of eqn (4.7) gives

$$\ln(D/D_r) = \frac{B\beta(\phi_0 - \phi_{0r})}{f_r^2 + f_r\beta(\phi_0 - \phi_{0r})} \tag{4.9}$$

so that a plot of $1/[\ln(D/D_r)]$ against $1/(\phi_0 - \phi_{0r})$ should give a straight line with slope f_r^2/β and intercept f_r if B is taken as 1 as is usually done [154, 156, 56].

The reference state is sometimes taken as the pure polymer, in which case $\phi_{0r} = 0$. In this case, since D_r is then usually impossible to measure, an iterative fitting procedure is used to find a value of D_r for which the plot of $1/[\ln(D/D_r)]$ against $1/\phi_0$ is linear [151, 154].

If the data of Kosfeld [151] for C_6H_{12} diffusion in PS-C_6H_{12} solutions at 40°C is plotted as $1/[\ln(D/D_r)]$ against $1/(\phi_0-\phi_{0r})$ with the reference concentration chosen as their highest experimental concentration, ($D_r = 1.06 \times 10^{-10}$ m^2s^{-1}, $\phi_{0r} = 0.455$) a straight line with a slope of 0.101 and intercept at 0.164 is found. These values are of the same order of magnitude as those found by von Meerwall et al. [156] for the diffusion of hexafluorobenzene in polystyrene-THF solutions and by Nemoto et al. [56] for the diffusion of methyl red in polystyrene-THF solutions. The parameters derived from this fit can be used to to apply a correction for the concentration dependent local friction to the polymer self diffusion data presented in the first part of this chapter. This type of correction has been mentioned several times in the literature [145, 156, 56] and was discussed in section 4.1.3. Here, the correction has been made by multiplying the polymer diffusion coefficients by $D(0)/D(\phi)$ where D is the solvent self diffusion coefficient. As

was mentioned earlier, $D(0) = 1.93 \times 10^{-9}$ m^2s^{-1} and $D(\phi)$ is calculated from the free volume fit discussed above. The result of this correction is shown in Fig. 4.15. A linear least squares fit to the data above ϕ^* gives a slope of -2.8 when the last point is excluded and -3.0 when it is included.

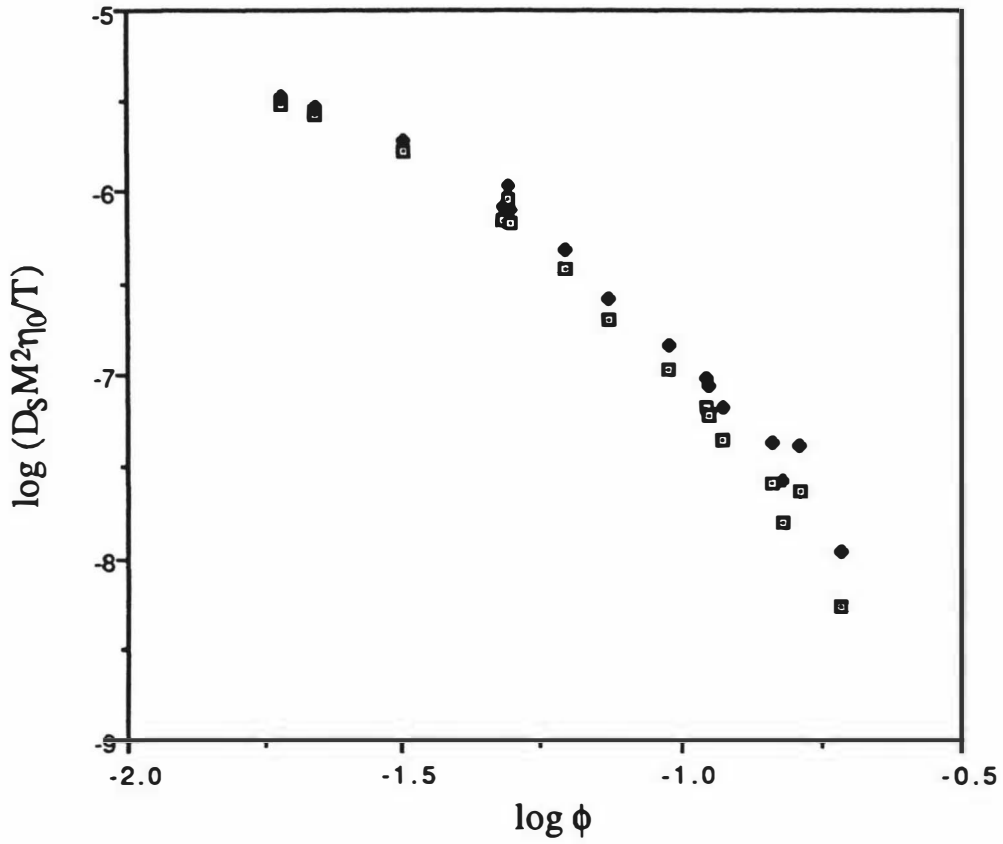

Figure 4.15 The reduced polymer self diffusion coefficient before (▫) and after (•) correction for local friction effects (M = 350,000 g mol^{-1}, T = 40.5°C).

It is well known that the basic assumptions of free volume theory are invalid at low polymer concentrations where the solution is far from the glass transition temperature [156]. In section 2.2.6, several alternative theoretical models for solvent self diffusion are discussed. The equations derived by Wang (the modified version is given in eqn (2.67)) and Jönsson (eqn (2.69)) apply to the diffusion of solvent in a colloidal dispersion of large, impermeable particles. The equation of Mackie and Meares (eqn (2.68)) describes solvent diffusion in a swollen network. These results are plotted with experimental data for cyclohexane diffusion in polystyrene-cyclohexane solutions in Fig. 4.16. It is immediately apparent that neither the modified Wang equation nor the Jönsson equation fits the data. In

fact the plot of Wang equation has the wrong shape and becomes negative at higher volume fractions. To this extent, the Jönsson equation is clearly an improvement over the Wang equation.

Although equation (2.69) accounts well for the concentration dependence of solvent self diffusion in dispersions of latex and silica spheres [73, 152], it does not fit the data for solvent diffusion in polymer solutions.

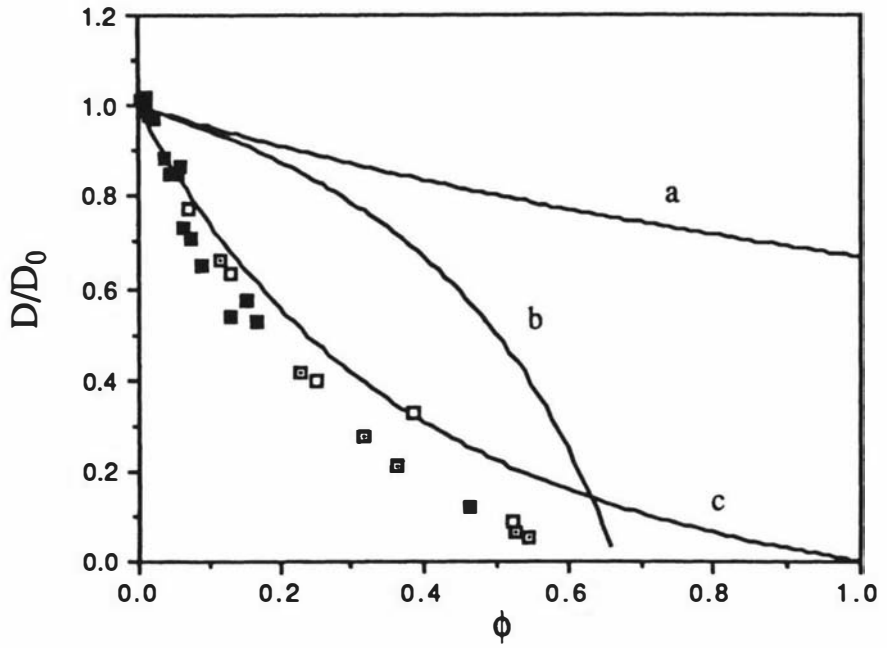

Figure 4.16 The reduced solvent self diffusion coefficient D/D_0 versus polymer volume fraction, ϕ. The data points are from Kosfeld ◘, Blum □, and this work ■. (Three of the low concentration data points from C_6H_{12} diffusion experiments which were clearly affected by convection effects have been omitted for clarity.) The curves were calculated using the theories of (a) Jönsson, (b) Wang (no hydration effect), (c) Mackie and Meares.

The equation of Mackie and Meares gives the correct qualitative behaviour but still does not fit the data well. Due to free volume effects, the data could be expected to deviate from this curve at high volume fractions. Another difficulty with the Mackie and Meares equation is that it cannot explain the slight solvent quality dependence of D_s observed by Moseley and Stilbs [157]. Also, at low polymer concentrations, the swollen network model upon which the Mackie and Meares equation is based breaks down.

The Wang and Jönsson equations can be modified to account for the effect of solvation. In the case of an aqueous solution of a globular protein, for example, it is expected that a layer of water molecules are bound to the surface of the hydrated protein. The extension of this concept to random coil polymers has been considered by Callaghan and Lelievre [158]. They derived a first order approximation to the Wang equation including solvation effects and applied it to their data on solvent self diffusion in polysaccharide solutions. Their results showed that the solvation effect is very large for random coil molecules; approximately 1.8 g of solvent per gram of solute was required to obtain a good fit to their data. This figure corresponds to a ratio of a solvation sphere radius to the hydrodynamic radius of 0.7 for dextran in water. A similar treatment of the cyclohexane diffusion data given here gives a value of approximately 2 g g^{-1}. Although this modification allows for a better fit to the data, the meaning of the extra parameter is not clear. It may comprise the dominant term in the equation used for data analysis but it cannot be measured independently [158].

5 FRACTIONATION AND CHARACTERIZATION OF PVME

Poly(vinyl methyl ether) (PVME) has been the subject of many experimental studies recently, mainly because of its compatibility with polystyrene both in blends and in ternary solutions with appropriate solvents. PVME is available from commercial sources, but only as a polydisperse and relatively poorly characterized raw material. For some of the experiments reported in Chapter 6, it was necessary to reduce the polydispersity of the original material by fractional precipitation and then characterize the fractions.

5.1 Preparation of PVME fractions

5.1.1 Raw Materials

PVME is also known as poly(methoxyethylene). The structure of PVME is shown in Fig. 5.1.

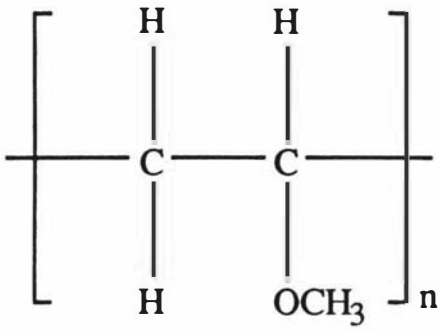

Figure 5.1 The structure of poly(vinyl methyl ether).

The PVME was obtained from two sources. At first, PVME purchased from Polysciences Inc. of Warrington, Pennsylvania USA was used. This PVME is delivered as neat polymer - an amber coloured, translucent material which is very viscous and tacky. In this form it is quite difficult to handle. Approximate molar mass characteristics for this product were provided by the manufacturers. For a typical lot, M_w obtained from static light scattering in butanone was given as 70,600 g mol^{-1} and M_n obtained from gel permeation chromatography was 31,700 g mol^{-1} so $M_w/M_n = 2.23$.

The other samples of PVME were kindly donated by GAF (Australasia) Pty Ltd, Grey Lynn, Auckland, New Zealand. GAF provides PVME in several different forms; the commercial product names of the samples obtained for this work were Gantrez M-154, M-

555 and M-574. The M-154 comes as cloudy dispersion (50% solids) in water. The specific viscosity ($\eta_{sp} = (\eta - \eta_0) / \eta_0$) at 1% w/v in benzene is quoted as 0.47 in the data provided by GAF. The M-574 is supplied in the form of a 70% solution in toluene. This product has $\eta_{sp} = 0.47$ at 1% in benzene. The M-555 is a 50% solution in toluene with $\eta_{sp} = 0.77$ at 1% w/v in benzene.

The molar masses estimated using the equation for the intrinsic viscosity of PVME in benzene at 30°C given by Manson and Arquette [159], were 45,000 g mol^{-1} (M-154, M-574) and 102,000 g mol^{-1} (M-555). The experiments which were planned required as high a molar mass of PVME as possible, so the M-555 PVME was used. Another GAF PVME, (M-556) which is described in the GAF catalogue as a high molecular weight material, was not available at the time. (However, it was later found that the difference between the molar masses of the M-555 and M-556 products is small.) GAF were not able to provide information about the polydispersity of their PVME, but it is reasonable to expect it to be approximately the same as it is for the Polysciences product.

5.1.2 Fractionation

The fractionation of a polydisperse sample of polymer into fractions with narrower molecular weight distributions can be achieved in many different ways. A general discussion of fractionation techniques is provided by Flory [161] and a recent survey of the literature on experimental methods is provided by Pollock and Kratz [162].

The solvent quality of a polymer solution can be changed by varying either the composition of the solvent or by varying the temperature. The method of fractional precipitation exploits the variation of the precipitation temperature (or solvent composition) with molar mass. This leads to two basic types of fractional precipitation.

In the first, the polymer is dissolved in a solvent chosen so that a critical solution temperature is accessible. The temperature of the solution is then raised or lowered depending on whether the lower or upper critical solution temperature is closer. The solution becomes turbid when precipitation begins. At this point, the high molar mass material is precipitating, but lower molar mass molecules are still in solution. The solution is allowed to achieve equilibrium and slowly separates into two phases, one containing the dissolved lower molar mass fraction and the other containing the precipitated higher molar mass fraction. The two phases can then be separated by removing the supernatant or the precipitate.

The second method of fractional precipitation relies on a change in solvent quality at constant temperature. The polymer is dissolved and a non-solvent is then added to the

solution until the solvent quality has been reduced to the extent that precipitation occurs. As before, the high molar mass molecules precipitate first and the separation of phases proceeds as it did in the previous case.

Flory [161] has recommended that the ratio of volumes of the supernatant and precipitated phases should be at least ten for maximum efficiency of separation. This leads to the requirement that the solution should be dilute. The suggested range of concentrations is from 0.5 to 1.0% corresponding to molar masses in the range 10^6 to 10^4 [161].

Manson and Arquette [159] have described two methods of fractionation of PVME by fractional precipitation. The first consisted of precipitation from solution in benzene by the addition of hexane, heptane or decane. This method has also been used recently by Bauer et al. [160]. The second was precipitation from aqueous solution by gradually raising the temperature. (This implies that PVME in water has a LCST close to room temperature; see Fig. 2.1.)

Both methods suggested by Manson and Arquette were tried. Precipitation by the addition of non-solvent to a solution of PVME in toluene was found to be the most convenient method for this work and will be described in more detail below. The fractional precipitation of PVME by raising the temperature of a PVME/water solution was found to have disadvantages. It is very difficult to completely remove all traces of water from the final fractions. If the polymer is to be redispersed in an organic solvent, trace contamination by water could be a severe problem. Also, the separation of the precipitated phase from the rest of the solution was very slow in this method, possibly due to a small difference in density between the precipitate and the supernatant.

It is worth mentioning here that the method of purification adopted by Kwei et al. [163] i.e. precipitation from benzene solution with methanol, only works with the crystalline form of PVME. Atactic PVME is soluble in methanol [164].

The fractionations performed in this work were the simplest variation of a potentially very sophisticated technique. The object was to reduce the polydispersity of the PVME by as much as possible with the minimum of effort. To this end, it was considered adequate to "top and tail" the distribution, i.e. to remove the low and high molar mass portions of the distribution and keep the middle fraction.

The procedure used in the fractional precipitation was as follows. The sample was dissolved in analytical grade toluene at an initial concentration of approximately 5% w/w in a 1 litre round bottomed flask. For the GAF PVME this corresponded to 10 g of the 50% solution in 100 g of toluene. (Note that the solution becomes more dilute as non-solvent is

added.) A two necked flask with ground glass stoppers is a convenient vessel for these fractionations. Other items of equipment used were; an overhead stirrer, a precise temperature controller (Thermomix 1460, B. Braun, Melsungen AG, West Germany), and a glass water bath.

The flask was placed into the water bath and the temperature was allowed to stabilize at 25°C. The solution was stirred vigorously as the non-solvent (petroleum spirit, analytical grade, boiling range 40 - 60°C obtained from BDH chemicals) was gradually added. Turbidity was first observed after the addition of approximately 350 - 400 ml of petroleum spirit. The amount of precipitate formed was adjusted by adding more non-solvent. The solution was then warmed by a few degrees to redissolve the precipitate. When the solution became clear, the thermostat was returned to its original setting, the stirrer was removed, the flask was stoppered and the solution was allowed to slowly approach equilibrium at the original temperature. When the precipitated phase had settled, the supernatant was removed with a syphon or a large syringe, taking great care not to disturb the settled layer of precipitate. The precipitate was then redissolved in toluene and completely removed from the flask. The supernatant was returned to the flask for the next precipitation. It is best to keep the supernatant warm and avoid evaporation of solvents so that the remaining PVME does not precipitate. Otherwise, it is necessary to redissolve the residue in toluene before continuing. (A convenient way of avoiding this problem would be to transfer the supernatant directly to another flask in the water bath, ready for further fractionation.)

The process was repeated with the addition of more non-solvent (approximately 120 ml) to produce the second fraction. The amount of non-solvent used to produce the second fraction varies according to the quantity of precipitate desired. An adjustment to the quantity of non-solvent must also be made if any of the solvent has evaporated or if the addition of toluene was required to redissolve unintentionally precipitated polymer. After the second precipitation, the precipitate (the middle fraction) was retrieved and the remaining supernatant and the first fraction were discarded.

The solvents were most effectively removed from the products of the fractionation by the following method. The sample was diluted in a 100 ml flask and dried at room temperature using a rotary evaporator. A fast rotation rate was necessary to spread the polymer in a thin layer around the wall of the flask for the most effective drying. When most of the solvent had evaporated, the sample was removed from the rotary evaporator and dried under a vacuum of 0.2 mm Hg for a few hours to remove residual solvent. (It was occasionally observed that a longer period under vacuum resulted in the formation of insoluble rubbery

aggregates of polymer when redissolution was attempted. DLS experiments on these samples revealed anomalously high polydispersities, even after filtering.)

Particular care was taken to avoid exposing the polymer to excessive heat because PVME is susceptible to oxidative degradation. The colour of the PVME gradually changes to dark brown during oxidation. A method of storage which seemed effective in preventing oxidation was to redissolve the polymer in toluene and keep the solution in a well sealed (and solvent resistant) container, minimizing the surface area of the solution exposed to air. This stock solution was stored in a cool, dark place. Further precautions which others [165] have taken include storage in an atmosphere of inert gas and addition of antioxidant. Neat PVME absorbs moisture, so storage in an organic solvent also prevents contamination by water.

Redispersion in other solvents was readily achieved by drying the solution using the technique described above and adding the new solvent.

5.2 Characterization of PVME Fractions

5.2.1 Gel Permeation Chromatography

Gel Permeation Chromatography (GPC), was used to examine fractions obtained in an early fractional precipitation experiment on the Polysciences PVME (P-PVME). The fractionation was achieved by raising the temperature of a solution of PVME in water.

The theory and practice of GPC are discussed at an introductory level in [17] and [162] and in more detail in reference [166]. The basic principles of the technique are straightforward; the polymer solution is passed through a column packed with porous gel beads. The polymer molecules are partitioned between the insides of the pores and the interstitial volume between the gel particles. Dynamic equilibrium exists, with the smaller molecules spending more time inside the pores than the larger ones. Therefore the largest molecules are eluted from the column first and separation takes place on the basis of hydrodynamic size. For a suitably calibrated column, the log of the molar mass is usually proportional to the retention volume V_r (the volume eluted from the column during the time between injection of the sample and detection of the peak).

The apparatus used in these experiments consisted of a 60 cm PL Gel column (Polymer Laboratories Ltd. UK) containing 10 μm gel particles of mixed pore sizes, a Waters chromatography pump and a Waters R401 differential refractometer. The differential refractometer cell was held at a constant temperature by recirculating water from a constant temperature water bath around it, but the column temperature was not controlled.

The best results were obtained using chloroform (AR grade, containing 1% ethanol as stabilizer, filtered before use) as solvent. Both toluene and carbon tetrachloride were tried but the refractive index difference between these solvents and PVME was too small to give a useful signal on the differential refractometer.

A GPC column requires calibration with well characterized molar mass standards before it can be used to measure the molar masses of unknown samples. No PVME standards are available, so the calibration was done with polystyrene standards. Since the hydrodynamic radii of polystyrene and PVME have different M dependences, this calibration is only useful for semiquantitative determinations of the molar masses of PVME samples. Universal calibration can usually be obtained for different polymers in a given solvent by plotting $\log[\eta]M$ against V_r. However, $[\eta]$ was not measured in these experiments, so the calibration is precise for polystyrene and only approximate for PVME.

Fig. 5.2 shows a chromatogram obtained for a solution of mixed polystyrene standards. The calibration plot for polystyrene standards averaged over four runs is shown in Fig. 5.3. This calibration plot was obtained by plotting $\log M_w$ against the retention volume for the corresponding peak. (For narrow distribution polymers, it is adequate to assume that the peak molar mass M_p is equal to the value of M_w given by the manufacturer but in general, M_p is not equal to M_w.) Note that calibrations performed on different GPC systems with the same column may differ slightly due to small differences in pump speeds.

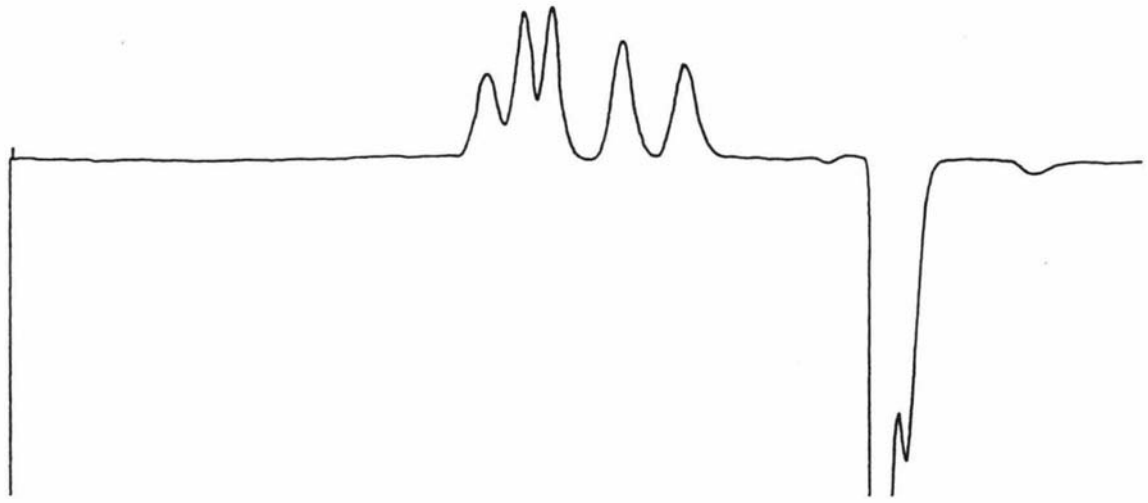

Figure 5.2 GPC chromatogram for a solution of mixed polystyrene standards. The sharp peak at the beginning of the chromatogram is a marker peak corresponding to the injection of the sample and the large peak at the end is a solvent peak due to solvent impurities.

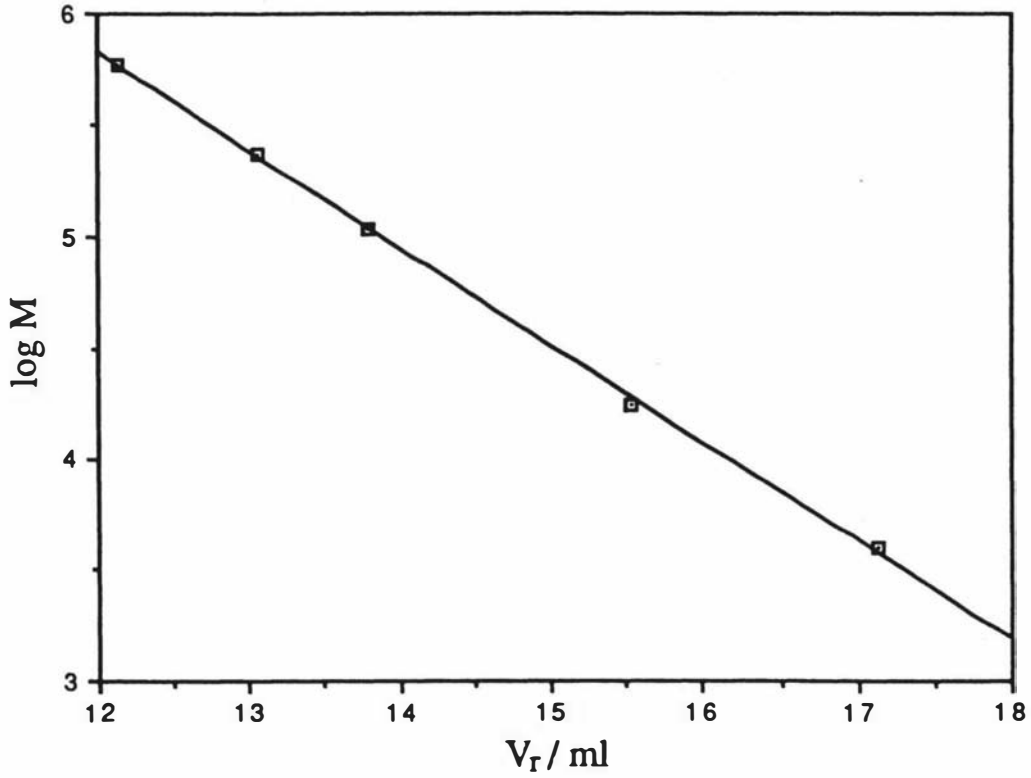

Figure 5.3 GPC calibration plot for polystyrene standards in chloroform.

The output signal from a refractive index detection system is proportional to the difference in refractive index between a reference (usually pure solvent) and the sample which is eluted from the column. If the degree of polymerization is greater than roughly ten, the refractive index increment is independent of molar mass so the detector output is given by

$$F(V_r) \propto \Delta n = \left(\frac{\partial n}{\partial C}\right) C \ . \tag{5.1}$$

Assuming that a calibration of the form

$$V_r = k_1 - k_2 \log M \tag{5.2}$$

holds, it is then straightforward to show that

$$M_w = \int M\, F(V_r)\, dV_r \ / \ \int F(V_r)\, dV_r \tag{5.3}$$

and

$$M_n = \int F(V_r)\, dV_r \ / \ \int (1/M)\, F(V_r)\, dV_r \ . \tag{5.4}$$

In practice, these integrals were approximated using the trapezoid rule. The interval ΔV_r was allowed to vary to increase the efficiency of the integration.

The method was checked by calculating M_w and M_n from the chromatogram obtained for a standard polystyrene (M_w = 110,000 g mol^{-1}, M_w/M_n = 1.06). The results gave M_w = 121,000 g mol^{-1}, M_n = 115,000 g mol^{-1} and M_w/M_n = 1.05. These values are acceptable considering that the column temperature was not controlled, the calibration assumed that $M_p = M_w$ and no attempts were made to account for the effects of column dispersion or the use of finite concentration samples.

The unfractionated Polysciences PVME and fractions obtained by fractional precipitation in water were studied using GPC. The averaged results from two runs on the unfractionated PVME gave M_w = 44,000 g mol^{-1} and M_n = 11,000 g mol^{-1}, so M_w/M_n = 4. The first of these two runs is shown in Fig. 5.4. A long tail on the low molar mass end of the distribution is apparent. The values of M_w and M_n are both lower than the values quoted by manufacturer, and the value of M_w/M_n found here seems high. However, it should remembered that the manufacturer's data is subject to variation from lot to lot and furthermore, the column calibration was not absolute.

Fig. 5.5 shows the chromatogram obtained for the fraction taken at 35°C (f2/2). An analysis of the chromatogram gave M_w = 101,000 g mol^{-1} and M_n = 71,000 g mol^{-1} so M_w/M_n = 1.4. This clearly shows that the fractionation was successful.

5.2.2 Dynamic Light Scattering

Dynamic light scattering is a convenient technique for routine characterization of polymers. Values of the mutual diffusion coefficient, which are easily measured by DLS, can be extrapolated to zero concentration to give the z-average value of D_0. The normalized second moment of the distribution of decay rates, $\mu_2/\langle\Gamma\rangle^2$, obtained from a cumulant fit to DLS data, (see section 2.4.1) can give an estimate of the polydispersity of a solution of non-interacting molecules. As soon as the DLS apparatus was in running condition, the products of fractionations were routinely checked using DLS.

Some DLS experiments were performed on samples of the unfractionated Polysciences PVME. Samples made in butanone showed evidence of aggregation even after filtering. Manson and Arquette [159] remarked that the values of R_G obtained from their experiments on PVME in butanone were higher than expected, and the results were scattered suggesting the presence of dust or aggregates. This casts some doubt on the value of M_w for the Polysciences PVME provided by the manufacturer because it was obtained by static light scattering using butanone as the solvent.

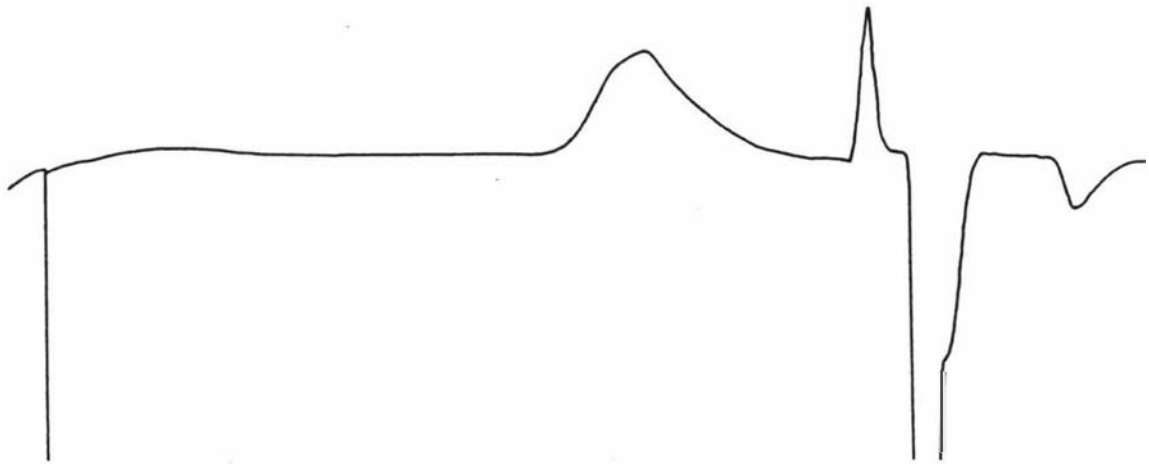

Figure 5.4 GPC chromatogram for the unfractionated Polysciences PVME in chloroform.

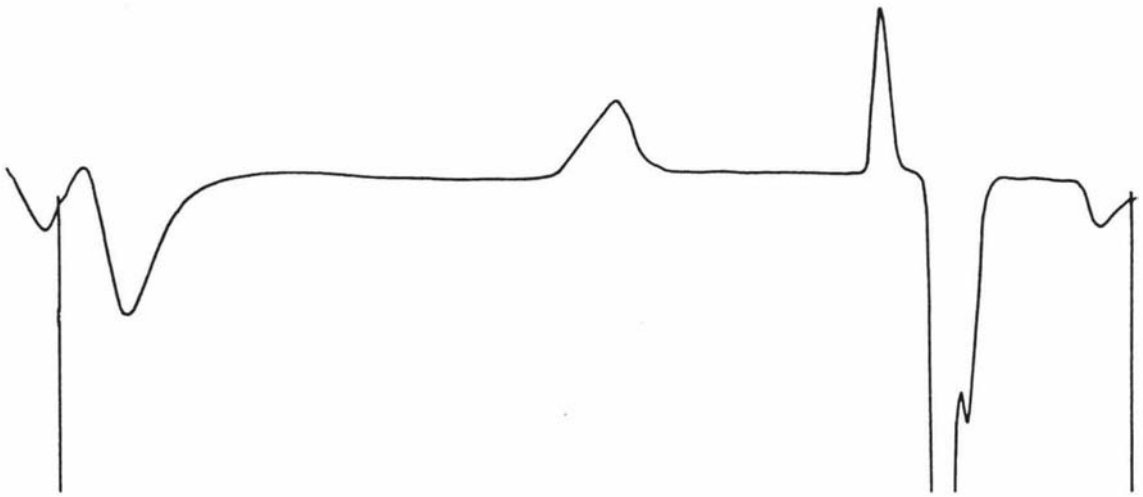

Figure 5.5 GPC chromatogram for a fraction of the Polysciences PVME in chloroform. The broad peaks on the left were from the previous injection.

All further DLS measurements for the purpose of characterization were performed using ethyl acetate as the solvent as suggested by Bauer et al. [160].

High quality square cells were used for all of the DLS experiments in this chapter so that the stray light detected at low angles was minimized. It was often necessary to exclude the first one or two points of the correlation function from the data analysis because of distortion produced by correlated afterpulsing in the photomultiplier.

Experiments on unfractionated Polysciences PVME dissolved in ethyl acetate at a concentration of 57 mg g^{-1} gave $D = (1.40\pm0.01) \times 10^{-10}$ m^2s^{-1} and $\mu_2/\langle\Gamma\rangle^2 = 0.23\pm0.08$.

The GAF PVME, dissolved in ethyl acetate at a concentration of 49 mg g^{-1} gave D = $(1.30\pm0.01) \times 10^{-10}$ m^2s^{-1} and $\mu_2/\langle\Gamma\rangle^2 = 0.19\pm0.08$. These values were obtained from second order cumulant fits to correlation functions spanning approximately three decay times. The measurements were all made at an angle of 21° and a temperature of 25°C. The mean count rate was roughly 900 s^{-1} for each sample.

Pusey [94] has derived a relationship between the commonly used polydispersity index M_w/M_n and the second moment obtained from a cumulant fit which holds at low polydispersities for symmetrical molar mass distributions, i.e.

$$M_w/M_n \approx M_z/M_n \approx 1+\frac{1}{\alpha^2}\frac{\mu_2}{\langle\Gamma\rangle^2} \tag{5.5}$$

where α is defined by the relationship $D_0 \sim M^{\alpha}$. Although α is not known for PVME in ethyl acetate, it is between 0.5 and 0.55 for most polymer-solvent pairs over the range of molar masses usually encountered. The maximum value of M_w/M_n is obtained by taking α = 0.5 giving $M_w/M_n \approx 1.92$ for the P-PVME and 1.76 for the G-PVME. Pusey [94] has shown that this method underestimates M_w/M_n by more than 20% for $\mu_2/\langle\Gamma\rangle^2$ above approximately 0.05. Furthermore, the cumulant fit results for $\mu_2/\langle\Gamma\rangle^2$ quoted here can be expected to underestimate the true values because the fits were made to correlation functions spanning two or three decay times. Strictly speaking, correlation functions should be measured at different values of the sample time and the results of the cumulant fits should be extrapolated to zero sample time to obtain the true initial slope and second moment for such polydisperse samples [94], but these results are at least indicative of the polydispersity of the unfractionated polymer.

Several series of fractionations were carried out to refine the fractionation technique, check the reproducibility of characterization and provide samples for various experiments.

The concentration dependence of the mutual diffusion coefficient D was measured by DLS for G-PVME fraction B2 in ethyl acetate at 25°C. Due to the limited quantity of fractionated polymer available, it was necessary to conserve the polymer. The first measurements were made with the highest concentration sample which was then diluted before each subsequent set of measurements. The results of these experiments showed considerable scatter, probably due to poor sample handling techniques which were improved in later experiments. The intensity of the light scattered by these samples was quite weak, so the baseline of the correlation function only reached 10^4 or 10^5 counts for a typical run. Each diffusion coefficient was the result of a cumulant fit to a normalized correlation function obtained by averaging two or three runs to improve the precision. However, correlation

function baselines of about 10^6 counts are generally required to reduce the uncertainty in the second moment to ±0.01.

Fig. 5.6 shows D plotted against C for G-PVME fraction B2 in ethyl acetate. To convert the concentrations from mass fractions to mass/volume units, $\bar{v}$ for ethyl acetate was taken as 1.11×10^{-3} m^3kg^{-1} and $\bar{v}$ for PVME was taken as 0.983×10^{-3} m^3kg^{-1} which is the value given in [167] for PVME in amyl alcohol at 23.5°C. The positive initial slope of the plot of D against concentration indicates that ethyl acetate is a good solvent for PVME. (Note that k_D can be negative for a low molar mass polymer in a good solvent, but is never positive for a polymer in a poor solvent.) Extrapolation to zero concentration gives $D_0 = 7.5 \times 10^{-11}$ m^2s^{-1}. Values of the second moment, while clearly lower than for the unfractionated sample, were higher than expected. However, the data were not precise enough to allow very accurate estimations of this quantity. The values of $\mu_2/\langle\Gamma\rangle^2$ obtained were in the range 0.08±0.2 to 0.27±0.3.

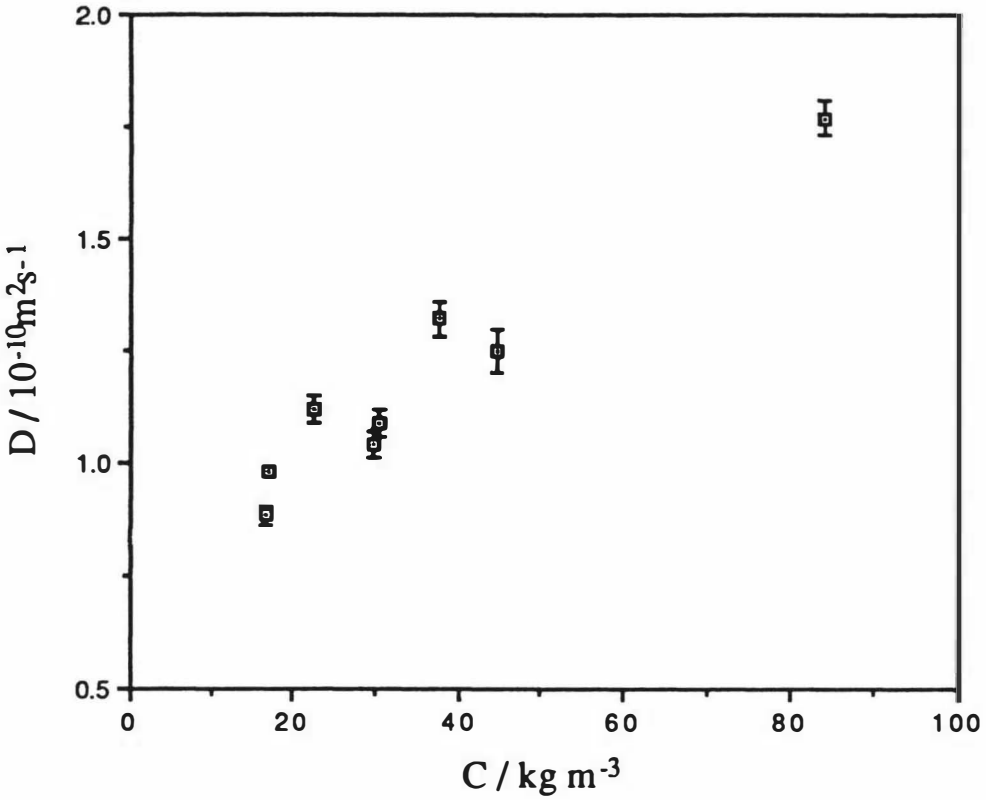

Figure 5.6 Concentration dependence of the mutual diffusion coefficient for G-PVME fraction B2 in ethyl acetate.

The concentration dependence of D for G-PVME fraction C2 in ethyl acetate was also measured. These measurements gave much better results than the G-PVME B2 experiments because of improvements in the sample handling technique, particularly in isolating the fractionated PVME. Measurements were mainly made at an angle of 17° so that a larger value of the sample time could be used, giving an increase in the number of counts per sample time and hence the S/N ratio. The mutual diffusion coefficient D is plotted against concentration in Fig. 5.7. A linear fit to the four lowest concentration points gives $D_0 = (5.67 \pm 0.03) \times 10^{-11}$ $m^2 s^{-1}$ and $k_D = (0.032 \pm 0.0003)$ $kg^{-1} m^{-3}$.

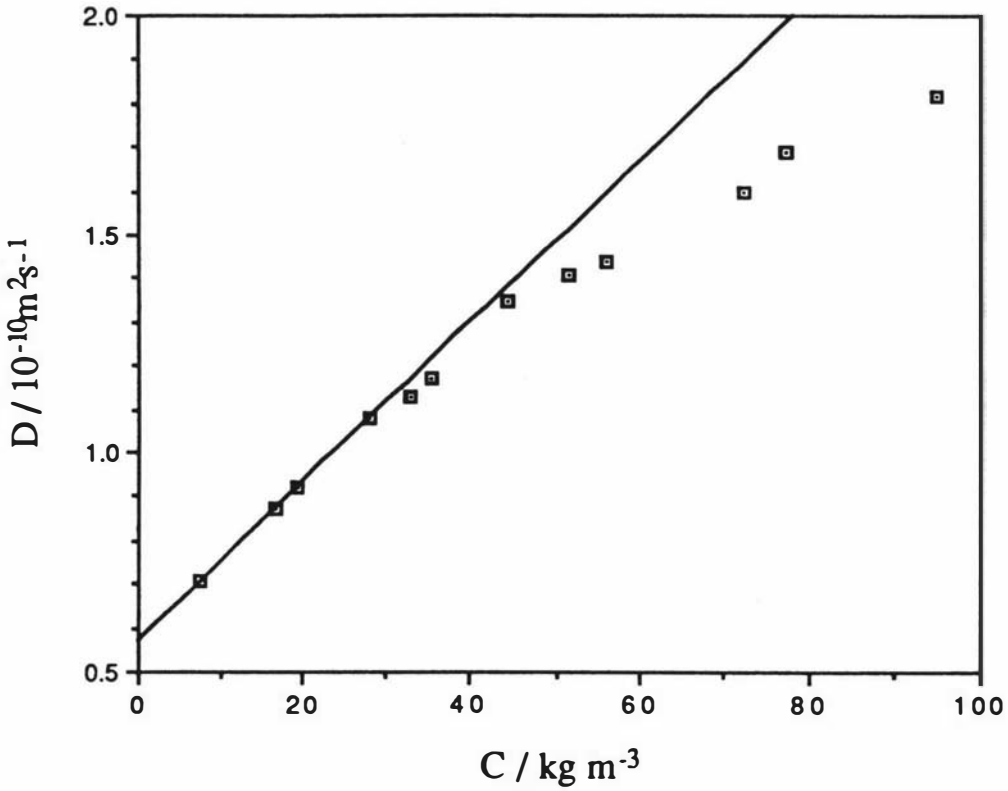

Figure 5.7 Concentration dependence of the mutual diffusion coefficient for G-PVME fraction C2 in ethyl acetate.

A detailed study of angular dependence of the mean decay rate $\langle\Gamma\rangle$ of the field autocorrelation function was made for the C = 28 kg m^{-3} sample. Fig. 8a shows $\langle\Gamma\rangle$ as a function of q^2 for this sample. The intercept is zero to within experimental error. An alternative way of presenting this information is to plot ln S_i against $q^2\tau$. (The S_i are the experimental estimates of the electric field autocorrelation function, i.e. $[\hat{g}^{(2)}(q,\tau_i)-1]^{1/2}$.) Fig. 8b shows correlation functions measured at 17°, 27° and 60° plotted this way. The

17° correlation function shown represents an average of two runs with approximately 1.4×10^6 counts on the baseline for each run. At 27° eight runs with $B = 1.3 \times 10^5$ were averaged and at 60°, six runs with $B = 2 \times 10^4$ were averaged. The normalization of the correlation functions has been adjusted so that the intercept of $\ln S_i$ calculated with a quadratic fit is equal to zero. The scatter is obviously greater for the 60° data because of the smaller number of counts accumulated. The data fall on a common curve, indicating that the diffusion coefficient $D = \langle \Gamma \rangle / q^2$ is independent of q as expected. It is also worth noting that the residuals of the second order cumulant fits to $\ln S_i$ showed no trends in either the actual values or their magnitudes, indicating respectively that the functional form of the fitting function was adequate to describe the data and also that the weighting factors included in the least squares fits had the correct τ dependence.

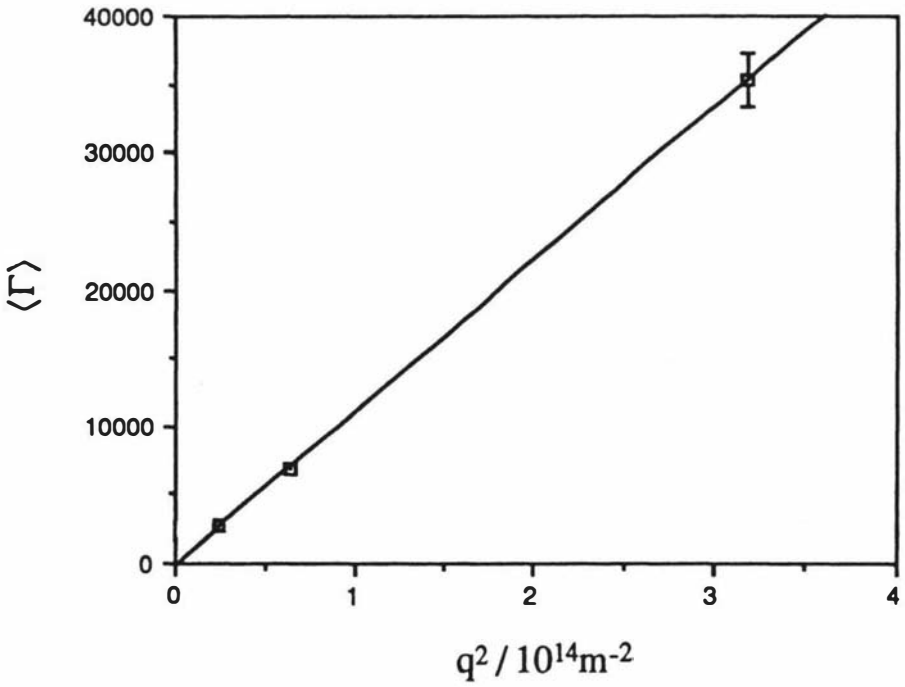

Figure 5.8a The mean decay rate of the field autocorrelation function versus the magnitude of the scattering vector squared for the 28 kg m^{-3} sample of G-PVME fraction C2.

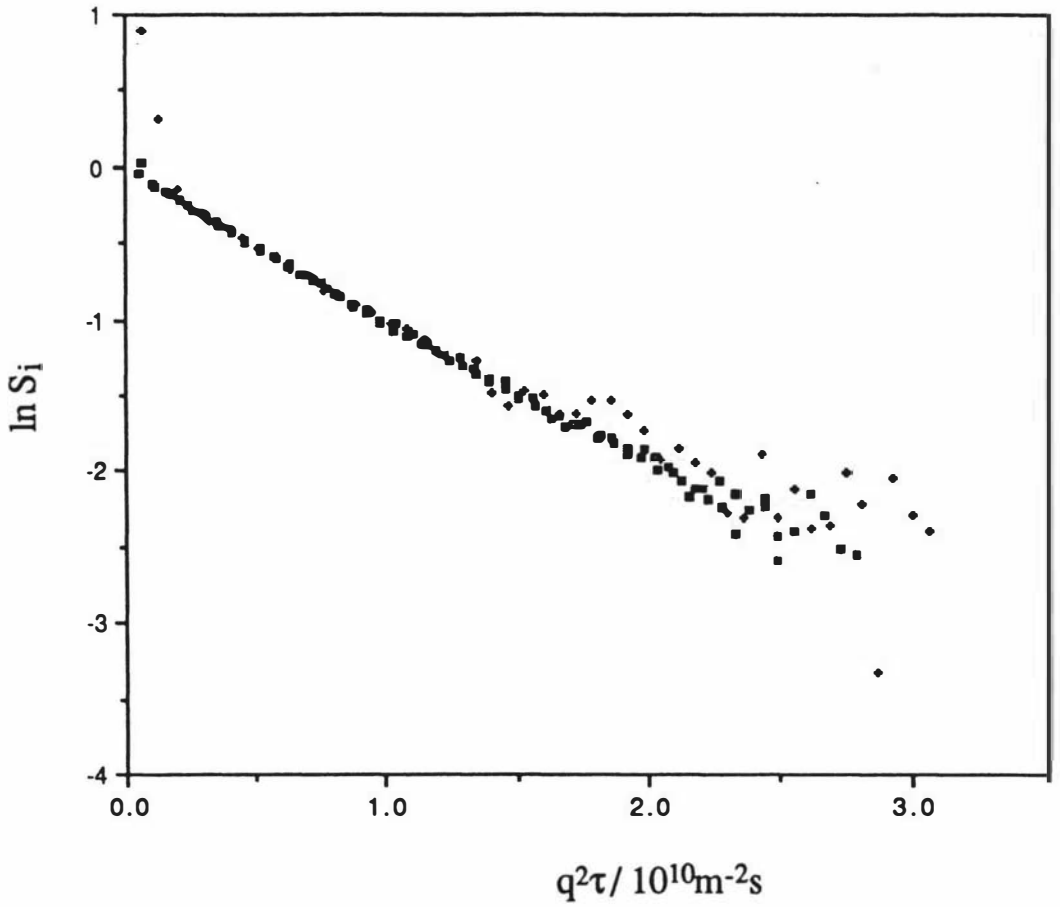

Figure 5.8b Normalized field autocorrelation functions versus $q^2\tau$ for the 28 kg m^{-3} sample of G-PVME fraction C2 at angles of 17°(□), 27°(■) and 60°(+). Note the distortion at very short times due to photomultiplier afterpulsing.

The run rejection scheme described in Chapter 3 was used in all of these experiments. Each run consisted of typically 1000 or 2000 short, self normalized runs with $N = 10^5$. The number of runs rejected was typically less than 20 for every 1000 accepted.

Values of $\mu_2/\langle\Gamma\rangle^2$ obtained in these experiments were in the range 0.06±0.03 to 0.15±0.06. Most of the samples had $\mu_2/\langle\Gamma\rangle^2 = 0.08\pm0.02$. If it is assumed that $\alpha = 0.5$, the value of M_w/M_n is found to be 1.32, confirming that the width of the molar mass distribution has been reduced by the fractionation procedure.

Only one sample of fraction D2 was studied using DLS. At a concentration of 23.59 kg m^{-3} the results gave $D = (8.99\pm0.04) \times 10^{-11}$ m^2s^{-1} with a second moment of 0.10±0.04.

Sample G-PVME E2 was studied by both DLS and sedimentation velocity experiments to give the absolute molar mass calculated using the Svedberg equation. The concentration dependence of D for G-PVME E2 is plotted in Fig. 5.9. A linear least squares fit to the data gives $D_0 = (5.35\pm0.2) \times 10^{-11}$ m^2s^{-1} and $k_D = (0.038\pm0.003)$ kg^{-1} m^3.

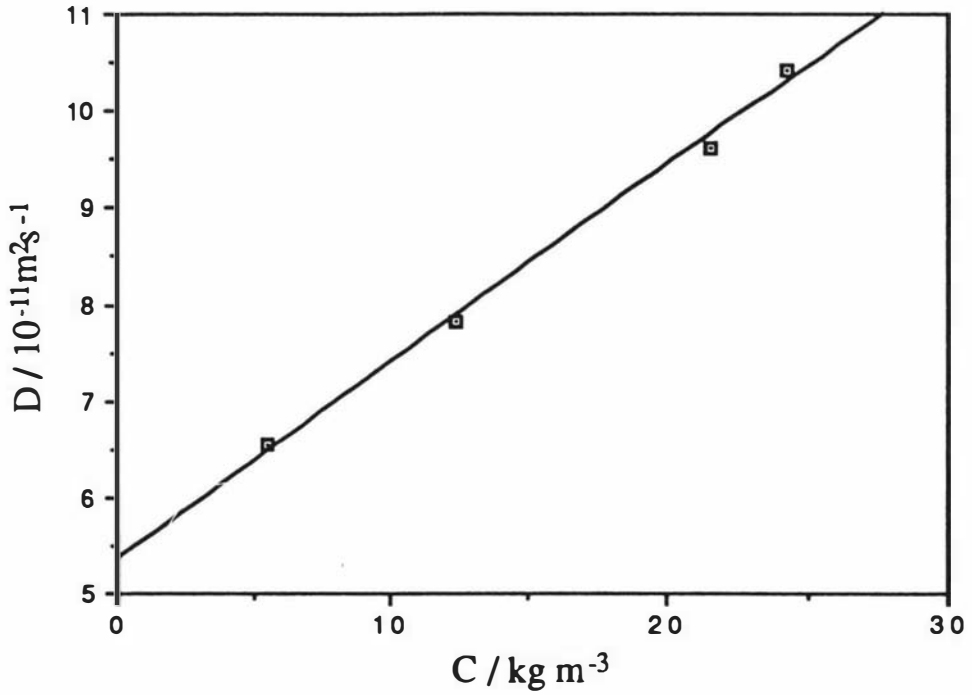

Figure 5.9 Concentration dependence of the mutual diffusion coefficient for G-PVME fraction E2 in ethyl acetate.

The combined data for the concentration dependence of the G-PVME fractions are plotted in Fig. 5.10. The consistency of the values of D obtained for samples originating from different fractionation runs indicates that the fractionations were reproducible.

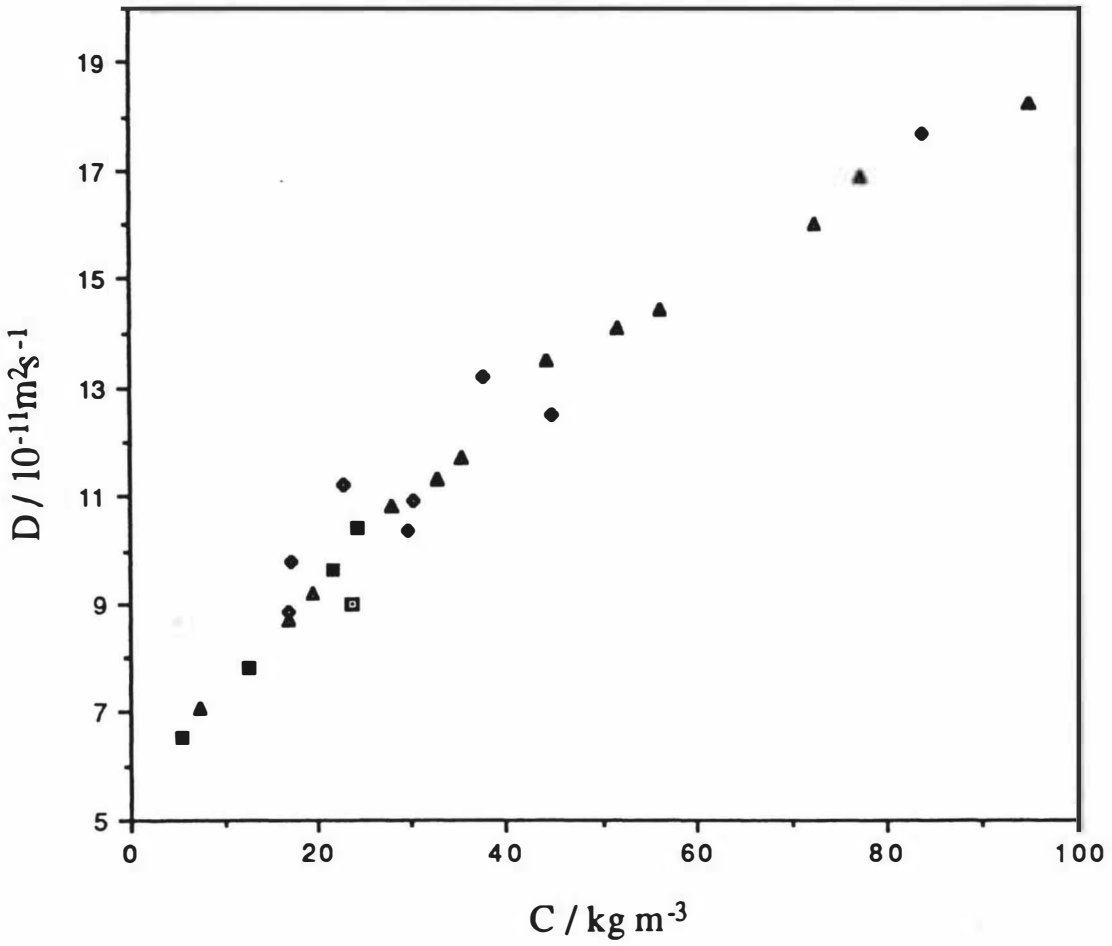

Figure 5.10 Plot of the combined data for the concentration dependence of mutual diffusion of G-PVME fractions in ethyl acetate; ● fraction B2, ▲ fraction C2, ▫ fraction D2, ■ fraction E2.

5.2.3 Sedimentation Velocity

PVME molar mass standards were not available, so the GPC results presented above are only semiquantitative. As was stated earlier, absolute molar masses cannot be measured directly by DLS. However, it is possible to calculate the weight average molar mass from the z-average diffusion coefficient and the weight average sedimentation coefficient (see [94] and references therein) using the Svedberg equation (eqn (2.28)). A series of sedimentation velocity experiments was performed on four samples of G-PVME E2 in ethyl acetate at concentrations up to 13 kg m^{-3}. The values of the sedimentation coefficient were extrapolated to zero concentration to give s_0 which was then combined with D_0 to give M_w.

The sedimentation coefficients were measured with the assistance of Dr. J. A. Lewis on a Beckman Model E analytical ultracentrifuge by the following method. The sample was

loaded into a 2° single sector aluminium cell and placed into the rotor (type AN-H) with an appropriate counterbalance. The temperature was adjusted to 25°C and the rotor speed was uniformly increased to 48,000 rpm. Due to the finite time taken to reach the running speed, zero time is conventionally taken as the time at which the angular velocity is two thirds of the final value. Schlieren optics were used to give an image representing dC/dr against r, the distance from the axis of rotation. Photographs of the Schlieren profile were taken at appropriate intervals (approximately every 30 min). The peak of the Schlieren profile gives the position of the boundary between the sedimenting polymer molecules and the pure solvent which is left behind. A typical series of Schlieren profiles is shown in Fig. 5.11. The peak position was determined with a Nikon 6CT2 Profile Projector and the distance from the axis of rotation, r, was calculated using a previously determined calibration point on the rotor and the appropriate magnification factor [168]. The sedimentation coefficient was determined from the slope of a plot of ln r against t using the equation

$$s = \frac{1}{\omega^2} \frac{d}{dt} \ln r \qquad (5.6)$$

where ω, the angular frequency of rotation (expressed in rad s^{-1}) was measured for each run. This method gives the weight average sedimentation coefficient if the peak is symmetrical; otherwise the second moment of r must be used [169]. The plot used to obtain s for the 9.3 kg m^{-3} sample is shown in Fig. 5.12. The point at low t is significantly higher than the least squares fit to the other points. This is due to an inadequate estimate of the time origin t_0. Possible reasons for this inadequate estimate are firstly, non-uniform angular acceleration of the rotor during the time taken to reach the running angular velocity, and secondly, there is a time delay between the beginning of rotation and the sedimenting macromolecules leaving the meniscus. This delay has been calculated by Fujita [170] and it depends on D, s, ω and the value of r at the meniscus. The strongest effect on the time delay comes from the proportionality to ω^{-4}. Therefore, the easiest way to reduce the effect would be to increase ω. Provided that the low time data are excluded from the analysis, the true value of t_0 need not be estimated if a linear fit to the plot of ln r against t is performed. On the other hand, if a quadratic fit is necessary, it is important to correct the data for the t_0 effects first. This was only necessary for the highest concentration sample where concentration dependence of s, combined with the dilution effect due to the sector shape of the cell, produced a non-linear plot of ln r against t. The t_0 correction was found by fitting the uncorrected data to a quadratic, extrapolating to the value of r corresponding to the position of the meniscus and denoting the corresponding value of t as the origin. Then the initial slope of the corrected data was used to evaluate s.

The values of s obtained in these experiments are plotted in Fig. 5.13 as 1/s against C. It is immediately apparent that the plot is not linear over the range of concentrations covered in

these measurements. The data are well described by a quadratic curve which is consistent with eqn (2.37). From the quadratic fit, $s_0 = (2.68 \pm 0.08) \times 10^{-13}$ s and $k_s = 6.4 \times 10^{-3}$ $kg^{-1}m^3$ were obtained. The molar mass of G-PVME fraction E2 obtained from the Svedberg equation with all quantities extrapolated to zero concentration is (110±10) kg mol^{-1}.

It is also possible to estimate the second virial coefficient for PVME in ethyl acetate by using equation (2.39) and taking $k_s = k_f$. The result is $A_2 = 2.1 \times 10^{-4}$ $kg^2mol^{-1}m^{-3}$ which compares well with values obtained for other flexible polymers.

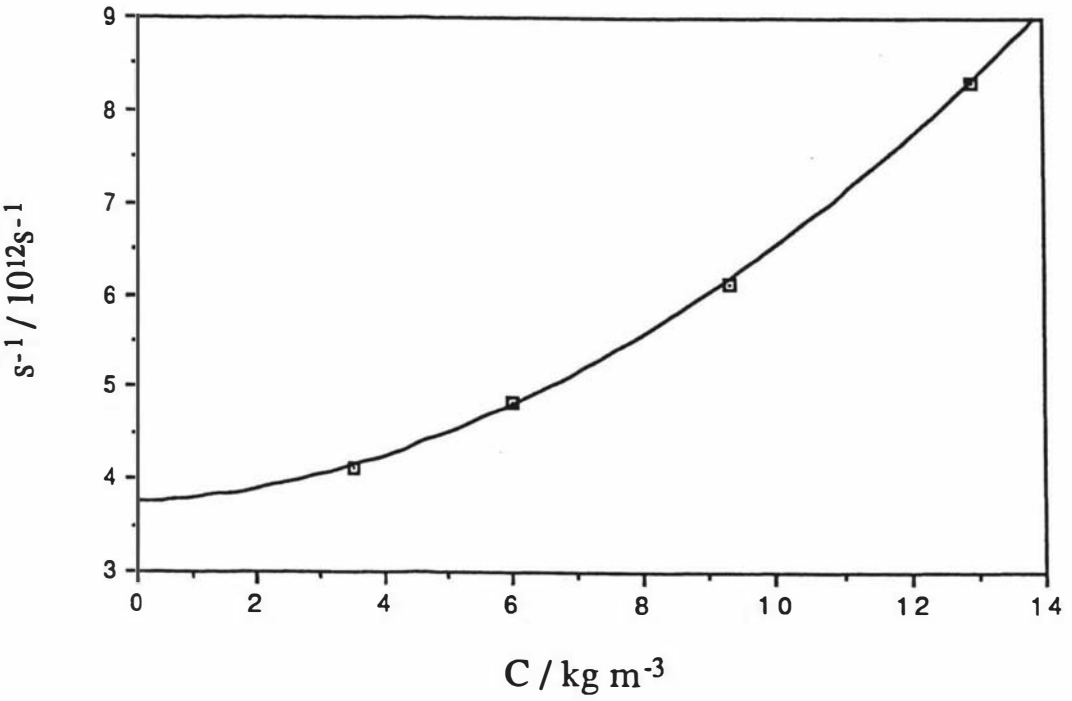

Figure 5.13 The reciprocal of the sedimentation coefficient versus concentration. The quadratic fit gives $s_0 = 2.68 \times 10^{-13}$ s and $k_s = 6.4 \times 10^{-3}$ $kg^{-1}m^3$.

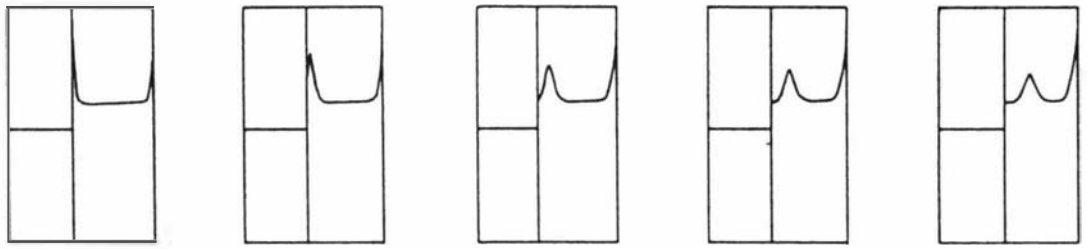

Figure 5.11 Schlieren profiles for the sedimentation velocity experiment on G-PVME fraction E2 in ethyl acetate at a concentration of 9.3 kg m^{-3}.

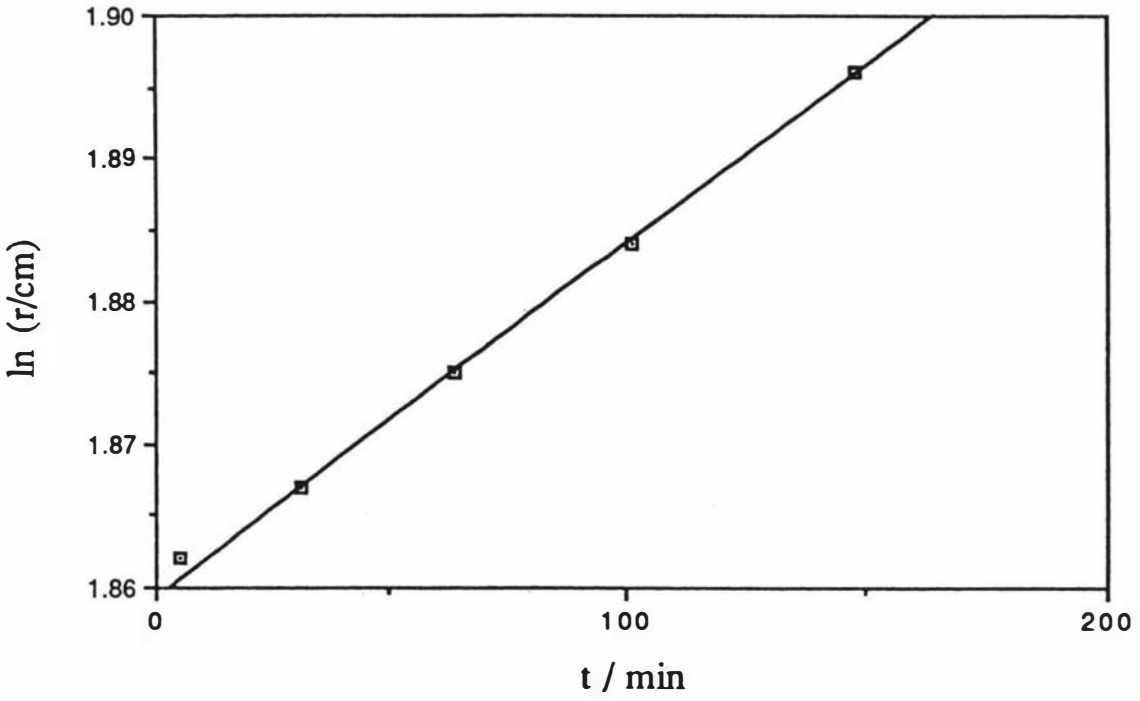

Figure 5.12 Plot of ln r against time for G-PVME fraction E2 in ethyl acetate, C = 9.3 kg m^{-3}. The sedimentation coefficient calculated from the slope is 1.63×10^{-13} s.

6. TERNARY SOLUTIONS

The first section of this chapter (section 6.1) deals with optical tracer DLS experiments which reproduce the results obtained in 1984 by Martin [68]. Martin measured the correlation function of light scattered from a trace component of polystyrene (PS) in an isorefractive solution of poly(vinyl methyl ether) (PVME) in toluene as a function of PVME concentration. Martin identified the diffusion coefficient obtained in such a measurement as the self diffusion coefficient of the trace component, polystyrene.

Section 6.2 describes similar measurements on the PS-PVME-CCl_4 system. Carbon tetrachloride is a particularly convenient solvent for PGSE NMR measurements because it contains no hydrogen atoms, but the PS-PVME-CCl_4 system is thermodynamically quite different from the PS-PVME-toluene system. The measurements presented in section 6.2 show that the thermodynamic conditions of the solution can have a strong effect on the results of DLS experiments. It is shown that even though the matrix polymer is isorefractive with the solvent and the probe polymer is present only as a trace component, the self diffusion coefficient of the probe polymer is not necessarily measured.

Dynamic light scattering and PGSE NMR experiments on PS-PVME-(toluene d8) solutions are described in section 6.3. The solvent in this case is deuterated toluene. The low glass transition temperature of PVME made it possible to investigate very high total polymer concentrations (up to approximately sixty percent) in these experiments. The effect of increasing the concentration of polystyrene is investigated and a direct comparison of the diffusion coefficients measured by DLS with those measured by PGSE NMR is made.

6.1. DLS Experiments on PS-PVME-Toluene

6.1.1. Experimental

These experiments were designed to replicate as closely as possible an early set of optical tracer dynamic light scattering experiments reported by Martin [68]. Martin performed DLS experiments on solutions of PVME in toluene to which a trace of polystyrene had been added.

The PVME used in Martin's experiments was Gantrez M-556 obtained from GAF. The molar mass of this material evaluated from the intrinsic viscosity was given as 110,000 g mol^{-1} [68]. No numerical estimate of the polydispersity was provided by Martin, but the value of M_w/M_n was probably in the region of 2 (see also the discussion in section 5.1.1). The polystyrene used by Martin had a nominal M_n of 900,000 g mol^{-1} and $M_w/M_n = 1.10$, giving M_w = 990,000 g mol^{-1}. The PVME concentration was varied between

approximately 30 kg m^{-3} and 260 kg m^{-3} and the polystyrene concentration was maintained at 0.2 kg m^{-3} in all of Martin's experiments. (Martin gives two conflicting values of the PS concentration in his paper; the value given in the text is 0.2 mg ml^{-1} = 0.2 kg m^{-3} but his Table I gives the PS mass fraction as 0.2%, which is approximately 2 mg ml^{-1}.)

The PVME used in the work presented here was the unfractionated G-PVME (Gantrez M-555) discussed previously in Chapter 5. The molar mass of this polymer was previously estimated as 102,000 g mol^{-1}. Note that this estimate is based on the value of the solution viscosity at 1% given by the manufacturer, while the value quoted by Martin was probably obtained by extrapolation to zero concentration. If the concentration dependence of the solution viscosity is significant, the estimates of M based on unextrapolated values can be expected to overestimate M. The polystyrene was a narrow fraction with M_w = 929,000 g mol^{-1} and M_w/M_n = 1.10 obtained from Polysciences (lot no. 23590). The PVME concentration was varied and the polystyrene mass fraction (mass of PS per unit mass of solution) was kept at approximately 0.2 mg g^{-1}.

The procedure used in making the solutions for these experiments was as follows. The PVME was used as received from the manufacturer (50% solution in toluene). The concentration of the stock material was determined by weighing a sample before and after evaporation of the solvent. Several diluted samples of the PVME stock were made. These samples were filtered directly into cleaned scattering cells using 0.2 μm pore size teflon filters (Millipore). The mass of solution in each cell was determined by weighing and the appropriate amount of a filtered stock solution of the polystyrene (of concentration 24.41 mg g^{-1}) was added to each cell to give an overall polystyrene mass fraction of 0.2 mg g^{-1}. A microlitre chromatography syringe was used to deliver the required volume of polystyrene stock solution to the cells.

The mass fractions were converted to mass/volume concentrations and volume fractions by taking the partial specific volumes $\bar{v}$ of PVME, polystyrene and toluene at 25°C to be 0.98 $\times 10^{-3}$ m^3 kg^{-1}, 0.916 $\times 10^{-3}$ m^3 kg^{-1} and 1.154 $\times 10^{-3}$ m^3 kg^{-1} [167] respectively.

The measurements were made at a temperature of 25°C.

Diffusion coefficients were obtained from second order cumulant fits to correlation functions. Whenever it was possible, several measurements were averaged at each of two or three different angles, usually 27°, 60° and 90°. Measurements were not usually made at angles higher than 90° because of the low count rates observed at such angles. Measurements on the most concentrated sample at low angles were made difficult by slow fluctuations in the count rate, possibly due to a weak aggregation effect. Experiments on this sample were repeated over a period of three months, but showed no improvement with

time. There were no obvious signs of dust contamination when the scattering volume was observed through a polarizing filter rotated so that the singly scattered (vertically polarized) light was strongly attenuated. (Dust, or particulate contamination usually produces a strong component of depolarized scattering which is easily observed through a "crossed" polarizing filter.)

It was often found that afterpulsing affected the first channel of the correlation function due to the low number of counts detected per sample time. This effect was particularly evident at higher angles where the count rate was small. When afterpulsing distortion was observed, the affected channels were omitted from the data analysis.

As was also noted by Martin, the intensity of the light scattered by the PVME-toluene solutions was no greater than that scattered by the pure solvent.

6.1.2. Results

Fig. 6.1 shows a correlation function representative of the data obtained in these experiments. As is clearly shown in Fig. 6.1, there was no sign of any significant deviation from single exponential behaviour in the measured correlation functions.

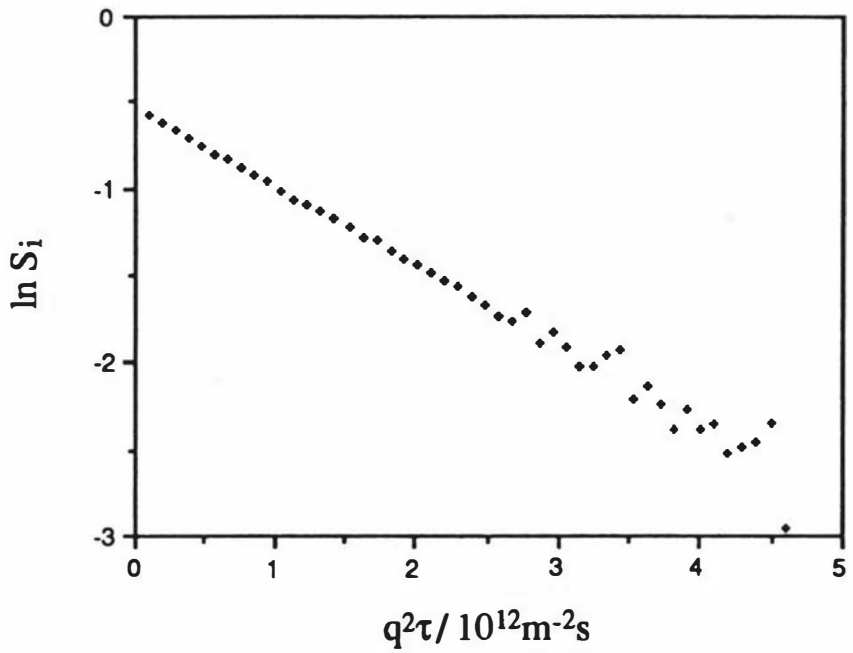

Figure 6.1 A typical correlation function for the PS-PVME-toluene system, measured at an angle of 27° with a sample time of 1.5 ms. The total polymer volume fraction ϕ was 0.144 and the total polystyrene mass fraction was 0.00018.

The values of the effective diffusion coefficient, $D_{eff} = \langle\Gamma\rangle / q^2$, extracted from cumulant fits to the averaged data typically varied by less than 10% over the angular range covered. Within this variation, there was a weak tendency of the lower values to occur at lower angles. Figures 6.2a and 6.2b show the dependence of the measured diffusion coefficient on scattering vector (i.e. angle) for the two cases in which measurements were extended to angles greater than 90°. It is apparent that even for these samples, the change in the effective diffusion coefficient is small. In the first instance this effect was neglected, so the diffusion coefficients obtained at different angles were averaged to produce the values plotted in Fig. 6.3. Martin's results are also plotted for comparison. The scattering vector dependence of the effective diffusion coefficient will be considered in more detail in section 6.1.3.

The values of the normalized variance of the distribution of decay rates, $\mu_2/\langle\Gamma\rangle^2$, were typically in the region of 0.05±0.02. These very low values confirm that the polystyrene had a narrow molar mass distribution and that the correlation function was effectively a single exponential over the concentration range covered by these measurements.

6.1.3. Discussion

The intensity of light scattered from a polymer in a solvent at infinite dilution is proportional to $C M (\partial n/\partial C)^2$, where $(\partial n/\partial C)$ is the refractive index increment [1]. The refractive index increment of PVME in toluene can be estimated by using the approximation [171] $(\partial n/\partial C) \approx \bar{v}\Delta n$ where Δn is the difference between the polymer and solvent refractive indices. At T = 20°C and λ = 589 nm, the refractive indices of PVME and toluene are 1.467 and 1.496 respectively [167], giving $(\partial n/\partial C) \approx -0.028$ cm^{3}g^{-1}. Polystyrene dissolved in toluene has a refractive index increment of 0.111 cm^{3}g^{-1} [171], so the ratio of the intensities scattered by PS and PVME molecules with equal molar masses and concentrations in a dilute solution is approximately 10:1. The higher PS molar mass used in these experiments increases this ratio to 80:1. These considerations suggest that the scattering from polystyrene dominates the scattering from PVME in very dilute ternary solutions, provided that the polystyrene concentration remains greater than approximately one tenth of the PVME concentration.

The same simple arguments cannot, however, be used to predict the ratio of intensities scattered by the two polymer components in more concentrated solutions. The scattered intensity is more generally proportional to $C(\partial\Pi/\partial C)^{-1}(\partial n/\partial C)^2$ for a solution of a polymer in a solvent [1]. As was mentioned at the end of section 6.1.1, the intensity scattered by PVME alone in toluene even at high concentrations is small. This is not only due to the small refractive index increment. The substitution of scaling laws for $(\partial\Pi/\partial C)$ into the above expression shows that the scattered intensity decreases as the concentration increases;

concentration fluctuations are suppressed and the scattered intensity therefore decreases. Similarly, the amplitudes of the two modes measured in a DLS experiment on a ternary system depend on thermodynamic factors and diffusion coefficients, as well as the refractive index increments [99, 100, 101].

The correlation functions measured in this work comprised a single relaxation mode, suggesting that the PVME-toluene pair is a sufficiently good approximation to an isorefractive system to give single exponential behaviour at low PVME concentrations and that the other factors influencing the mode amplitudes are strong enough to guarantee single exponential behaviour at higher concentrations.

There is now theoretical [100] and experimental [172] evidence that an optical tracer DLS measurement on a compatible polymer-polymer-solvent system such as the PS-PVME-toluene system studied here does in fact yield the self diffusion coefficient of the trace component. The theoretical results of Benmouna et al. [100] show that the amplitude of the cooperative mode is zero in the limit of zero tracer concentration for an isorefractive solution of the matrix polymer. In addition, their result for the decay rate of the interdiffusion mode (eqn (2.155)) calculated for a special case (case A, see section 2.4.3) approaches $D_s q^2$ in the limit of zero tracer concentration provided that the polymers are compatible, the solvent is good for both of them (i.e. $\chi/\upsilon < 1$) and the single molecule form factor P(q) is close to 1. Note that this result was derived under the assumption that the molar masses of the polymers are equal. The compatibility of PS and PVME in toluene has been well verified [20].

On the experimental side, Chang et al. [172] have recently made a direct comparison of results obtained from optical tracer DLS and forced Rayleigh scattering experiments on the PVME-PS-(o-flourotoluene) system. They concluded that the diffusion coefficients from optical tracer DLS were equal, within experimental errors, to the self diffusion coefficients of the trace component measured by forced Rayleigh scattering, although the DLS values were consistently marginally higher than the FRS values. They also studied the effect of small departures from true optical tracer conditions by varying the concentration of polystyrene between 0.5 and 3.0 kg m^{-3} in their DLS measurements. Only a weak dependence on polystyrene concentration was found, and they concluded that little error is introduced by assuming that the measured diffusion coefficient is equal to D_s in this concentration range. In the experiments reported here, the polystyrene concentration was 0.2 mg g^{-1} ($\approx$ 0.2 kg m^{-3}), and the PS concentration as a fraction of the total polymer concentration (expressed as mass fractions) varied from 0.0055 down to 0.0007. On the basis of the conclusions of Chang et al. [172], these concentrations are low enough for the

diffusion coefficient measured here to be identified with the self diffusion coefficient of the polystyrene.

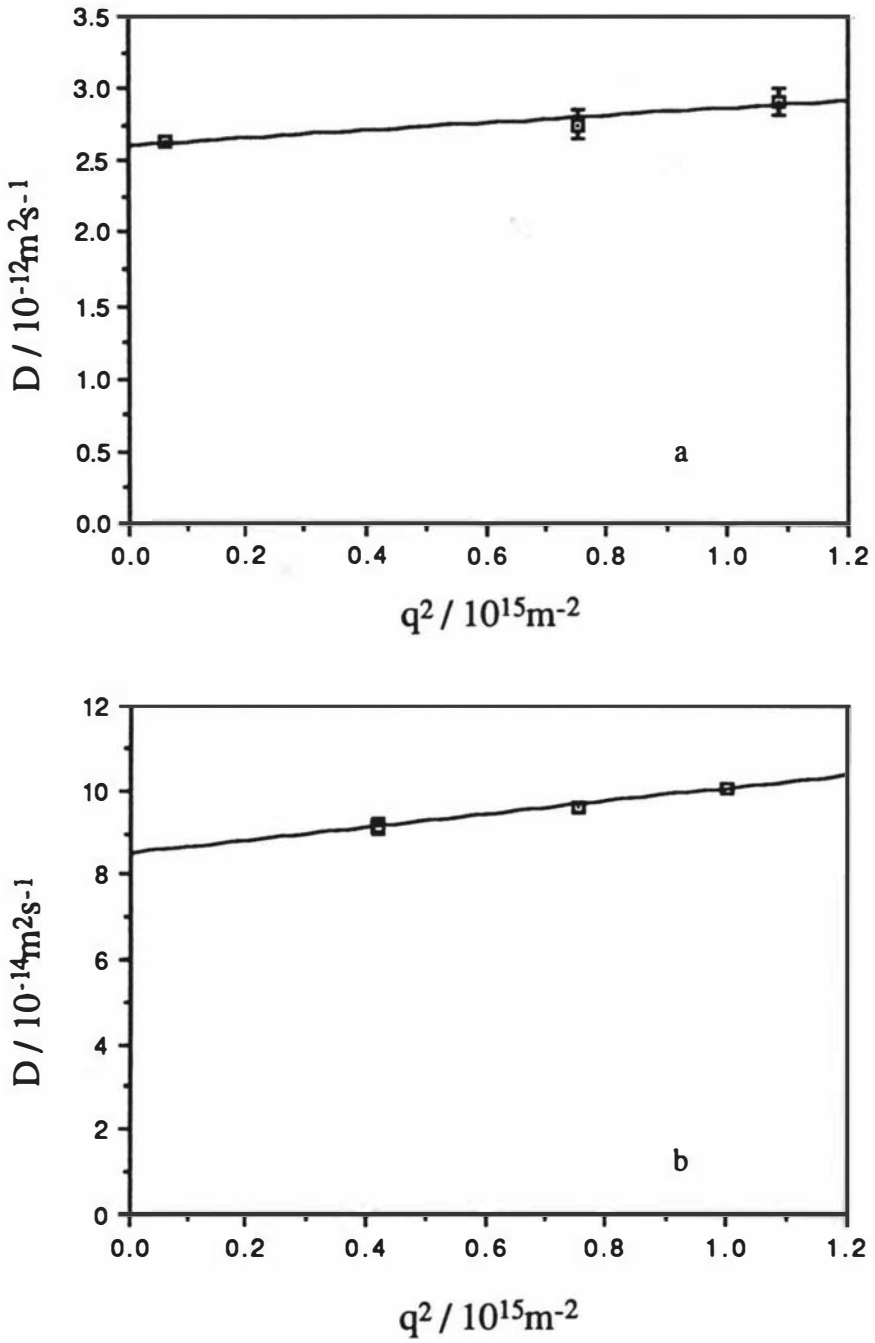

Figure 6.2 The scattering vector dependence of the effective diffusion coefficient, $\langle\Gamma\rangle / q^2$ obtained from second order cumulant fits to DLS data. (a) The polymer volume fraction was 0.056. The slope of the linear fit gives R_G = 17±3 nm, using equation (6.2). (b) The polymer volume fraction was 0.246. The slope of the linear fit gives R_G = 23±1 nm, using equation (6.2).

The q dependence of the effective diffusion coefficient shown in Fig 6.2 was at first unexpected, because there was no suggestion that the diffusion coefficient was q dependent in Martin's work [68]. The data analysis techniques used by Martin were, however, different from the cumulant analysis used here. Martin commented that two modes of relaxation were present in the correlation functions measured at higher angles throughout the entire concentration range, with the fast component having its smallest amplitude at the highest concentrations. Martin attributed the fast decays to internal modes. He used two different methods to account for their effect. The first was to delete several of the initial channels from the data analysis and the second was to fit a sum of two exponentials to the data, including a term accounting for the relaxation of the internal modes and a diffusive term. The results of these two methods of data reduction agreed to within 3% [68]. The q dependence of the diffusion coefficients obtained from this analysis was not discussed in detail, except to say that the diffusion coefficient for his sample 11 (the most concentrated one) was independent of scattering vector.

The method of data analysis used in the work presented here, in contrast to Martin's, emphasizes the short time data in the calculation of the effective diffusion coefficient, $\langle\Gamma\rangle / q^2$. Martin's data analysis method effectively eliminated the q dependence by calculating the diffusion coefficient from the long time part of the correlation function rather than the initial slope which contains rapidly decaying contributions due to internal relaxations. When measured at sufficiently long times so that the internal modes have decayed completely, Martin's diffusion coefficients are equivalent to the $q = 0$ limit of the effective diffusion coefficients measured here.

The theoretical treatment of Benmouna et al. [100], based on earlier work (see references in [96, 179]), has elucidated the q dependence of the effective diffusion coefficient in ternary systems. It has already been established that D_I is approximately equal to the self diffusion coefficient of the trace component (PS) for the system discussed here, so equation (2.157) can be used as the basis of the data interpretation. This equation simply gives the initial decay rate for a polymer at infinite dilution in the free draining (Rouse) approximation with D_0 replaced by D_S.

Equation (2.157) indicates that the effective diffusion coefficient, $\langle\Gamma\rangle / q^2$, measured in an optical tracer DLS experiment should be q dependent unless P(q) is close to 1. Note that P(q) may differ appreciably from 1 before the amplitudes of the internal modes become sufficiently large for the internal modes to be resolvable as a separate decay process. For example, even when P(q) has dropped to 0.75, the amplitude of the first significant internal mode is still only 0.01 [24].

The radius of gyration of polystyrene with M = 929,000 g mol^{-1} in toluene at infinite dilution is 45 nm (using a relationship given in [173]) and the value of q at 120° was roughly 3×10^7 m^{-1} giving $qR_G \approx 1.4$. The form factor for a Gaussian random coil drops from 1.0 to about 0.6 as qR_G goes from zero to 1.4 [24]. This would give an increase in the effective diffusion coefficient ($\langle\Gamma\rangle / q^2$) by a factor of 1.7 in going from zero angle to 120°. This is far larger than the change observed in the measurements reported here, implying that the radius of gyration of polystyrene in PVME-toluene solutions may be smaller than it is in toluene at infinite dilution.

It is possible to estimate the radius of gyration of the polystyrene from the observed q dependence of the effective diffusion coefficient using the theory of Benmouna et al [100]. Equation (2.157) can be simplified by assuming that

$$\frac{1}{P(q)} = 1 + \frac{1}{3}q^2R_G^2 \qquad (6.1)$$

which is valid for $qR_G < 1$, independent of particle shape [24]. In this case, a plot of $D_{eff} = \Gamma_S / q^2$ against q^2 should have an initial slope proportional to R_G^2. Assuming that equation (6.1) is valid, D_{eff} becomes

$$D_{eff} = D_s (1 + \frac{1}{3}q^2R_G^2) \quad . \qquad (6.2)$$

The slopes observed in Fig. 6.2 are consistent with an R_G of 20±4 nm. The data are not detailed or precise enough to allow a more definite conclusion to be reached, but it appears that the radius of gyration of polystyrene in a PS-PVME-toluene solution is significantly less than it is in the pure solvent. In fact the radius of gyration of polystyrene in cyclohexane at the theta temperature is of the order of 30 nm [135] so the collapse of the polystyrene in the presence of PVME appears to be quite severe under the conditions investigated here.

The concentration dependence of the polystyrene self diffusion coefficients shown in Fig. 6.3 will now be discussed.

It is possible to calculate the value of D_0 for polystyrene in toluene at zero PVME concentration using the relation between D_0 and M given by Appelt and Meyerhoff [173] for polystyrene in toluene at 20°C. With a temperature and viscosity temperature correction to 25°C, D_0 is found to be 1.43×10^{-11} m^2s^{-1} giving $\log D_0 = -10.85$. This value is consistent with the low concentration data in Fig. 6.3.

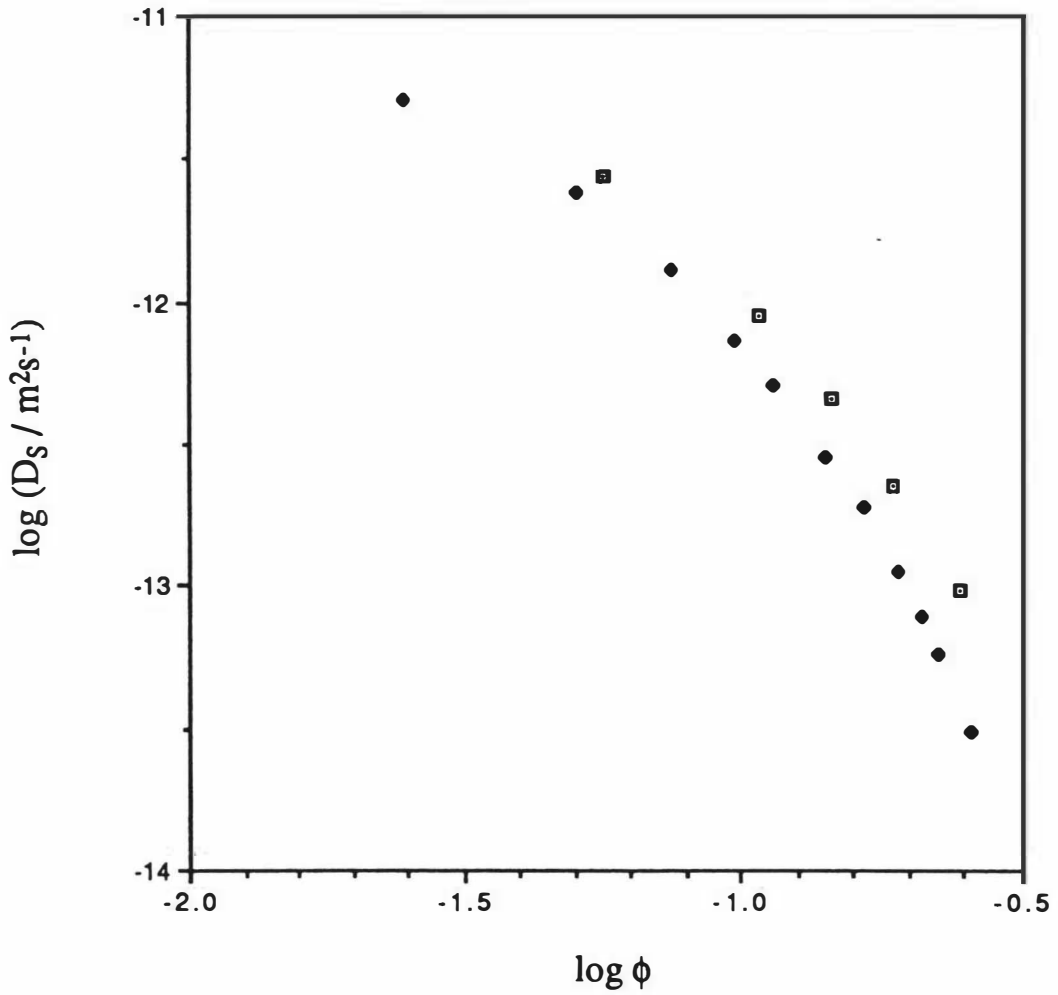

Figure 6.3 The concentration dependence of the polystyrene self diffusion coefficient in PS-PVME-toluene solutions obtained from DLS experiments; this work ▫, and Martin ♦. The PVME and PS molar masses were 102,000 and 929,000 g mol^{-1} in this work and 110,000 and 990,000 g mol^{-1} in Martin's work.

The systematic difference between the results of Martin and those of this work almost certainly results from the difference between the molar masses of the polymers used in the two sets of experiments. Both the PVME and the polystyrene used in the work presented here had slightly lower molar masses than the polymers used in Martin's work (see section 6.1.1). These molar mass differences would both tend to increase the values of D_S reported here compared to Martin's results.

The variation of R_G with molar mass for PVME in toluene is not known, so C^* is difficult to calculate. An approximate value of C^* can be estimated by the following method. The molar mass dependence of the unperturbed mean square end to end distance of PVME is

given in reference [167]. The expansion factor of a polystyrene molecule with the same number of monomers as a 110,000 g mol^{-1} PVME can be estimated as 1.3 in toluene at 25°C. Assuming that the PVME used here has the same expansion factor, a C^* of 45 kg m^{-3} is found. This seems a reasonable figure, because the value of C^* for 110,000 g mol^{-1} polystyrene in benzene is around 60 kg m^{-3} and a PVME molecule has a larger radius of gyration than a PS molecule of the same molar mass.

If this estimate of C^* is correct, it is likely that all of the data points in Fig. 6.3 were measured in the semidilute regime for the PVME matrix. However, the molar mass of the polystyrene is much higher than the matrix molar mass, so that reptation is not expected to be the dominant mechanism for the diffusion of the polystyrene tracer molecules. Instead, Martin has suggested that the polystyrene molecules diffuse according to the Stokes-Einstein equation (eqn (2.62)) with the macroscopic solution viscosity being the dominant influence on the polystyrene self diffusion. If the hydrodynamic radius of the polystyrene remains constant as the PVME concentration is increased, the product of the polystyrene self diffusion coefficient and the macroscopic viscosity of the solution should be independent of concentration, assuming that the PS diffuses by the Stokes-Einstein mechanism. Martin has plotted his data in this form and finds that ηD_S remains relatively constant up to a volume fraction of 0.14 where it begins to rise steadily. Martin interpreted this upturn as being due to either a crossover of the dominant mechanism for diffusion from Stokes-Einstein diffusion to reptation or a concentration dependent collapse of the hydrodynamic radius of the polystyrene molecules. The results presented here indicate that significant contraction of the polystyrene might already occur in relatively dilute solutions, suggesting that the change in the behaviour of Martin's ηD_S - ϕ plot should be attributed to a change in the mechanism of diffusion. Evidence for the existence of a crossover from Stokes-Einstein diffusion to reptation has also been provided by the optical tracer DLS, static light scattering and viscosity measurements on the PS-poly(methyl methacrylate)-benzene system made by Numasawa, Kuwamoto and Nose [69].

Martin gave the first discussion of scaling results for the self diffusion coefficient in solutions containing two chemically different polymers. Martin's discussion [68] of scaling laws for ternary polymer solutions assumes that the matrix polymers do not screen the excluded volume interactions between the blobs of the tracer polymers if the tracer and matrix are chemically different (more precisely, if $\chi \neq 0$). His results are left in terms of the excluded volume parameter, which in general will depend in a complicated way on the polymer-polymer interaction parameter χ, the concentration of the matrix ϕ, and the molar masses of the probe and matrix polymers N and P. Nose [22] has extended this treatment and derived expressions for the blob excluded volume parameter in ternary solutions

consisting of a dilute probe in a semidilute matrix solution. Martin's result for R_G corresponds to a special case (χ large and negative) in Nose's treatment.

The $\chi < 0$ case treated by Nose is appropriate to the compatible PS-PVME pair [163]. Nose's results (ref. [22], Fig. 4) show that the radius of gyration of the probe molecule is expected to decrease as ϕ increases, with the onset of the change occurring at lower values of ϕ as N/P increases. The change in R_G is predicted to be small and asymptotes to a constant value which depends on χ. As χ approaches zero, the change in dimensions increases and approaches the behaviour expected of a bimodal distribution of chemically identical polymers. Although measurements of the composition and temperature dependence of χ in PS-PVME blends [174] and concentrated benzene solutions [163] have been reported, no measurements on semidilute solutions are available. Kwei et al. [163] found that χ was independent of benzene concentration for benzene volume fractions less than 0.2, and also that χ tended to zero in the limit of high PVME/PS ratios. Shibayama et al. [174] found $\chi = -2.74 \times 10^{-2}$ at room temperature in PS-PVME blends composed of 10% PS.

Additional evidence for a severe contraction of the polystyrene at low matrix concentrations is provided by the results of the optical tracer DLS experiments of Wheeler et al. [175]. They found that their plots of log D/D_0 against log C/C_{ps}^* for different molar mass polystyrenes in PVME-(o-flourotoluene) solutions fall on a master curve only if C_{ps}^* is calculated assuming that $C_{ps}^* \sim M^{-0.5}$ as it does in a theta solvent.

The evidence assembled above therefore suggests that in the concentration range covered by these experiments, χ is probably negative but small for PS-PVME interactions in semidilute PS-PVME-toluene solutions. This implies that the contraction of PS in PS-PVME-toluene solutions takes place at a lower concentration than is suggested by Martin.

6.2. DLS Experiments on PS-PVME-Carbon Tetrachloride

The PS-PVME-toluene system examined in the previous section is not suitable for PGSE NMR measurements of polymer diffusion for two reasons. Firstly, the presence of protons in the toluene means that there is a very large solvent signal which can make PGSE NMR measurements on the polymer difficult. Secondly, the very low concentration of polystyrene in these solutions makes it impossible to do a direct measurement of PS self diffusion by PGSE NMR, so that only the PVME self diffusion may be measured, even if the solvent signal is absent.

The solvent signal can be eliminated by using a deuterated solvent, or more conveniently, by using a solvent such as carbon tetrachloride which contains no hydrogen atoms. The

experiments discussed in this section were conducted to assess the possibility of substituting carbon tetrachloride for toluene in optical tracer DLS experiments. The thermodynamic incompatibility of PS and PVME in CCl_4 strongly influences these DLS experiments. It is found that even when the PS concentration is low, D_I and D_S may differ due to thermodynamic effects, so that optical tracer measurements do not necessarily give the self diffusion coefficient of the trace component.

6.2.1. Experimental

The refractive index of carbon tetrachloride at a wavelength of 589 nm and temperature 20°C is 1.460 [167] which actually provides a better refractive index match with PVME (n = 1.467) than toluene. (The match is still not quite as good as that provided by o-fluorotoluene which has a refractive index of 1.468 [167].) Therefore, the PS-PVME-CCl_4 system would appear to be suitable for optical tracer DLS measurements.

The PVME used in these experiments was a fractionated sample, G-PVME fraction B2, which has already been discussed in section 5.2.2. Considering the similarity of the concentration dependences of the mutual diffusion coefficients of fractions B2 and E2 shown in Fig. 5.10, the molar mass of this fraction must be close to the molar mass of fraction E2, which was determined using the Svedberg equation as 110,000 g mol^{-1} (see section 5.2.3). The polystyrene was the same as that used for the experiments in the preceding section. The carbon tetrachloride was a spectroscopic grade solvent which was used as received.

The sample preparation technique for this series of experiments was slightly different from that used for the PS-PVME-toluene experiments. Only a limited quantity of the G-PVME B2 fraction was available, so the most concentrated sample was made first and then diluted as required to cover the desired concentration range. After each dilution, it was necessary to add a small quantity (less than 100 µl) of the stock polystyrene solution (3.28 mg g^{-1}) to maintain the total polystyrene concentration at 0.2 mg g^{-1}. The range of concentrations covered in these measurements was from 36 to 94 kg m^{-3}. The sample was contained in a tightly stoppered 1 cm square cross-section fluorimeter cell. Evaporation of solvent during the course of the measurements was checked by weighing and found to be negligible.

When the measurements at each concentration were completed, a small quantity (approximately 70 µl) of solution was removed and placed in an NMR tube to be used later for PGSE NMR measurements.

The concentration of a portion of one of the dilute samples was measured by weighing the sample before and after the evaporation of solvent, and the concentrations of the other samples were calculated from the masses before and after dilutions.

The technique used in the DLS experiments was the same as that described in the previous section, except that a more systematic examination of the q dependence was made. Experiments were performed at 27°, 60°, 90° and 120°. Several runs were made, often over a period of a few days, at each angle. Correlation functions measured at a given angle were averaged after adjusting the intercept of each run to the same value (see section 3.2.4). Quadratic cumulant fits were used to extract the effective diffusion coefficient and second moment at each angle (see section (2.4.1).

The value of D_0 for the polystyrene alone in CCl_4 at 0.2 mg g^{-1} was also measured by DLS. These measurements were performed at low angles (17° and 27°) because the low scattered intensity combined with shorter sample times made measurements at higher angles more difficult and time consuming.

All measurements were made at a temperature of 30°C.

PGSE NMR experiments were performed to measure the self diffusion of the PVME. These experiments were performed using the old PGSE probe ($G = 0.1577\ T\ m^{-1}A^{-1}$, see section 3.1.1). The calibration of G was checked by measuring the self diffusion coefficients of pure water and cyclohexane at 30°C and was found to be within 2 percent of the value previously used. These measurements were started about six weeks after the light scattering measurements were finished. By this time, the most concentrated samples, which were made the earliest, had suffered some oxidative degradation. This was made evident by a brown tinge which the samples had acquired. It appeared that the small volume of the NMR sample, combined with a large volume of air above the sample in the NMR tube, provided an ideal environment for degradation. The two most dilute, and therefore most recently made samples were the least affected and gave reasonable results. These are plotted and discussed with similar results in section 6.3. The other samples gave scattered results and anomalously high self diffusion coefficients, so they were discarded.

An interesting phenomenon was noticed when the polystyrene solution was mixed with the PVME solutions. Within an hour of the addition of the polystyrene-CCl_4 solution (or even sooner at the lower concentrations), fingers of polystyrene-rich solution could be seen flowing slowly upwards from the bottom of the cell. This was first observed when a cell was placed in the path of the unfocused laser beam to check whether the the polystyrene had completely dissolved. At the tips of the fingers, cloudiness due to phase separation could be seen. In the most concentrated solution, the fingers persisted for about 24 hours.

A similar effect has been observed before in ternary polymer solutions. Preston et al. [176] observed structured flows in several different multicomponent solutions containing polymers, one of which was the poly(vinyl pyrrolidone)-dextran-water system. The structured flows were observed when a dextran solution was layered on top of a similar solution containing a small additional concentration of PVP, even though gravitationally stable initial conditions had been established (i.e. by placing the more dense solution at the bottom of the cell). McDougall and Turner [177] and Comper, Checkley and Preston [178] have presented detailed explanations of the effect in terms of convection due to the formation of gravitationally unstable regions near the boundary between the two solutions. Their explanations propose that cross-diffusion effects (i.e. diffusion of one component due to a gradient of another) are responsible for the creation of the instabilities.

In the case of the PS-PVME-CCl_4 system discussed here, it was observed that the polystyrene solution which was added to the cell sank to the bottom and formed a layer immediately. This is reasonable because the PS solution was dilute and therefore had a higher density than the surrounding solution due to the high density of CCl_4. The fingers in this case may have developed by a mechanism involving phase separation, because, as was mentioned earlier, a slight cloudiness was seen at the tips of the upward moving fingers. Once the fingers had dissipated, there was no observable sign of any cloudiness or non-uniform distribution of polystyrene in the solutions. The depolarized component of the scattered light was weak, indicating the absence of multiple scattering.

6.2.2. Results

Correlation functions measured in DLS experiments on the highest and lowest concentration samples are shown in Figures 6.4a and 6.4b. A feature of the data which is immediately apparent is the distinct non-exponentiality of the correlation function measured at the higher concentration. The values of $\mu_2/\langle\Gamma\rangle^2$, measured at 27° (the most precise values) fell from 0.25 to 0.09 as the PVME concentration decreased. The non-exponentiality of the correlation functions measured at higher concentrations is attributed to polydispersity rather than the appearance of the collective mode for the following reasons. If a collective mode were to appear, it would have a faster decay rate than the interdiffusion mode. The correlation functions collected in these experiments showed a general curvature of the log plots rather than the onset of a fast mode at short times. The decay rate of the collective mode would be expected to increase while that of the interdiffusion mode would be expected to decrease at higher concentrations, increasing the resolution of the two modes. This was not observed in the experiments discussed here.

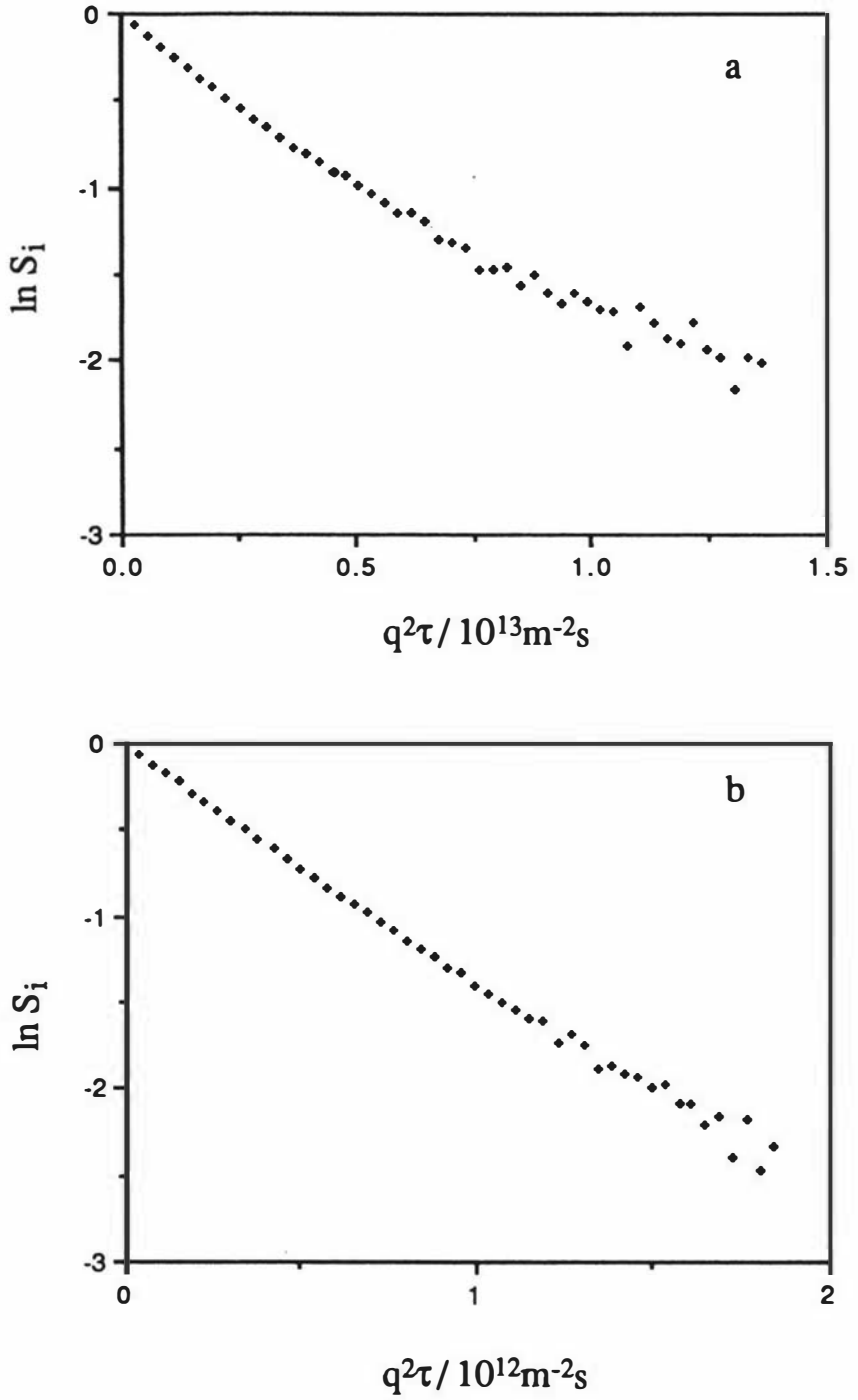

Figure 6.4 DLS data obtained for the PS-PVME-CCl_4 system. (a) The total polymer volume fraction was 0.092 and the polystyrene mass fraction was 0.00021. The correlation function shown here is an average of four correlation functions measured at an angle of 90°, each having a baseline, B for the unnormalized photocount correlation function of about 4.3×10^4. Note that the intercept was adjusted before averaging the correlation functions. (b) The total polymer volume fraction was 0.035. Seven runs measured at an angle of 27°, each having a baseline $B = 4 \times 10^5$ were averaged to produce this correlation function.

The q dependence of the effective diffusion coefficient ($D_{eff} = \langle \Gamma \rangle / q^2$) for the highest concentration sample is shown in Fig. 6.5. Similar plots were obtained for the other samples and the results of linear fits to these plots are given in Table 6.1. As was mentioned in section 6.1.3, the theory of Benmouna, Benoit, Duval and Akcasu [100] gives a particularly simple expression for the q dependence of the effective diffusion coefficient when the optical tracer conditions are satisfied, the polymers are compatible and the solvent is good for both of them. In this case, D_I is equal to D_S, the "bare" diffusion coefficient in the theoretical treatment of [100]. Values of the radius of gyration calculated from the slope of D_{eff} against q^2 using equation (6.2) are given in Table 6.1. The theory of [100] is only valid above C^* and the particular expressions used here were derived for a special case which may not be applicable to these experiments, so these values must be treated cautiously. More explicitly, equation (6.2) was actually derived for the case of two compatible polymers of equal molar mass, one of which has no contrast with the solvent, the other being present only at trace concentrations, dissolved in a solvent which is good for both of them.

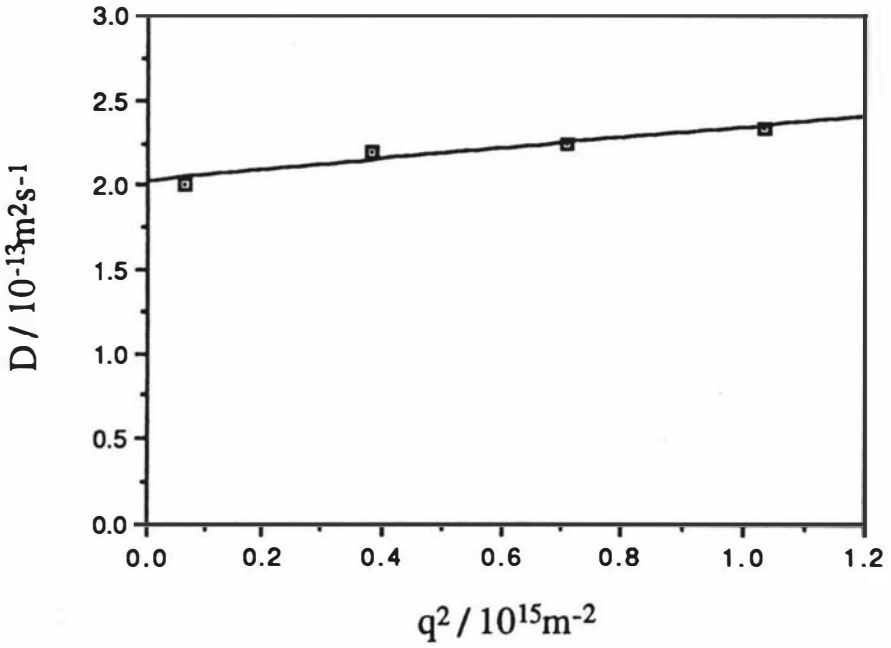

Figure 6.5 Scattering vector dependence of the effective diffusion coefficient in the PS-PVME-CCl_4 system. The polymer volume fraction was 0.092. A linear fit using equation (6.2) gives R_G = 22±2 nm.

The general theoretical framework of [100] does not include the effect of hydrodynamic interactions. This is not a serious omission at high concentrations due to the screening of hydrodynamic interactions, but at lower concentrations, hydrodynamic interactions are not screened. The calculation of the equivalent "bare" effective diffusion coefficient including the effects of hydrodynamic interactions has already been performed by Burchard, Schmidt and Stockmayer [179]. They calculated the q dependence of the effective diffusion coefficient for a polymer in a solvent at infinite dilution using the non-preaveraged Oseen tensor to incorporate hydrodynamic interactions. All that is required to adapt their expression to the purpose of this work is to replace their D_0 by D_s. This provides an expression for the q dependence of D_{eff} which may be compared with eqn (6.2).

Whereas D_{eff} is independent of q for a monodisperse system of rigid, spherical scatterers, the internal motion of polymer molecules results in q dependence for a monodisperse polymer solution. In the small q region, this q dependence has been calculated by Burchard et al. [179] as

$$D_{eff} = D_0 \left(1 + \frac{13}{75} q^2 R_G^2\right) \quad . \tag{6.3}$$

It should be noted that polydispersity has a weak effect on the value of the constant appearing in eqn (6.3); if the polydispersity is increased from M_w/M_n = 1.0 to 2.0, the value of the constant only changes from 0.17 to 0.20 [179]. Values of R_G calculated using eqn (6.3) are also given in Table 6.1.

Table 6.1 Results of linear fits to the scattering vector dependence of the effective diffusion coefficient.

Polymer volume fraction, ϕ	Intercept D_I / 10^{-13} m^2s^{-1}	Slope / 10^{-29} m^4s^{-1}	R_G / nm from eqn (6.2)	R_G / nm from eqn (6.3)
0.035	14.8	12.4	15.9	22.6
0.057	6.55	5.36	15.7	21.9
0.072	3.80	4.67	19.2	26.9
0.087	2.55	2.79	18.1	25.4
0.092	2.02	3.16	21.7	30.3

The values of D_{eff} extrapolated to zero angle are plotted against concentration in Fig. 6.6. The results from section 6.1.2 are also shown for comparison.

DLS measurements on the M = 929,000 g mol^{-1} polystyrene at a concentration of 0.2 mg g^{-1} in CCl_4 gave $D_0 = 1.02 \times 10^7$ m^2s^{-1} ($\log D_0 = -10.99$).

6.2.3. Discussion

The values of D_I obtained in these experiments clearly differ from those obtained for the PS-PVME-toluene system. Several factors contribute to differences between the two sets of experiments. The temperature and solvent viscosity have been changed from 25°C and 5.516×10^{-4} Pa s in the case of the PS-G-PVME-toluene experiments to 30°C and 8.43×10^{-4} Pa s in these experiments. In addition, the unfractionated G-PVME was used in the previous experiments, while those discussed here used G-PVME fraction B2. The combined effects of these factors are still insufficient to explain the large deviation seen in Fig. 6.6. The temperature and viscosity effects can be estimated using a similar procedure to that used in Chapter 4. The net effect would be an upward shift of $\log D_I$ for the CCl_4 points by only 0.18 units. The diffusion coefficients of fraction B2 and the unfractionated G-PVME discussed in Chapter 5 were virtually identical, suggesting that their molar masses were also similar. Therefore, the lower diffusion coefficients are unlikely to have been caused by the use of fractionated rather than unfractionated PVME as the matrix polymer.

If the mechanism of the polystyrene diffusion is assumed to be Stokes-Einstein diffusion, as it was in section 6.1, and it is assumed that D_I is equal to D_s in these measurements, there are two possible explanations for the lower diffusion coefficients in the PS-PVME-CCl_4 system. The first is an increase in the viscosity of the matrix polymer solution, and the second is an increase in the hydrodynamic radius of the polystyrene. However, a simple change of solvent would be unlikely to increase either of these quantities by the factor of three required to bring the two sets of data in Fig. 6.6 into coincidence, so this explanation must be discarded.

It is well known that PS-PVME blends formed from solutions in toluene exhibit behaviour characteristic of a well mixed single phase system. Such blends are optically clear and exhibit a single glass transition in differential scanning calorimetry experiments [180]. NMR experiments on PS-PVME blends made from toluene solutions give a single longitudinal relaxation time, T_1 [163]. However, blends cast from solutions of PS and PVME in solvents such as chloroform and trichloroethylene are cloudy and exhibit two glass transitions at temperatures characteristic of the component polymers [180]. This indicates that the PS and PVME exist in separate phases distributed throughout the blended

material. The behaviour of PS-PVME mixtures in carbon tetrachloride, which is chemically very similar to chloroform and trichloroethylene, can be expected to be similar.

The reduced compatibility of polystyrene and PVME in carbon tetrachloride had a strong influence on these experiments. The cloudiness, due to local phase separation, which was observed when polystyrene was added to the solution soon disappeared as the local concentration of polystyrene decreased, but the effective solvent quality of the PVME-CCl_4 solution for the polystyrene must nevertheless have been quite poor. The increase of $\mu_2/\langle\Gamma\rangle^2$ at higher concentrations might therefore be attributed to increased polydispersity due to aggregation of the polystyrene.

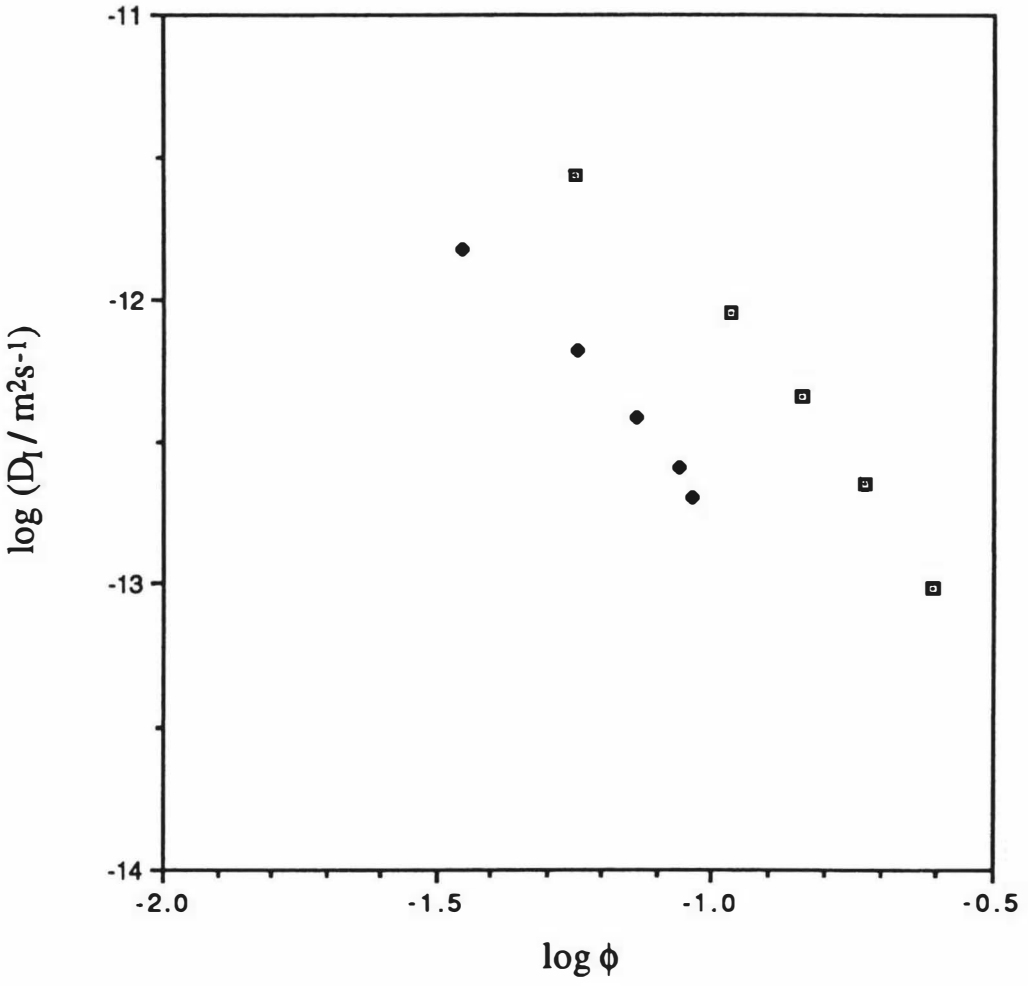

Figure 6.6 Concentration dependence of D_I (equation (2.155)) for the PS-PVME-CCl_4 system (●). The D_S values obtained in section 6.1 for the PS-PVME-toluene system are also shown (▫) for comparison. In both cases, the PS molar mass was 929,000 g mol^{-1}. In the toluene measurements the PVME molar mass was 102,000 g mol^{-1} and in the CCl_4 measurements, the PVME molar mass was 110,000 g mol^{-1}.

The decrease in the values of D_I for the PS-PVME-CCl_4 solutions relative to those found in the PS-PVME-toluene solutions can be qualitatively understood in terms of the theory of Benmouna et al. [100]. One of the two special cases which they discussed, the case of two polymers of equal molar mass, one of them having no contrast with the solvent, in a solvent of the same quality for both polymers, (case A) can be compared with the experiments of this section. The molar masses of the PS and PVME used in the experiments of this section were not equal, but the PVME is, to a good approximation, isorefractive with the CCl_4. The solvent quality of CCl_4 for PS is known to be moderately good, but its quality as a solvent for PVME is unknown. Leaving aside these differences for the moment, it is instructive to focus on the result obtained by Benmouna et al. [100] for the decay rate of the interdiffusion mode, equation (2.155).

Although the derivation of eqn (2.155) contains several restrictive assumptions, it does show that D_I can be less than D_s under certain circumstances. In particular, if χ/υ is large and the value of x is close to 0.5, the difference is maximized. Only small values of x were used in these measurements, but a large value of χ/υ would result from a large, positive value of χ or a small value of υ. This would correspond to incompatible polymers or a poor solvent. Carbon tetrachloride is a moderately good solvent for polystyrene, but its solvent quality for PVME is unknown. The solubility of PVME in CCl_4 indicates that it is at least a theta solvent. The value of χ for PS-PVME blends in the melt is composition dependent, but is generally negative, indicating that the polymers are compatible in the melt. The value of χ is, however, possibly also solvent dependent. The low values of D_I are therefore consistent with a reduction in the PS-PVME compatibility in the presence of carbon tetrachloride, but a more quantitative investigation is not possible here.

The q dependence of the effective diffusion coefficient is a more subtle issue. If the reduction of D_I is due to an increase in the second term of eqn (2.155), eqns (6.2) and (6.3) are inadequate and the complete form of eqn (2.155) must be used to interpret the data. Parameters such as A_2 and χ/υ are unknown for the PS-PVME-CCl_4 system, but Fig. 6.6 shows that the values of D_I (extrapolated to q=0) and D_s differ by an approximately constant factor of about 3 after the viscosity and temperature corrections are taken into account. Using this in eqn (2.155) leads to radii of gyration which are approximately 0.6 of the values calculated from eqn (6.2) (Table 6.1); i.e. the q dependence of D_{eff} may be just as strong as it was for the PS-PVME-toluene samples, even though the radius of gyration is smaller, due to thermodynamic effects. If the values of R_G for polystyrene in the PS-PVME-toluene solutions (section 6.1) and the PS-PVME-CCl_4 solutions found here are correct, the difference could be attributed to the incompatibility of the polymers in CCl_4. The values of R_G in the PS-PVME-toluene system were already lower than the theta solvent dimensions. The radius of a compact sphere containing a totally collapsed polystyrene

molecule of molar mass 929,000 g mol^{-1} would be approximately 6.9 nm. The radius of gyration of such a sphere would be equal to $(3/5)^{1/2}R$ = 5.3 nm, so the polystyrene molecules are still far from totally collapsed, and radii of gyration 0.6 times the values given by eqn (6.2) are therefore not unrealistic. These calculations involve several strong assumptions, but they give at least a qualitative understanding of the behaviour of this system.

6.3. DLS and PGSE NMR Experiments on PS-PVME-Toluene

A direct comparison of the diffusion coefficients obtained by optical tracer DLS and PGSE NMR was not possible for the systems studied in sections 6.1 and 6.2. PGSE NMR measurements with the current technology require polymer concentrations of at least 5 mg g^{-1}, even under favourable conditions, but the polystyrene concentrations in the experiments of sections 6.1 and 6.2 were only 0.2 mg g^{-1}. Trial experiments were conducted to determine whether PS-PVME-CCl_4 solutions with sufficiently high polystyrene concentrations for PGSE measurements could be prepared. As the polystyrene concentration was increased, the solutions approached the cloud point and finally, phase separation occurred. (A solution with a PVME mass fraction of 0.112 and a polystyrene mass fraction of 0.013 underwent phase separation during a preliminary light scattering experiment and the portion of the sample in the focused beam started to char after becoming opaque!) Phase separation also occurred when the samples were made with deuterated chloroform.

The solution to these difficulties was to use deuterated toluene ($C_6D_5CD_3$ or toluene d8) as the solvent. The refractive index match between toluene and PVME is acceptable, and compatibility is assured.

The molar mass of the polystyrene was chosen so that Stokes-Einstein diffusion would not be the dominant mechanism for diffusion over most of the concentration range as it was in the experiments of section 6.1. This required a PS molar mass less than or comparable to the PVME molar mass. Equal molar masses were preferred because of the correspondence with a special case of the theory of Benmouna et al. [100].

6.3.1. Experimental

It was intended that both PGSE NMR and DLS experiments should be performed on the same samples in this set of experiments. The polystyrene concentration was therefore increased above the 0.2 mg g^{-1} used in the experiments of sections 6.1 and 6.2. The effect of the additional polystyrene on the measurements was investigated by varying the proportions of PS and PVME in the solutions.

The concentration of polystyrene as a proportion of the total polymer concentration can be conveniently defined as

$$x = C_{ps} / (C_{ps} + C_{pvme}) \tag{6.4}$$

where C_i is the mass/volume concentration of component i. Samples with four different values of x were made. One of the samples contained too little polystyrene for PGSE NMR or DLS measurements of the polystyrene diffusion, but it was still possible to measure the PVME self diffusion in this sample by PGSE NMR. Lower concentrations of the samples were made by successive dilutions, without adding any polymer. This differs from the technique of sections 6.1 and 6.2 in which the PS concentration was maintained at 0.2 mg g^{-1}. The characteristics of the components of the four series of samples are summarized in Table 6.2.

Table 6.2 Components of samples.

Series	Solvent	PVME	$x = C_{ps} / (C_{ps} + C_{pvme})$
D	C_7H_8	G-PVME D2	0.001
E6	C_7D_8	G-PVME E2	0.056
E11	C_7D_8	G-PVME E2	0.114
E25	C_7D_8	G-PVME E2	0.246

The polystyrene used in these experiments was a standard polystyrene with M_w = 110,000 g mol^{-1} and M_w/M_n = 1.06 (lot 4b), obtained from the Pressure Chemical Co., USA.

The G-PVME fraction E2 was discussed in Chapter 5. The molar mass of this fraction obtained from sedimentation and diffusion measurements using the Svedberg equation was 110,000 g mol^{-1} and M_w/M_n was estimated from DLS measurements as 1.3. The G-PVME D2 fraction can be expected to have similar molar mass characteristics to the G-PVME E2 fraction.

The deuterated toluene used in these experiments was obtained from two sources; CEA, Service des Molécules, Marquées, France (DMM-5, lot 179-780) and the Sigma Chemical Co., USA (Lot 58C-0099). Each of these solvents had a 99+% deuteration rating.

The undeuterated toluene was a chromatography grade solvent manufactured by BDH Chemicals, England.

The compositions of the samples studied in this set of experiments are listed in Table 6.3.

Table 6.3 Compositions of samples.

Sample name	PS mass fraction	PVME mass fraction	Total polymer conc., C / kg m^{-3}	Total polymer vol. fraction
D-1	0.00030	0.51463	480.5	0.472
D-2	0.00025	0.42265	388.5	0.382
D-3	0.00018	0.31041	280.1	0.275
D-4	0.00012	0.21230	188.5	0.185
D-5	0.00008	0.13491	118.3	0.116
D-6	0.00005	0.09448	82.3	0.081
E6-1	0.02992	0.50547	525.1	0.514
E6-2	0.02560	0.43250	446.3	0.437
E6-3	0.01799	0.30383	310.0	0.304
E6-4	0.01322	0.22335	226.3	0.222
E6-5	0.00891	0.15049	151.5	0.148
E6-6	0.00670	0.11321	113.6	0.111
E11-1	0.06568	0.51291	570.7	0.557
E11-2	0.05318	0.41532	457.6	0.447
E11-3	0.03887	0.30356	330.8	0.323
E11-4	0.03151	0.24611	266.7	0.260
E11-5	0.01789	0.13968	149.8	0.146
E11-6	0.01336	0.10434	111.5	0.109
E25-1	0.14023	0.42942	564.0	0.546
E25-2	0.09212	0.28207	363.6	0.352
E25-3	0.05586	0.17105	217.4	0.210
E25-4	0.03816	0.11685	147.5	0.143
E25-5	0.02548	0.07804	98.1	0.095
E25-6	0.01794	0.05495	68.8	0.067

The mass/volume concentrations and volume fractions were calculated using the following relationships assuming simple additivity of volumes [19];

$$1 / \rho = \sum_{i=1}^{3} w_i \bar{v}_i \tag{6.5}$$

$$C_i = w_i \rho \tag{6.6}$$

$$\phi_i = C_i \bar{v}_i \ . \tag{6.7}$$

Here, ρ is the solution density, w_i is the mass fraction of component i, $\bar{v}_i$ is the partial specific volume of component i, C_i is the mass/volume concentration of component i and ϕ_i is the volume fraction of component i. The partial specific volume of PVME was taken as 0.983×10^{-3} m^3kg^{-1} [167]. The partial specific volume of polystyrene in toluene was taken as the value at infinite dilution interpolated to 30°C using the temperature dependence given by Scholte [181]. The value of $\bar{v}$ for undeuterated toluene was taken as the reciprocal of the density at 30°C using the value of ρ at 25°C and the temperature coefficient of density given in [183]. The density of deuterated toluene was calculated approximately by assuming that the volume per molecule remains the same as it is for undeuterated toluene and multiplying ρ by the ratio of the molar masses (100.15 / 92.1). This method is suggested in the technical literature provided by a supplier of deuterated solvents [182].

These experiments were subject to a number of severe constraints. A limited quantity of fractionated PVME was available, so small samples were necessary. Duplication of samples was not possible, so the PGSE NMR and DLS experiments had to be done on exactly the same samples. This meant that the samples had to be contained in 4 mm diameter NMR tubes so that they would fit into the high gradient PGSE probe. Specially modified NMR tubes were used for these measurements. Ground glass sockets were added to the tops of the tubes so that they could be sealed with teflon stoppers during experiments and then be easily reopened for dilutions. The optical quality of the NMR tubes was adequate for the DLS experiments, but careful alignment was required and stray reflections were carefully avoided. The high viscosities of the most concentrated solutions presented some difficulties in sample preparation and handling.

The sample preparation technique was as follows. Dilute solutions of the fractionated PVME (about 50 mg g^{-1}) and polystyrene (15 mg g^{-1}) were made. The PVME solution was filtered into a clean light scattering cell. The solvent was slowly evaporated under an aspirator pump vacuum until the desired PVME concentration and sample volume (about 100 µl) was reached. An appropriate quantity of the filtered, dilute polystyrene solution was then added. The solutions were mixed thoroughly over a period of days. Mixing was

assisted by tilting the cell and allowing the solution to slowly flow from one corner of the cell to another. Stirring with a foreign object was avoided in order to prevent contamination of the samples with particulate matter. The distribution of polystyrene was checked by examining the solution in an unfocused laser beam. If necessary, the overall concentration was adjusted after addition and mixing of the dilute polystyrene solution by further evaporation of solvent.

When the solutions had mixed completely, they were transferred to the modified NMR tubes for measurements. (The evaporation and mixing steps would have taken far too long if the samples had been contained in NMR tubes from the beginning.) The transfer was a difficult task to perform because the solutions were too viscous to be drawn into a syringe. It was essential to avoid spreading the solution over the internal wall of the NMR tube during the transfer, because the solutions had to remain as nearly as possible dust free for the DLS experiments. After some trial (and considerable error!) a method of transferring the solutions satisfying these requirements was devised. A length of 11 gauge stainless steel hypodermic tubing was purchased and made into a tubular spatula by grinding one end at a shallow angle to the axis of the tube. It was necessary to remove a thin layer from the outer diameter of the tube so that it slid comfortably into a 4 mm NMR tube. A plunger with a teflon head which slid smoothly inside the hypodermic tube was also manufactured.

The samples could then be transferred using the following method. The hypodermic tube was held horizontally in a retort stand with the plunger withdrawn enough to allow the sample to be loaded. The sample was carefully collected with a fine spatula and deposited in the open end of the hypodermic tube. A cleaned NMR tube was then slipped over the hypodermic tube and the two parts were moved to an upright position. The sample was then gently pushed out of the hypodermic tube into the bottom of the NMR tube. The plunger was withdrawn and the hypodermic tube was removed from the NMR tube. This technique worked well with small volumes (approximately 100 μl) of viscous solutions.

One problem with this method of sample preparation is that some degree of solvent evaporation is inevitable. It was therefore necessary to measure the concentration of the samples again after the experiments were finished.

The E25 and D samples were originally so concentrated that they required an initial dilution before they could be used for measurements.

DLS experiments were performed on the samples of series E6, E11 and E25. The scattering from the series D samples was too weak to allow useful DLS measurements to be made.

Corrections to the refractive indices of the samples due to changes in concentration and wavelength were calculated approximately using equations and data given in [167], [181] and [183].

After each dilution, at least a week of equilibration time was allowed. The equilibration of the samples was quicker than it would have been if extra polymer had been added after each dilution. Mixing was assisted by tilting the tube and allowing the solution to slowly flow from one side to another, or gently agitating the more dilute solutions. The uniformity of each sample was then checked by making measurements at several locations along the tube. The sample was allowed to equilibrate until the results were independent of position.

Experiments were repeated several times over a period of days for each sample. Measurements were made at at least two angles for each sample, and three or four angles for some. The results were independent of angle and wavelength, within experimental errors. Correlation functions measured at different angles for two samples are shown in Fig. 6.7. The correlation functions were well described by second order cumulant fits at all concentrations.

Apart from a very weak enhancement of the first channel which was observed in some of the lower concentration data for series E11 and E25, there was no sign of a fast mode for any of the samples studied here. In fact, the weak enhancement which was observed could not be distinguished from the distortion caused by photomultiplier afterpulsing which becomes apparent at short sample times and low count rates.

At the highest concentrations, long sample times (of the order of 10 ms) were necessary because of the low diffusion coefficients being measured, so the number of counts detected per sample time was high. The incident power was reduced to well below 50 mW with a variable neutral density filter to give a count rate close to one count per sample time. As the concentration of the samples was decreased, higher incident power was required and difficulties due to local heating in the sample were encountered. Fluorescence from the samples was observed, indicating that the heating was probably due to strong absorption of the incident light. The local heating produced a thermal lens effect (spatial variation in refractive index due to temperature differences) which enlarged the diameter of the transmitted beam. Correlation functions were also affected by the local heating. Plots of ln S_i exhibited a downward curvature due to convection in the sample and negative values of $\mu_2/\langle\Gamma\rangle^2$ were obtained. The simplest solution to this problem is to reduce the incident power. In some cases, the power had to be reduced so much that measurements became very difficult. Instead of reducing the incident power further, it was more effective to increase the wavelength of the incident light. At longer wavelengths, less fluorescence was observed, presumably because the resonant absorption was no longer occurring. For some

of these measurements, it was sufficient to change the wavelength of the Ar ion laser from 488.0 nm to 514.5 nm, but it was more often necessary to use a He-Ne laser operating at 632.8 nm.

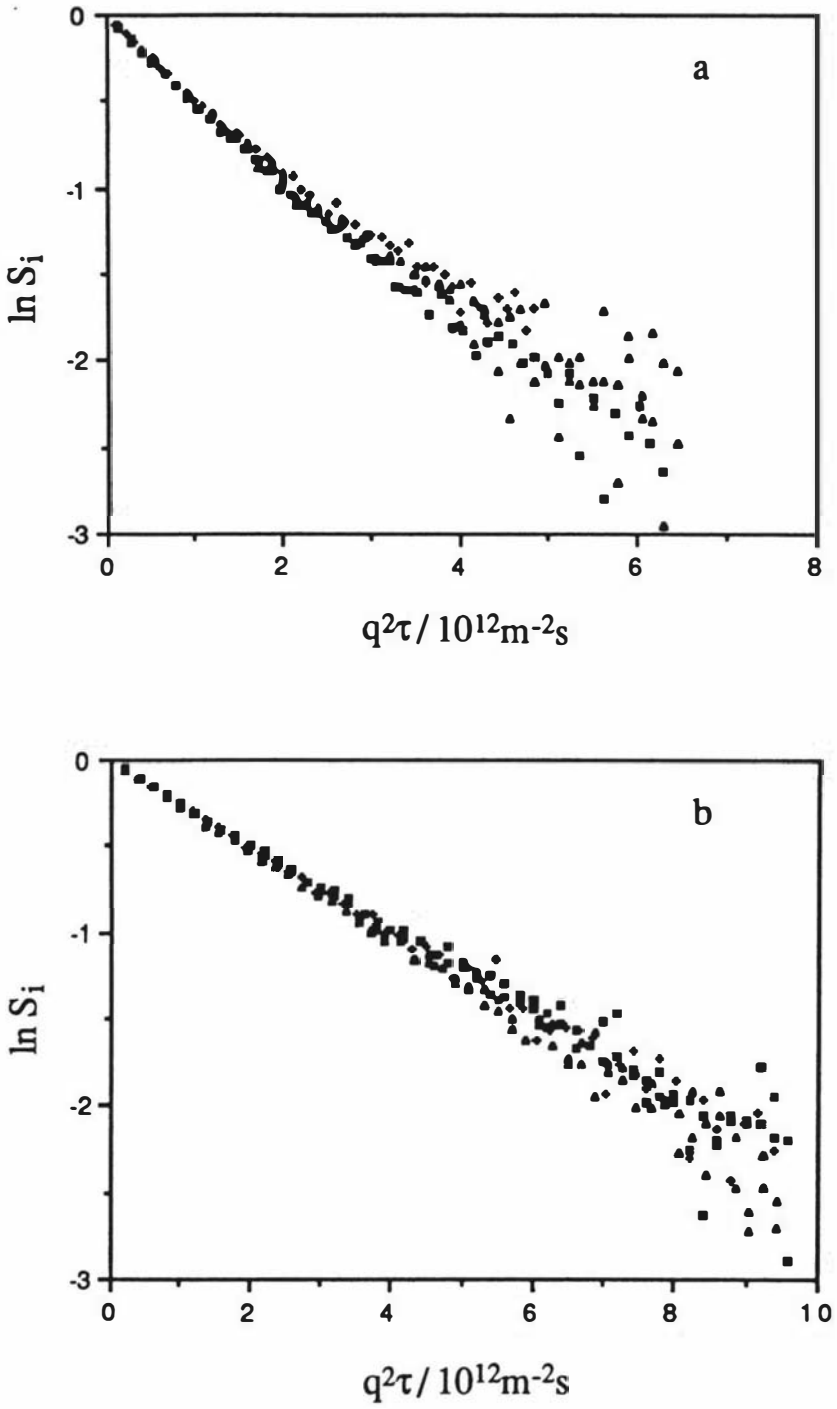

Figure 6.7 Dynamic light scattering data for sample E25-3 (a) and sample E11-4 (b). The correlation functions were measured at angles of 60° (+), 90° (▲) and 120° (■) in (a) and at angles of 30° (▲), 45° (+) and 90° (■) in (b). In each case, correlation functions measured at different angles superimposed when plotted against $q^2\tau$, indicating that D_{eff} was q-independent.

The high field gradient probe (see section 3.1.1) was used for the PGSE NMR experiments discussed in this section. This probe has the particular advantage that the uniformity of the field gradient along the vertical axis allows long samples to be used. The sample length was not a critical parameter, so it was not necessary to remove any of the sample to set the correct sample length after a dilution.

The relative positions of the peaks in the proton NMR spectra of polystyrene, PVME and toluene are particularly important to these experiments. A high resolution spectrum showing the positions of the peaks is given in Fig. 6.8. The names of the functional groups to which the resonances have been assigned are also shown for reference. Figures 6.9 and 6.10 give some examples of spectra measured under different conditions and demonstrate the resolution obtained with the PGSE probe on the JEOL FX60 spectrometer. Figures 6.9 and 6.10 show that the resonances of the polystyrene aliphatic protons overlap with the unresolved PVME peaks, but the peak due to the polystyrene aromatic protons does not. The spectra shown in Fig. 6.10 indicate that the resolution of the PS aromatic proton peak from the peak containing all of the other resonances improved as the concentration of polystyrene as a proportion of the total polymer concentration (i.e. the value of x) was increased.

The normalized echo attenuation A(k)/A(0) was measured as a function of k for three spectral windows in the experiments on the E6, E11 and E25 series samples. The first window (window α) covered all of the peaks and was used by the auto-phasing routine of program PGSE to calculate the first order phase correction. The second spectral window (window β) covered the peak corresponding to the polystyrene aromatic protons, and the third (window γ) covered the region containing the PVME methoxy and methine resonances as well as all of the PVME and polystyrene aliphatic (mainly methylene) resonances. (The PGSE probes have low resolution; high resolution spectra of PVME and polystyrene can be found in Fig. 6.8 and references [184, 185, 186].) Provided that the peaks are sufficiently well resolved and the windows are set appropriately, the echo attenuation plots for window β should directly give the polystyrene self diffusion coefficient. Plots of ln A(k)/A(0) for window β were therefore expected to be linear due to the narrow molar mass distribution of the polystyrene. A representative echo attenuation plot for window β is shown in Fig. 6.11.

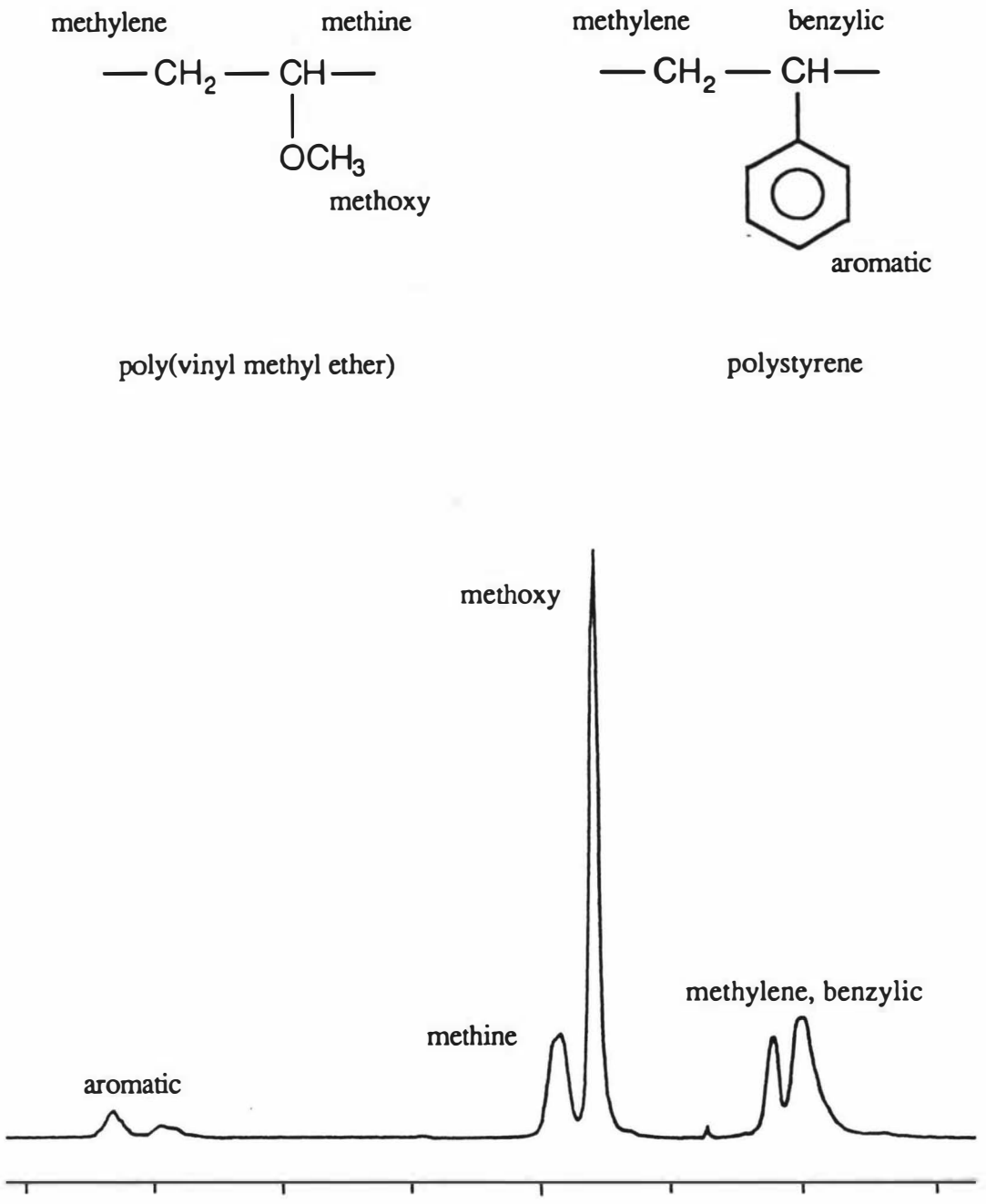

Figure 6.8 At the top of this Figure, the structures of the PVME and polystyrene monomer units are shown. The names of the protons on different functional groups are given for reference. At the bottom, a high resolution spectrum recorded on a JEOL GX270 NMR spectrometer is shown. The sample was a PS-PVME-(toluene d8) solution made with unfractionated G-PVME (Gantrez M555) and the 110,000 g mol^{-1} polystyrene mentioned in the text. The total polymer volume fraction was approximately 0.4 and x was approximately 0.11.

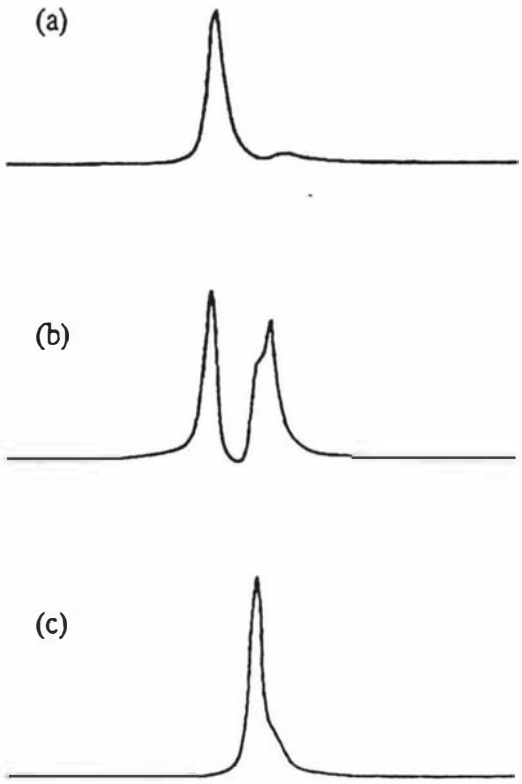

Figure 6.9 Spectra recorded at low resolution with the PGSE probe on the JEOL FX60 spectrometer. Spectrum (a) shows the spectrum of polystyrene ($M = 2 \times 10^6$ g mol^{-1}) in CCl_4 at a concentration of $C = 154$ kg m^{-3}. This spectrum was obtained using a two pulse spin echo pulse sequence (Fig. 2.4) with $\tau = 15$ ms. The aromatic resonances comprise the peak on the left and the methylene and benzylic resonances comprise the peak on the right. The methylene and benzylic resonances have smaller values of T_2 than the aromatic resonances, so their intensities are attenuated more rapidly than the aromatic resonance as τ is increased. Spectrum (b) shows the spectrum of a D series sample obtained using the two pulse spin echo pulse sequence with $\tau = 15$ ms. When the pulsed gradient was included in the pulse sequence, spectrum (c) was obtained. The aromatic resonances were strongly attenuated and the peak containing the other resonances changed shape, due to the strong attenuation of the signal from the undeuterated toluene which contains both aromatic and aliphatic (CH_3) protons. The toluene diffuses rapidly and is strongly attenuated, but the attenuation of the PVME signal is weaker due to its relatively slow diffusion. Note that the peak containing the polystyrene methylene and benzylic resonances in (a) occurs in the same region of the spectrum as the peak containing the PVME resonances in (c).

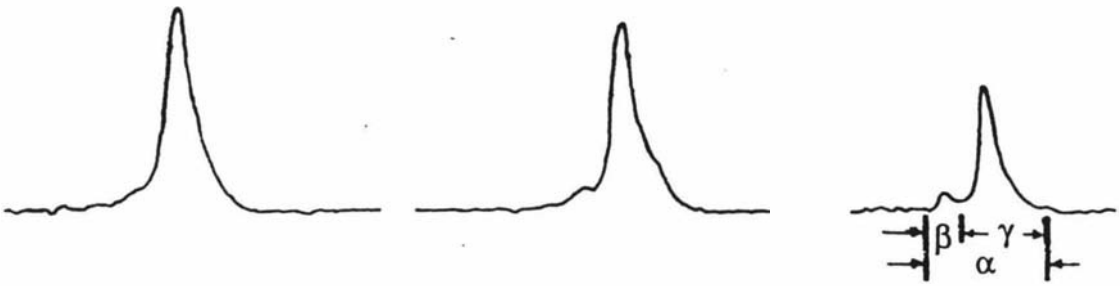

Figure 6.10 Spectra obtained in PGSE experiments at τ = 20 ms and k = 0 for samples E6-3, E11-3 and E25-2, showing the resolution obtained in PGSE experiments. The horizontal scale is the same in each case, but the vertical scales are arbitrary. Approximate positions of the integration windows (α, β, γ) used to calculate the echo attenuations are shown. The polystyrene aromatic peak becomes more well defined as x is increased.

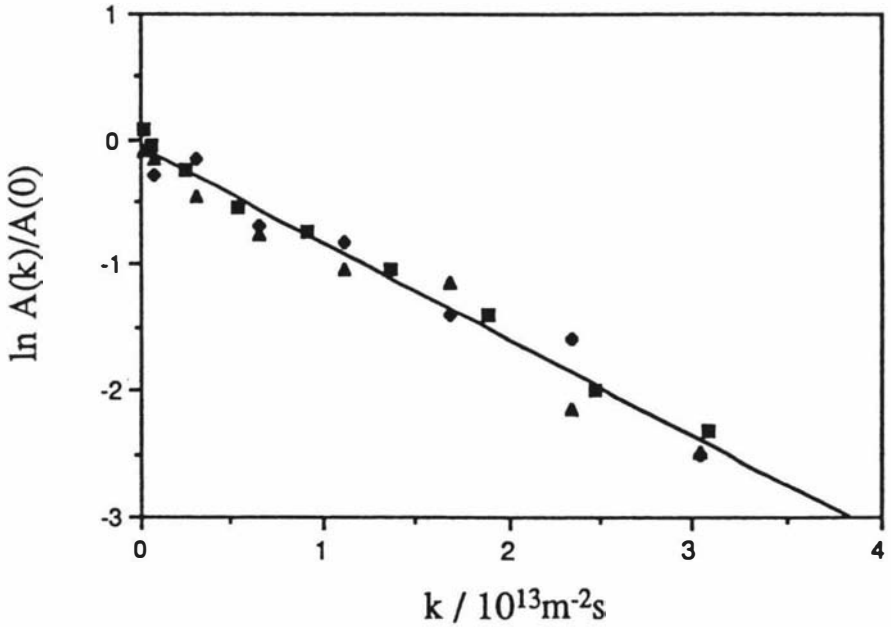

Figure 6.11 Echo attenuation plot for window β for sample E6-2. The parameters used in the experiments were; $\tau = \Delta$ = 20 ms, G = 10.71 T m^{-1}, δ varied from 1 to 16 ms (■, ●); $\tau = \Delta$ = 20 ms, G = 11.90 T m^{-1}, δ varied from 1 to 16 ms (▲).

The echo attenuation plots for window β were analysed using linear least squares fits to ln A(k)/A(0) and a diffusion coefficient, designated as D_β, was calculated from the slope. The echo attenuation plots for window β were often noisy and they were also sensitive to any small changes in peak position due to interactions between the pulsed field gradient and the field lock circuit. The spectral windows were frequently checked and were adjusted if any small drifts in peak positions had occurred. Occasionally, it was necessary to reject data showing anomalously severe apparent echo attenuations due peak shifts. Within experimental errors, the plots of ln A(k)/A(0) for the data from window β were linear, providing support for the assumption that the self diffusion coefficient of the polystyrene alone was being measured.

There was no detectable peak within the spectral region of window β for the D series samples due to the low concentration of polystyrene present in these samples.

Nonlinear plots of ln A(k)/A(0) for window γ were expected for both the D and E series samples. The polydispersity of the PVME ($M_w/M_n = 1.3$) was expected to contribute to the nonlinearity of ln A(k)/A(0) for all samples. The nonlinearity of ln A(k)/A(0) for the E series samples was also expected to contain a small contribution from the PS echo attenuation due to the overlap of PS and PVME peaks (assuming that the PS and PVME have different diffusion coefficients). Typical echo attenuation plots for window γ obtained from D and E series samples are shown in Fig. 6.12 and Fig. 6.13 respectively. The curvature of ln A(k)/A(0) due to polydispersity has been discussed in section 2.3.4. The discussion of section 2.3.4 focused on the effect of polydispersity in dilute solutions, but the arguments leading to equation (2.114) are equally valid for concentrated solutions. (The same extension cannot generally be made in the case of dynamic light scattering [187], except when the self dynamic structure is being measured. This is true, for example, at infinite dilution. PGSE NMR always measures the self dynamic structure factor whereas DLS generally measures the full dynamic structure factor.) Assuming that ln A(k)/A(0) can be adequately described by a second order polynomial fit and that T_2 remains independent of M at higher concentrations, A(k)/A(0) can be written as

$$A(k)/A(0) = A_0 \exp[-k\langle D\rangle_w + \tfrac{1}{2} V_D (k\langle D\rangle_w)^2] \qquad (6.8)$$

where V_D is the normalized variance of the distribution of diffusion coefficients, defined as

$$V_D = (\langle D^2\rangle_w - \langle D\rangle_w^2) / \langle D\rangle_w^2 \quad . \qquad (6.9)$$

The form of A(k)/A(0) is more complicated for the E series samples. The most general expression for the echo attenuation retains the τ dependence of the amplitudes of each

resonance included in the window. For two monodisperse polymers in a deuterated solvent, this would give

$$A(2\tau,k) = \sum_{i=1}^{n} A_{1i}(2\tau) \exp(-kD_1) + \sum_{j=1}^{m} A_{2j}(2\tau) \exp(-kD_2) \qquad (6.10)$$

where n and m are the number of resonances of polymers 1 and 2 contained in the spectral window, $A_{1i}(2\tau)$ and $A_{2j}(2\tau)$ are the echo amplitudes (or peak areas in the frequency domain) obtained at $k = 0$ for each resonance and D_1 and D_2 are the self diffusion coefficients of polymers 1 and 2. It is often assumed that $A(2\tau)$ can be written in terms of the spin-spin relaxation time T_2, as is done in equation (2.86), but other effects such as spin-spin scalar coupling [82] may also influence $A(2\tau)$ so, for generality, the explicit form of the τ dependence of $A(2\tau)$ has not been given.

Provided that all of the points on a given echo attenuation plot are measured at a constant value of τ, $A(2\tau,k)$ is a simple sum of two exponentials with amplitudes $A_1(2\tau)$ and $A_2(2\tau)$;

$$A(2\tau,k) = A_1(2\tau) \exp(-kD_1) + A_2(2\tau) \exp(-kD_2) \ . \qquad (6.11)$$

Allowing for the polydispersity of the PVME, this becomes

$$A(2\tau,k) = A_1(2\tau) \exp[-kD_1 + \tfrac{1}{2} V_D (kD_1)^2] + A_2(2\tau) \exp(-kD_2) \qquad (6.12)$$

where $D_1 = \langle D \rangle_w$ is the weight averaged self diffusion coefficient of the PVME and D_2 is the self diffusion coefficient of the PS.

The value of k was varied by changing δ or G in these experiments. The r.f. pulse separation τ was kept constant during the measurement of points on a given echo attenuation plot and echo attenuation plots with different τ values were not combined in the data analysis.

Each $A_{1i}(2\tau)$ is proportional to $A_{1i}(0)$ which in turn, is proportional to the total number of nuclei contributing to resonance i that are contained in the receiver coil. The value of $A_1(0)$ is therefore a sum of terms proportional to the number of protons per molecule contributing to each resonance of polymer 1 included in the spectral window and the total number of molecules of polymer 1 contained in the receiver coil. The ratio of amplitudes contributed by each polymer to a given peak is then simply related to the number densities, or concentrations, of the polymers. A calculation based on these considerations shows that the ratio of the PVME signal to the PS signal in window γ at $\tau = 0$ should be approximately 11 for the E25 series and 61 for the E6 series, so the PVME signal should dominate, i.e. $A_1(0) > A_2(0)$.

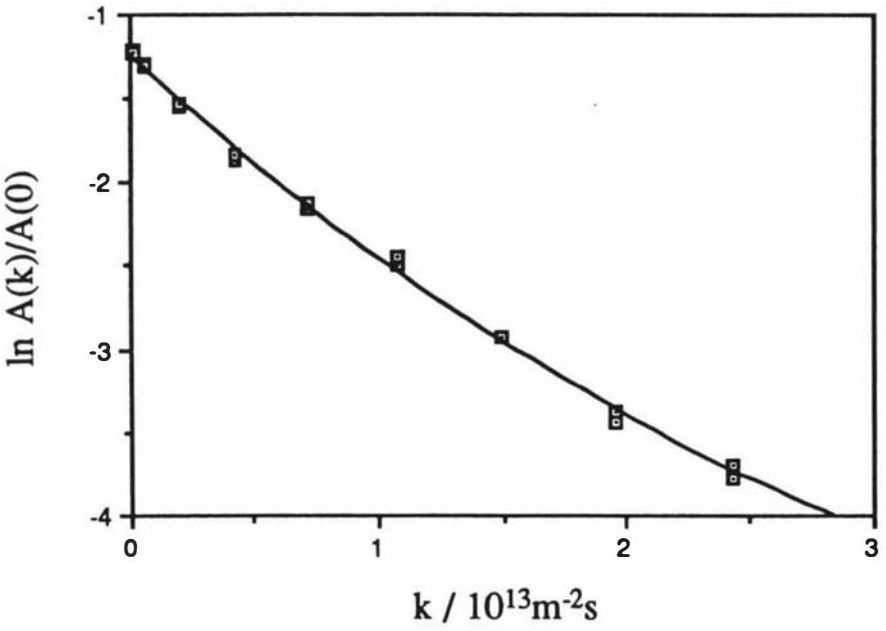

Figure 6.12 Echo attenuation plot for window γ for sample D-1. The parameters used in the experiments were; $\tau = \Delta = 20$ ms, G = 9.52 T m^{-1}, δ varied from 1 to 16 ms .

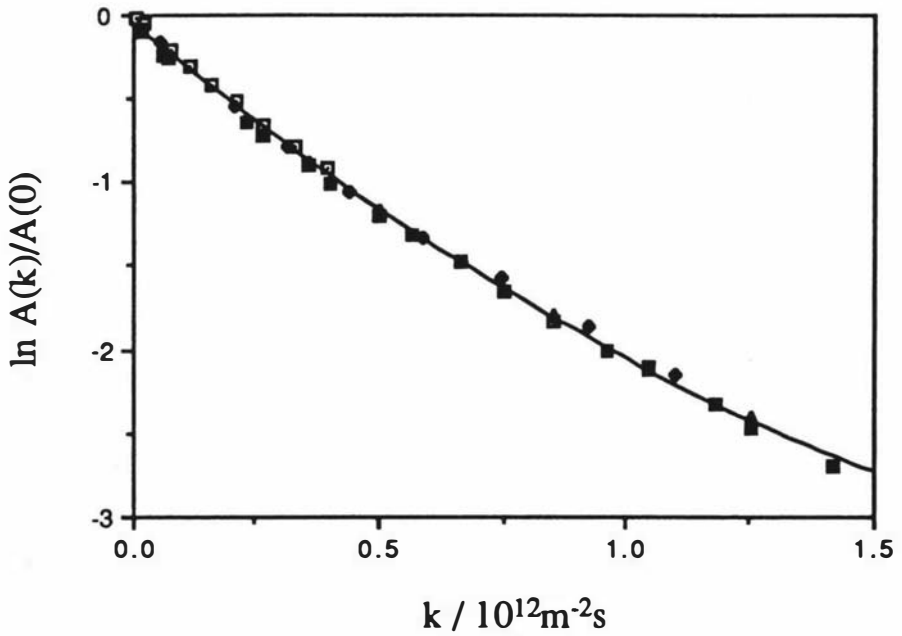

Figure 6.13 Echo attenuation plot for window γ for sample E11-6. The parameters used in the experiments were; $\tau = \Delta = 15$ ms, δ varied from 1 to 16 ms, G = 2.182 T m^{-1} (▫), 3.636 T m^{-1} (●, ■), 3.878 T m^{-1} (▲) and 4.121 T m^{-1} (■).

In practice, finite values of τ must be used in spin echo experiments. The value of τ used in these experiments was decreased from 30 ms down to 15 ms as the concentration was decreased to allow Δ and δ, the gradient pulse separation and width, to be varied appropriately. Window γ contains the PS methylene and benzylic resonances as well as the PVME methoxy, methine and methylene resonances. The PVME methoxy group protons were expected to have a longer relaxation time than any of the PS protons with resonances in window γ due to their freedom of rotation, being located on a side group rather than the main chain backbone [188]. Therefore it was expected that the PVME signal would continue to dominate window γ, even at non-zero values of τ. The PVME was not monodisperse, so eqn (6.8) was used to analyze the data from window γ for the E series samples.

Quadratic fits to ln A(k)/A(0) gave a fair description of the window γ data for the E series samples in most cases except for a few of the high concentration samples which were better described by linear fits. A self diffusion coefficient designated as D_γ was obtained from the slope in the case of the linear fits or the initial slope (given by the linear term) in the case of the quadratic fits (see equation (2.114)).

Peaks due to residual ^1H atoms in the deuterated toluene and traces of solvents not removed in the sample preparation procedure were not detectable for the E6, E11 and E25 series samples because of their small amplitude and the overlap with polystyrene resonances (Fig 6.9). Their contribution to the A(0) signal was estimated as less than 5% from the intercepts of echo attenuation plots.

The spectra of the D series samples, however, showed strong aromatic and methyl peaks due to the undeuterated toluene which was used as the solvent for this series of samples (see Fig. 6.9). The solvent peak was very strongly attenuated when the PGSE parameters were set for a polymer diffusion measurement, because of the vast difference between the solvent and polymer self diffusion coefficients. The rapid attenuation of the solvent signal resulted in echo attenuation plots with low intercepts for PVME diffusion measurements on the D series samples. Spectra (b) and (c) in Figure 6.9 and the echo attenuation plot for a D series sample shown in Fig. 6.12 vividly show this. The methyl peak of the toluene also falls within this window, so measurements of A(0) include a contribution from them, with an amplitude dependent on the concentration and T_2. Figure 6.9 shows that the PS aromatic proton peak was totally insignificant due to the very low concentration of polystyrene in the D series samples.

6.3.2. Results

The values of D_I obtained from quadratic cumulant fits to the DLS data are plotted against the total polymer volume fraction in Fig. 6.14. No systematic variation of D_I was observed over the range of x values studied in these experiments. The estimated uncertainty in values of D_I was generally less than ±5%, giving error bars of ±0.02 on Fig. 6.14. The exception was sample E25-1, (the highest concentration of the E25 series) with an error bar of ±0.06. These uncertainties were estimated from the reproducibility of the measurements, so the absolute uncertainties are probably slightly greater. Fig. 6.14 shows that D_I decreases as the concentration is increased, in keeping with the behaviour expected of the interdiffusion mode and the self diffusion coefficient.

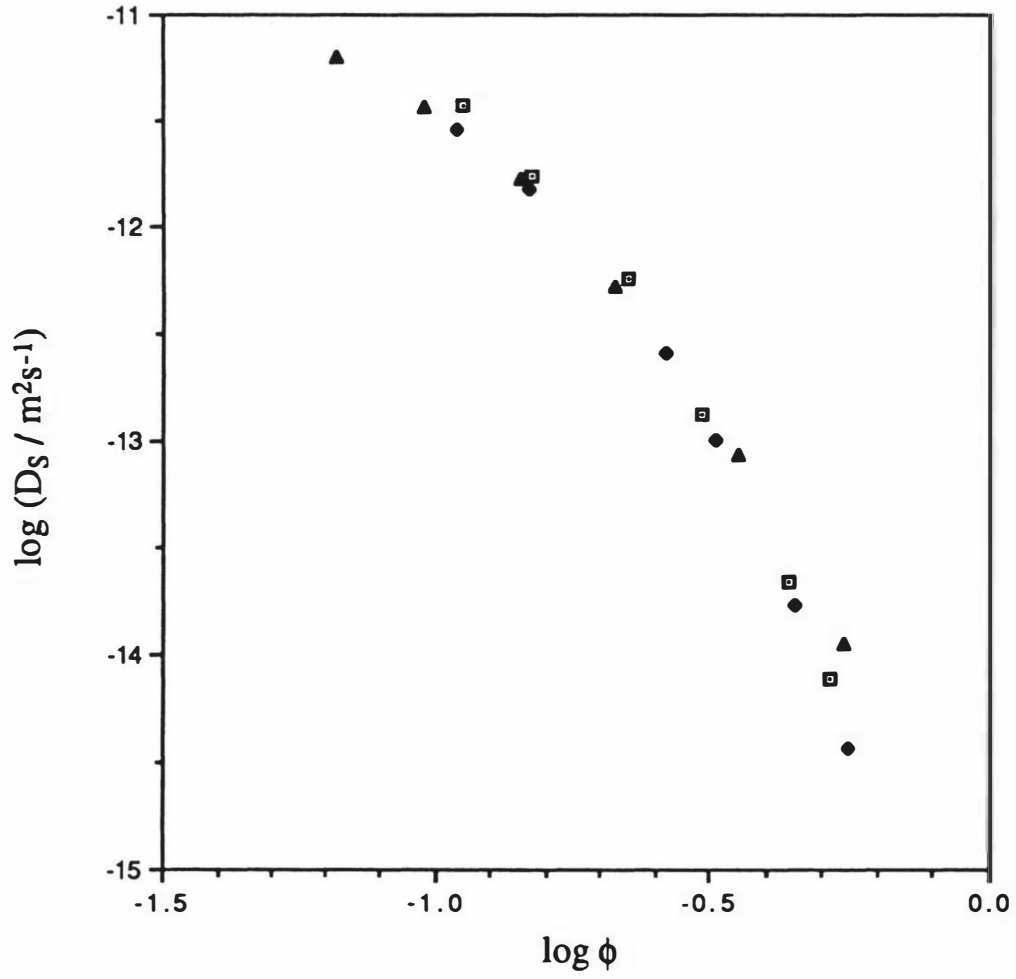

Figure 6.14 The concentration dependence of diffusion coefficients obtained from dynamic light scattering experiments on the E6 (■), E11 (●) and E25 (▲) series samples of the PS-PVME-(toluene d8) system. The PS and PVME molar masses are both 110,000 g mol^{-1}.

The values of $\mu_2/\langle\Gamma\rangle^2$ obtained at higher concentrations were consistently higher than the values obtained at lower concentrations. Samples of the E25 series gave values of $\mu_2/\langle\Gamma\rangle^2$ which were consistently higher than those obtained for the E6 and E11 series. Typical values of $\mu_2/\langle\Gamma\rangle^2$ for the E25 samples ranged from 0.25 down to 0.10. For the E6 and E11 samples, the range was from 0.20 down to 0.05. The uncertainty in values of $\mu_2/\langle\Gamma\rangle^2$ was typically ±0.05.

Fig. 6.15 shows the concentration dependence of the values of D_β obtained from linear fits to the PGSE NMR echo attenuation plots for window β. As was mentioned in the experimental section, D_β was assumed to be equal to the self diffusion coefficient of polystyrene. The uncertainties in the values of D_β estimated from their reproducibility were of the order of 10%, giving error bars on the log plot of ±0.05.

Fig. 6.16 shows the values of D_γ obtained from the initial slopes of quadratic fits to the echo attenuation plots for window γ. The reproducibility of these values was approximately ±7% giving error bars on the log plot of ±0.03. The quadratic term from the quadratic fits to ln A(k)/A(0) gave the variance of the distribution of diffusion coefficients (see eqn (6.9)) which tended to take lower values at higher concentrations for the E series samples. The values obtained for the D series samples tended to cluster around 0.12 and remained essentially constant over the entire concentration range.

6.3.3. Discussion

Previous work on self diffusion in polymer solutions has often focused on polystyrene because it is readily available as a well characterized, monodisperse polymer, but polystyrene solutions suffer from one major limitation. Neat polystyrene is a glassy solid at room temperature. At high concentrations, the effective local friction, which is often described in terms of a reduction in free volume, increases due to the proximity of the glass transition and adds complexity to the interpretation of self diffusion data (see the discussion in sections 4.1.3 and 4.2.3.) It is usually desirable to reduce this effect as much as possible. Many experimentalists have done this by using high molar mass polystyrenes so that the overlap concentration C^* is low. Concentrations well above C^* can then be studied while keeping the absolute concentration low and minimizing the free volume effects.

The major polymer component in the solutions studied here is PVME, which has a lower glass transition temperature than polystyrene. The glass transition temperatures of neat PVME and PS measured by Bank et al. [180] were –29°C and 102°C respectively. This means that PVME is a liquid at room temperature whereas PS is a glassy solid. Even concentrated solutions of PVME are therefore expected to be far above the glass transition

at room temperature. This has made it possible to measure self diffusion at concentrations as high as 570 kg m^{-3} in this series of experiments.

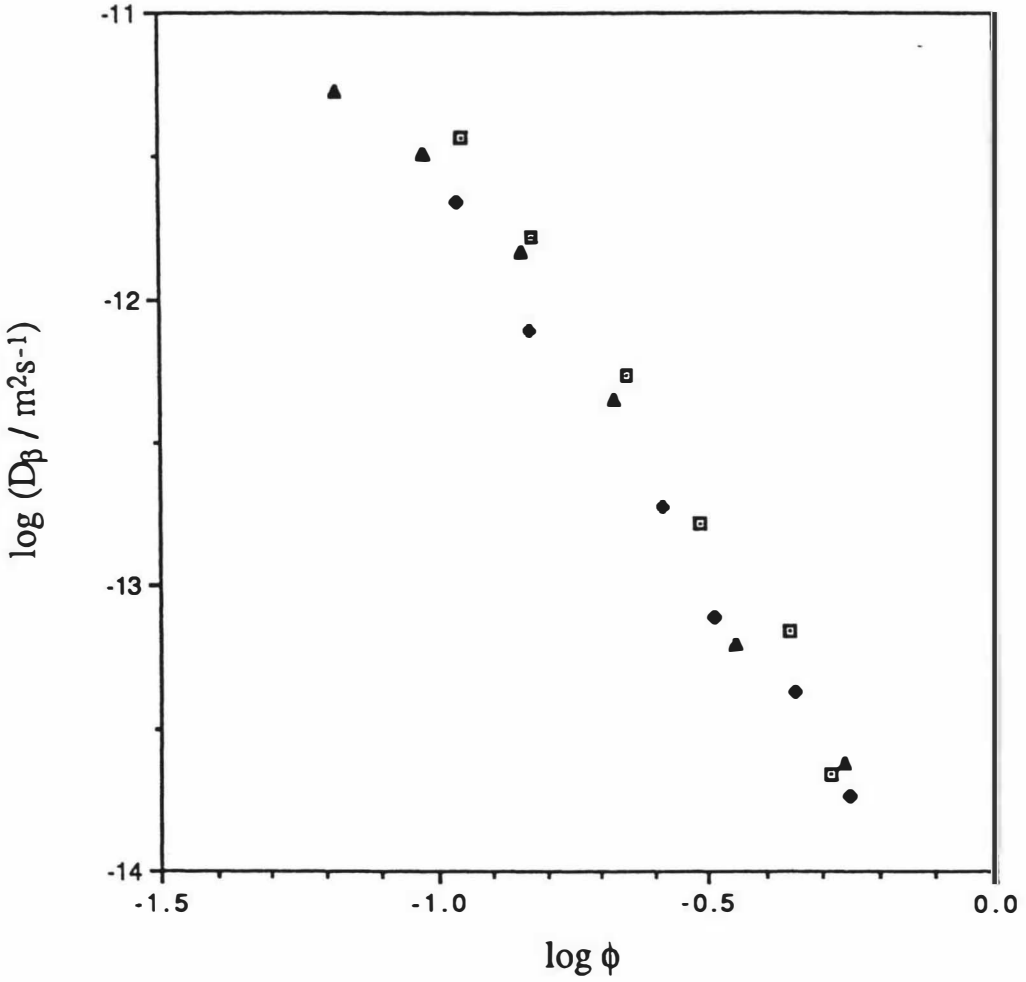

Figure 6.15 The concentration dependence of diffusion coefficients obtained from linear fits to PGSE echo attenuation plots for window β. The results for series E6 (▫), E11 (●) and E25 (▲) are shown. These values are interpreted as the self diffusion coefficients of the PS. The PS and PVME molar masses are both 110,000 g mol^{-1}.

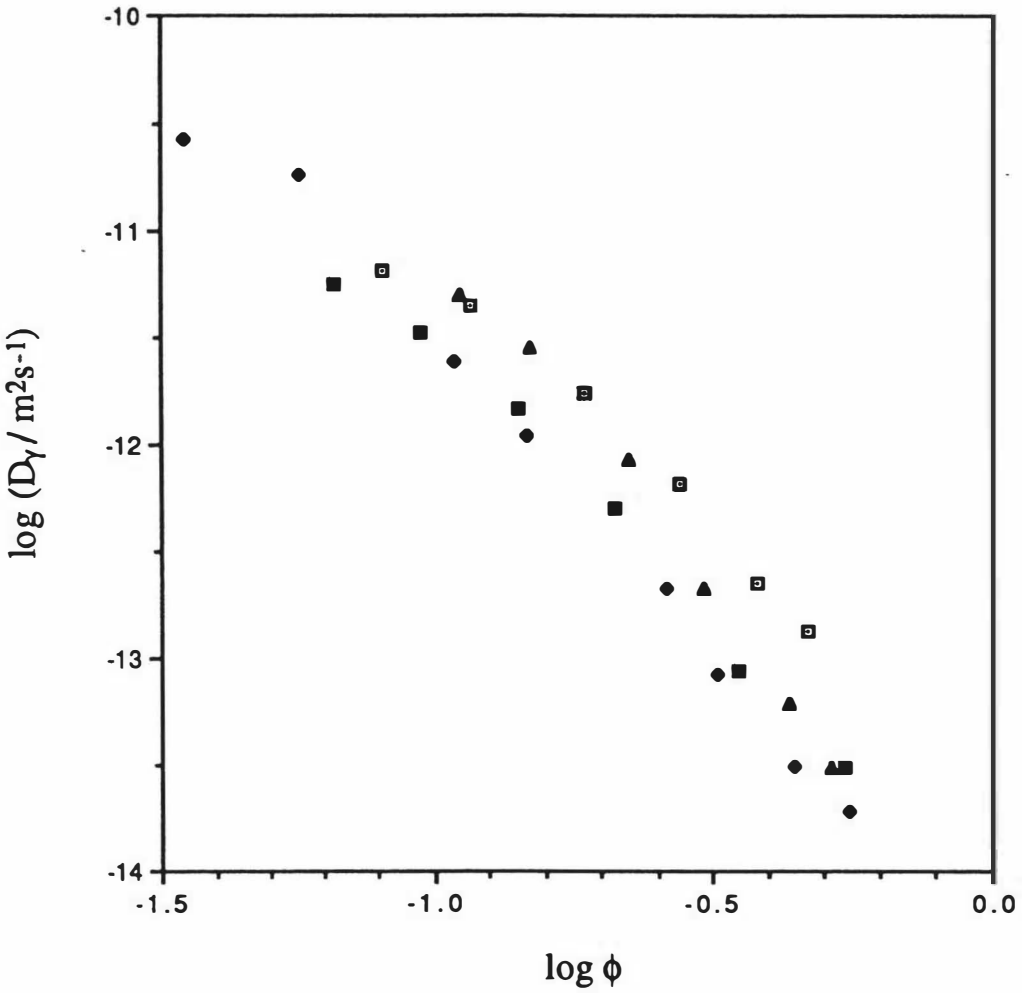

Figure 6.16 The concentration dependence of diffusion coefficients obtained from quadratic, or, at the highest concentrations for the E series samples, linear fits to PGSE echo attenuation plots for window γ. The results for series B2 (●), D (▫), E6 (▲), E11 (●) and E25 (■) are shown. The PS and PVME molar masses are both 110,000 g mol^{-1} except in the case of the B2 series sample. The B2 series samples were the two lowest concentration samples of the series discussed in section 6.2 and the PS and PVME molar masses were 929,000 and 110,000 g mol^{-1}. The B2 results were corrected to account for viscosity and temperature differences between the two sets of experiments. The diffusion coefficients plotted here can only be definitely identified as the PVME self diffusion coefficients for the B2 and D series samples.

A feature of the light scattering results of this section which is at first surprising is that the cooperative mode was not observed, even when polystyrene comprised 25% of the total concentration of polymer in the solution. This can be understood in terms of the theory of Benmouna et al. [100]. A plot of the relative amplitude of the cooperative mode against x is

shown in Fig. 6.17. The contribution of the cooperative mode decreases with increasing total polymer concentration at a given value of x, and decreases as x decreases if the total polymer concentration remains fixed. If x is less than 0.25 (which is the case in the experiments described here) the contribution of the cooperative mode is less than 0.15 at the overlap concentration and decreases as the concentration is increased. The ratio of D_C to D_S for polystyrene in toluene at C^* is approximately 24 [140, 189]. Assuming equal mode amplitudes, $\ln|g^{(1)}(\tau)|$ for the fast mode would decay to -1.4 in the time taken for the slow mode to decay to -0.06 (this time corresponds approximately to the width of the first channel of our correlator if $D_{slow}q^2\tau_{max} \approx 3$). When these factors are considered, it is quite understandable that the cooperative mode was not observed in these experiments. More favourable conditions for the extraction of both modes from DLS data would exist at x values of approximately 0.5 to 0.75. The cooperative mode would have a large amplitude, but it would decay quickly. (Note that D_I will generally differ from D_S at high x values.)

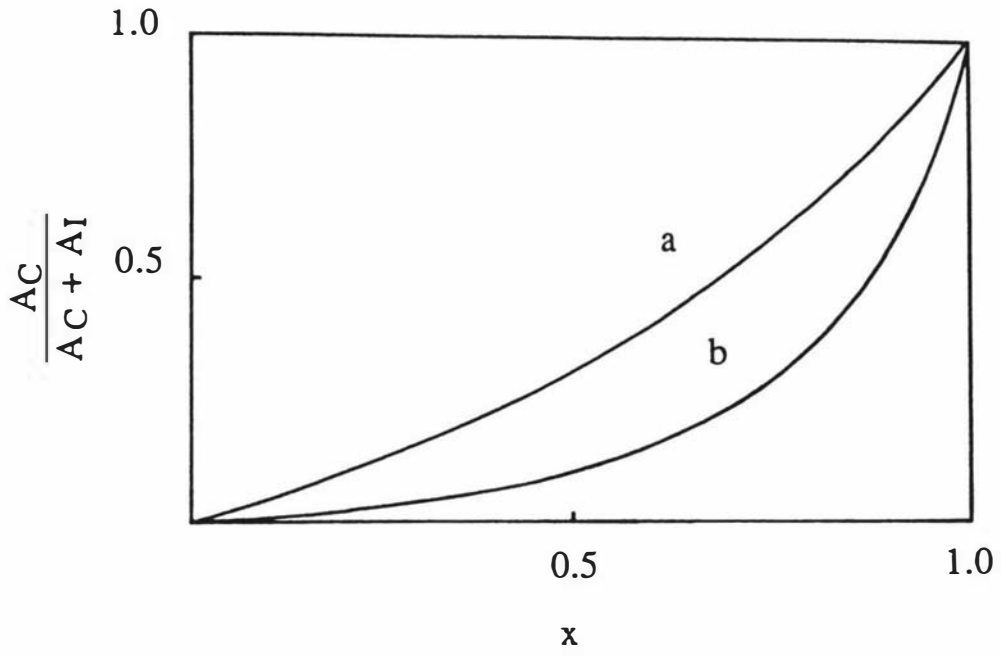

Figure 6.17 The dependence of the cooperative mode amplitude on the proportion of "visible" polymer in the q = 0 limit, taken from Benmouna et al. [100]. The parameter x is defined in equation (6.4). In the case described here, it is assumed that the solution contains two polymers of equal molar mass, one of them having no optical contrast with the solvent. The quality of the solvent is assumed to be the same for both polymers, and χ/υ is taken as 5×10^{-2}. Curve (a) is for $C/C^* = 0.5$ and curve (b) is for $C/C^* = 2.5$. In the limit of small values of x, the interdiffusion mode is dominant but when x approaches unity, the cooperative mode is dominant.

Martin [190] has published results of experiments on the PS-PVME-toluene system which can be directly compared with those presented here. Martin measured the concentration dependence of D_s for a trace of PS in PVME-toluene solutions for a range of PS molar masses. The polystyrene used in Martin's experiments with the closest molar mass to that used here (110,000 g mol^{-1}) had M_w = 106,000 g mol^{-1} and M_w/M_n = 1.06 and the PVME was unfractionated Gantrez M-556 ($M_w \approx$ 110,000 g mol^{-1}, $M_w/M_n \approx 2$). The results of Martin's experiments taken from his Figure 1 are plotted with the results of this work in Fig. 6.18. Also shown is the value of D_0 for polystyrene (110,000 g mol^{-1}) in toluene calculated using the relationship between D_0 and M given by Appelt and Meyerhoff [173]. The Stokes-Einstein equation was used to correct this result to 30°C.

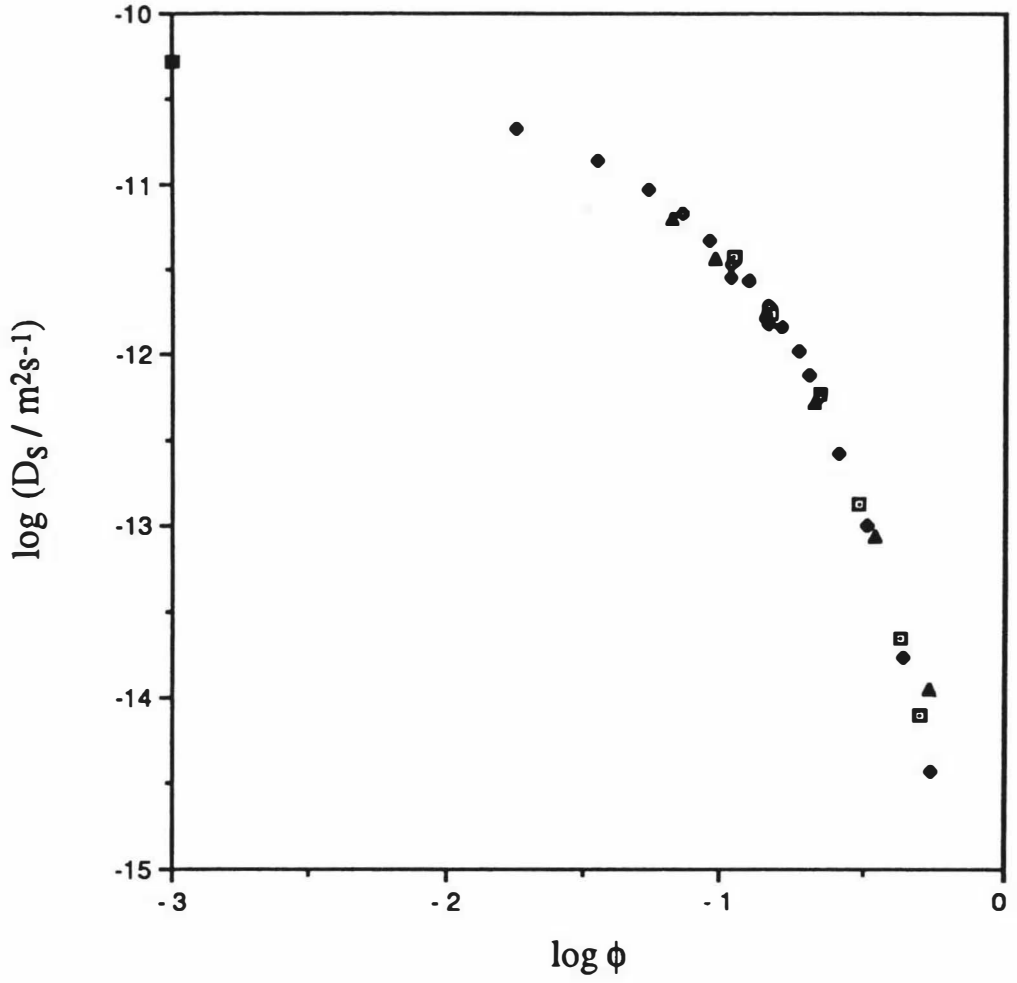

Figure 6.18 A comparison of the self diffusion coefficients obtained in the DLS experiments of this work (E6 ▫, E11 ♦, E25 ▲) with those of Martin (♦) [190]. Also shown is the value of D_0 (■) calculated using the relationship between D_0 and M given by Appelt and Meyerhoff [173] and corrected to 30°C.

The results obtained in this work agree well with those of Martin, and extend to higher concentrations. The precise agreement found in Fig. 6.18 may, however, be fortuitous. Martin did not specify the temperature at which his experiments were performed, so his results have not been corrected for any temperature or viscosity differences. Martin's PVME had the same average molar mass as that used in this work, but it was unfractionated.

Fig. 6.14 shows that the variation of D_I with x is very weak, if it exists at all, for the samples studied here. Interpreted in terms of the theory of Benmouna et al., this suggests that the product $A_2M\chi/\upsilon$ appearing in eqn (2.155) is close to zero, so that $D_I \approx D_s$. This effectively means that the polymers are compatible and the solvent is good for both of them.

Chang et al. [172] have studied the dependence of the diffusion coefficient obtained in a DLS experiment on polystyrene concentration in the PS-PVME-(o-fluorotoluene) system. At small values of C_{ps}, they found a linear relationship between the measured diffusion coefficient D_{eff} and C_{ps} for a given value of C_{pvme} which could be written as

$$D_{eff} = D_s (1 + k_{De} C_{ps} + \dots) \ . \qquad (6.13)$$

The value of k_{De} was positive at low PVME concentrations and gradually decreased to zero and then became negative as the PVME concentration was increased. Chang et al. [172] have pointed out that the behaviour of k_{De} is similar to the behaviour of k_D for the mutual diffusion coefficient (section 2.2.3). As the solvent quality is decreased, keeping the molar mass constant, k_D decreases and then becomes negative. This analogy is, however, not entirely appropriate. The concentration of polystyrene as a proportion of the total polymer concentration changes considerably as the PVME concentration is changed in [172]. In fact the value of x decreases from 1 down to 0 as C_{pvme} is increased and C_{ps} is decreased. The theory of Benmouna et al. [100] is strictly only valid above C^*, but if it is used to interpret the behaviour of the mode amplitudes at the relatively low concentrations employed in [172], it implies that that the cooperative mode is measured at high values of x and the interdiffusion mode is measured at low values. Interpreted in this way, the change in k_D observed by Chang et al. is therefore not only due to a change in the effective solvent quality seen by the PS as the PVME concentration is increased; it is also due to a change in the character of the quantity being measured. According to this interpretation, D_I is only measured at high PVME concentrations and low PS concentrations in [172], but x is always small in the experiments described in this section, so D_I is always measured.

If the arguments presented above are correct and the values of D_I measured in the experiments reported in this section are equal to D_s, they should agree with the values of D_β measured in PGSE NMR experiments on the same samples. Fig. 6.19 gives a comparison

of the values of D_β and D_I obtained from PGSE and DLS measurements. The agreement between the two techniques is within experimental error over most of the concentration range, which suggests that D_I and D_β are equal and identical to the self diffusion coefficient of the polystyrene for the samples studied here.

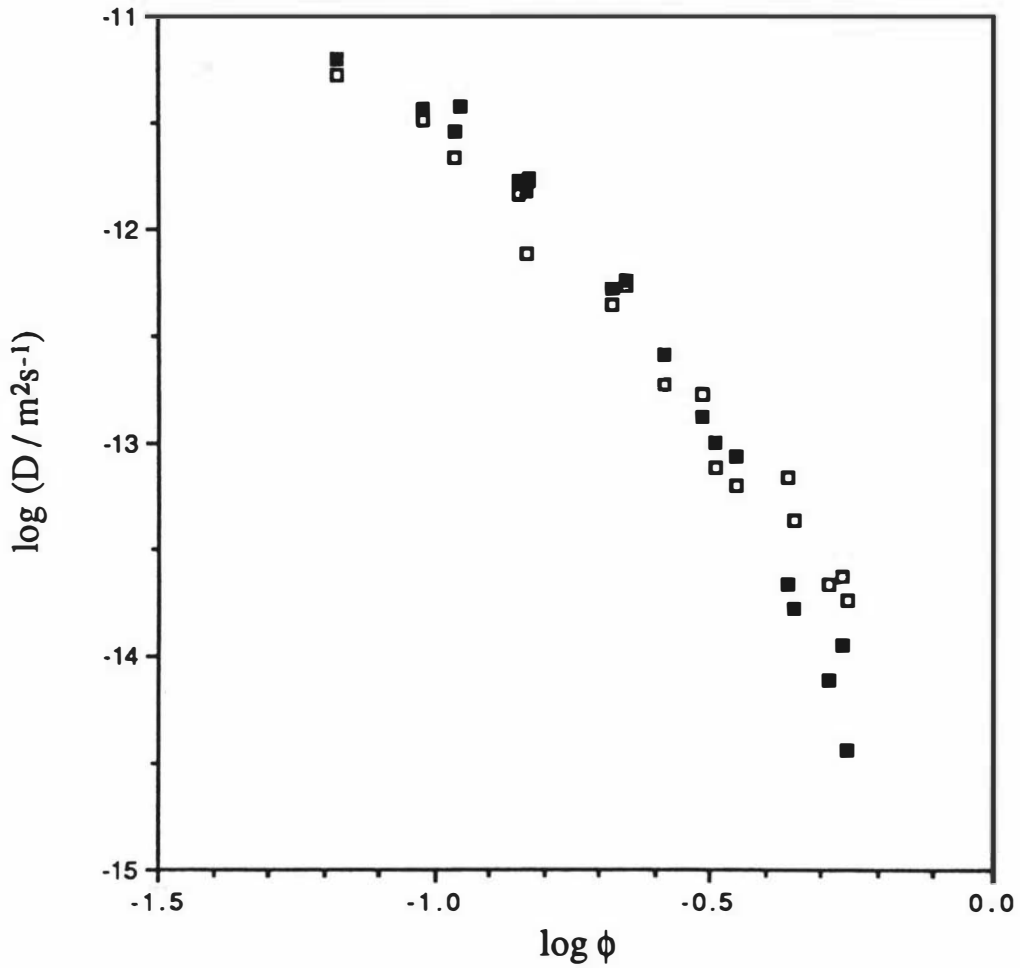

Figure 6.19 A comparison of the diffusion coefficients obtained from DLS experiments (■) with those obtained from PGSE experiments on window β (□). The agreement between the two sets of results leads to the conclusion that the diffusion coefficient measured in these DLS experiments is equal to the self diffusion coefficient of the polystyrene.

A discrepancy between the DLS and PGSE values of D_β is apparent at high polymer concentrations. The DLS values appear to fall more rapidly than the PGSE values above volume fractions of approximately 0.4. The discrepancy could be due to weak aggregation

effects. DLS is more sensitive to aggregation than PGSE because the average diffusion coefficient obtained from DLS is the z-average whereas PGSE gives the weight average. The z-average diffusion coefficient is more strongly influenced by high molar mass components of the molar mass distribution than the weight average. Aggregation is also suggested by the increase in $\mu_2/\langle\Gamma\rangle^2$ with increasing concentration which was observed in the light scattering experiments. The sample preparation procedure may have been responsible for the formation of these aggregates. It is possible that strongly entangled clumps of polymer were formed during the evaporation of solvent. These would have disentangled much more slowly than the surrounding solution in the concentrated samples, and then gradually dissipated as the samples were diluted, leading to the observed decrease in $\mu_2/\langle\Gamma\rangle^2$.

The results of the PGSE NMR measurements on window γ (see Fig. 6.10) will now be discussed. As was mentioned earlier, the plots of ln A(k)/A(0) for data from window γ were nonlinear (see Fig. 6.12 and Fig. 6.13). The curvature of the plots for the D series samples was attributed to the polydispersity of the PVME so quadratic polynomial fits were used to analyze the data (equation (2.114)). It is possible to estimate the polydispersity of the G-PVME D2 fraction from the quadratic term of the polynomial fits to ln A(k)/A(0) using equation (2.119) if a log normal molar mass distribution for the PVME is assumed and a value of the exponent in the relationship $D_0 = aM^{-\alpha}$ is estimated. Taking $\alpha = 0.55$ (a typical value for polymer-good solvent systems) and using $V_D = 0.12$ (section 6.3.2) M_w/Mn is estimated as 1.45. This is consistent with the polydispersity of 1.3 obtained from DLS measurements on similar fractions in section 5.2.2. This treatment is valid at infinite dilution. The effects of polydispersity at higher concentrations are more complicated. The exponent for the molar mass scaling of the self diffusion coefficient at semidilute concentrations and in the melt is generally closer to -2. This result applies to solutions and melts of monodisperse polymers. It has previously been shown by Callaghan and Pinder [82] that a polymer in a polydisperse solution does not have the same diffusion coefficient as it does in a solution of polymers of its own molar mass at the same concentration. This leads to a narrower distribution of diffusion coefficients than would be expected on the basis of the naive approach of substituting the semidilute molar mass scaling exponent for α in the treatment described above.

Fig. 6.16 shows the concentration dependence of the diffusion coefficients obtained from the window γ data. As was mentioned in section 6.3.2, D_γ was assumed to be equal to the PVME diffusion coefficient in these measurements. The values of $D\gamma$ for samples with very low PS concentrations (the D series and the B2 series) fall on a smooth curve which tends to power law behaviour at higher concentrations. The reptation model suggests that the concentration scaling exponent should be -1.75 for a polymer in a good solvent and -3

for a polymer in a theta solvent (section 2.2.4). When the blob model is applied to self diffusion, it predicts that the concentration scaling exponent of D_S should gradually change from -1.75 to -3 as the concentration increases (see Appendix 3). The behaviour of D_S for PVME in the D and B2 samples shown in Fig. 6.16 is consistent with the description provided by the blob model. The observation of an extended C^{-3} scaling region for polystyrene in a good solvent at high concentrations is made difficult by the onset of an increase in the local friction related to a reduction in free volume, but this effect is expected to be absent or at least comparatively weak in PVME solutions.

The $D\gamma$ values for the E series samples shown in Fig. 6.16 display unexpected behaviour. Most of the points fall below the $D\gamma$ values obtained for the D series samples. At high concentrations, the $D\gamma$ values for the E6 samples are in agreement with the E11 and E25 data and at low concentrations, they agree better with the D series values.

Several explanations for this behaviour could be advanced.

The most obvious explanation would be that the presence of the polystyrene changed the diffusion coefficient of the PVME. This seems very unlikely, because the polystyrene only comprised at most 25% of the total polymer in the solution. If a direct interaction between the polystyrene and PVME such as association had occurred in the samples, the polystyrene diffusion coefficients should have been influenced even more strongly than those of the PVME. An x and C dependent aggregation would be required to produce the variation in D_γ values shown in Fig. 6.16. The DLS results show no sign of such an effect; the x independence of D_I, and the agreement with Martin's results obtained for samples having very low values of x shows this particularly well.

There were several differences between the D series samples and the E series samples. The PVME used in the D series samples was G-PVME fraction D2 whereas the E series samples were made with G-PVME fraction E2. However, there is no reason to suspect that molar mass or other differences between the D2 and E2 fractions are responsible for the unexpected form of Fig. 6.16, because the two fractions were prepared and treated identically. Indeed, the results of the DLS experiments on these fractions discussed in section 5.2.2 were virtually identical.

Another difference between the D series and E series experiments was that undeuterated toluene was used to prepare the D series samples but deuterated toluene was used for the E series samples. Fig. 6.9 clearly shows that the solvent signal was very strongly attenuated when PGSE experiments were performed on the D series samples, so there is no solvent diffusion component in the measured values of $D\gamma$. The different densities of the deuterated and undeuterated solvents were accounted for by using polymer volume fraction rather than

mass fraction as the concentration variable when the data were plotted. The results of measurements on the PS-(G-PVME B2)-CCl_4 samples shown in Fig. 6.16 merge well with the D series results, providing support for the D series data. Additionally, the results for the E6 series (which has the lowest proportion of polystyrene present of all the E series samples) merge with the D series results at lower concentrations.

In all of the preceding discussion, it has been assumed that the area of window γ was dominated by the contribution made by PVME protons (see section 6.3.1). The values of $D\gamma$ were usually obtained from the initial slopes of quadratic fits to ln A(k)/A(0). The results obtained for window γ can be explained if $D\gamma$ contains a major contribution from the PS diffusion coefficient. The diffusion coefficient obtained from the initial slope of ln A(k)/A(0) for the window γ data can be written as

$$D_\gamma = (A_1 D_1 + A_2 D_2) / (A_1 + A_2) \ . \qquad (6.14)$$

The value of D_γ is approximately equal to D_1 if $A_1 >> A_2$, as was mentioned in section 6.3.1. This condition was expected to be satisfied, based on the amplitudes at $\tau = 0$ but more information is required to determine whether it still valid at $\tau > 0$. This question can only be answered by considering the τ dependence of the spin echo amplitudes for the resonances within window γ.

Window γ contains the resonances of the aliphatic polystyrene protons as well as the PVME resonances. Figure 6.9 shows spectra which demonstrate this point. Spectra (a) and (b) were measured using a two pulse spin echo pulse sequence (i.e. the PGSE pulse sequence with zero magnetic field gradient; see Fig. 2.4), and spectrum (c) was measured with the PGSE pulse sequence. All of these spectra were subject to τ dependent attenuation, the most important contribution to which is spin-spin relaxation with relaxation time T_2 (section 2.3.2). Generally speaking, nuclei which are very mobile due to rapid diffusive motion or the rotation about bonds for example, have resonances with long relaxation times, corresponding to narrow spectral peaks. This is demonstrated in spectrum (a), which was obtained for a sample of polystyrene ($M_w = 2 \times 10^6$ g mol^{-1}) dissolved in carbon tetrachloride at a concentration of 154 kg m^{-3}. The ratio of the area of the aromatic peak to the methylene+benzylic peak at $\tau = 0$ would be 5:3 based on the numbers of hydrogen atoms belonging to each group in the monomer, but the peak corresponding to the methylene+benzylic protons is clearly attenuated with respect to the aromatic resonance because of the shorter T_2 values of its component resonances. The shorter values of T_2 can be attributed to restrictions on the motions of the polystyrene backbone compared to the pendant aromatic group. These restrictions arise from chain connectivity, entanglements and free volume effects. It was not possible to determine the τ dependence of the spin echo attenuation for each resonance in window γ separately due to the poor resolution of the

PGSE probe. A set of measurements was made at high resolution on a sample of unfractionated G-PVME and PS (M = 110,000 g mol^{-1}) dissolved in toluene d8 at concentrations similar to sample E11-2. These measurements were made using the JEOL GX270 270 MHz spectrometer by Dr K. Jolley. The spectrum of the sample is shown in Fig. 6.8. By fitting the plots of peak height against 2τ with a single exponential curve, apparent T_2 values were obtained for the resonances falling within window γ in the PGSE measurements. The apparent T_2 values for the PVME methoxy and methine peaks were 81 ms and 13 ms respectively. The resonances corresponding to the PS and PVME methylene protons and the PS benzylic proton (see Fig. 6.8) were not fully resolved, but the two peaks in this region gave apparent T_2 values of 4 ms and 7 ms. As expected, the protons directly bonded to the backbones of the two polymers had shorter T_2 values than the pendant methoxy group. Therefore, the effect of the τ variation of the spin echo amplitudes of the different resonances within window γ would be to enhance the PVME contribution as τ is increased, so T_2 effects could not be responsible for the lower values of D_γ measured on the E series samples.

Another question which must be considered is whether the initial slope of ln A(k)/A(0) is really being measured. Pusey has shown that cumulant fits to DLS data for polydisperse samples contain a large systematic error when correlation functions span more than two or three decay times. The results of cumulant fits need to be extrapolated to zero delay time in order to give correct values. The values of k employed in these experiments were always chosen so as to give a decay of ln A(k)/A(0) to about –3 for the window β data. The same parameters were used in the measurements on window γ. The results for the D series samples given in Fig. 6.16 show that the PVME diffusion coefficients were as much as a factor of three higher than the PS diffusion coefficients obtained from DLS. Therefore, it is likely that the PVME signal would have been attenuated quite early on the echo attenuation plots for window γ. The mean diffusion coefficient for a polydisperse sample such as the PVME should be obtained from the initial slope, but this was not possible with the k values chosen in these experiments, so a lower value was always obtained. It is apparent that the large values of k used in the measurements, combined with the polydispersity of the PVME, produced a systematic bias of the results of the fits to the echo attenuation plots for window γ towards the PS self diffusion coefficient rather than the PVME self diffusion coefficient as would initially have been expected. Fig. 6.20 shows the similarity of the D_γ and the D_β values. This explains why the results from window β gave the PS self diffusion coefficient despite the poor spectral resolution of the PS aromatic resonance. It also explains why the D_γ values for the E6 series samples tended towards the results obtained for the D series samples as the concentration decreased. Another feature of the results which is consistent with this explanation is the decrease of V_D for the window γ echo attenuation plots at higher polymer concentrations. Linear plots of ln A(k)/A(0) were

obtained at the highest polymer concentrations of the E series samples but not for the D series samples.

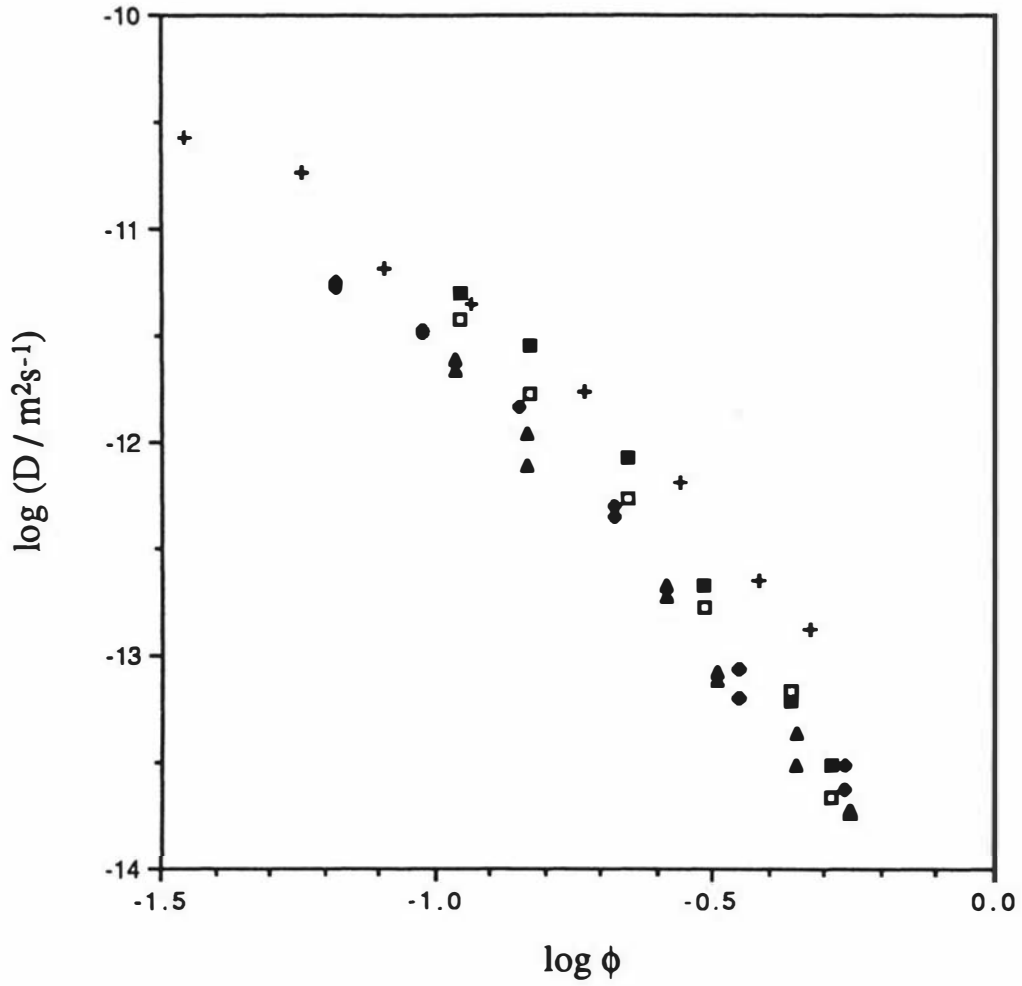

Figure 6.20 A comparison of the diffusion coefficients obtained from the window β data with those from the window γ data. The window β points are; E6 ▫, E11 ▲ and E25 ♦ and the window γ points are; B2 and D +, E6 ■, E11 ▲ and E25 ♦. The + points are self diffusion coefficients of PVME and the open squares, triangles and diamonds are the self diffusion coefficients of polystyrene. The E6 diffusion coefficients for window γ, represented by filled squares, agree with the PS diffusion coefficients at high polymer concentrations but tend towards the PVME diffusion coefficients at lower concentrations.

These ideas were tested by reanalysing the data for window α for sample E6-3. The large k portion of the echo attenuation plot was linear, suggesting that it was due to the PS. Extrapolation of this portion back to the k = 0 intercept gave a relative amplitude for this

mode of 0.41. This is greater than expected on the basis of the number densities of the protons contributing to the PVME and PS resonances, but could be in error if the PVME echo attenuation contained a slowly decaying component due to polydispersity. The exponential decay with an amplitude of 0.41 and diffusion coefficient given by the long time, linear part of the echo attenuation plot was subtracted from A(k)/A(0) and the resultant echo attenuation plot was fitted with a quadratic, giving a PVME diffusion coefficient in agreement with the D series curve at the appropriate concentration. A closer examination of the shape of other echo attenuation plots for the E series samples confirmed the existence of a rapidly decaying component and a linear decay at large k values consistent with this explanation.

A more correct analysis of the data would involve fitting echo attenuation plots for windows α or γ with equation (6.12). However, the large number of parameters fitted would require more precise data over a larger range of k values than was investigated here. Attempts to fit the data with functional forms similar to eqn (6.12) were not successful due to the non-convergence of the nonlinear curve fitting algorithm.

Fig. 6.21 gives a comparison of the concentration dependence of the PS self diffusion coefficient obtained here with that obtained for other systems. It is a remarkable feature of these results that the PS self diffusion coefficient, corrected for solvent viscosity and temperature, is the same in PVME+toluene as it is in benzene and carbon tetrachloride. (The results for the PS-(toluene d8) system given in [140] also agree, but cover a smaller concentration range. For the sake of clarity, they are not shown in Fig. 6.21.) This implies that the reduction in the radius of gyration of PS in the presence of PVME is less severe in this case than was inferred in section 6.2 where the PS molar mass was much greater than the PVME molar mass. This would be consistent with the theoretical results of Nose [22].

Fig. 6.21 also shows that the chemical difference between PS and PVME makes little difference to the self diffusion of PS when the molar masses of the two polymers are equal. This implies that χ is indeed small for PS and PVME in toluene and confirms that the PS and PVME do not form long-lived aggregates in PS-PVME-toluene solutions. It would be interesting to test whether a reduction in the size of a high molar mass PS molecule in a matrix of low molar mass PS is observed analogous to the effect observed for PS in a matrix of PVME seen in section 6.2. If $\chi = 0$ for PS and PVME in toluene, exactly the same behaviour should be observed for a bimodal PS solution.

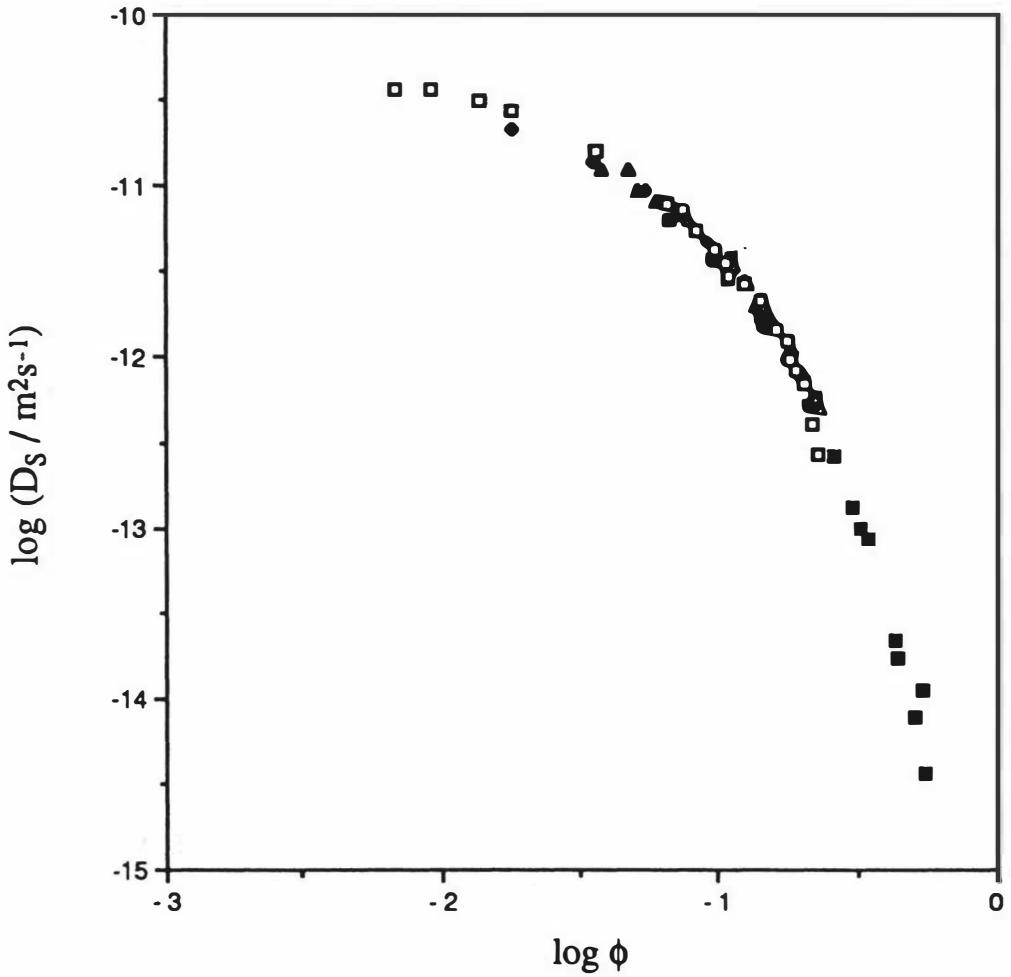

Figure 6.21 Comparison of the polystyrene self diffusion coefficients for the PS-PVME-(toluene d8) system studied in this section (■) with the results of Martin [185] (●) and PGSE measurements of self diffusion in PS-(benzene d6) (▲) and PS-CCl_4 (□) solutions (Callaghan and Pinder [62]). In all cases, the polystyrene molar mass was 110,000 g mol^{-1}. The PS-(benzene d6) and PS-CCl_4 results have been corrected to account for temperature and viscosity differences.

If there is any difference between the behaviour of PS solutions and the PS-PVME solutions shown in Fig. 6.21, it is that the CCl_4 data begin to fall rapidly due to effective local viscosity effects (proximity to glass transition) at high concentrations, whereas the PS-PVME data do not.

Fig. 6.22 gives a comparison of the concentration dependence of the PVME self diffusion coefficient with that of the PS self diffusion coefficient. The PVME diffusion coefficients do not decrease as rapidly with increasing concentration as the PS diffusion coefficients. This is most likely a reflection of the difference in the glass transition temperatures of the

two polymers. Although a PVME chain is expected to be longer than a PS chain of the same molar mass due to its lower molar mass per monomer, the PVME diffusion coefficients shown in Fig. 6.22 are higher than the values for PS. The larger polydispersity of the PVME is probably responsible for this difference.

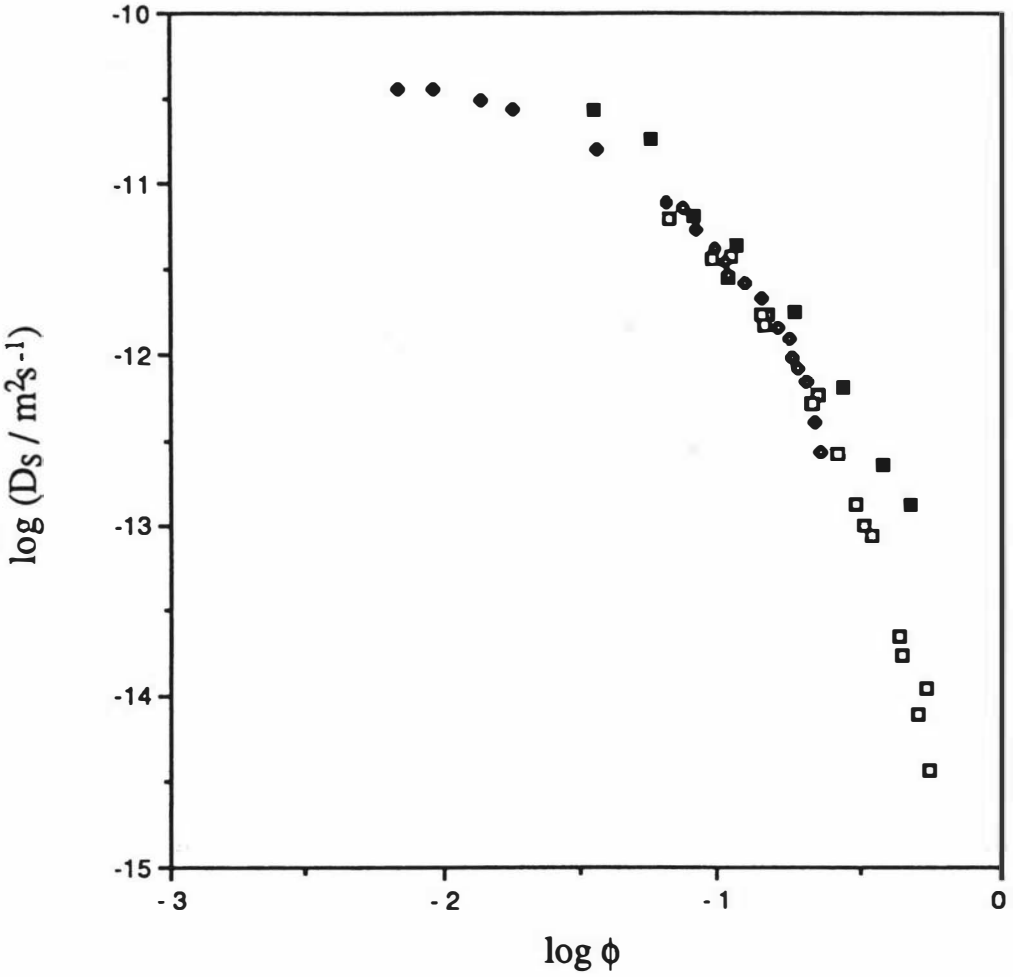

Figure 6.22 Comparison of the PVME self diffusion coefficients for the PS-PVME-toluene and PS-PVME-CCl_4 systems (■) with the polystyrene self diffusion coefficients obtained from DLS experiments (□) and PGSE experiments on the PS-CCl_4 system (●) [62].

7. CONCLUSION

7.1. Conclusions

Chapter Two mainly summarized existing results which could be found in the literature, but the development of this chapter included some new work. The relationship between the diffusion coefficient measured in a dynamic light scattering experiment and the mutual diffusion coefficient defined in non-equilibrium thermodynamics was clarified in Appendix 2. The blob model was used to find the concentration and solvent quality dependence of the cooperative and self diffusion coefficients in Appendix 3 and a discussion of effective exponents was also given, extending previous work.

The circumstances under which a nonlinear time dependence of the mean square displacement for a diffusing polymer could be measured were discussed in sections 2.3.3 and 2.3.4.

Chapter Three described experimental techniques used in this work and introduced some original work. The standard deviation of the echo attenuation measured in a PGSE NMR experiment was derived and the results were discussed in relation to the weighting of least squares fits. A computer program which runs DLS experiments and provides several options for data analysis was described. A "dust discrimination" scheme for DLS experiments was also discussed.

The results of measurements of the polymer and solvent self diffusion coefficients as a function of polymer concentration in polystyrene-cyclohexane solutions near the theta temperature were presented in Chapter Four. The measurements were made on solutions close to the theta temperature for the following reasons. According to scaling theories, a polymer in a good solvent is subject to crossover effects; that is, a change from good solvent behaviour to theta solvent behaviour at concentrations near ϕ^{**}. The crossover effect is absent for solutions which are already under theta conditions, making the interpretation of the data more straightforward. The molar mass of the polystyrene used in these measurements was 350,000 g mol^{-1}. The value of D_0 for the polymer, obtained by extrapolation of the dilute solution results ($C < C^*$) to zero concentration, was found to agree well with literature values. The exponent of the concentration dependence of the self diffusion coefficient in the semidilute region was found to be -3.1 without any correction for the increase in local friction which occurs at higher concentrations. When solvent diffusion data were used to estimate this correction, the exponent was found to equal -2.8. These results are consistent with the exponent of -3 predicted by the reptation model.

The concentration dependence of the self diffusion coefficient of polystyrene in cyclohexane was compared with that of polystyrene in another theta solvent, cyclopentane (Deschamps and Léger, [144]). It was suggested that the systematic difference between the two sets of results seen at higher concentrations in the plots of $\log(D_s M^2 \eta_0 / T)$ against polymer volume fraction was due to the solvent dependence of local friction effects related to the glass transition. Solvent diffusion measurements indicated that the local friction effects were not negligible for the polystyrene-cyclohexane solutions, but it was suggested that they may be weaker for polystyrene-cyclopentane solutions.

A comparison of the theta solvent data and good solvent data from the literature was made and the "universal" plot of D_s / D_0 against ϕ / ϕ^* which has been used by other workers was discussed. The plot does not unify good solvent and theta solvent data. It was concluded that this plot is only genuinely universal if the solvent quality is independent of concentration. This is not the case for a polymer in a good solvent because of the crossover effect.

The theta solvent results were used to plot the self diffusion data of Kim et al. in the form suggested by the reptation model and the blob model (Appendix 3) as $D_s / D_{s,\theta}$ against C. Kim's results for D_s were expected to be free of constraint release and contour length fluctuation contributions, because they had been extrapolated to infinite matrix molar mass. Therefore, the analysis of Appendix 3, combining the reptation model and the blob model, was expected to describe the data well. Reasonable qualitative agreement was obtained, and discrepancies at high concentrations were attributed to local friction effects.

Chapter Five presented a discussion of the fractionation and characterization of poly(vinyl methyl ether) (PVME). The fractionations were performed by batch fractional precipitation from toluene solution with petroleum spirit. Gel permeation chromatography, dynamic light scattering and sedimentation velocity measurements were used to characterize the fractions. An absolute measurement of the molar mass of one of the fractions was obtained by combining the sedimentation coefficient and the diffusion coefficient in the Svedberg equation.

Three sets of experiments were presented in Chapter Six. In the first, dynamic light scattering experiments were performed on PS-PVME-toluene solutions. PVME and toluene are very close to being isorefractive. The molar mass of the PVME was approximately 102,000 g mol^{-1} and the molar mass of the PS was 929,000 g mol^{-1}. The polystyrene concentration was maintained at 0.2 mg per gram of solution and the PVME concentration was varied over a wide range. The experiments gave results in agreement with those obtained by Martin [68], and the diffusion coefficient obtained from the measurements was interpreted as the self diffusion coefficient of the polystyrene. The

recently published theory of Benmouna et al. [100] was used to interpret the results, and similar experiments reported in the literature were discussed.

The second section of Chapter Six described DLS measurements on a system similar to the one investigated in section 6.1. The solvent was changed from toluene to carbon tetrachloride to examine the possibility of performing pulsed gradient spin echo NMR measurements on PS-PVME-CCl_4 samples. The concentration of polystyrene in these samples was too low for the self diffusion coefficient of PS to be measured, but PVME diffusion coefficients (discussed later in section 6.3) were obtained. The diffusion coefficients obtained from DLS measurements were significantly lower than those obtained for the PS-PVME-toluene system. It was concluded that the decay rate of the interdiffusion mode did not yield the PS self diffusion coefficient as it had in the PS-PVME-toluene experiments. The difference was attributed to thermodynamic effects. The literature indicates that PS and PVME are likely to be much less compatible in carbon tetrachloride than they are in toluene. Indeed, phase separation was observed in later attempts to make samples with increased polystyrene concentrations. The effective diffusion coefficient (the decay rate of the correlation function divided by the square of the scattering vector) was found to be dependent on the scattering vector, q. The results were interpreted in terms of the theory of Benmouna et al. and values of the radius of gyration were obtained from the slopes of plots of the effective diffusion coefficient against q^2.

In the third section of Chapter Six, PGSE NMR and DLS experiments on PS-PVME-toluene solutions were described. The PS and PVME molar masses were both equal to 110,000 g mol^{-1} in these experiments. Four series of samples were studied. The polystyrene concentration as a fraction of the total polymer concentration, x, for the four series of samples was 0.001, 0.056, 0.114 and 0.246. The experiments were designed to allow the measurements to be made on the same samples using both techniques. This was possible for all samples except for the one with x = 0.001 which had a very low polystyrene concentration. The only measurements possible with this sample were measurements of the PVME self diffusion coefficient using PGSE NMR.

The results of the DLS experiments showed that the cooperative mode could not be measured within the range of concentrations and x values studied here. The effective diffusion coefficient was not q dependent because of the low molar mass of the polystyrene. The diffusion coefficient obtained from the decay rate of the interdiffusion mode was independent of x and agreed to within experimental errors with the self diffusion coefficient of the polystyrene measured by PGSE NMR. The x independence of the diffusion coefficient obtained from the interdiffusion mode was attributed to the

compatibility of PS and PVME and the good solvent quality of toluene for the two polymers.

PGSE NMR measurements of the PVME self diffusion coefficients for the three series of samples with x values greater than 0.001 were hampered by the the overlap of PS and PVME peaks in the proton NMR spectra and the moderate polydispersity of the PVME, even after fractionation to $M_w / M_n = 1.3$. However, measurements of the PVME self diffusion coefficient were possible for the series of samples with the lowest x values.

7.2. Suggestions for Further Work

The agreement of the theta solvent concentration scaling exponent found in Chapter Four with the reptation result suggests that constraint release and tube fluctuation effects are absent under theta conditions. This surprising result could be checked by measuring the self diffusion coefficient as a function of matrix molar mass for a polymer in a theta solvent.

An interesting check on the possibility of a molar mass dependent local friction effect could be made by examining the concentration dependence of the cooperative diffusion coefficient as a function of molar mass. The cooperative diffusion coefficient is expected to be molar mass independent in the semidilute region, but the onset of local friction effects at high concentrations could occur at different concentrations for different molar masses.

It would be highly desirable to increase the resolution of spectra obtained in PGSE experiments. This would make it easier to simultaneously measure the self diffusion coefficients of different polymers in multicomponent solutions.

Now that the theory of DLS experiments on ternary polymer solutions is developing, the interpretation of measurements on solutions of two polymers of the same chemical type but with different molar masses should become easier. Such experiments promise to reveal much, not only about diffusion mechanisms in polymer solutions, but also about ternary diffusion coefficients.

Martin [195] has already used DLS experiments on high molar mass polystyrenes dissolved in isorefractive solutions of PVME in toluene to investigate the concentration dependence of the internal dynamics of polymer molecules. Other experiments which exploit isorefractivity are also possible. For example, the mean square displacement of a polymer segment in a concentrated solution could be measured by labeling an otherwise isorefractive polymer with non-isorefractive segments. Such measurements would provide valuable information about the mechanism of self diffusion at times shorter than the tube renewal time.

APPENDIX 1 - EQUIVALENT EQUATIONS FOR THE MUTUAL DIFFUSION COEFFICIENT

Beginning with equation (2.26), we can write several different but equivalent expressions for D.

If the thermodynamic factor is written in terms of the reciprocal of the osmotic compressibility, we have (see [19], equation 1.4.62)

$$C\left(\frac{\partial\mu}{\partial C}\right)_{T,P} = (1-\phi)\left(\frac{\partial\Pi}{\partial C}\right)_{T,P} \qquad \text{(A1.1)}$$

provided that the solvent volume fraction is defined as $\bar{v}_0^0 C_0$ where $\bar{v}_0^0$ is the solvent partial specific volume in the limit of pure solvent, and C_0 is the concentration of solvent (see Kurata, equation 1.1.30). Then equation (2.26) becomes

$$D = \frac{M(1-\phi)}{f}\left(\frac{\partial\Pi}{\partial C}\right)_{T,P} \qquad \text{(A1.2)}$$

where f is the molar friction factor defined with respect to the volume fixed reference frame. Equation (A1.2) is given by Yamakawa (ref.[4], eqn. 30.43) and by Chu [1] with f expressed as friction per molecule. When the friction factor is defined relative to the reference frame moving at the mean solvent velocity it becomes [23]

$$f^s = f\,(1-\phi)\ . \qquad \text{(A1.3)}$$

It is often necessary to use osmotic pressure data which are acquired under conditions of constant solvent pressure rather than the constant solution pressure conditions which apply for the usual diffusion measurements. In such situations, caution is required [19, 27], but for polymer solutions it is adequate to assume that (ref.[19], eqn.3.1.133)

$$C\left(\frac{\partial\mu}{\partial C}\right)_{T,P} = (1-\phi)\left(\frac{\partial\Pi}{\partial C}\right)_{T,\mu_0} \qquad \text{(A1.4)}$$

so the reciprocal of the osmotic compressibility in eqn. (A1.2) could be given by either (A1.1) or (A1.4).

APPENDIX 2 - MICROSCOPIC EXPRESSION FOR THE MUTUAL DIFFUSION COEFFICIENT

Equations for the mutual diffusion coefficient in terms of microscopic quantities have been derived previously. Pusey (p 99 of [26]) gives a derivation which starts from an expression for the dynamic structure factor and identifies the result as the cooperative diffusion coefficient measured in a dynamic light scattering experiment. Pusey's result is

$$D = (S(0)\, 3\, N)^{-1} \sum_{i=1}^{N} \sum_{j=1}^{N} \int_0^{\infty} \langle\, \mathbf{v}_i(0) \cdot \mathbf{v}_j(t)\, \rangle \, dt \qquad \text{(A2.1)}$$

where S(0) is the static structure factor at zero scattering vector (see section 2.4.1) and the summations are performed over N macroparticles dissolved in a solvent. Equation (A2.1) leads to a generalized Stokes-Einstein equation

$$D = \frac{1}{\zeta} \left(\frac{\partial \Pi}{\partial \rho} \right)_T \qquad \text{(A2.2)}$$

where ρ is the number density of solute molecules, S(0) is related to the osmotic compressibility $\kappa_\pi = (\partial\rho/\partial\Pi)_T / \rho$ by

$$S(0) = k_B T \left(\frac{\partial \Pi}{\partial \rho} \right)_T^{-1} \qquad \text{(A2.3)}$$

and the friction factor appearing in (A2.2) is defined as

$$\zeta = (3Nk_BT)^{-1} \sum_{i=1}^{N} \sum_{j=1}^{N} \int_0^{\infty} \langle \mathbf{v}_i(0) \cdot \mathbf{v}_j(t) \rangle \, dt \quad . \qquad \text{(A2.4)}$$

Equation (A2.2) appears to differ from the results obtained from non-equilibrium thermodynamics (see Appendix 1). The interpretation of the friction factor in eqn (A2.4) has been a matter of some debate in the literature. Hess (p 34 of [90]) suggested that ζ was the solvent-fixed frame friction factor. A paper by Yoshida [28] summarizes some of the discussion.

Recent work by Raineri and Timmerman [29] has made it possible to derive eqn (A2.1) from the standard expressions provided by linear response theory (see e.g. [25]) and non-equilibrium thermodynamics. For a two component system, the mutual diffusion coefficient can be written as [29]

$$ {}_{V}D_{11} = \frac{{}_{V}L_{11}}{\phi_0}\left(\frac{\partial \mu_1}{\partial c_1}\right)_{T,P} \tag{A2.5} $$

where ${}_{V}L_{11}$ is the phenomenological coefficient [23] referred to the volume fixed frame, ϕ_1 is the solute volume fraction, μ is the chemical potential in J mol^{-1} and c is the molar concentration.

Linear response theory gives the phenomenological coefficient ${}_{V}L_{11}$ as [29]

$$ {}_{V}L_{11} = c_1^2 \; {}_{V}F_{11} \tag{A2.6} $$

where ${}_{V}F_{11}$ is

$$ {}_{V}F_{11} = \int_0^\infty \lim_{\infty} \{ V\langle (\bar{v}_1(t)-\bar{w}\ (t))\cdot(\bar{v}_1(0)-\bar{w}\ (0)) \rangle \}\, dt\ .\ \propto \frac{1}{k_B T} \tag{A2.7} $$

Here $\bar{w}$ is the reference velocity, in this case the mean volume weighted velocity. Equation (A2.7) can be derived from the usual expressions for phenomenological coefficients given by linear response theory which are written using the mass weighted velocity as the reference velocity [29]. If there is no volume change on mixing, $\bar{w}$ = 0 in a diffusion experiment. Therefore,

$$ {}_{V}F_{11} = \int_0^\infty \lim_{\infty} \{ V\langle \bar{v}_1(t)\cdot\bar{v}_1(0) \rangle \}\, dt\ .\ \propto \frac{1}{k_B T} \tag{A2.8} $$

The $\lim_{\infty}$ symbol represents the thermodynamic limit, i. e. V, N_1 and N_2 become very large with N_1/V and N_2/V remaining finite. Assuming that these conditions are satisfied, we will omit the limit symbol from here on.

The mean molecular velocity $\bar{v}_1$ of species 1 is given by

$$ \bar{v}_1 = \frac{1}{N}\sum_{i=1}^{N} v_i \tag{A2.9} $$

where v_i is the velocity of the i^{th} particle of species 1. The index runs over all of the particles of species 1 in the volume V.

Then

$$vF_{11} = \frac{V}{3N^2k_BT}\int_0^\infty \langle \sum_{i=1}^{N} \mathbf{v}_i(0)\cdot\sum_{j=1}^{N} \mathbf{v}_j(t) \rangle \, dt \qquad \text{(A2.10)}$$

which becomes

$$vF_{11} = \frac{V}{3N^2k_BT}\int_0^\infty \sum_{i=1}^{N}\sum_{j=1}^{N} \langle \mathbf{v}_i(0)\cdot\mathbf{v}_j(t) \rangle \, dt) \ . \qquad \text{(A2.11)}$$

Substitution of

$$vD_{11} = \frac{c_1^2 \, vF_{11}}{\phi_0}\left(\frac{\partial\mu_1}{\partial c_1}\right)_{T,P} \qquad \text{(A2.12)}$$

and (see Appendix 1)

$$c_1\left(\frac{\partial\mu}{\partial c_1}\right)_{T,P} = \phi_0\left(\frac{\partial\Pi}{\partial c_1}\right)_{T,P} \qquad \text{(A2.13)}$$

into equation (A2.11) gives

$$vD_{11} = \frac{1}{3Nk_BTN_A}\left(\frac{\partial\Pi}{\partial c_1}\right)_{T,P}\int_0^\infty \sum_{i=1}^{N}\sum_{j=1}^{N} \langle \mathbf{v}_i(0)\cdot\mathbf{v}_j(t) \rangle \, dt) \ . \qquad \text{(A2.14)}$$

In terms of ~~(the number density $\rho = c_1N_A$ and)~~ $S(0)$, the osmotic pressure derivative is

$$\left(\frac{\partial\Pi}{\partial c_1}\right)_{T,P} = \frac{N_Ak_BT}{S(0)}$$

so we finally obtain

$$vD_{11} = \frac{1}{3NS(0)}\int_0^\infty \sum_{i=1}^{N}\sum_{j=1}^{N} \langle \mathbf{v}_i(0)\cdot\mathbf{v}_j(t) \rangle \, dt)$$

which is the same as Pusey's result.

Note that Pusey's ζ can be related to the usual friction factor f (eqn (2.26)) by a comparison of eqns (A2.2) and (A1.2). The result is

$$\zeta = \frac{f}{N_A(1-\phi_1)} \ .$$

The results of this analysis are in agreement with the conclusions which Yoshida [28] reached by a different route.

APPENDIX 3 - APPLICATION OF THE BLOB MODEL TO THE CALCULATION OF THE SELF DIFFUSION COEFFICIENT

The blob model has already been applied to the quantitative calculation of the expansion factors for the radius of gyration and the hydrodynamic radius at infinite dilution by Akcasu and Han [6]. Before extending these calculations to properties in the semidilute region, it is worthwhile to summarise the main features of their approach.

The blob model is a model for the mean square distance between two segments of a polymer molecule. A mathematical statement of the blob model is given in eqns (2.4) and (2.5). When these equations are substituted directly into the definition of the radius of gyration, the result is [6, 32]

$$R_G^2 = a^2 N_\tau \left(\frac{2\nu-1}{2(2\nu+1)} x - \frac{2\nu-1}{3(2\nu+2)} x^2 + \frac{1}{(2\nu+1)(2\nu+2)} x^{-2\nu} \right) \qquad (A3.1)$$

where $x=N_\tau / N$.

With $\nu = 3/5$ this becomes

$$R_G^2 = a^2 N_\tau (24x - 11x^2 + 75x^{-2\nu}) / 528 . \qquad (A3.2)$$

In the dilute theta region, ($x \geq 1$) the radius of gyration is given by

$$R_G^2 = a^2 N / 6 \qquad (A3.3)$$

according to the blob model.

Likewise, equations (2.4) and (2.5) can be substituted into the Kirkwood equation for D_0 to give an equation for the hydrodynamic radius [6, 32];

$$R_H^{-1} = (12 / [6\pi]^{1/2}) a^{-1} N_\tau^{-1/2} \left(\frac{1-2\nu}{1-\nu} x + \frac{2\nu-1}{3(2-\nu)} x^2 + \frac{1}{(1-\nu)(2-\nu)} x^\nu \right) \qquad (A3.4)$$

which, with $\nu = 3 / 5$ becomes

$$R_H^{-1} = (12 / [6\pi]^{1/2}) a^{-1} N_\tau^{-1/2} (-21x + 2x^2 + 75x^\nu) / 42 . \qquad (A3.5)$$

In the dilute theta region, R_H is given by

$$R_H = ([6\pi]^{1/2} / 16) a N^{1/2} \qquad (A3.6)$$

according to the blob model.

These results can be used to construct quantities which depend only on x. The expansion factors α_S and α_H depend only on x and are therefore universal. To simplify the algebra, it is convenient to define the following quantities;

$$B = 24x - 11x^2 + 75x^{-2\nu} \tag{A3.7}$$

and

$$G = -21x + 2x^2 + 75x^{\nu} \ . \tag{A3.8}$$

Then α_S and α_H are given by

$$\alpha_S = (Bx / 88)^{1/2} \tag{A3.9}$$

and

$$\alpha_H = x^{1/2}\, 56 / G \ . \tag{A3.10}$$

The relationship between $x = N_\tau / N$ and the experimentally accessible quantities M and τ is

$$1 / x = (\tau / \tau^*)^2 \tag{A3.11}$$

where

$$(\tau^*)^2 = k_1 nA / M \tag{A3.12}$$

and k_1 is the constant of proportionality relating N_τ to τ^2, i.e.

$$N_\tau = k_1 / \tau^2, \tag{A3.13}$$

n is the number of monomers in a statistical segment and A is the molar mass per monomer. The value of the product $k_1 n$ is expected to depend insensitively on the type of solvent and the structure of the monomer units. Akcasu and Han [6] have determined that $k_1 n = 4$ for polystyrene in cyclohexane by matching the theoretical expression for α_S with experimental data in the large N / N_τ limit where the blob model is expected to be most accurate. They then used the same value to plot data for other solvents, although they leave open the possibility of determining $k_1 n$ separately for each polymer-solvent pair.

When the blob model is applied to semidilute polymer solutions, the idea that ideal chain statistics exist within a group of N_τ segments (called a temperature blob) is maintained. In addition, the concept of thermodynamic screening is used to justify the assumption that each group of g segments (called a concentration blob) between interchain contact points behaves as a noninteracting unit [5, 46]. Therefore, if a chain is made up of N / g

concentration blobs, each of radius of gyration ξ, the total end to end distance is $\xi(N/g)^{1/2}$. Note that g varies with both the temperature (solvent quality) and concentration.

By analogy with the dilute solution case, the radius of gyration of a blob ξ_S is given by eqn (A3.1) with N replaced by g. The hydrodynamic radius of a blob ξ_H is found by the same method from eqn (A3.4). To construct a universal quantity, we proceed by the same method as was used for the dilute case. For example, the expansion factor for the radius of gyration (the static radius) in the semidilute region is written as

$$\alpha_S = R_G / R_G(\theta) \qquad \text{(A3.14)}$$

$$= [\xi_S(N/g)^{1/2}] / [\xi_{S\theta}(N/g_\theta)^{1/2}] \ .$$

It is necessary to distinguish between g and g_θ because the concentration and temperature dependence of g depends on concentration and temperature. The ratio g_θ / g must be written in terms of x before this equation can be developed. The critical concentration for overlap of polymer molecules is

$$c^* = \frac{N}{k_2 R_G^3} \qquad \text{(A3.15)}$$

where k_2 is a parameter determined by experiment and c is the number density of segments ($C = cnAN_A$). At higher concentrations, the analogous relationship

$$c = \frac{g}{k_2 \xi_S^3} \qquad \text{(A3.16)}$$

holds. Therefore, at a given concentration, we have

$$g_\theta / g = (\xi_{S\theta} / \xi_S)^3 \qquad \text{(A3.17)}$$

or

$$g_\theta / g = [88\ g_\theta / (B\ N_\tau)]^{3/2} \ . \qquad \text{(A3.18)}$$

Since

$$g_\theta / N_\tau = g_\theta / (xg) \qquad \text{(A3.19)}$$

we then find that

$$g_\theta / g = (Bx / 88)^3 \ . \qquad \text{(A3.20)}$$

The final result for the static expansion factor in the semidilute regime is

$$\alpha_S = (Bx / 88)^{1/2} \quad . \tag{A3.21}$$

It is necessary to find a relationship between x and the experimental variables M, C and τ before this equation can be used quantitatively. This has been done by Daoud and Jannink [46] who showed that the ratio C / τ could be written as a function of x only. (Note that eqn.(14) of [46] contains a misprint; N_τ should be replaced by τ. Also, Daoud and Jannink appear to have assumed that $k_1 = k_2 = 6$ for their numerical calculations.) Here, we will follow their method to find a result which retains experimental factors so as to enable a direct comparison between theory and experiment.

The mass/volume concentration is $C = cnA / N_A$ and the reduced temperature τ is $\tau = (k_1 / N_\tau)^{1/2}$ so with eqn (A3.16) we find

$$C / \tau = \frac{C_\theta^*}{\tau^*} F(x) \tag{A3.22}$$

where

$$C_\theta^* = M / (k_2 N_A R_{G\theta}^3) \quad , \tag{A3.23}$$

$$\tau^* = (nk_1 A / M)^{1/2} \tag{A3.24}$$

and

$$F(x) = \frac{1}{x}(88 / B)^{3/2} \, . \tag{A3.25}$$

On the C/C_θ^* - τ/τ^* plane, a given value of x corresponds to a straight line through the origin, the slope being given by $1 / F(x)$. Slopes less than one correspond to $x > 1$ (semidilute theta) and slopes greater than one correspond to $x < 1$ (semidilute good).

We can use the same procedure to determine k_2 as was used by Akcasu and Han to determine k_1. First, data for a universal ratio involving a static property is plotted against C/τ on a log-log plot. Then the theoretical curve for the universal ratio as a function of F(x) is plotted on the same axes. The shift factor on the $\log(C/\tau)$ axis which is required to give a good fit in the small x (small C/τ) region where the property obeys a power law is recorded. This gives the value of C_θ^* / τ^*. If nk_1 is already known from a fit to dilute solution data, the value of k_2 can be determined. This has been done with the data of Cotton et al. [47] for the temperature dependence of α_S for a deuterated polystyrene chain in a semidilute solution of deuterated polystyrene in cyclohexane. Fig. A3.1 shows the

data of Cotton et al. plotted with the theoretical curve from the blob model taking $C_\theta^* / \tau^* =$ 7400 kg m^{-3}. This value of C_θ^* / τ^* leads to $k_2 = 0.51$ when A is taken as 112 g mol^{-1} and eqn (10) of reference [47] is used to calculate R_G for deuterated polystyrene. On the other hand, data taken from the same paper for $\xi_S / \xi_{S\theta}$ measured on polystyrene in deuterated cyclohexane gives $C_\theta^* / \tau^* = 14800$ kg m^{-3}. The value of k_2 (0.13) obtained from this result seems unreasonably low, but more experiments would need to be analyzed before a more informed discussion of this discrepancy could be attempted. In both cases, nk_1 was taken as 4 which was obtained for undeuterated polystyrene in C_6H_{12}. Measurements of crossover effects made well inside the semidilute regime ($C/C_\theta^* > 3$ taking $k_2 = 1$) are rare and more work needs to be done in this area. The measurements of Cotton et al. concentrate on temperature crossover effects, corresponding to a variation of τ, keeping C constant. Alternatively, concentration crossover effects could be studied by varying C while keeping τ constant (see Fig. 2.2).

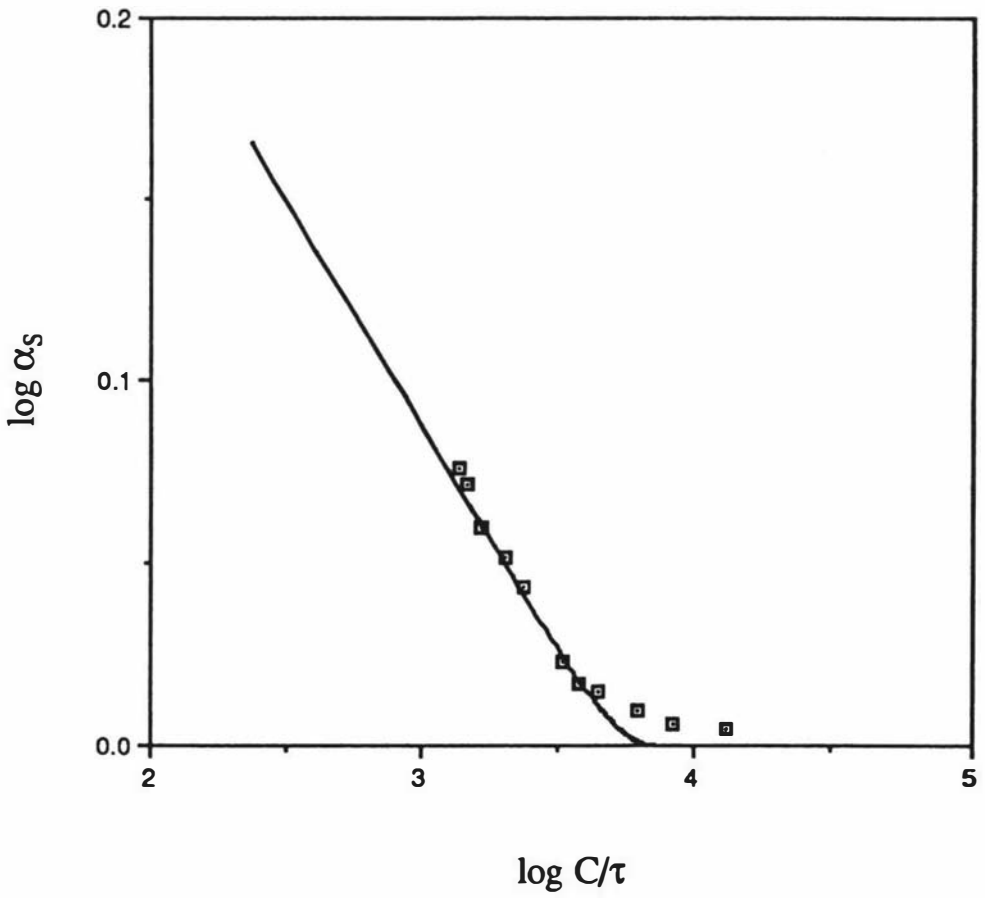

Figure A3.1 The expansion factor for the radius of gyration, α_S. Experimental data were taken from the work of Cotton et al. [47] and the curve was plotted using eqns (A3.21) and (A3.22) with $C_\theta^*/\tau^* = 7400$ kg m^{-3}.

The blob model can also be used to give a theoretical curve for the cooperative diffusion coefficient, D_c. Referring to equation (2.34), we see that a universal quantity independent of temperature and viscosity effects would be $D_c\eta T_\theta / D_{c\theta}\eta_\theta T$ which is equivalent to $\xi_{H\theta} / \xi_H$. This ratio is given by

$$\xi_{H\theta} / \xi_H = (xG / 56)\,(B / 88)^{3/2} \quad . \qquad \text{(A3.26)}$$

Taking $C_\theta^* / \tau^* = 7400$ kg m^{-3}, we obtain the curve shown in Fig. A3.2. Also plotted are the data of Adam and Delsanti [48], which show a similar slope. As has already been observed in the case of the hydrodynamic radius, dynamic properties approach the asymptotic power law behaviour very slowly. Exact agreement between theory and experiment is not to be expected, because even in the dilute regime, the agreement between the blob model and experimental data for the hydrodynamic radius expansion factor is not particularly good [6]. This discrepancy need not be entirely attributed to a failure of the blob model. The Kirkwood equation for the hydrodynamic radius involves severe approximations in its treatment of hydrodynamic interactions (the draining effect). The blob model has the advantage of providing a useful unified framework for the interpretation of many different properties of polymer solutions.

Now we are in a position to apply the blob model to the analysis of crossover effects on the self diffusion coefficient.

Equation (2.56) can be generalized to account for the crossover between the semidilute good solvent and semidilute theta regions of the τ - ϕ diagram if we allow both the hydrodynamic radius ξ_H and the static radius ξ_S of a blob to vary with concentration and temperature [6, 32, 46].

When hydrodynamic and static lengths are distinguished, eqn. (2.56) becomes [62]

$$D_S = \frac{k_B T}{18\eta\pi}\left(\frac{N}{g}\right)^{-2} \xi_H^{-1} \quad . \qquad \text{(A3.27)}$$

One approach to the investigation of crossover effects is to examine the effective exponents which are found when data collected in the semidilute good to semidilute theta crossover region are force fitted to a power law [46, 49, 62]. True power law behaviour is only expected in a theta solvent or in the asymptotic region for a good solvent.

For a theta solvent,

$$\xi_S \sim g^{1/2} \qquad \text{(A3.28)}$$

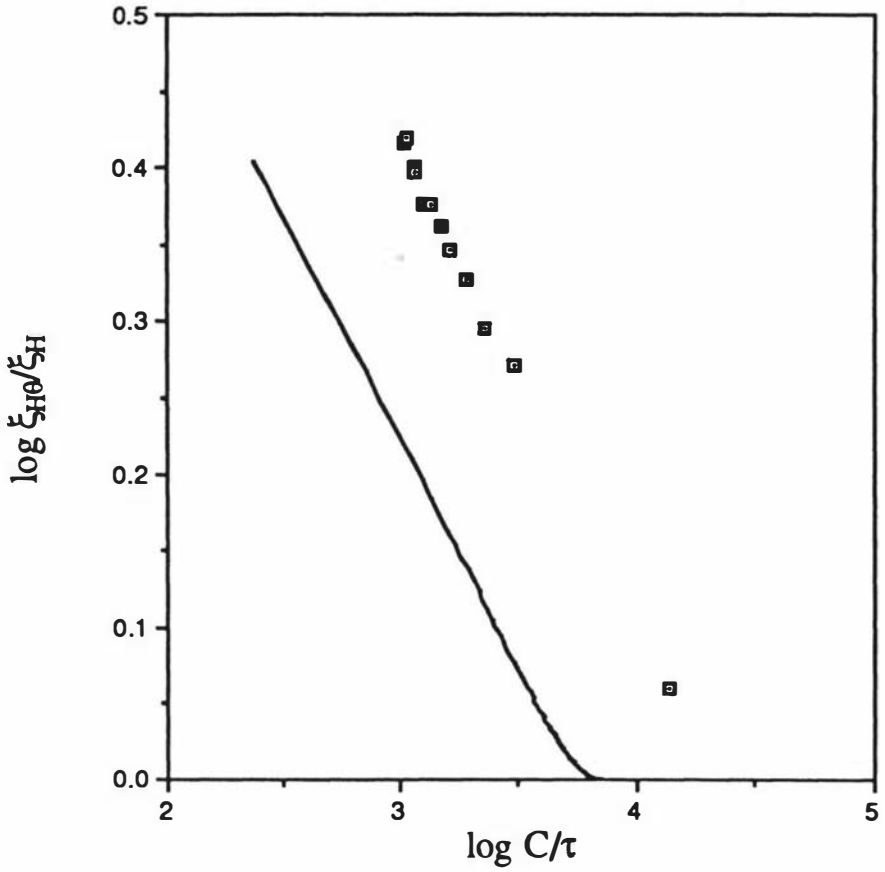

Figure A3.2 Universal plot for the blob hydrodynamic radius ξ_H. Experimental points were taken from Adam and Delsanti [48] and the curve was calculated using the blob model (eqn (A3.26)). The value of C^*_θ/τ^* was taken as 7400 kg m^{-3} which was obtained by matching theory and experiment in Fig. A3.1.

whereas in the asymptotic region for a good solvent,

$$\xi_S \sim g^\nu \tag{A3.29}$$

with similar equations holding for ξ_H.

In the crossover region, the effective exponents of ξ_S and ξ_H are defined as

$$\nu_S = \frac{\partial \log \xi_S}{\partial \log g} \tag{A3.30}$$

$$= \frac{g}{\xi_S} \frac{\partial \xi_S}{\partial x} \frac{\partial x}{\partial g}$$

and

$$\nu_H = \frac{\partial \log \xi_H}{\partial \log g} \qquad \text{(A3.31)}$$

$$= \frac{g}{\xi_H} \frac{\partial \xi_H}{\partial x} \frac{\partial x}{\partial g} .$$

Callaghan and Pinder [62] determined the effective exponent for the concentration dependence of D_s by the following procedure. It was assumed that D_s could be written in terms of an effective exponent α as

$$D_s \sim c^{\alpha} . \qquad \text{(A3.32)}$$

Eqn (A3.27) shows that with $\xi_S \sim g^{\nu_s}$, D_s can also be written as

$$D_s \sim N^{-2} \xi_S^{2/\nu_S} \xi_H^{-1} . \qquad \text{(A3.33)}$$

Using eqn (A3.16) with $\xi_S \sim g^{\nu_s}$ and $\xi_H \sim g^{\nu_H}$ it is found that

$$\xi_S \sim C^{\nu_S/(1-3\nu_S)} \qquad \text{(A3.34)}$$

and

$$\xi_H \sim C^{\nu_H/(1-3\nu_S)} \qquad \text{(A3.35)}$$

so the effective exponent, α is

$$\alpha = \frac{2-\nu_H}{1-3\nu_S} . \qquad \text{(A3.36)}$$

The explicit formulae for ν_H and ν_S which are found when ν is taken to be 3/5 are

$$\nu_H = \frac{-21x + 4x^2 + 45x^{\nu}}{-21x + 2x^2 + 75x^{\nu}} \qquad \text{(A3.37)}$$

and

$$\nu_S = -\frac{12x - 11x^2 - 45x^{-2\nu}}{24x - 11x^2 + 75x^{-2\nu}} . \qquad \text{(A3.38)}$$

Alternatively, it is possible to find an expression for the effective exponent α using the method of Daoud and Jannink [46] who calculated the effective exponents for the

concentration and temperature dependence of the cooperative diffusion coefficient in semidilute solutions. (Note that ref.[46] contains several misprints.)

The general scaling form of g is [46]

$$g \sim C^{-5/4}\,\tau^{-3/4}\,f(C/\tau) \tag{A3.39}$$

so that

$$D_s \sim g^2\,\xi_H^{-1} \sim \tau^{-3}\,f(C/\tau)\,. \tag{A3.40}$$

In terms of effective exponents, D_s is

$$D_s \sim C^{\alpha}\,\tau^{\beta}\,. \tag{A3.41}$$

Since we are insisting on a power law for D_s, the relationship between α and β can be found by equating (A3.40) and (A3.41) with $f(C/\tau) = (C/\tau)^z$ where z is as yet undetermined. This gives

$$\beta = -(3+\alpha)\,. \tag{A3.42}$$

The effective exponent α is easily found by the following method. First, we write the effective exponent as

$$\alpha = \left(\frac{\partial \log D_s}{\partial \log c}\right)_{\tau} \tag{A3.43}$$

$$= \left(\frac{\partial \log D_s}{\partial \log g}\right)_{\tau}\left(\frac{\partial \log g}{\partial \log c}\right)_{\tau}$$

Then, since

$$D_s \sim \xi_S^{2/\nu_S}\;\xi_H^{-1} \tag{A3.44}$$

we find

$$\left(\frac{\partial \log D_s}{\partial \log g}\right)_{\tau} = 2-\nu_H\,. \tag{A3.45}$$

Daoud and Jannink [46] give an expression for the second factor in (A3.43)

$$\left(\frac{\partial \log g}{\partial \log c}\right)_{\tau} = \frac{24x - 11x^2 + 75x^{-2\nu}}{60x - 44x^2 - 60x^{-2\nu}}\,. \tag{A3.46}$$

Substitution of (A3.45) and (A3.46) into (A3.43) then gives the desired result

$$\alpha = (2-\nu_H)\frac{24x - 11x^2 + 75x^{-2\nu}}{60x - 44x^2 - 60x^{-2\nu}} . \qquad \text{(A3.47)}$$

Note that eqns. (A3.47) and (A3.37) are equivalent. Both α and C/τ can be calculated as functions of x ($x = N_\tau/g$) so that α can then be plotted against C/τ, as is done in Figure A3.3.

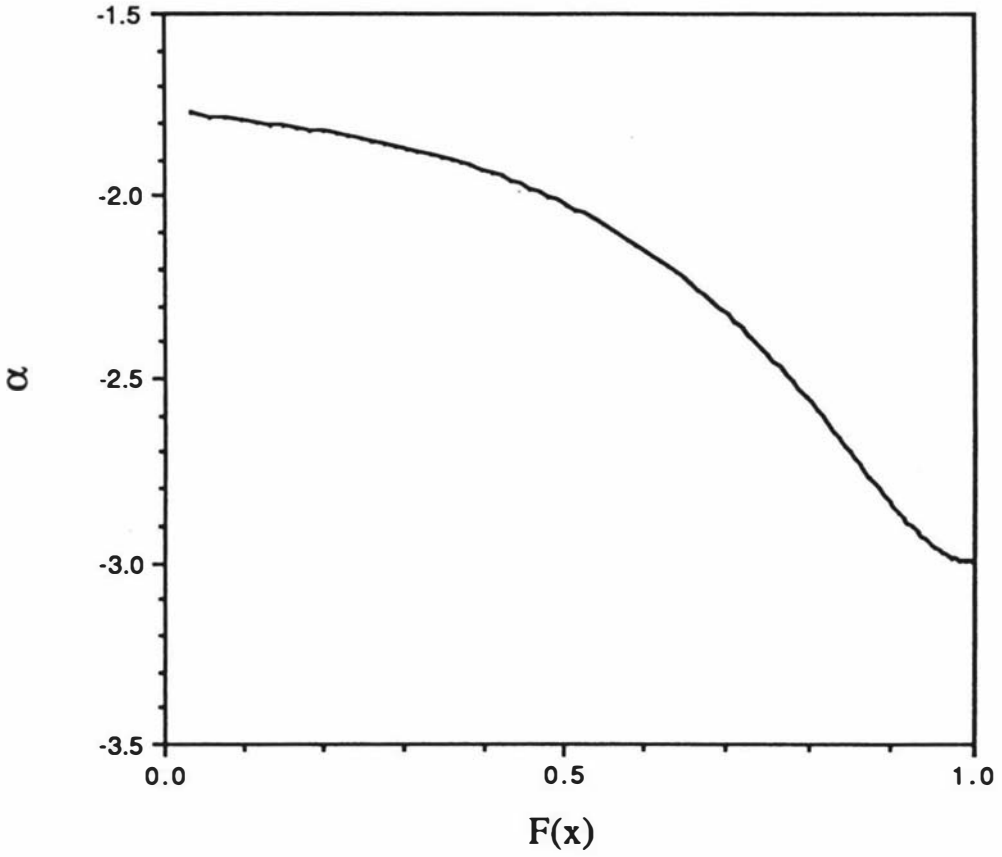

Figure A3.3 The effective exponent for the concentration dependence of the self diffusion coefficient (eqn (A3.42)) according to the blob model. The horizontal axis is $F(x) = (C/C_\theta^*) / (\tau/\tau^*)$ (eqn (A3.22)).

We can define a universal quantity involving D_s by rearranging the right hand side of (A3.41) in terms of C/τ :

$$D_S \sim (C/\tau)^{3+\alpha}\ C^{-3} . \qquad \text{(A3.48)}$$

Therefore

$$D_s C^3 \sim (C/\tau)^{3+\alpha} \tag{A3.49}$$

is a function of C/τ only and is therefore universal.

It is also possible to construct a universal ratio involving the self diffusion coefficient D_s by the method used for other properties above. If we remove the molar mass, temperature and viscosity variations in D_s, the quantity we are left with is the reduced diffusion coefficient

$$D_s N^2 \eta T_\theta / D_{s\theta} N_\theta^2 \eta_\theta T = (g/g_\theta)^2 (\xi_{H\theta}/\xi_H) \tag{A3.50}$$

which can be written, using previously calculated results, as

$$D_{red} = (88/B)^{9/2} (G/56) / x^5 \ . \tag{A3.51}$$

This result is clearly dependent only on x and it is plotted in Fig. A3.4.

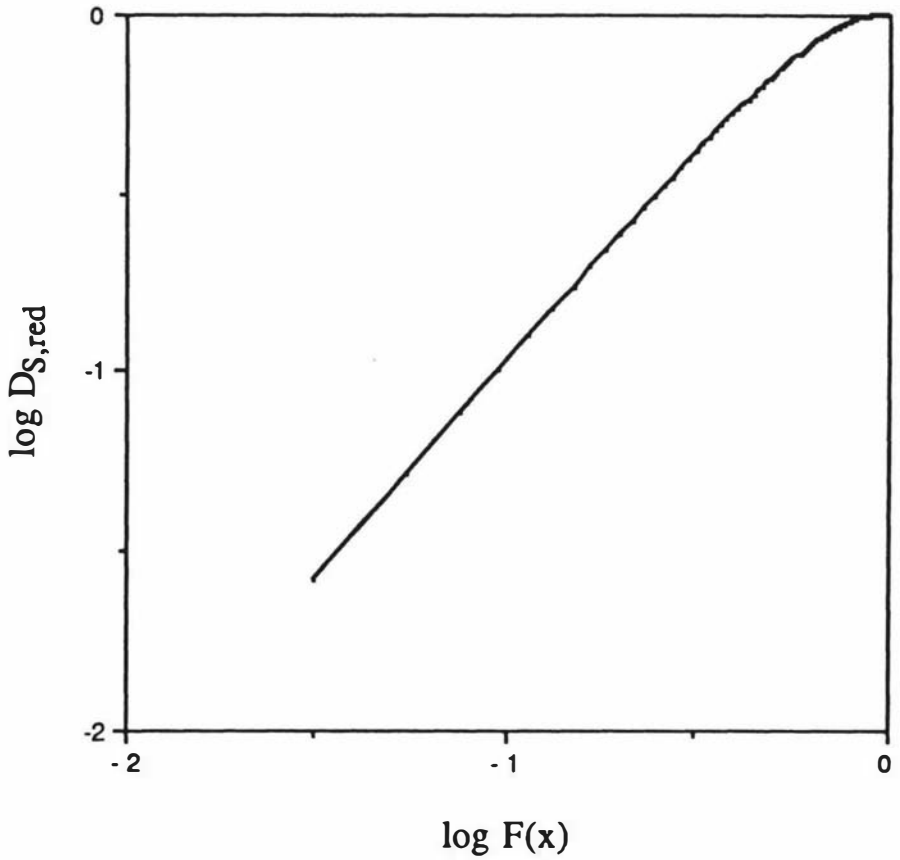

Figure A3.4 The reduced self diffusion coefficient calculated using the blob model (eqn (A3.51)) plotted against $F(x) = (C/C_\theta^*) / (\tau/\tau^*)$.

APPENDIX 4 - THE FREE ENERGY DENSITY IN TERMS OF OSMOTIC PRESSURE

The solution osmotic pressure measured at constant solution pressure is given by [19]

$$\Pi = -\frac{1}{V_0^0}\Delta_m\mu_0\,(T, P, x_1) \tag{A4.1}$$

where V_0^0 is the pure solvent partial molar volume, x_1 is the solute mole fraction, P is the solution pressure and $\Delta_m\mu_0$ is the change in solvent chemical potential due to the addition of solute. Equation (A4.1) can also be written as

$$\Pi V_0^0 = -\left(\frac{\partial\Delta_m G}{\partial n_0}\right)_{T,P,n_1} \tag{A4.2}$$

where $\Delta_m G$ is the change in the Gibbs free energy on mixing and n_i is the number of moles of component i.

Since

$$\left(\frac{\partial\Delta_m G}{\partial n_0}\right)_{T,P,n_1} = \frac{1}{V}(1 - c_0V_0)\left(\frac{\partial\Delta_m G}{\partial c_0}\right)_{T,P,n_1} \tag{A4.3}$$

where c_0 is the molar concentration of solvent and V is the total volume, we can now write (A4.2) in terms of the molar concentration;

$$\Pi V_0^0 = \frac{1}{V}(1 - \phi_0)\left(\frac{\partial\Delta_m G}{\partial c_0}\right)_{T,P,n_1} \tag{A4.4}$$

where $c_0V_0 = \phi_0$ is the solvent volume fraction. Finally, using

$$\left(\frac{\partial c_0}{\partial c_1}\right) = -\frac{V_1}{V_0} \tag{A4.5}$$

we find

$$\Pi V_0^0 = \frac{c_1V_0}{V}\left(\frac{\partial\Delta_m G}{\partial c_1}\right)_{T,P,n_1} \tag{A4.6}$$

Equation (A4.6) can be written directly in terms of the free energy density which we define as $G^V = (\Delta_m G) / V$. Using the relationship

$$\left(\frac{\partial G^V}{\partial c_1}\right)_{T,P,n_1} = \frac{1}{V}\left(\frac{\partial \Delta_m G}{\partial c_1}\right)_{T,P,n_1} - \frac{\Delta_m G}{V}\left(\frac{\partial V}{\partial c_1}\right)_{T,P,n_1} \tag{A4.7}$$

we find that

$$\begin{aligned} \Pi V_0^0 &= V_0 \left(c_1 \left(\frac{\partial G^V}{\partial c_1}\right)_{T,P,n_1} - G^V \right) \\ &= c_1^2 V_0 \frac{\partial}{\partial c_1}\left(\frac{G^V}{c_1}\right)_{T,P,n_1} \end{aligned} \tag{A4.8}$$

or, assuming that V_0 is independent of concentration,

$$\Pi = c_1^2 \frac{\partial}{\partial c_1}\left(\frac{G^V}{c_1}\right)_{T,P,n_1} \tag{A4.9}$$

The same relationship holds when C_1 or ϕ_1 is substituted for c_1 in eqn. (A4.9). De Gennes [7] gives a relationship similar to eqn.(A4.9) (his eqn. III.12) which is missing a factor of a^3. This factor reappears in the following equation (de Gennes' III.13).

APPENDIX 5 - PGSE NMR IN THE NARROW PULSE LIMIT

Equation (2.106) can be derived from Stepisnik's equation for the echo attenuation (eqn (2.95)) by assuming that the gradient pulses are a pair of appropriately normalized Dirac delta functions $\delta_D(t - t_p)$.

The normalization required is that the pulse area A must equal $G\delta$, so

$$G_{eff}(t) = A\delta_D(t - d) - A\delta_D(t - d - \Delta) \tag{A5.1}$$

where the times d and τ are defined in Fig. 2.5.

The spectrum $S(\omega,t)$ of $G_{eff}(t)$ can be found using eqns (2.97) and (2.98) giving

$$S(\omega,t) = \frac{A^2}{\omega^2}\,(2 - e^{-i\omega\Delta} - e^{i\omega\Delta}) \tag{A5.2}$$

Substitution of (A5.2) into eqn (2.95) gives $\beta(t)$ as

$$\beta(t) = \frac{\gamma^2 G^2 \delta^2}{2\pi}\,(2I_1 - I_2 - I_3) \tag{A5.3}$$

where

$$I_1 = \int_{-\infty}^{\infty} \frac{C(\omega)}{\omega^2}\,d\omega\ , \tag{A5.4}$$

$$I_2 = \int_{-\infty}^{\infty} \frac{C(\omega)}{\omega^2}\,e^{i\omega\Delta}\,d\omega \tag{A5.5}$$

and

$$I_3 = \int_{-\infty}^{\infty} \frac{C(\omega)}{\omega^2}\,e^{-i\omega\Delta}\,d\omega\ . \tag{A5.6}$$

These integrals can be simplified using

$$\langle x(t_1)\, x(t_2)\rangle = \frac{1}{\pi}\int_{-\infty}^{\infty} \frac{C(\omega)}{\omega^2}\exp[i\omega(t_1 - t_2)]\, d\omega \qquad \text{(A5.7)}$$

which is given by Stepisnik [81]. Eqn (A5.7) can be proven using a well known property of correlation functions [31]

$$\frac{d^2}{dt_1 dt_2}\langle x(t_1)\, x(t_2)\rangle = \langle v(t_1)\, v(t_2)\rangle$$

and the inverse transform of eqn (2.96).

Integral I_1 is therefore

$$I_1 = \pi\langle x^2\rangle \qquad \text{(A5.8)}$$

and integral I_3 is

$$I_3 = \pi\langle x(0)\, x(\Delta)\rangle \qquad \text{(A5.9)}$$

where $t_2 - t_1 = \Delta$. Since time correlation functions are even functions , $I_2 = I_3$.

The position correlation function is related to the mean square displacement by

$$\langle\, |x(\Delta) - x(0)|^2\,\rangle = 2(\langle x^2\rangle - \langle x(0)\, x(\Delta)\rangle) \qquad \text{(A5.10)}$$

(provided that x is a stationary random variable) so that $\beta(t)$ becomes

$$\beta(t) = \frac{\gamma^2 G^2 \delta^2}{2}\langle\, |x(\Delta) - x(0)|^2\,\rangle \qquad \text{(A5.11)}$$

which is the desired result.

APPENDIX 6 - THE VARIANCE OF THE MEAN COUNT RATE IN A DYNAMIC LIGHT SCATTERING EXPERIMENT

This discussion is based on the review by Jakeman [122].

The sampling scheme used in digital correlation is shown in Fig. A6.1. Photoelectron pulses are counted for N intervals, each of length T at intervals T_p. In practice, the sampling scheme for digital correlation has $T_p = T$. The estimator for the mean number of counts detected per sample time is defined as

$$\hat{n} = \frac{1}{N}\sum_{i=1}^{N} n(t_i,T) \ . \tag{A6.1}$$

Each run of N samples gives one value of $\hat{n}$.

Consider the commonly encountered case of a scattering process for which the magnitude of the instantaneous electric field is a gaussian random variable and the spectrum of the scattered light is lorentzian (i.e. the autocorrelation function is a single exponential). The distribution of measured values of $\hat{n}$ for gaussian-lorentzian scattered light has a variance Var $\hat{n}$ which is the sum of two contributions [122]. The first,

$$\frac{\text{Var } n}{N} = \frac{1}{N}\left(\langle n\rangle + \langle n\rangle^2\left(\frac{1}{\gamma} - \frac{1}{2\gamma^2} + \frac{e^{-2\gamma}}{2\gamma^2}\right)\right) \tag{A6.2}$$

is just the variance which would be obtained if the samples were separated by a sufficient time for them to be considered independent (T_p is large). In eqn (A6.2) the term which is linear in $\langle n\rangle$ is the variance due to the discrete nature of the detection process (Poisson noise), and the quadratic term is due to intensity fluctuations. Even if the source had a constant intensity, the number of counts detected per sample time would still fluctuate due to the probabilistic nature of the photodetection process.

The second contribution to Var $\hat{n}$, reflecting correlations between the samples (when T_p is not large) is

$$\frac{2\langle n\rangle^2 \exp(-2\Gamma T_p)}{1-\exp(-2\Gamma T_p)} + \frac{2\langle n\rangle^2 \exp(-2\Gamma T_p)\,[1-\exp(-2N\Gamma T_p)]}{[1-\exp(-2\Gamma T_p)]^2\, N} \ . \tag{A6.3}$$

The second term of eqn (A6.3) is negligible if N is large [122].

Two cases will be examined in more detail. First, if $\langle n\rangle$ is small the Poisson noise is dominant and

$$\mathrm{Var}\,\hat{n} = \frac{\langle n \rangle}{N} \quad . \tag{A6.4}$$

The more common experimental situation is that $N >> 1$ and $\Gamma T \rightarrow 0$. The second term of (A6.3) is negligible and since ΓT is small, the remaining exponential terms in eqn (A6.2) and (A6.3) can be expanded, giving

$$\mathrm{Var}\,\hat{n} = \frac{1}{N}\left(\langle n \rangle + \langle n \rangle^2/\gamma\right) \quad . \tag{A6.5}$$

The variance in the total number of counts registered in a run (which may be more useful practically) is $\mathrm{Var}\,\hat{n}_r = N^2\,\mathrm{Var}\,\hat{n}$. In terms of the total time per run, $T_r = NT$ we then have

$$\mathrm{Var}\,\hat{n}_r = \langle n_r \rangle + \frac{\langle n_r \rangle^2}{\Gamma T_r} \tag{A6.6}$$

where $\langle n_r \rangle = N\langle n \rangle$. This expression differs slightly from the one obtained by Haller et al. [131]. Their expression includes an erroneous factor of 2 arising from their eqn (9) which is incorrect. The right hand side of their eqn (9) is essentially $\langle \delta P^2 \rangle \left| g^{(1)}(\tau) \right|^2$ (in their notation) so the exponent should be $-2\Gamma\tau$ rather than $-\Gamma\tau$.

As was pointed out by Haller et al. [131], the fluctuations in intensity will be reduced by integration of the signal over the finite detector area and will also be affected by the clipping level. These effects are responsible for the experimental factor C appearing in eqn (3.10). This quantity appears as a factor of C^2 in the $\langle n \rangle^2$ term of eqn (A6.5), and could easily be included in the calculation of the variance.

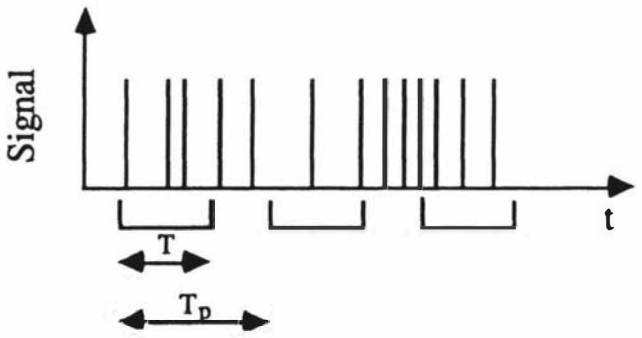

Figure A6.1 Sampling scheme for digital correlation.

REFERENCES

1. B. Chu, "Static and Dynamic Properties of Polymer Solutions", in [91].

2. M. Daoud and G. Jannink, *J. Physique*, **37**, 973-979 (1976).

3. D. W. Schaefer, *Polymer*, **25**, 387-394 (1984).

4. H. Yamakawa, *Modern Theory of Polymer Solutions*, Harper and Row, New York (1971).

5. B. Farnoux, F. Boué, J. P. Cotton, M. Daoud, G. Jannink, M. Nierlich and P. G. de Gennes, *Journal de Physique*, **39**, 77-86, (1978).

6. A. Z. Akcasu and C. C. Han, *Macromolecules*, **12**, 276-280 (1979).

7. P. G. de Gennes, *Scaling Concepts in Polymer Physics*, Cornell University Press, Ithaca (1979).

8. F. W. Billmeyer, *Textbook of Polymer Science*, Second Edition, John Wiley and Sons, New York (1971).

9. D. J. Lohse, *Macromolecules*, **14**, 1658-1667 (1981).

10. K. F. Freed, *Renormalization Group Theory of Macromolecules*, John Wiley and Sons, New York (1987).

11. Y. Oono, *Advances in Chemical Physics*, **61**, 301-437 (1985).

12. M. Daoud, J. P. Cotton, B. Farnoux, G. Jannink, G. Sarma, H. Benoit, R. Duplessix, C. Picot and P. G. de Gennes, *Macromolecules*, **8**, 804-818 (1975).

13. B. L. Hager and G. C. Berry, *Journal of Polymer Science: Polymer Physics Edition*, **20**, 911-928 (1982).

14. J. Roots and B. Nyström, *Polymer*, **20**, 148-156 (1979).

15. M. Doi and S. F. Edwards, *The Theory of Polymer Dynamics*, Oxford University Press, Oxford (1986).

16. G. Gee, *Contemporary Physics*, **11**, 313-334 (1970).

17. P. C. Hiemenz, *Polymer Chemistry*, Marcel Dekker, New York (1984).

18. H. J. V. Tyrrell and K. R. Harris, *Diffusion in Liquids*, Butterworths, London (1984).

19. M. Kurata, *Thermodynamics of Polymer Solutions*, Harwood Academic, Chur (1982).

20. S. Krause, "Polymer - Polymer Compatibility", in *Polymer Blends*, Vol. 1, Editors, D. R. Paul and S. Newman, Academic Press, New York (1978).

21. J. F. Joanny, P. Grant, L. A. Turkevich and P. Pincus, *J. Physique*, **42**, 1045-1051 (1981).

22. T. Nose, *J. Physique*, **47**, 517-527 (1986).

23. S. R. de Groot and P. Mazur, *Non-Equilibrium Thermodynamics,* North-Holland Publishing Company, Amsterdam (1962).

24. B. J. Berne and R. Pecora, *Dynamic Light Scattering*, John Wiley and Sons, New York (1976).

25. W. A. Steele, "Time Correlation Functions", in *Transport Phenomena in Fluids*, Ed. H. J. M. Hanley, Marcel Dekker, New York (1969).

26. *Dynamic Light Scattering*, Ed. R. Pecora, Plenum Press, New York (1985).

27. D. Stigter, *Journal of Physical Chemistry*, **64**, 114-118 (1960).

28. N. Yoshida, *J. Chem. Phys.*, **84**, 6529-6530 (1986).

29. F. O. Raineri and E. O. Timmermann, *Journal of the Chemical Society, Faraday Transactions* 2, **82**,1339-1350 (1986).

30. J. G. Albright and R. Mills, *Journal of Physical Chemistry*, **69**, 3120-3126 (1965).

31. J. P. Hansen and I. R. Mc Donald, *Theory of Simple Liquids*, Academic Press, London (1976).

32. G. Weill and J. des Cloizeaux, *Journal de Physique*, **40**, 99-105 (1979).

33. J. S. Lindner, W. W. Wilson and J. W. Mays, *Macromolecules*, **21**, 3304-3312 (1988).

34. A. Z. Akcasu, *Polymer*, **22**, 1169-1180 (1981).

35. P. G. de Gennes, *Macromolecules*, **9**, 587-593 and 594-598 (1976).

36. M. Muthukumar and S. F. Edwards, *Polymer*, **23**, 345-348 (1982).

37. Y. Shiwa, Y. Oono and P. R. Baldwin, *Macromolecules*, **21**, 208-214 (1988).

38. G. Rehage, O. Ernst and J. Fuhrmann, *Faraday Discussions of the Chemical Society*, **49**, 208-221 (1970).

39. Y. Shiwa, *Physical Review Letters*, **58**, 2102-2105 (1987).

40. B. Nyström and J. Roots, *Journal of Macromolecular Science - Reviews in Macromolecular Chemistry*, **C19**, 35-82 (1980).

41. M. Adam and M. Delsanti, *Macromolecules*, **10**, 1229-1237, (1977).

42. P. Wiltzius, H. R. Haller, D. S. Cannell and D. W. Schaefer, *Physical Review Letters*, **53**, 834-837 (1984).

43. D. W. Schaefer and C. C. Han, in [26].

44. G. Pouyet and J. Dayantis, *Macromolecules*, **12**, 293-296 (1979).

45. M. Adam and M. Delsanti, *Macromolecules*, **18**, 1760-1770 (1985).

46. M. Daoud and G. Jannink, *Journal de Physique Lettres*, **41**, L217-L220 (1980).

47. J. P. Cotton, M. Nierlich, F. Boué, M. Daoud, B. Farnoux, G. Jannink, R. Duplessix and C. Picot, *J. Chem. Phys.*, **65**, 1101-1108 (1976).

48. M. Adam and M. Delsanti, *J. Physique*, **41**, 713-721 (1980).

49. G. Pouyet, J. Francois, J. Dayantis and G. Weill, *Macromolecules*, **13**, 176-179 (1980).

50. J. D. Ferry, *Viscoelastic Properties of Polymers*, Third Edition, John Wiley and Sons, New York (1980).

51. G. C. Berry and T. G. Fox, *Advances in Polymer Science*, **5**, 261-357 (1968).

52. G. C. Berry, *Journal of Physical Chemistry*, **70**, 1194-1198 (1966).

53. E. D. von Meerwall, *Advances in Polymer Science*, **54**, 1-28 (1983).

54. M. Tirrell, *Rubber Chemistry and Technology*, **57**, 523-556 (1984).

55. G. Fleischer and E. Straube, *Polymer*, **26**, 241-246 (1985).

56. N. Nemoto, M. R. Landry, I. Noh, T. Kitano, J. A. Wesson and H. Yu, *Macromolecules*, **18**, 308-310 (1985).

57. R. Bachus and R. Kimmich, *Polymer*, **24**, 964-970 (1983).

58. P. G. de Gennes, *Journal of Chemical Physics*, **55**, 572-579 (1971).

59. W. W. Graessley, *Advances in Polymer Science*, **47**, 67-117 (1982).

60. R. H. Colby, L. J. Fetters and W. W. Graessley, *Macromolecules*, **20**, 2226-2237 (1987).

61. H. Deschamps and L. Léger, *Macromolecules*, **19**, 2760-2765 (1986).

62. P. T. Callaghan and D. N. Pinder, *Macromolecules*, **17**, 431-437 (1984).

63. W. Hess, *Macromolecules*, **19**, 1395-1404 (1986).

64. W. Hess, *Macromolecules*, **20**, 2587-2599 (1987).

65. N. Nemoto, S. Okada, T. Inoue and M. Kurata, *Macromolecules*, **21**, 1509-1513 (1988).

66. M. Daoud and P. G. de Gennes, *Journal of Polymer Science: Polymer Physics Edition*, **17**, 1971-1981 (1979).

67. P. F. Green and E. J. Kramer, *Macromolecules*, **19**, 1108-1114 (1986).

68. J. E. Martin, *Macromolecules*, **17**, 1279-1283 (1984).

69. N. Numasawa, K. Kuwamoto and T. Nose, *Macromolecules*, **19**, 2593-2601 (1986).

70. J. H. Wang, *Journal of the American Chemical Society*, **76**, 4755-4763 (1954).

71. M. E. Clark, E. E. Burnell, N. R. Chapman and J. A. M. Hinke, *Biophysical Journal*, **39**, 289-299 (1982).

72. J. S. Mackie and P. Meares, *Proceedings of the Royal Society of London*, **A232**, 498-509 (1955).

73. B. Jönsson, H. Wennerström, P. G. Nilsson and P. Linse, *Colloid and Polymer Science*, **264**, 77-88 (1986).

74. A. Abragam, *The Principles of Nuclear Magnetism*, Oxford University Press, Oxford (1985).

75. C. P. Slichter, *Principles of Magnetic resonance*, Springer-Verlag, Berlin (1980).

76. K. Blum, *Density Matrix Theory and Applications*, Plenum Press, New York (1981).

77. R. Lenk, *Brownian Motion and Spin Relaxation*, Elsevier Publishing Company, Amsterdam (1977).

78. E. O. Stejskal and J. E. Tanner, *Journal of Chemical Physics*, **42**, 288-292 (1965).

79. E. O. Stejskal, *Journal of Chemical Physics*, **43**, 3597-3603 (1965).

80. P. T. Callaghan, *Australian Journal of Physics*, **37**, 359-387 (1984).

81. J. Stepisnik, *Physica* , **104B**, 350-364 (1981).

82. P. T. Callaghan and D. N. Pinder, *Macromolecules*, **18**, 373-379 (1985).

83. P. T. Callaghan and D. N. Pinder, *Macromolecules*, **16**, 968-973 (1983).

84. E. D. von Meerwall, *Journal of Magnetic Resonance*, **50**, 409-416 (1982).

85. L. H. Peebles Jr, "Some Distribution Functions and their Properties", in [168].

86. G. Fleischer, D. Geschke, J. Kärger and W. Heink, *Journal of Magnetic Resonance*, **65**, 429-443 (1985).

87. B. J. Berne and R. Pecora, *Dynamic Light Scattering*, John Wiley and Sons, New York (1976).

88. *Photon Correlation and Light Beating Spectroscopy*, Ed. H. Z. Cummins and E. R. Pike, Plenum Press, New York (1974).

89. *Photon Correlation Spectroscopy and Velocimetry*, Ed. H. Z. Cummins and E. R. Pike, Plenum Press, New York (1977).

90. *Light Scattering in Liquids and Macromolecular Solutions*, Ed. V. Degiorgio, M. Corti and M. Giglio, Plenum Press, New York (1980).

91. *Scattering Techniques Applied to Supramolecular and Nonequilibrium Systems*, Ed. S. H. Chen, B. Chu and R. Nossal, Plenum Press, New York (1981).

92. P. N. Pusey and J. M. Vaughan, "Light Scattering and Intensity Fluctuation Spectroscopy", in *Dielectric and Related Molecular Processes*, Vol. 2, Ed. M. Davies, Specialist Periodical Reports of The Chemical Society, London (1975).

93. D. E. Koppel, *Journal of Chemical Physics*, **57**, 4814-4820 (1972).

94. P. N. Pusey, "Measurement of diffusion coefficients of polydisperse solutes by intensity fluctuation spectroscopy", in *Industrial Polymers : Characterization by Molecular Weight*, Ed. J. H. S. Green and R. Dietz, Transcripta Books, London (1973) and J. C. Brown, P. N. Pusey and R. Dietz, *Journal of Chemical Physics*, **62**, 1136-1144 (1975).

95. T. A. King and M. F. Treadaway, *Journal of The Chemical Society Faraday TRansactions II*, **73**, 1616-1626 (1977).

96. A. Z. Akcasu, M. Benmouna and C. C. Han, *Polymer*, **21**, 866-890 (1980).

97. G. D. J. Phillies, *J. Chem. Phys.* , **60**, 983-989 (1974).

98. P. N. Pusey, H. M. Fijnaut and A. Vrij, *J. Chem. Phys.* ,**77**, 4270-4281 (1982).

99. B. Hanley, S. Balloge and M. Tirrell, *Chem. Eng. Commun.*, **24**, 93-113 (1983).

100. M. Benmouna, H. Benoit, M. Duval and Z. Akcasu, *Macromolecules*, **20**, 1107-1112 (1987).

101. G. Foley and C. Cohen, *Macromolecules*, **20**, 1891-1896 (1987).

102. H. Benoit and M. Benmouna, *Macromolecules*, **17**, 535-540 (1984).

103. R. Borsali, M. Duval, H. Benoit and M. Benmouna, *Macromolecules*, **20**, 1112-1115 (1987).

104. R. Borsali, M. Duval and M.Benmouna, *Macromolecules*, **22**, 816-821 (1989).

105. E. L. Cussler, *Multicomponent Diffusion*, Elsevier Scientific Publishing Company, Amsterdam (1976).

106. E. Fukushima and S. B. W. Roeder, *Experimental Pulse NMR A Nuts and Bolts Approach*, Addison - Wesley Publishing Company Inc., Reading, Massachusetts (1981).

107. M. L. Martin, J.-J. Delpuech and G. J. Martin, *Practical NMR Spectroscopy*, Heyden, London (1980).

108. P. T. Callaghan, C. M. Trotter and K. W. Jolley, *Journal of Magnetic Resonance*, **37**, 247-259 (1980).

109. C. D. Eccles, Ph D Thesis, Massey University, New Zealand (1987).

110. Y. Xia, M Sc Thesis, Massey University , New Zealand (1988).

111. R. Mills, *Journal of Physical Chemistry*, **77**, 685-688 (1973).

112. P. T. Callaghan, unpublished.

113. P. T. Callaghan, unpublished.

114. P. T. Callaghan, unpublished.

115. R. C. O'Driscoll, unpublished.

116. R. C. O'Driscoll, unpublished.

117. I. Butler, Ph D Thesis, University of Manchester, UK (1984).

118. C. J. Oliver, "Correlation Techniques", in [88].

119. D. Jolly and H. Eisenberg, *Biopolymers*, **15**, 61-95 (1976).

120. R. C. O'Driscoll, Ph D Thesis, Massey University, New Zealand (1982).

121. R. C. O'Driscoll and D. N. Pinder, *J. Phys. E: Sci. Instrum.*, **13**, 192-200 (1980).

122. E. Jakeman, "Photon Correlation", in [88].

123. C. M. Trotter, Ph D Thesis, Massey University, New Zealand (1980).

124. R. C. O'Driscoll, unpublished.

125. *Light Scattering from Polymer Solutions*, Ed. M. B. Huglin, Academic Press, London (1972).

126. B. E. Tabor, "Preparation and Clarification of Solutions", in [125].

127. H. Z. Cummins and P. N. Pusey, "Dynamics of Macromolecular Motion", in [89].

128. C. J. Oliver, "Correlation Techniques", in [88].

129. C. J. Oliver, "Recent Developments in Photon Correlation and Spectrum Analysis Techniques: I. Instrumentation for Photodetection Spectroscopy" in [91].

130. C. J. Oliver, "Recent Developments in Photon Correlation and Spectrum Analysis Techniques: II. Information From Photodetection Spectroscopy" in [91].

131. H. R. Haller, C. Destor and D. S. Cannell, *Review of Scientific Instruments*, **54**, 973-983 (1983).

132. S. W. Provencher, J. Hendrix and L. De Mayer, *Journal of Chemical Physics*, **69**, 4273-4276 (1978).

133. P. R. Bevington, *Data Reduction and Error Analysis for the Physical Sciences*, McGraw-Hill, New York (1969).

134. *Handbook of Chemistry and Physics*, 61st Edition, CRC Press Inc., Boca Raton, Florida (1981).

135. P. Vidakovic and F. Rondelez, *Macromolecules*, **16**, 253-261 (1983).

136. C. Strazielle and H. Benoit, *Macromolecules*, **8**, 203-205 (1975).

137. P. Stepanek, R. Perzynski, M. Delsanti and M. Adam, *Macromolecules*, **17**, 2340-2343 (1984).

138. T. A. King, A. Knox and J. D. G. McAdam, *Journal of Polymer Science: Polymer Symposia*, **44**, 195-202 (1974).

139. P.T. Callaghan and D. N. Pinder, *Macromolecules*, **14**, 1334-1340 (1981).

140. P.T. Callaghan and D. N. Pinder, *Polymer Bulletin*, **5**, 305-309 (1981).

141. W. Brown, P. Stilbs and R. M. Johnsen, *Journal of Polymer Science: Polymer Physics Edition*, **21**, 1029-1039 (1983).

142. J. A. Wesson, I. Noh, T. Kitano and H. Yu, *Macromolecules*, **17**, 782-792 (1984).

143. P. T. Callaghan and D. N. Pinder, unpublished results.

144. H. Deschamps and L. Léger, *Macromolecules*, **19**, 2760-2765 (1986).

145. M. F. Marmonier and L. Léger, *Physical Review Letters*, **55**, 1078-1081 (1985).

146. H. Kim, T. Chang, J. M. Yohanan, L. Wang and H. Yu, *Macromolecules*, **19**, 2737-2744 (1986).

147. N. Boden, S. A. Corne, P. Halford-Maw and K. W. Jolley, To be published in *Journal of Magnetic Resonance* (1989).

148. D. E. O'Reilly, E. M. Peterson and D. L. Hogenboom, *Journal of Chemical Physics*, **57**, 3969-3976 (1972).

149. R. Mills, *Journal of Physical Chemistry*, **79**, 852-853 (1975).

150. J. Jonas, D. Hasha and S. G. Huang, *Journal of Physical Chemistry*, **84**, 109-112 (1980).

151. R. Kosfeld and K. Goffloo, *Kolloid Zeitscrift und Zeitschrift für Polymere*, **247**, 801-810 (1971).

152. F. D. Blum, S. Pickup and K. R. Foster, *Journal of Colloid and Interface Science*, **113**, 336-341 (1986).

153. D. H.-S. Yu and J. M. Torkelson, *Macromolecules*, **21**, 1033-1041, (1988).

154. B. D. Boss, E. O. Stejskal and J. D. Ferry, *Journal of Physical Chemistry*, **71**, 1501-1506 (1967).

155. A. F. Collings and L. A. Woolf, *Journal of the Chemical Society, Faraday Transactions I*, **71**, 2296-2298 (1975).

156. E. D. von Meerwall, E. J. Amis and J. D. Ferry, *Macromolecules*, **18**, 260-266 (1985).

157. M. E. Moseley and P. Stilbs, *Chemica Scripta*, **16**, 114-116 (1980).

158. P. T. Callaghan and J. Lelievre, *Analytica Chimica Acta*, **189**, 145-166 (1986).

159. J. A. Manson and G. J. Arquette, *Makromolekulare Chemie*, **37**, 187-197 (1960).

160. B. J. Bauer, B. Hanley and Y. Muroga, *Polymer Communications*, **30**, 19-21 (1989).

161. P. J. Flory, *Principles of Polymer Chemistry*, Cornell University Press, London (first published 1953, tenth printing, 1978).

162. D. J. Pollock and R. F. Kratz, "Polymer Molecular Weights", in *Methods of Experimental Physics*, Vol. 16 "Polymers", Part A "Molecular Structure and Dynamics", Ed. R. A. Fava, Academic Press, New York (1980).

163. T. K. Kwei, T. Nishi and R. F. Roberts, *Macromolecules*, **7**, 667-674 (1974).

164. E. J. Vandenberg, *Journal of Polymer Science: Part C*, **1**, 207-236 (1963).

165. T. P. Lodge and P. Markland, *Polymer*, **28**, 1377-1384 (1987).

166. B. G. Belenkii and L. Z. Vilenchik, *Modern Liquid Chromatography of Macromolecules*, (Journal of Chromatography Library - Volume 25), Elsevier, Amsterdam (1983).

167. *Polymer Handbook*, Second Edition, Ed. J. Brandrup and E. H. Immergut, John Wiley and Sons, New York (1975).

168. J. A. Lewis, personal communication.

169. C. Tanford, *Physical Chemistry of Macromolecules*, John Wiley and Sons, New York (1961).

170. H. Fujita, *Mathematical Theory of Sedimentation Analysis*, Academic Press, New York (1962).

171. M. B. Huglin, "Specific Refractive Index Increments", in [125].

172. T. Chang, C. C. Han, L. M. Wheeler and T. P. Lodge, *Macromolecules*, **21**, 1870-1872 (1988).

173. B. Appelt and G. Meyerhoff, *Macromolecules*, **13**, 657-662 (1980).

174. M. Shibayama, H. Yang, R. S. Stein and C. C. Han, *Macromolecules*, **18**, 2179-2187(1985).

175. L. M. Wheeler, T. P. Lodge, B. Hanley and M. Tirrell, *Macromolecules*, **20**, 1120-1129 (1987).

176. B. N. Preston, T. C. Laurent, W. D. Comper and G. J. Checkley, *Nature*, **287**, 499-503 (1980).

177. T. J. McDougall and J. S. Turner, *Nature*, **299**, 812-814 (1982).

178. W. D. Comper, G. J. Checkley and B. N. Preston, *Journal of Physical Chemistry*, **88**, 1068-1076 (1984).

179. W. Burchard, M. Schmidt and W. H. Stockmayer, *Macromolecules*, **13**, 580-587 (1980).

180. M. Bank, J. Leffingwell and C. Thies, *Macromolecules*, **4**, 43-46 (1971).

181. Th. G. Scholte, *Journal of Polymer Science*, **A2**, 841-868 (1970).

182. BDH Chemicals, England.

183. B. L. Johnson and J. Smith, "Refractive Indices and Densities of Some Common Polymer Solvents", in [125].

184. P. Caravatti, P. Neuenschwander and R. R. Ernst, *Macromolecules*, **18**, 119-122 (1985).

185. M. W. Crowther, I. Cabasso and G. C. Levy, *Macromolecules*, **21**, 2924-2928, (1988).

186. P. A. Mirau, H. Tanaka and F. A. Bovey, *Macromolecules*, **21**, 2929-2933 (1988).

187. A. Z. Akcasu, B. Hammouda, T. P. Lodge and C. C. Han, *Macromolecules*, **17**, 759-766 (1984).

188. F. Heatley, *Progress in NMR Spectroscopy*, **13**, 47-85 (1979).

189. J. Roots, B. Nyström, L.-O. Sundelöf and B. Porsch, *Polymer*, **20**, 337-346 (1979).

190. J. E. Martin, *Macromolecules*, **19**, 922-925 (1986).

191. J. Hadgraft, A. J. Hyde and R. W. Richards, *Journal of the Chemical Society, Faraday Transactions 2*, **75**, 1495-1505 (1979).

192. T. P. Lodge, *Macromolecules*, **16**, 1393-1395 (1983).

193. D. B. Cotts, *Journal of Polymer Science; Polymer Physics Edition*, **21**, 1381-1388 (1983).

194. P. Daivis, I. Snook, W. van Megen, B. N. Preston and W. D. Comper, *Macromolecules*, **17**, 2376-2380 (1984).

195. J. E. Martin, *Macromolecules*, **19**, 1281-1284 (1986).